DESIGN AND REALIZATION OF DIGITAL TOMOGRAPHIC FILTERS FOR RADIOGRAPHS

by

José M. Costa Vela

Department of Electrical Engineering

A Thesis submitted in conformity with the requirements
for the Degree of Doctor of Philosophy in the
University of Toronto

Design and Realization of Digital Tomographic Filters for Radiographs

J.M. Costa Vela

ABSTRACT

Radiographs are two-dimensional representations of three-dimensional objects. Using conventional X-ray imaging techniques a shadow view of the body under examination is produced which does not contain explicit information of the depth of details and structures. Due to the finite size of the X-ray source, the image of each layer of a three-dimensional object exposed to X-rays is blurred to an extent which depends on the distance from that layer to the X-ray source and to the film plane. Taking advantage of this fact, a radiograph can be processed in such a way that the image of a particular layer is deblurred while the other layers are not. This method is referred to as a tomographic filtration process and can be implemented using digital techniques.

In this dissertation, a model for the radiologic process from the viewpoint of communication system theory is developed and is used to determine what characteristics the tomographic filters should have. Based on these characteristics, theoretical evaluations both in the space and frequency domains show that tomographic filters can improve the usefulness of conventional radiographs with respect to three-dimensional information.

Two-dimensional digital signal processing techniques are developed which can be used to design digital tomographic filters as well as other

useful types of digital filters for the restoration and enhancement of imagery. The data management problems which arise in image processing are considered and some solutions are proposed.

Finally, digital tomographic filters are used to process both computer simulated radiographs and actual radiographs. Pictorial results are shown for different set-ups of the X-ray system and different parameters of the filtration process. The performance of tomographic filtering is compared with that of conventional radiology and that of standard tomography in terms of several measures, such as: the thickness of the tomographic layer, the rate of change of the Modulation Transfer Function and the signal-to-noise ratios. Some recommendations for possible extensions of this research are also given.

ACKNOWLEDGEMENTS

I am gratefully indebted to Professor Anastasios N. Venetsanopoulos under whose supervision this research was accomplished for the continuing support and encouragement he has offered throughout the course of my graduate studies.

I wish to express my gratitude to Dr. Martin Trefler for suggesting this research problem as stated in the introduction and for his helpful comments. While at the Radiological Research Laboratories, University of Toronto, he also provided the actual radiographs used in some of the experiments in this dissertation.

I would like to thank Dr. Michael L.G. Joy for his interest and constructive criticism on the manuscript, which led to significant improvements in this dissertation.

I sincerely acknowledge the stimulating discussions with my past fellow graduate students of the Communications Group. In particular, the efficient and careful proofreading of the manuscript of this dissertation by Mr. Brian J. Frohlich is deeply appreciated.

I am thankful to the staff of the Computer Research Facility, University of Toronto, under the direction of Mr. Dennis Smith, for their help and efforts in obtaining better image displays and photographs.

I gratefully acknowledge the financial support between 1973 and 1976 through various fellowships administered by the School of Graduate Studies. This work was also supported in part by the National Research Council of Canada under Grant No. A-7387.

I sincerely thank Mrs. Amy Chan for her typing skills in incorporating alterations and additions to an ever-changing manuscript.

Finally, I would also like to express special gratitude to my parents for their love and assistance over the years; and to my wife and three children who have contributed so many of my hours which should have been theirs.

The Röntgen Rays, The Röntgen Rays
What is this craze,
The town's ablaze,
With the new phase
Of X-rays ways
I'm full of daze,
Shock and amaze,
For nowadays,
I hear they'll gaze,
Thro' cloack and gown — and even stays,
These naughty, naughty Röntgen Rays.

Old popular verse quoted by
John G. Taylor, New Worlds in Physics.
London: Faber & Faber, 1974, page 49.

TABLE OF CONTENTS

GLOSSARY

LIST OF ACRONYMS

		Page
BIBO	bounded-input bounded-output	83
DFT	discrete Fourier transform	221
FFT	fast Fourier transform	222
FIR	finite impulse response	66
FS	focal spot	14
IDFT	inverse discrete Fourier transform	221
IIR	infinite impulse response	66
MTF	modulation transfer function	11
PRP	pattern recognition process	18
PSF	point spread function	11
TFP	tomographic filtration process	34

LIST OF PRINCIPAL SYMBOLS

a	"agressiveness" of a restoration filter	53
a	real part of H	41
b	imaginary part of H	41
c	real part of H^{-1} with hard-limited magnitude	42
C_T	cosine taper data window	119
d	imaginary part of H^{-1} with hard-limited magnitude	42
d	focal spot to film distance	30
d_1	distance from a layer to the focal spot	13
d_2	distance from a layer to the film plane	13
E_i	attenuation factor	23
f	original image	38
f_N	Nyquist frequency (1/2T)	77

		Page
F	Fourier transform of f	38
g	blurred image	38
G	Fourier transform of g	38
h	PSF or impulse response (in general)	24,26
h_a	approximation to the ideal impulse response of a digital filter	71
H_g	transfer function of a family of restoration filters	52
h_i	PSF of the space-variant model at the origin	26
h_{io}	PSF of the space-variant model	26
h_ℓ	hard-limit of the magnitude response	42
h_o	PSF of the space-invariant model at the origin	24
H_r	resultant frequency response of a digital filter	69
h_s	separable PSF	62
H	transfer function (in general)	
H_d	desired frequency response of a digital filter	68
H_s	separable transfer function	62
H_t	transfer function for the tomographic layer	49
I	X-ray intensity distribution	13
I_o	modified zeroth-order Bessel function of the first kind	71
I_o	X-ray intensity distribution in the focal spot	14,23
J_1	first-order Bessel function of the first kind	74
L	linear path of a single X-ray from the point (x_o,y_o) in the focal spot to the point (x,y) on the film	14
m_i	object magnification in radiology	13
s	size of a focal spot	45
S_x, S_y	sampling intervals of the focal-spot pin-hole images	111

		Page
t	distance from a layer to the plane of cut	45
T	linear transformation	86
T	sampling interval	77
T_x, T_y	sampling intervals of the radiographs	111
x,y	coordinates on the film plane	21
x_i,y_i	coordinates on the plane of the i^{th} layer	21
x_{io},y_{io}	coordinates of the position of a pin-hole on the i^{th} layer	23
x_o,y_o	coordinates on the plane of the focal spot	21
w	window function	69
w_K	Kaiser window	70
α	angle of the plane of the focal spot with the film plane	26
β	parameter for the Kaiser window	70
γ	parameter for a family of restoration filters	53
Δ_1	distance from the focal spot to the plane of a pin-hole	111
Δ_2	distance from the pin-hole to the film plane	111
Φ_R	ratio of the power spectrum of the noise and the power spectrum of the image	53
μ	total linear attenuation coefficient	13

LIST OF FIGURES

Figure		Page
5.3	Tomographic filter used to obtain Figure 5.10(c). (a) Magnitude response. (b) Magnitude response in dB.	115
5.4	Tomographic filter used to obtain Figure 5.17(b). (a) Magnitude response. (b) Magnitude response in dB.	116
5.5	Tomographic filter used to obtain Figure 5.17(c). (a) Magnitude response. (b) Magnitude response in dB.	117
5.6	Cosine taper data window. (a) One-dimensional. (b) Two-dimensional.	119
5.7	Simulated radiographs with different focal-spot intensity distributions. (a) Uniform-square. (b) Gaussian. (c) Gaussian (50% object absorption). (d) Point source.	124
5.8	(a)-(d) Magnification of the centre parts of the radiographs in Figure 5.6 [(a)-(d), respectively] multiplied by a two-dimensional cosine taper data window.	125
5.9	(a)-(d) Two-dimensional Fourier transforms (in dB) of the radiographs in Figure 5.7 (a)-(d), respectively.	126
5.10	Results of filtering Figure 5.7(a) with tomographic filters. For layer 2: (a) h_ℓ=10dB, (b) h_ℓ=20dB. For layer 1: (c) h_ℓ=20dB, (d) h_ℓ=30dB.	128
5.11	Results of filtering Figure 5.7(b) with tomographic filters. For layer 2: (a) h_ℓ=10dB, (b) h_ℓ=20dB. For layer 1: (c) h_ℓ=20dB, (d) h_ℓ=40dB.	129
5.12	Results of filtering Figure 5.7(c) with tomographic filters. For layer 2: (a) h_ℓ=10dB, (b) h_ℓ=20dB. For layer 1: (c) h_ℓ=20dB, (d) h_ℓ=40dB.	130
5.13	(a)-(d) Portions of the actual radiographs to be processed. The characteristics and geometries of the radiologic system are given in Table 5.4.	134
5.14	(a)-(d) Magnification of the centre parts of the radiographs in Figure 5.13 [(a)-(d), respectively], digitized, windowed, and reconstructed.	135
5.15	(a)-(d) Results of filtering Figure 5.14(b) with tomographic filters. The parameters are given in Table 5.6	138

Figure		Page

LIST OF TABLES

Chapter I

INTRODUCTION

1.1 Nature of the Problem and Research Motivation

To date, almost all theory of incoherent imaging has dealt with two-dimensional objects. The very nature of the radiologic process, however, forces one to consider three-dimensional objects in all imaging problems. Amazing as it may seem, this problem has not been fully appreciated in conventional radiology and even the most current analyses of standard X-ray imaging systems treat them as if they were designed to project two-dimensional objects. Nevertheless some special procedures have been devised to image three-dimensional objects which will be reviewed in the next section.

Let us consider the nature of the X-ray beam that forces us to develop new imaging theories: 1) the beam penetrates the object and thus information from all depths in the object is displayed; 2) lack of imaging devices for X-rays such as lenses and mirrors, force the use of a shadow casting geometry; and 3) this geometry is complicated by a) the size, shape and intensity distribution of the source of X-rays; b) beam divergence which implies that parts of the object located directly above each other are not imaged at the same point in the image plane, causing at best serious distortion of size and shape relationships and at worst complete obliteration of information due to overlapping of images of different parts of the object; and c) the angle of the source of X-rays , which implies that all the factors mentioned in a) and b) depend strongly on the location in the object field.

The previous considerations relating to the X-ray imaging problem have usually been ignored. However, they can be studied from two points of view. First, the properties of the X-ray imaging system itself with regard to design and use of X-ray systems. Second, the design of restoration filters to compensate for the degrading effects in the system. These are not really different problems but only two related aspects of the same problem.

In this work we shall be concerned with the problem of retrieving three-dimensional information from radiographs, without altering the specifications or operating conditions of the X-ray system. Using conventional X-ray imaging techniques, a shadow view of the body under examination is produced which does not contain explicit information of the depth of details and structures. This drawback has been overcome partially by standard tomography and three-dimensional radiography or computerized tomography. With these techniques care must be taken to avoid complexity, excessive patient dose, cost, and time consumption.

Our approach consists in the design of digital filters for conventional radiographs. These filters will emphasize the structures and details contained in a given depth of the body. This is done by deblurring the image of the layer of interest while the other layers are left partially blurred to an extent which depends on the position of each layer. We will refer to these filters as tomographic filters.

1.2 Antecedents

This section contains the historical development of the problem. A brief review of the relevant literature and pertinent background references are given here. More specific references are given whenever needed within the text.

Three-dimensional techniques

As early as 1916 [1] special radiographic procedures were invented to obtain clear images of certain parts of an object by blurring redundant images of other parts. These techniques have been reinvented, modified and improved over the years, and are all based on the same principle, which will be discussed and used in Chapter III. These methods have received different names such as laminagraphy, stratigraphy, tomography, stereoradiography, etc. The most commontly used is that of tomography: from the greek words "to write a cut".

Another approach to solve the problem consists in using more than one X-ray image or projection of the object to reconstruct any layer by digital or optical methods. A comprehensive review of these methods has been done by Mersereau [2], [3]. He even proved that in theory, bandlimited functions of finite order can be reconstructed exactly from a single projection. Nevertheless this method is so sensitive to noise that it can not be used in any practical application [2].

Another technique [4] uses a spatially-modulated X-ray source, such as a Fresnel zone plate pattern, which produces a shadow image of the object, but in a coded form. Decoding is done using optical techniques and only a thin slice of the object is in focus at one time, but other slices may be brought into focus by changing lens positions in the reconstruction system. Alternatively, digital techniques can also be used in the reconstruction.

To our knowledge no other attempts to recover three-dimensional information from a single projection have been published.

Two-dimensional techniques

The work done in radiograph processing is vast and it may be catalogued or studied from several points of view. Rather than give here a list of references we include them in Chapter II in a more organized way, in parallel with the description of a model for the radiologic process.

Background

The background material required for this research includes topics from various disciplines such as radiologic systems, communication systems, image processing, and digital signal processing.

For the reader unfamiliar with radiologic systems we have found the monographs of Meredith and Massey [5] and Brinker and Skucas [6] quite comprehensive and readable.

In the general field of image processing there exists tutorial material [7]-[11] which includes extensive lists of additional references.

Since we are interested in filtering images using a computer, background material on two-dimensional digital signal processing techniques can be found in [12]-[15].

1.3 Research Contribution

The original contribution of this research consists basically in the derivation, evaluation, and implementation of tomographic filters using digital techniques. A list of specific contributions toward this goal follows.

1) A study of the characteristics of the space-invariant and space-variant models of the X-ray image formation process and determination of their impulse responses (Ch. II).

2) The conversion of the space-variant problem, due to lack of parallelism between focal spot and film, to a space-invariant one (Ch. II).

3) The development of a tomographic filtration process to emphasize three-dimensional information in conventional radiographs (Ch. III).

4) The theoretical evaluation of tomographic filters both in the space and frequency domains (Ch. III).

5) The approximation of the transfer functions by separable functions (Ch. III).

6) A new technique for cascading rotated filters that is capable of approximating better circularly-symmetric two-dimensional recursive filters as well as certain types of non-circularly-symmetric recursive filters (Ch. IV).

7) A group of linear spectral transformations for two-dimensional digital filters (Ch. IV).

8) The development of data management techniques for processing large two-dimensional arrays of data stored sequentially in auxiliary storage. These include recursive techniques and FFT algorithms (Ch. IV).

9) The design and implementation of tomographic filters in a digital computer (Ch. V).

10) The practical evaluation of tomographic filters with both computer-simulated radiographs and actual radiographs (Ch. V).

11) A comparative assessment of tomographic filtering taking as benchmarks two well-established radiological procedures: standard tomography and conventional radiology (Ch. VI).

12) Some recomendations for future research (Ch. VII).

13) A novel derivation of the linear model of conventional radiology by considering it as a special case of standard tomography and generalization of the concept of tomographic filtering to both conventional radiographs and standard tomograms (App. A).

14) The simulation of a three-dimensional radiologic process in a digital computer (App. A).

15) A suggestion to use the projection-slice theorem as an alternative to the Henkel transform for computing the Fourier transform of circularly symmetric functions without the need for Bessel functions (App.B).

16) The development of a number of software programmes for the design and realization of both recursive and non-recursive two-dimensional digital filters (App. C).

1.4 Organization of the Contents

This work is divided into six parts. A complete model for the radiologic process, on which this research is based, is developed in Chapter II. The core of this research is then presented in Chapter III, where the tomographic filters are proposed and discussed; and their performance evaluated theoretically. After studying in Chapter IV the two-dimensional digital signal processing tools, they are used in the synthesis and practical evaluation of tomographic filters in Chapter V. The comparative performance of tomographic filters with respect to conventional radiology and standard tomography is developed and discussed in Chapter VI using several measures. Finally, the conclusions of this research and some recommendations for future work are given in Chapter VII.

For the sake of continuity in the text, the development of auxiliary mathematical expressions and computational algorithms are given in four appendices.

Chapter II

A MODEL FOR THE RADIOLOGIC PROCESS

2.1 Introduction

Before we attempt any improvement of radiographs we must study the characteristics of the image formation process to find out what are the degradations which should be corrected.

The radiologic process consists of a sequence of transformations intimately related in that the result of one forms the input to the next [16]. The process begins with the generation of X-rays, continues with the exposure of an object, and ends with a diagnosis.

The degradations introduced at each stage of the radiologic process have been studied in great detail from the viewpoint of image quality [16]-[20]. However, most researchers assume that the object being X-rayed is two-dimensional; thus, the problems due to object depth are usually ignored.

In this chapter we develop a block diagram of the radiologic process which is valid for three-dimensional objects and we study the characteristics of each block.

2.2 Block Diagram

In Figure 2.1 we propose a block diagram model for the radiologic process. In general, block inputs and outputs are two-dimensional functions representing distributions of intensities. Unless otherwise specified we will deal with intensity images rather than density images†.

† An intensity image is defined to be an image represented by values

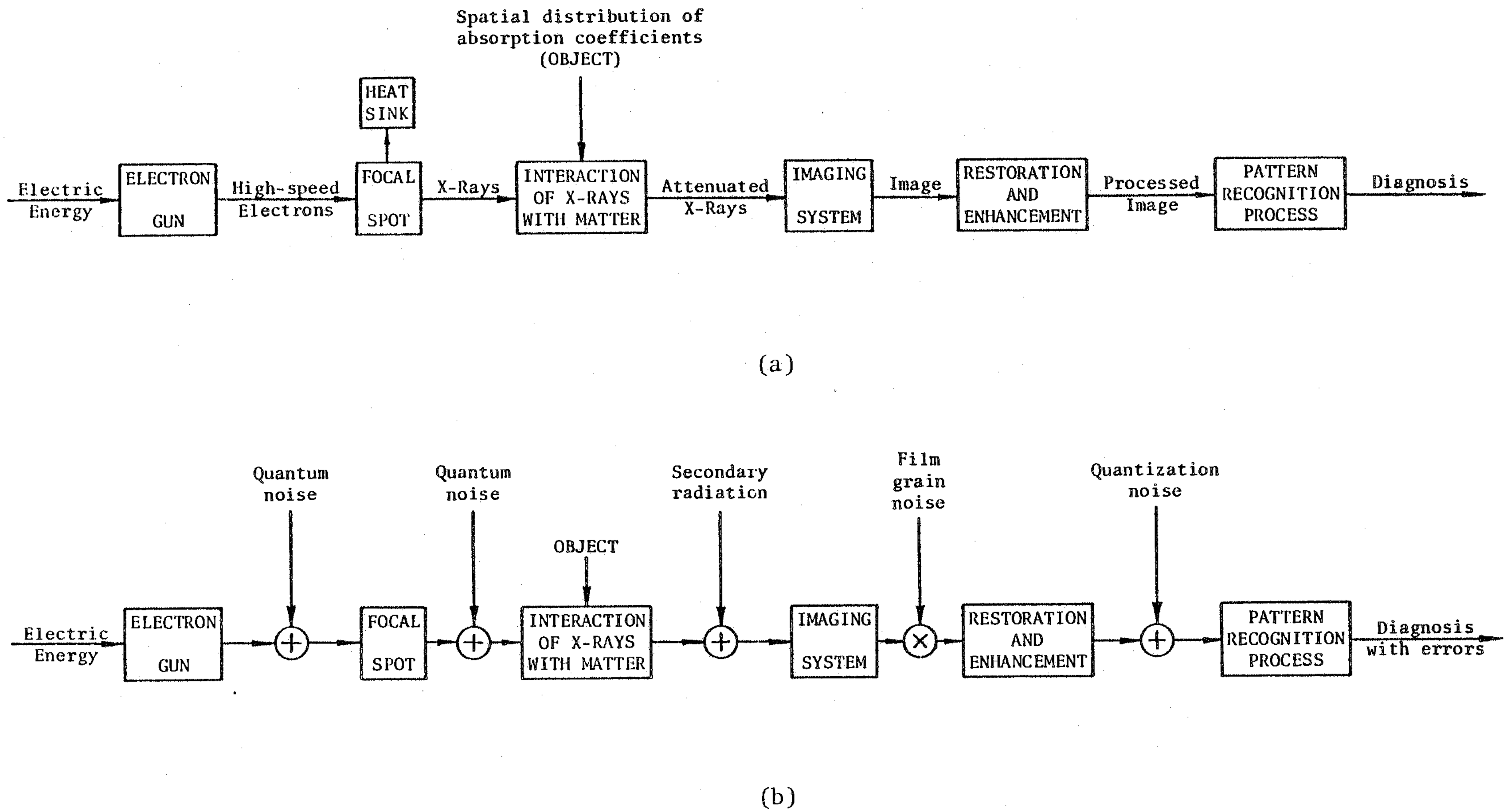

Figure 2.1. Block diagram model for the radiologic process. (a) Noiseless. (b) With noise.

The operation in each block can be represented by mathematical equations relating the output to the input. There are many factors, especially those which are random in nature, not taken into account in the block diagram of Figure 2.1(a). These factors are considered to be noise and they are modelled by a perturbing noise source at the output of each block in Figure 2.1(b). The manner in which the noise is combined with the image depends on how the image has been formed and the nature of the noise process. Usually additive or multiplicative noise is assumed.

2.2.1 Electron Gun

The first block represents the electron gun consisting of a heated filament or cathode emitting electrons which are focused and accelerated at high speed towards the anode. Some heat is also produced. The input to this block is therefore electric energy and the output is the spatial distribution of the current of high-speed electrons. The distribution and speed of the electrons in space depends upon various factors [21], such as the position and shape of the filament, the voltage and current in the filament, and the voltage and current in the anode.

2.2.2 Focal Spot

The focal spot is the source of X-rays. When the beam of high-speed electrons is stopped by a tungsten target some of its kinetic energy is converted into electromagnetic energy. A very large amount

---

which are linearly proportional to the intensity of the original radiant energy component involved in the image formation. A density image is defined to be an image in which the values are proportional to the logarithm of the intensity of the original radiant energy component involved in the image formation [37].

of heat is also produced. The region in the target where the X-rays and heat are produced is called the focal spot. The angle formed by the target surface and the direction of the centre X-ray is referred to as the target angle.

The X-rays emitted by the focal spot are not all of one frequency but constitute a complex spectrum made up of two different parts. There is a continuous spectrum consisting of frequencies from a certain maximum downwards, and upon this there is superimposed a line spectrum consisting of a relatively small number of separate frequencies [5, pp. 45-51].

The spatial distribution of X-rays is not uniform and depends on the target thickness, material, and roughness, as well as on the applied voltage between the cathode (filament) and the anode (target). The intensity of the radiation tends to be greater in the direction of movement of the electrons. However, for applied voltages in the 50-150 kV range, used in diagnostic radiology, X-rays are emitted more or less uniformly in all directions.

Many studies have been published about the characteristics of focal spots in X-ray tubes [22]-[27]. The shape and size of focal spots have been determined as well as their modulation transfer functions (MTF's), both theoretically and experimentally. The MTF is the magnitude of the Fourier transform of the point spread function (PSF) or impulse response of the focal spot. The PSF is defined here as a pin-hole image of the focal spot. Nevertheless, for mathematical simplicity many researchers assume that the focal spot can be represented by a geometrical shape (e.g. a square or a circle) with definite edges. In this case the MTF of a focal spot is some form of a two-dimensional sampling function. The radiation from outside the edges is referred to as off-focus radiation. Real focal spots are not defined by sharp edges; instead there is an edge gradient shaped like a Gaussian function. Indeed, it has been stated in the literature [22], [25], [28], that the MTF of a focal spot more resembles a Gaussian function rather than a sampling function and that this approximation is better in certain directions than others. This is a reasonable assumption because even if we had an ideal point source of electrons, it would be very difficult to focus the electron beam onto a single point in the target. Therefore, the impact of the electrons and the subsequent emission of X-rays takes place in a region of finite dimensions. A spatial Gaussian function seems a good approximation to the spatial distribution of X-rays over that region. When the source of electrons is of finite size, the distribution of X-rays results in an image of the filament with the edges approximated by Gaussian functions.

Since our purpose is not the design of radiologic systems but the design of filters that will compensate for the degradations in existing systems, we will assume that the output of the focal spot block, that is, the distribution of X-rays emitted by the focal spot, can be measured. Therefore, we will not consider any further the characteristics of the first two blocks.

2.2.3 X-Ray Image Formation

The attenuation of X-rays with matter may be modelled by the differential equation in (2.1), where $I(x)$ is the intensity of a narrow X-ray beam as a function of the distance x in the direction of propagation and $\mu(x)$ is a total linear attenuation coefficient.

$$\frac{dI(x)}{dx} + \mu(x)\, I(x) = 0 \tag{2.1}$$

The solution of (2.1) is given in (2.2).

$$I(x) = I(0)\, e^{-\int_0^x \mu(\sigma)\, d\sigma} \tag{2.2}$$

X-rays propagate in straight lines. This fact controls the size, shape, and position on the radiographic film of the shadow or image of the various structures of the object being exposed.

Due to the diverging nature of the X-rays emitted by the focal spot, the size of the shadow is different from that of the object casting the shadow. The ratio of the size of the image to that of the object is called the magnification. For a three-dimensional object, the magnification is a constant in a layer parallel to the film plane. If we denote by d_1 the distance from the focal spot to the i^{th} layer and by d_2 the distance from that layer to the film plane, the magnification for that layer is given by

$$m_i = \frac{d_1 + d_2}{d_1} \tag{2.3}$$

We are next to study the effects of the finite size of the focal spot.

The X-ray intensity distribution that reaches the imaging system is a function of both the object and the X-ray intensity distribution in the focal spot. To maintain generality in our block diagram, we model the interaction of X-rays with matter as a system with two inputs.

We denote by $I_o(x_o,y_o;x,y)$ the X-ray intensity emitted from the point (x_o,y_o) in the focal spot toward the point (x,y) in the film plane. The other input is denoted by $\mu_L(\ell)$ and corresponds to the spatial distribution of absorption coefficients in the object. $\mu_L(\ell)$ is defined along a line L from (x_o,y_o) to (x,y).

The interaction between these two inputs can then be modelled by the following integral equation:

$$I(x,y) = \iint_{F.S.} I_o(x_o,y_o;x,y)\, e^{-\int_L \mu_L(\ell)\, d\ell}\, dx_o\, dy_o \qquad (2.4)$$

which is a generalization of (2.2) and is obtained by integrating over the region of existence of the focal spot (denoted here by F.S.). The integral in the exponential is along a line L defined by the point (x_o,y_o) in the focal spot and the point (x,y) in the film plane. Since this is a line in space, (2.4) can be used with any three-dimensional object, in general.

The pragmatic approach to conventional radiographic image formation systems has been dominant in past efforts in this field [37]; namely, a linear space-invariant model is assumed, the thickness of the object is neglected, and the point spread function is estimated by approximations. The implications of (2.4) will be studied in detail in Section 2.3, where the questions of linearity and space-invariance will be examined and some simplifications will be made. Nevertheless, we must exphasize here that the salient feature of (2.4), as well as of subsequent equations which will be derived from (2.4), is that it shows what happens when X-rays are attenuated by three-dimensional objects, thus setting the basis for the recovery and separation of the information which is projected on the film. Other effects such as the inverse square law and scattered radiation are not relevant here, because they do not contribute to differentiate among layers. The inverse square law determines the attenuation of the radiation due to its divergent nature and may be modelled independently of the object and (2.4) if necessary.

The integrals in (2.4) can be approximated by summations. This discretization is suitable for implementation in a digital computer and is useful in performing simulations. For this purpose we coded the routine XRAY in FORTRAN IV. The details are given in Appendix A.

Due to the finite size of the focal spot, the shadow image of a point or edge in the object extends over a finite region on the film plane. Each edge or shadow is composed of two parts, the umbra and the penumbra or edge gradient†. These effects will be discussed further and exploited in Chapter III.

Several researchers have investigated the removal of penumbras in radiographs using optical signal processing techniques: Minkoff [30], Krusos [31], and Trefler [32].

† Umbra is defined as the zone of lucence formed on a film when a radiopaque object intervenes between the film and a source emitting X-rays. Penumbra, or more accurately edge gradient, is defined as the gradation in density which occurs at the margin of any given radiological image, delineated medially by the point of maximum image lucence and laterally by the point of minimum image lucence [29].

When X-rays interact with matter, they are not only attenuated in intensity, but also they are scattered through a finite solid angle tending to produce a hazy background in the image only indirectly related to absorption coefficients in the object [33]. Therefore, we model this secondary radiation as additive noise. The problem of estimating the PSF due to radiation scattering and the realization of a compensating filter using digital techniques has been studied by Hunt [34], [35].

2.2.4 Imaging System

The imaging system is the conversion process of an X-ray image to a light one. X-rays, at the energy levels used in radiology, have very poor capabilities for impressing film. Consequently, additional devices, such as image intensifiers or screens, must be used. The function of these devices is to create a large number of light photons in the device output for each X-ray photon in the input. These imaging devices introduce degradations which can be characterized by their PSF's or their frequency responses.

The input to the imaging system is the X-ray intensity distribution just before it enters a screen-film combination or an image intensifier and the output is a film image or a television image, respectively.

In addition to the low-pass characteristics of the frequency response of the imaging device, the main distortions in the recording (film) or display (television monitor) of images are due to random noise and nonlinearities. The source of noise in film is due to the finite size and random distribution of the light-sensitive grains in the film (film-grain noise). The main characteristic of this kind of noise is that it appears to be multiplicative rather than additive [36], [37]. If the images are sampled somewhere in the process, nonlinearities can be compensated for in a digital computer [37]. All these effects have been studied in detail by several authors [36]-[40].

2.2.5 Restoration and Enhancement

Restoration and enhancement, which are not normally present in conventional radiologic systems, are the principal objectives of this research. Given the characteristics of all other blocks, we have to design the restoration and enhancement methods that will improve the final output of the whole system, i.e. the diagnosis.

Restoration refers to that part of the system that corrects for degradations in other parts of the process. The design of the restoration filter requires knowledge of the degradations in the system, that is the transfer functions of the previous blocks. The way this knowledge is acquired may be represented in the block diagram by a feedforward path.

By enhancement we refer to the processing of images in general, to present to the viewer (or subsequent machine) additional information or insight into some factor concerning the pre-enhanced image. A comprehensive survey of image enhancement techniques has been published by Andrews [41]. It must be emphasized that the fidelity criterion of enhancement is not attempting better object representation; it will depend strongly on the type of pattern recognition process (PRP) used and on the relevant features in the image. If the PRP is automated, a mathematical criterion like the mean-square error will be in order; but if the image is to be viewed by a human viewer, such as the radiologist, then the psychophysics of vision and other human factors must be taken into account [39], [42]. Therefore, the design of an enhancement filter needs a feedback of the characteristics of the PRP following it.

Enhancement techniques have been applied to the processing of radiographs by Selzer [43], Hall [44], Hunt [45], and Hesse [46].

2.2.6 Pattern Recognition Process

This is the ultimate and most intelligent system block in the whole process which results in the diagnosis.

The pattern recognition may be performed by an automated process, a radiologist, or both in combination.

For a survey of automated PRP techniques for radiographs see for example Hall [47].

2.3 Point Spread Function of the System Block Representing the X-Ray Image Formation

In this section we further study the significance of (2.4) from the point of view of system theory. This part of the radiologic process is the most critical one because it is here that a three-dimensional object is projected into a two-dimensional radiograph. Depending upon the characteristics of this projection the recovery of depth information will or will not be possible.

In Section 2.2.3 we modelled the interaction of X-rays with matter as a system with two inputs. Now we consider one of the inputs as forming part of the system. The usual approach in existing work is to consider the intensity distribution of the focal spot as the input to the system and the object being X-rayed as belonging to the system. Using this formulation the input to the system is known and the system itself must be determined from a measurement of the output (system identification problem). Since the input cannot be specified arbitrarily and the object is three-dimensional, this model presents some problems. We will work with a second system model where the input is passive and the system is active, that is the focal spot belongs to the system and the input is a passive distribution of absorption coefficients. The problem now consists in finding the input, given the output and the system PSF (input identification problem).

From (2.4) it is clear that the radiologic process is linear with respect to I_o and nonlinear with respect to the attenuation coefficients μ. Since we consider the distribution of attenuation coefficients as the input to the system, some assumptions have to be made to make the problem mathematically tractable using linear system theory (cf. Appendix A).

In our approach to tomographic restoration, the radiologic image is to be processed by a filter which we assume will modify the image of each layer independently of the others. This means that the system is linearized by assuming that the exponential in (2.4) can be approximated by the linear terms in its Taylor series expansion. The validity of this assumption is based on how small the attenuation coefficients are and is discussed in [48], where it is also suggested that a better approximation may be obtained by writing $\mu=\mu_o+\Delta\mu$, where μ_o is the "background" linear attenuation coefficient and $\Delta\mu$ represents the changes in linear attenuation coefficient from μ_o in the object.

Once the system is linearized it can be described by convolution integrals if the system is also space-invariant. However, the radiologic system is space-variant for several reasons such as the obliquity of the X-rays when they reach the film, the superposition of the images of the layers in the object, the lack of parallelism of the focal spot and film planes, and the change with direction of the X-ray intensity emitted from the focal spot. The effect of the obliquity of the X-rays reaching the film can be corrected for if the area of the film to be processed is large, or it can be neglected if it small. In either case the error committed is quite small because of the distances normally used in diagnostic radiology, that is the focal spot to film distance is much greater than the focal spot size, say 1000:1. The space-variance due to the overlaying layers is avoided by dealing with one layer at a time; the effects of overlaying layers are discussed in Chapter V. In the remainder of this section we study separately the space-invariant and space-variant approximations taking into consideration the other factors.

2.3.1 Space-Invariant Model

If the plane of the focal spot and the plane of the film were

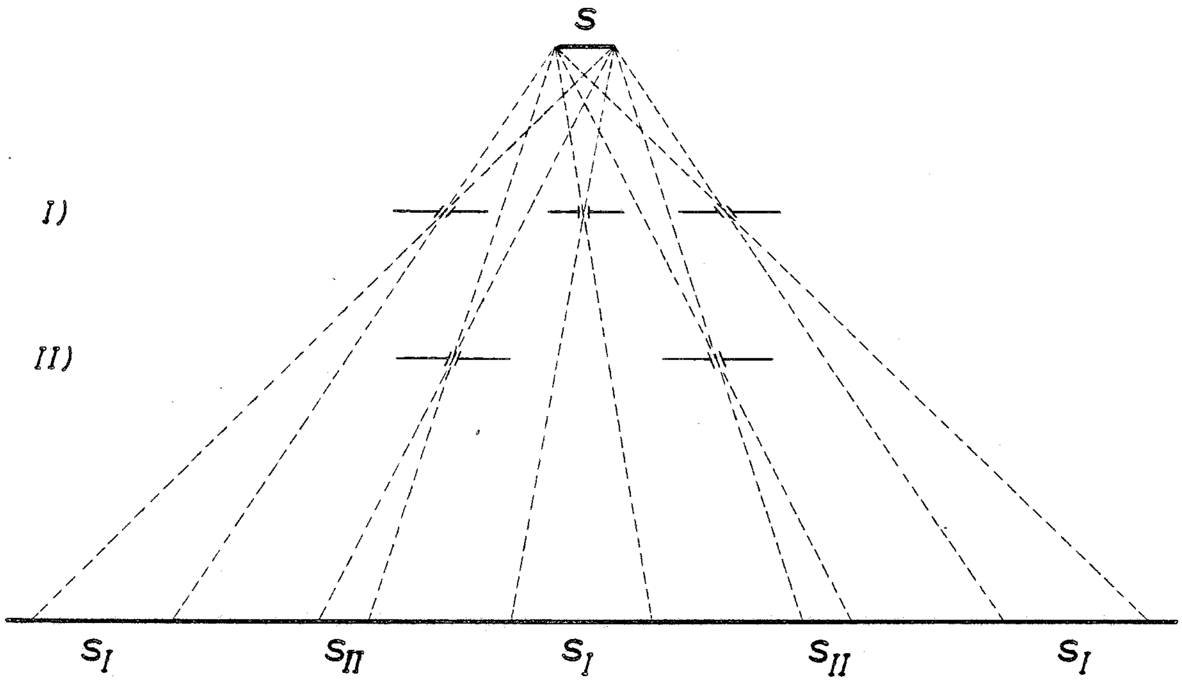

Figure 2.2. Comparison of impulse responses in the space-invariant model.

parallel, the system would be space invariant. Indeed, it can be proved that a translation of the unit-impulse input within a layer results in a translation of the PSF. Also, a translation of the unit-impulse input from one layer to another results in a similar PSF scaled in space (see Figure 2.2). A derivation of the dependence of the shifts and scalings on the position of the unit-impulse input follows.

Assume that the object is divided into very thin layers parallel to the film plane. Let $\mu_i(x_i,y_i)$ be the two-dimensional distribution of absorption coefficients in the i^{th} layer. The X-ray emitted from the point (x_o,y_o) in the focal spot and reaching the film at the point (x,y) intercepts the i^{th} layer at a point (x_i,y_i). This is illustrated in Figure 2.3. From the geometry of the system, these coordinates are given in (2.5).

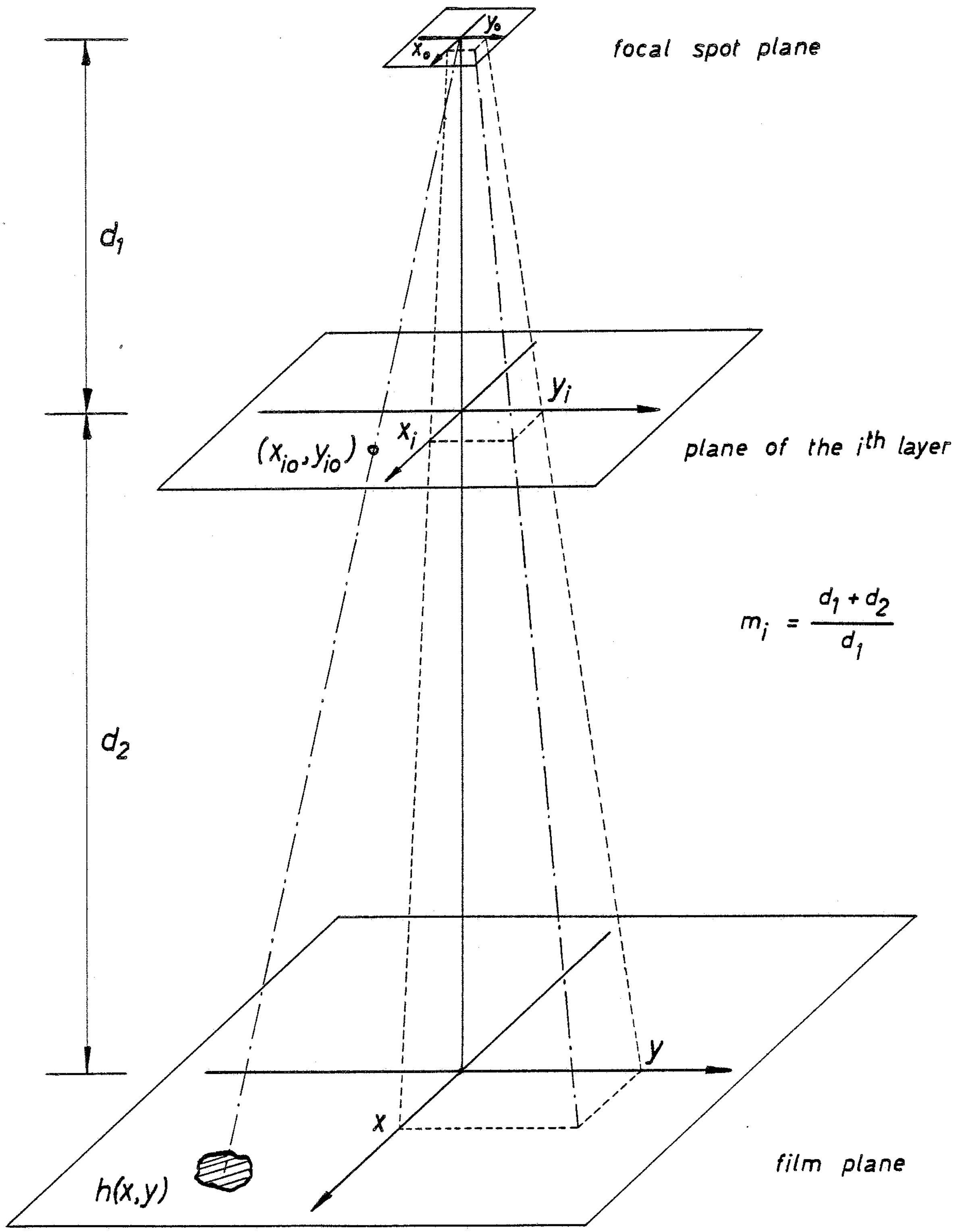

Figure 2.3. Relationship between coordinates on different planes in the space-invariant model.

$$x_i = \frac{x-x_o}{m_i} + x_o \tag{2.5a}$$

$$y_i = \frac{y-y_o}{m_i} + y_o \tag{2.5b}$$

where m_i is the magnification for the i^{th} layer as defined in (2.3). Assuming space invariance, the focal spot X-ray intensity distribution is a function of (x_o,y_o) only.

Under this conditions the integral in the exponential in (2.4) can be approximated by a summation which results in a product of exponentials as follows:

$$I(x,y) = \iint_{F.S.} I_o(x_o,y_o) \prod_i E_i(x_i,y_i)\, dx_o\, dy_o \tag{2.6}$$

where

$$E_i(x_i,y_i) = \exp\{-\mu_i(x_i,y_i)\,\Delta\ell\} \tag{2.7}$$

represents a two-dimensional distribution of total attenuation factors corresponding to the i^{th} layer. Since X-rays do not cross any layer perpendicularly (except the centre ray), the apparent thickness $\Delta\ell$ will depend on the position in the field. We neglect this effect and assume $\Delta\ell$ constant or else the variations can be included in the absorption coefficients thus becoming attenuation coefficients.

With the assumption of linearity, as previously discussed, the product of attenuation factors in (2.6) becomes a summation and the PSF of each layer can be determined independently of the others. The system PSF of the i^{th} layer is found by letting the input to be a unit-impulse located at the point (x_{io},y_{io}) in the i^{th} layer. Physically this is the same as a thin layer opaque to X-rays with a pin-hole at the point (x_{io},y_{io}).

$$h(x,y) = \iint_{F.S.} I_o(x_o,y_o) \quad \delta(x_i-x_{io},y_i-y_{io}) \; dx_o \; dy_o$$

$$= I_o\left(\frac{m_i x_{io}-x}{m_i-1} \; , \; \frac{m_i y_{io}-y}{m_i-1}\right)$$

$$= I_o\left(\frac{d_1}{d_2} (m_i x_{io}-x) \; , \; \frac{d_1}{d_2} (m_i y_{io}-y)\right) \qquad (2.8)$$

From (2.8) we conclude that the PSF of each layer is spatially scaled by the factor $-d_1/d_2$, which is a constant for a given layer, and is shifted depending upon the position of the unit-impulse within each layer.

Thus, the PSF of the i^{th} layer at the origin is

$$h_o(x,y) = I_o\left(-\frac{d_1}{d_2} x \; , \; -\frac{d_1}{d_2} y\right) \qquad (2.9)$$

The PSF anywhere else within the same layer can be found by shifting the PSF at the origin as follows:

$$h(x,y) = h_o\left(x - \frac{d_1+d_2}{d_1} x_{io} \; , \; y - \frac{d_1+d_2}{d_1} y_{io}\right) \qquad (2.10)$$

2.3.2 Space-Variant Model

A radiologic process is space-variant for the reasons previously mentioned. The following two are considered here:

1) The intensity of the X-rays emitted from the focal spot is different in each direction.

2) The film plane is not parallel to the plane of the focal spot.

A solution to the first problem could be to divide the X-ray image

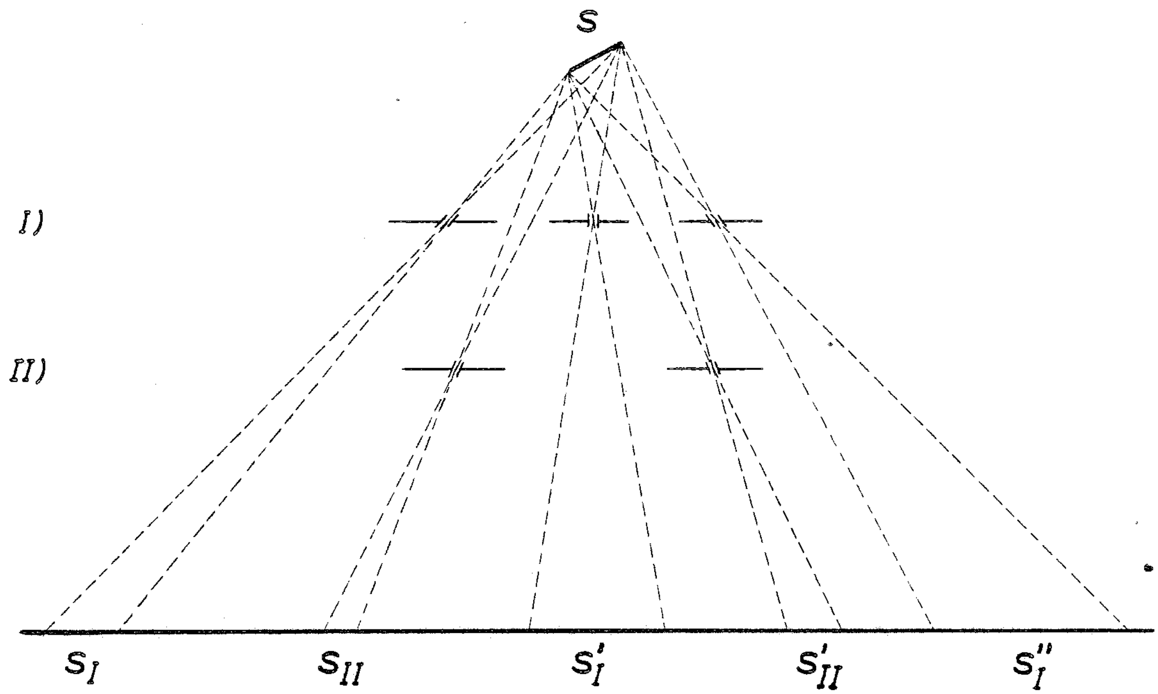

Figure 2.4. Comparison of impulse responses in the space-variant model.

into rectangular sections and assume a space-invariant PSF within each section. The PSF would be different from section to section. This solution seems to be the best unless a mathematical relationship between intensity and direction can be determined. In most cases, as we already mentioned in Section 2.2.2, the intensity is approximately the same in all directions, so that this cause of space-variance can usually be ignored.

The effect of the second reason is illustrated in Figure 2.4, where the focal spot and film planes are not parallel. It can be seen that the PSF has a different size and shape depending on the position of the pin-hole, even within the same layer. A mathematical formulation of the space-variant PSF can be derived from geometric considerations [22] as a function of the PSF at the origin.

If $h_i(x,y)$ is the PSF at the origin of the i^{th} layer, the PSF at an arbitrary position within the same layer can be expressed as follows [22] (see Figure 2.5):

$$h_{io}(x,y) = h_i(x+k_1 k_2 y \, , \, k_2 y) \tag{2.11}$$

where

$$k_1 = \tan\gamma = \frac{x_{io}\tan\alpha}{d_1+y_{io}\tan\alpha} \tag{2.12a}$$

$$k_2 = 1 + \tan\alpha \, \tan\beta = 1 + \frac{y_{io}\tan\alpha}{d_1} = \frac{d_1+y_{io}\tan\alpha}{d_1} \tag{2.12b}$$

The angle α of the focal spot is a constant that depends only on the system. The other parameter in the previous equations is d_1, the distance from the focal spot to the layer concerned.

Making a substitution of variables in (2.11) we obtain an expression in terms of coordinates rather than angles. The result is given in (2.13).

$$h(x,y;x_{io},y_{io}) \triangleq h_{io}(x,y) = h_i(x+kyx_{io} \, , \, y+kyy_{io}) \tag{2.13}$$

where $k=(\tan\alpha)/d_1$ is a constant which depends solely on the system and the layer concerned.

If the intensity also changes with direction and we denote this change by $I_{io}(x_{io},y_{io})$ we have the following result.

$$h(x,y;x_{io},y_{io}) = I_{io}(x_{io},y_{io}) \, h_i(x+kyx_{io} \, , \, y+kyy_{io}) \tag{2.14}$$

Here we have assumed that the shape of the PSF is the same everywhere, differing only in spatial and amplitude scalings. This implies that the rate of change of X-ray intensity with direction is the same everywhere in the focal spot. Without this assumption the only

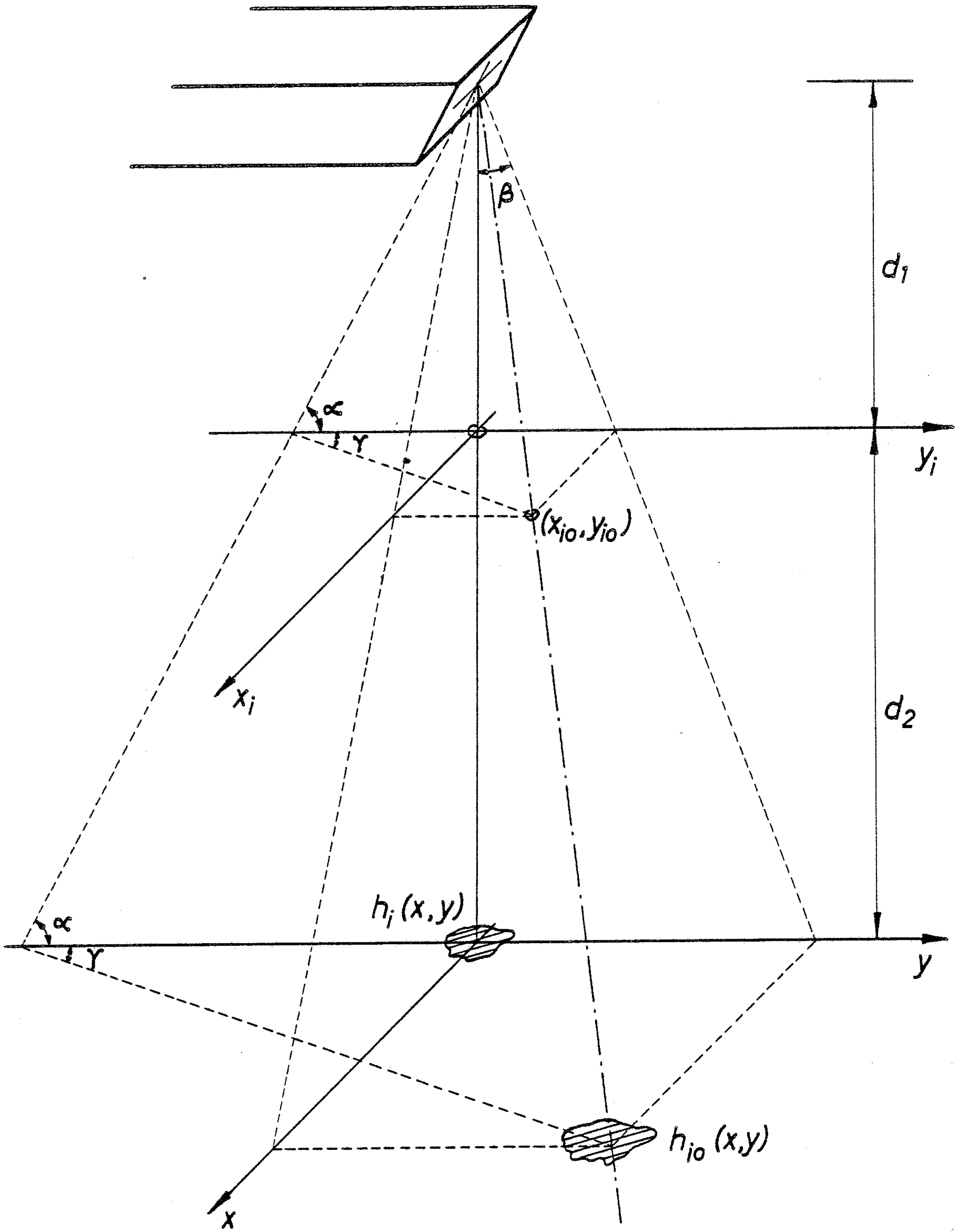

Figure 2.5. Point spread function formation in the space-variant model.

way to accurately characterize the system would be by measuring $h(x,y;x_{io},y_{io})$ everywhere, thus making the problem rather intractable†.

A solution was devised to convert the space-variant problem into a space-invariant one and the results are given in the next section.

2.4 Conversion of the Space-Variant Model into a Space-Invariant One

There is a simple way to correct for the space variability of the radiologic process in a digital computer. As shown in Figure 2.6 the radiologic image can be sampled uniformly and then a new image is calculated by interpolation. This new image is the one that would correspond to a plane parallel to the focal spot; therefore it has space-invariant properties. The new image can be calculated anywhere in the X-ray field. In order to minimize size distortions we have chosen the plane that, being parallel to the focal spot, passes through the intersection of the centre ray and the film plane. With this approach the reconstruction of the object is made on layers parallel to the focal spot. The information required for the conversion is the following: the angle of the focal spot, the focal spot to film distance, and the orientation of the film.

The relationships between the coordinates (x,y) over the film plane in the space-variant system and the coordinates $(\hat{x},\hat{y})$ over a plane parallel to the focal spot can easily derived by geometric considerations. Indeed, referring to Figure 2.7, since $\overset{\Delta}{FBO} \sim \overset{\Delta}{FAE}$ and $\overset{\Delta}{FOD} \sim \overset{\Delta}{FEC}$,

† We also derived an expression for (2.13) in polar coordinates and tried to use the Mellin transform to take care of the different scalings. The results are not reproduced here because there did not seem to be any apparent advantage in using polar coordinates.

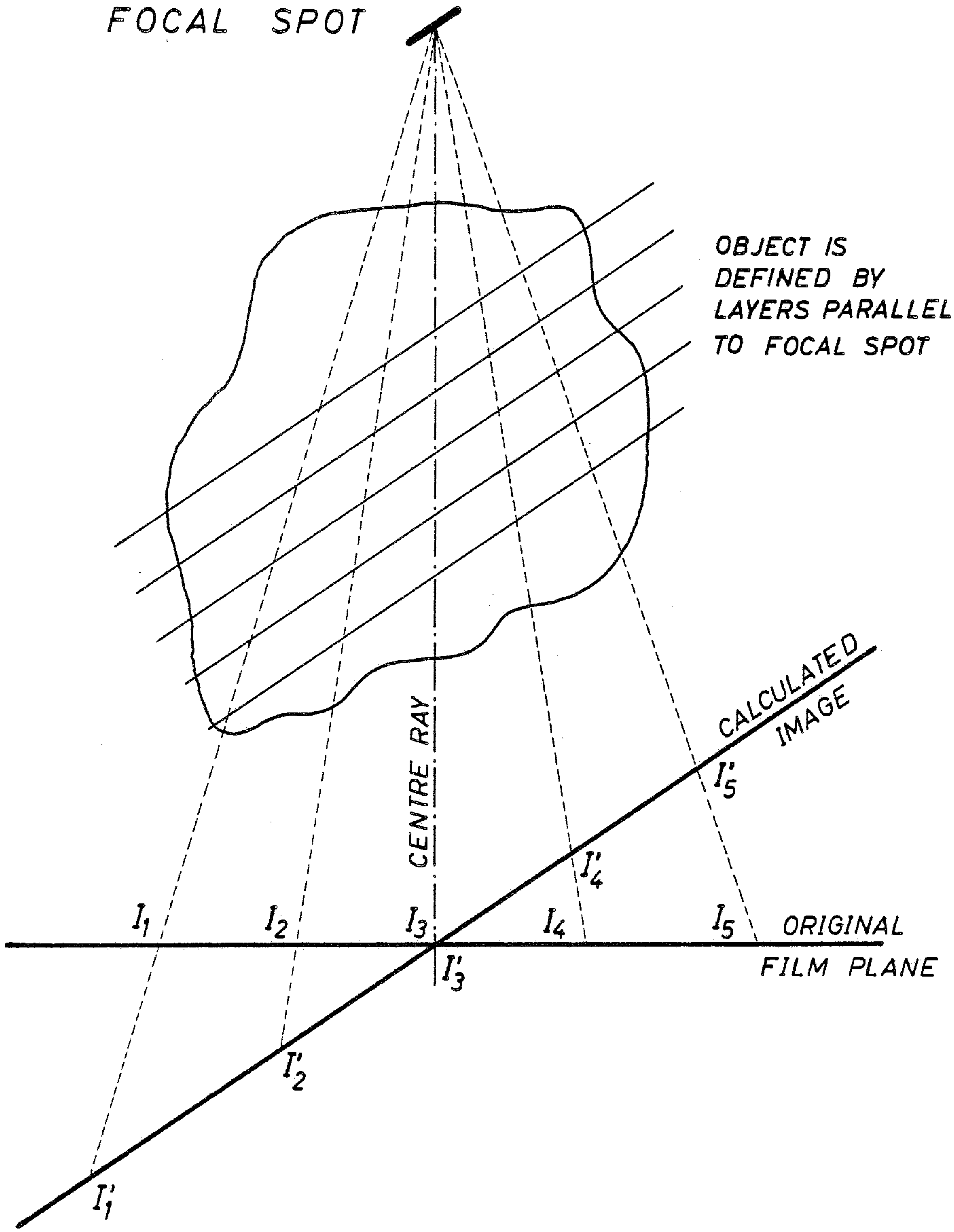

Figure 2.6. Conversion of the space-variant model into a space-invariant one.

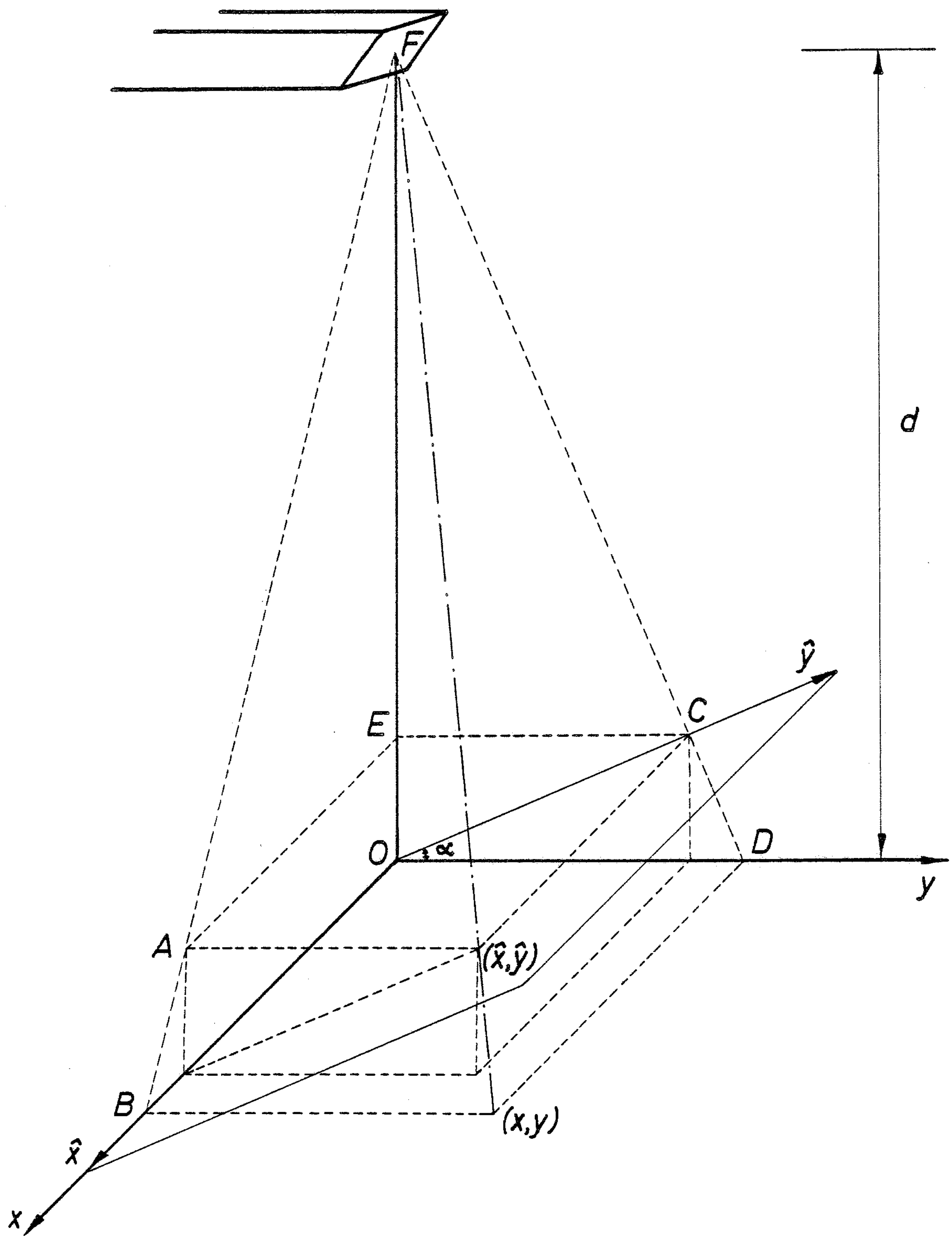

Figure 2.7. Relationship between the coordinates on the film plane in the space-variant model and in the equivalent space-invariant model.

we have:

$$\frac{\overline{FO}}{\overline{BO}} = \frac{\overline{FE}}{\overline{AE}} \; ; \qquad \frac{d}{x} = \frac{d-\hat{y}\ \sin\alpha}{\hat{x}} \; ; \qquad x = \frac{d\ \hat{x}}{d-\hat{y}\ \sin\alpha}$$

and

$$\frac{\overline{FO}}{\overline{OD}} = \frac{\overline{FE}}{\overline{EC}} \; ; \qquad \frac{d}{y} = \frac{d-\hat{y}\ \sin\alpha}{\hat{y}\ \cos\alpha} \; ; \qquad y = \frac{d\ \hat{y}\ \cos\alpha}{d-\hat{y}\ \sin\alpha}$$

Therefore, the intensity distribution $\hat{I}(\hat{x},\hat{y})$ of an equivalent space-invariant system can be expressed as a function of the intensity distribution $I(x,y)$ of the space-variant system as follows:

$$\hat{I}(\hat{x},\hat{y}) = I(x,y) = I\left(\frac{d\ \hat{x}}{d-\hat{y}\ \sin\alpha}\ ,\ \frac{d\ \cos\alpha\ \hat{y}}{d-\hat{y}\ \sin\alpha}\right) \qquad (2.15)$$

In a practical case (2.15) would be applied as follows: The radiograph is either sampled at non-uniform intervals as shown in (2.15) or a new set of samples is obtained by interpolating a uniformly sampled radiograph. This sampling rate should be sufficiently high so that the interpolating error is negligible. The new space-invariant intensity distribution $\hat{I}(\hat{x},\hat{y})$ is used and processed instead of $I(x,y)$ but taking into account the new geometry of the system, that is the focal spot to plane $\hat{x},\hat{y}$ distance.

It must be emphasized that this transformation gives a hypothetical image which does not really exist in the actual system but which results in a space-invariant system without loss of information. Indeed, if we wanted to calculate the true intensity in the actual system when the radiation crosses the plane $\hat{x},\hat{y}$ parallel to the focal spot, derived from the intensity distribution on the plane x,y, the inverse square law correction factor should be included to take into account the diverging nature of X-rays. However if we were to do that we would introduce another source of space variance due to the obliquity of the X-rays on impact over the plane $\hat{x},\hat{y}$ and therefore the resulting image would be distorted more than it would be corrected.

When the processed film area is small the transformation (2.15) may not be necessary because the variations of the impulse response within small areas is relatively small. A simple rule can be derived from (2.13) to determine the maximum percent variation V of the extent of the impulse response in the y-direction:

$$V = \frac{(y_2 - y_1)\sin\alpha}{d(\cos\alpha) + y_1\sin\alpha}\,100\%$$

where y_1 and y_2 are the ordinates of the film-area edges which are perpendicular to the y-axis. For example, if $\alpha = 70°$, d = 1000 mm, y_1= 50 mm and y_2= 100 mm, we obtain V = 12% only. On the other hand if we consider a larger area, say y_1= 50 mm and y_2= 300 mm, we obtain V = 60%; hence, in this case some correction would help.

Chapter III

A TOMOGRAPHIC FILTRATION PROCESS

3.1 Introduction

In this chapter we are going to establish the basis for the recovery of three-dimensional information from two-dimensional radiographs.

Rather than using special X-ray hardware in this approach, conventional radiographs will be processed using standard signal processing techniques. The utilization of conventional X-ray systems leads us to the use of the model developed in Chapter II.

When the object which can be visualized as a three-dimensional distribution of absorption coefficients is projected in a radiologic system, several types of transformations are introduced as discussed in the previous chapter. There is only one however which is depth dependent, namely the one due to the finite size of the focal spot. Indeed, if the source of X-rays were a perfect point source no depth information recovery would be possible at all from a single radiograph.

Making use of the depth-dependent focal-spot blur, our solution to the problem will be developed from two points of view; first, an analogy with standard tomographic techniques will be considered and second, a deblurring filtering process will be studied. Theoretical analyses in both the space and frequency domains will be used to evaluate the performance of the process. Finally, the effects of noise and the problem of determining the system transfer function in a practical application will be briefly considered. The implementation and practical evaluation of the process will be deferred to Chapter V.

3.2 Development of a Tomographic Filtration Process

3.2.1 Analogy with standard tomography

Standard tomographic techniques produce a tomogram by moving a point-like X-ray source and the recording film in a coupled manner, so that during the exposure the parts of the object lying in one specific plane parallel to the film plane are always projected on the same place on the film [1]. The X-ray shadows of the other parts of the object will move in relation to the film. Thus only a layer of a few millimeters of thickness in a predefined depth of the body is imaged sharply, whereas structures on both sides of this layer are blurred. The layer whose image is in focus is referred to as the plane of cut or tomographic layer. As shown in Figure 3.1, by moving the film from O_A to O_B in synchronism with the point source $I_o(x)$, which moves from A to B, we obtain the point O projected always on the same place.

A tomographic filtration process (TFP) must produce a focussing effect similar to that of standard tomography; but with no moving parts. In a TFP, instead of moving the X-ray tube, the finite size of the focal spot is used to advantage, and instead of moving the film, a filter is used to process a conventional radiograph. To see that a TFP is indeed analogous to a standard tomographic system in miniature, as far as the tomographic layer is concerned, consider the following model.

A focal spot is composed of a finite ordering of point sources. For example, the surface of a 300 micron square focal spot is composed of approximately $900 \cdot 10^8$ atoms of tungsten, each of which can act, if struck by an electron, as a true point source of X-rays [29]. Each

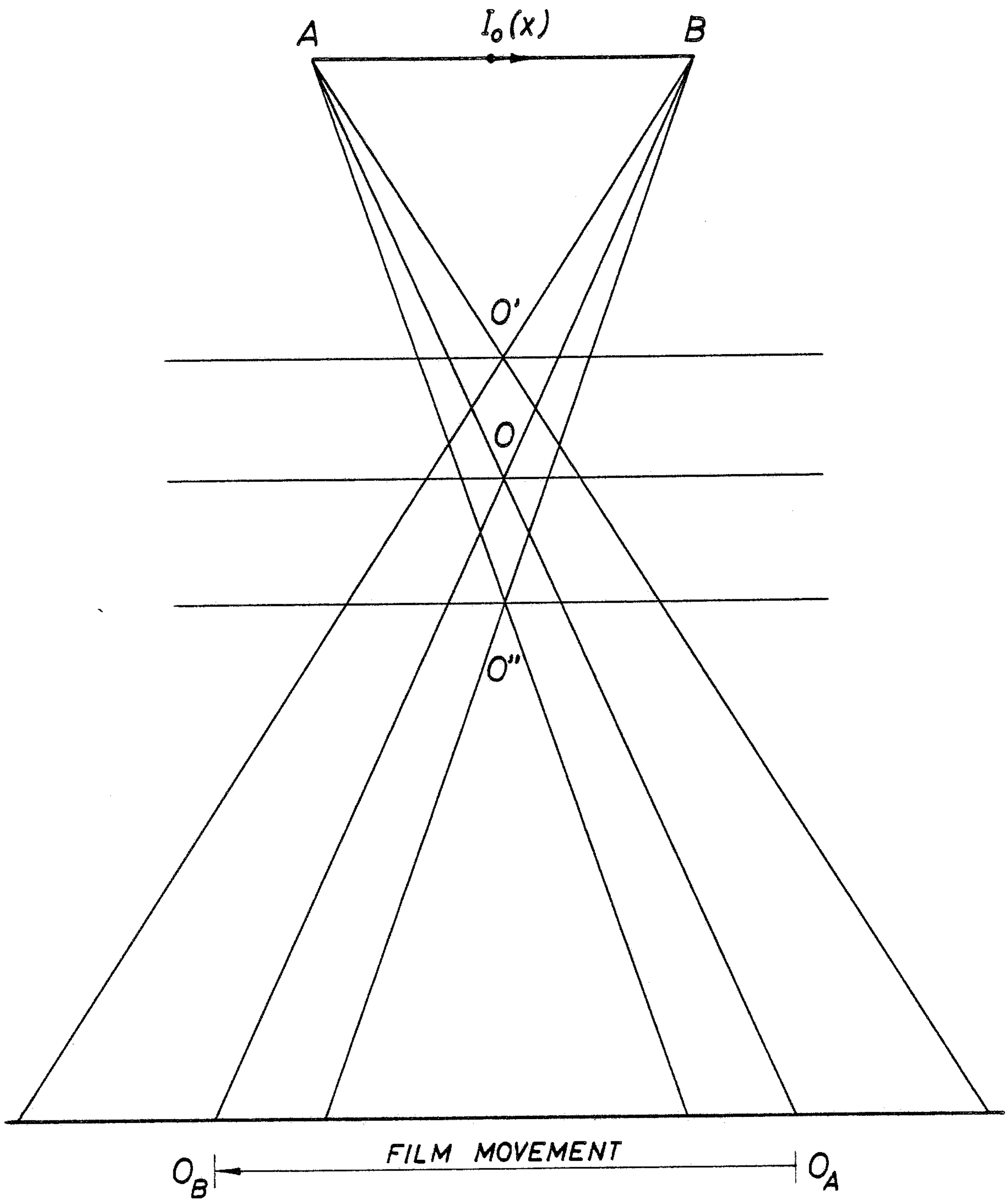

Figure 3.1. Simplified diagram of image formation in standard tomography.

emitting source produces its own image at a slightly different point in the image plane. The shadow from all these point sources add up to form the observed image; overlapping occurs throughout the entire image but will only be discernible at the edges where an intensity gradient is formed.

Since this system is linear we can apply superposition and make an equivalent focal spot by moving a true point source of X-rays all over a region which includes the real focal spot. In general the intensity of this ideal point source will change during its movement; because the X-ray intensity distribution over the focal spot is not uniform. With this model, (2.4) is still valid.

The movement of this point source is analogous to the movement of an X-ray tube in standard tomography. Since in conventional radiology the film does not move, the images of all the layers are blurred.

Therefore, in order to convert a radiograph into a tomogram we will pass the radiographic image through a filter that will produce on the image of the tomographic layer an effect equivalent to the motion of the film in standard tomography. Filters that produce a selective deblurring on a conventional radiograph will be referred to as tomographic filters. Mathematical details that clarify the analogy further are given in Appendix A.

The effect of overlaying layers is not the same in standard tomography as in the TFP. In standard tomography an intentional blur of the out of focus layers is produced, while the tomographic layer is kept in focus. On the other hand, in a conventional radiograph all the layers are blurred, although to a much lesser extent, and the tomographic filter deblurs the image of the tomographic layer.

3.2.2 Tomographic Filters

The mathematical characteristics of tomographic filters are derived here. The objective is to find a filter such that in cascade with the transfer function for the tomographic layer results in an overall transfer function equal to a constant for that layer. In Section 2.3 it was discussed how the contributions from the various layers to the total X-ray attenuation (that is, the X-ray image formation) can be approximated by an additive process. This is achieved by linearizing the exponential in (2.4), so that the effects of the various layers are separated and we can focus on a single layer at a time. With this linearization the problems of space-variance due to the object itself are also eliminated because the system is space-invariant when a single layer is considered (cf. Appendix A).

The overall transfer function for each of the overlaying layers should ideally be zero, however using a single radiograph this is not possible as it will be seen later. Due to these limitations in the system, the quality of the results will depend strongly on the characteristics of the object being exposed, such as the absorptions and spectra of the various layers, to be discussed in Chapter V.

In the following derivation of the transfer function of a tomographic filter we also assume that the PSF for the tomographic layer is known. The PSF for each layer of a three-dimensional object was derived in Section 2.3 as a function of the X-ray intensity distribution in the focal spot. The PSF's of different layers differ by a scaling factor only. Since the system is linearized, the image of a layer can be written as follows if the PSF is space-variant:

$$g(x,y) = \iint h(x,y;\alpha,\beta)\ f(\alpha,\beta)\ d\alpha\ d\beta \tag{3.1}$$

where $f(\alpha,\beta)$ is the two-dimensional distribution of attenuation factors in the layer, $h(x,y;\alpha,\beta)$ is the space-variant PSF of that layer, and $g(x,y)$ is the resultant image†. Since the object is three-dimensional, $g(x,y)$ represents the superposition of many layers; however we are interested in selecting one layer at a time only.

If the system is space-invariant or is converted into one by the technique of Section 2.4, then the integrals in (3.1) become convolution integrals.

$$\begin{aligned} g(x,y) &= \iint h(x-\alpha,y-\beta)\ f(\alpha,\beta)\ d\alpha\ d\beta \\ &= h(x,y) * f(x,y) \end{aligned} \tag{3.2}$$

Using the convolution property of the two-dimensional Fourier transform (see Table B.1), the convolution in (3.2) results in a product in the frequency domain.

$$G(f_x,f_y) = H(f_x,f_y) \cdot F(f_x,f_y) \tag{3.3}$$

To recover $F(f_x,f_y)$ from $G(f_x,f_y)$ the obvious technique is to inverse filter the radiologic image by multiplying $G(f_x,f_y)$ by $H^{-1}(f_x,f_y)$ as indicated in (3.4).

$$F(f_x,f_y) = \frac{G(f_x,f_y)}{H(f_x,f_y)} \tag{3.4}$$

---

† Unless otherwise specified the limits of integration are always from $-\infty$ to ∞.

The filtered image can then be obtained by finding the inverse two-dimensional Fourier transform of $F(f_x,f_y)$. Unfortunately $H(f_x,f_y)$ may have zeros and $G(f_x,f_y)$ is usually corrupted by noise. Thus the filtered image will include a large amount of noise at spatial frequencies in the neighborhood of a zero of $H(f_x,f_y)$. Nevertheless, in many cases of interest these zeros are located at frequencies which are higher than those where the relevant physiological information is contained. In these cases it is sufficient to restore up to the first zero and reject the band of higher frequencies.

When it is necessary to restore frequency bands with zeros in the transfer function, the modifications suggested in the literature to counteract the drawbacks of ideal inverse filtering are all *ad hoc* and intuitive [52]. Before we describe our method some of the alternatives available are reviewed briefly.

One of the earliest techniques that we have found in the literature to improve the results of inverse filtering for image processing was Harris' suggestion [52],[91],[92] of multiplying (3.3) by a function $H_o(f_x,f_y)$ before dividing by $H(f_x,f_y)$. Thus

$$\tilde{F}(f_x,f_y) = \frac{G(f_x,f_y)H_o(f_x,f_y)}{H(f_x,f_y)} + \frac{N(f_x,f_y)H_o(f_x,f_y)}{H(f_x,f_y)}$$

where the noise component $N(f_x,f_y)$ which corrupts $G(f_x,f_y)$ is explicitly shown in this equation. By choosing H_o to be zero over the region of the f_x,f_y plane where G is dominated by N we can reduce high-frequency noise. By choosing H_o/H to be finite wherever H is zero the problem with infinities can be eliminated. The price paid is that $\tilde{F}$ is no longer a noisy version of F but a noisy version of F blurred through the filter H_o. The requirements imposed on H_o are intuitively reasonable. However, there is a noncountable infinity of functions that satisfy these requirements and we must arbitrarily choose one [52].

Slepian [93],[94] notes that some *ad hoc* scheme for assigning a finite value at the pole positions of the inverse filter must be made and that just what these modified filters do to picture quality is not easy to analyze. He assumes that the image is of finite extent and considers a filter which restores correctly over the inverval spanned by the smeared image and gives an arbitrary output elsewhere (zero on one side and uninterpretable values on the other side).

Cutrona and Hall [95] exploit the same degree of freedom as Slepian but in a different manner and they arrive at a slight generalization of Slepian's results. They compare three classes of filters. The first class is basically inverse filtering attempting perfect reconstruction in the interval of the image and zero elsewhere. The second filter is similar but produces a nonzero output beyond the image interval (this essentially is Slepian's filter). The third class of filters correct the original blurring but giving a smeared version of the output of the second filter with smearing length set by the resolution required.

Brown *et al.* [96] have investigated replacing the inverse function beyond a certain frequency, say 1 cycle/inch, by a roll-off function. They have tested the Dolph-Chebyshev function. By "cutting-off" the filter function gradually instead of abruptly the ripples in the filtered image are reduced.

Dance *et al.* [97] have investigated three modifications of the ideal inverse function, each corresponding to deconvolution for values of the inverse filter magnitude response lower than a certain limit but being modified for values greater than that limit. The first method set terms above that limit to zero, the second gave terms above the limit a constant value but retained the phase, and the third was a compromise between the first two and made the inverse filter proportional to the transfer function of the degradation to correct.

It is interesting to note that all these techniques are quite similar and that no comparative assessment is available, but only subjective estimates in specific cases. Consequently, since our goal is not the determination of the best method of inverse filtering but to test the feasibility of tomographic filtering, we propose a simple technique which provides a means for hard-limiting the magnitude response of the inverse filter and cutting off the high frequencies dominated by noise. Both the hard-limit and cutoff frequency can be specified by the user. The astute reader will note its similarity to the techniques previously reviewed.

Suppose that $H = a + j\,b$ is the system transfer function for the tomographic layer. H, a, and b are functions of the spatial frequency (f_x, f_y) and j is the imaginary operator.

The magnitude response of the inverse filter is

$$\left| \frac{1}{H} \right| = \frac{1}{\sqrt{a^2 + b^2}} \tag{3.5}$$

and the phase response

$$\measuredangle \frac{1}{H} = \arctan \frac{-b}{a} \tag{3.6}$$

The transfer function of the inverse filter with hard-limited magnitude response is expressed as:

$$H^{-1} = c + j\,d \tag{3.7}$$

with the constraint

$$\sqrt{c^2 + d^2} \le h_\ell \tag{3.8}$$

where h_ℓ is the hard limit imposed on the magnitude response and c and d are given by

$$c = \frac{a}{a^2 + b^2} \quad \text{and} \quad d = \frac{-b}{a^2 + b^2} \quad \text{for} \quad \frac{1}{\sqrt{a^2 + b^2}} \le h_\ell \tag{3.9a}$$

$$c = \frac{a\,h_\ell}{\sqrt{a^2 + b^2}} \quad \text{and} \quad d = \frac{-b\,h_\ell}{\sqrt{a^2 + b^2}} \quad \text{for} \quad \frac{1}{\sqrt{a^2 + b^2}} > h_\ell \tag{3.9b}$$

$$c = h_\ell \quad \text{and} \quad d = 0 \quad \text{for} \quad a^2 + b^2 = 0 \tag{3.9c}$$

Equations (3.9) are consistent with (3.6) and (3.8); that is the phase response is preserved and the dynamic range of the magnitude response can be controlled with the parameter h_ℓ to prevent noise amplification and/or overflow of computer registers. In a digital computer all these operations are straightforward and we have coded them in the routine INVFHL, given in Appendix C. Examples of applications are given in Chapter V. It should be noted that under the transformations (3.9) a real PSF remains real, and an even PSF remains even.

In many cases it is convenient to assume a Gaussian shape for the system transfer function as pointed out in Section 2.2.2. The magnitude response of the tomographic filter then becomes an inverse Gaussian curve, which is readily implemented in a digital computer.

Since the system transfer function usually has a low-pass characteristic, the inverse filter has a high-pass characteristic. Therefore it is convenient to cascade the inverse filter with a low-pass filter to reduce the noise at high frequencies where the gain of the inverse filter is greatest. The choice of the cutoff frequency of the low-pass filter is a trade-off between the desired resolution and noise.

More sophisticated methods for overcoming the problems of inverse filtering will be considered in Section 3.4. In the next section we study the effectiveness of tomographic filters at different object depths.

3.3 Theoretical Evaluation of Tomographic Filters

A tomographic filter deblurs the image of the tomographic layer while leaving the images of all other layers blurred. After filtering the radiograph, the characteristics and extent of the blur on the image of each layer depends on the distance from that layer to the tomographic layer and the distance from the tomographic layer to the focal spot and to the film plane. In both the space-domain and frequency-domain analyses a one-dimensional model is considered for simplicity. The extension to two dimensions is straightforward.

3.3.1 Space-Domain Analysis

Suppose that the tomographic layer is at a distance d_1 from the focal spot and at a distance d_2 from the film plane. If O is a point on the tomographic layer, its image on the film extends over a distance U as shown in Figure 3.2. This blur U is the one that we want to eliminate. Here we define blur as the extent of the image of a point or edge due to the finite size of the focal spot. All other blurs corresponding to other layers, such as the blur V of the point X and the

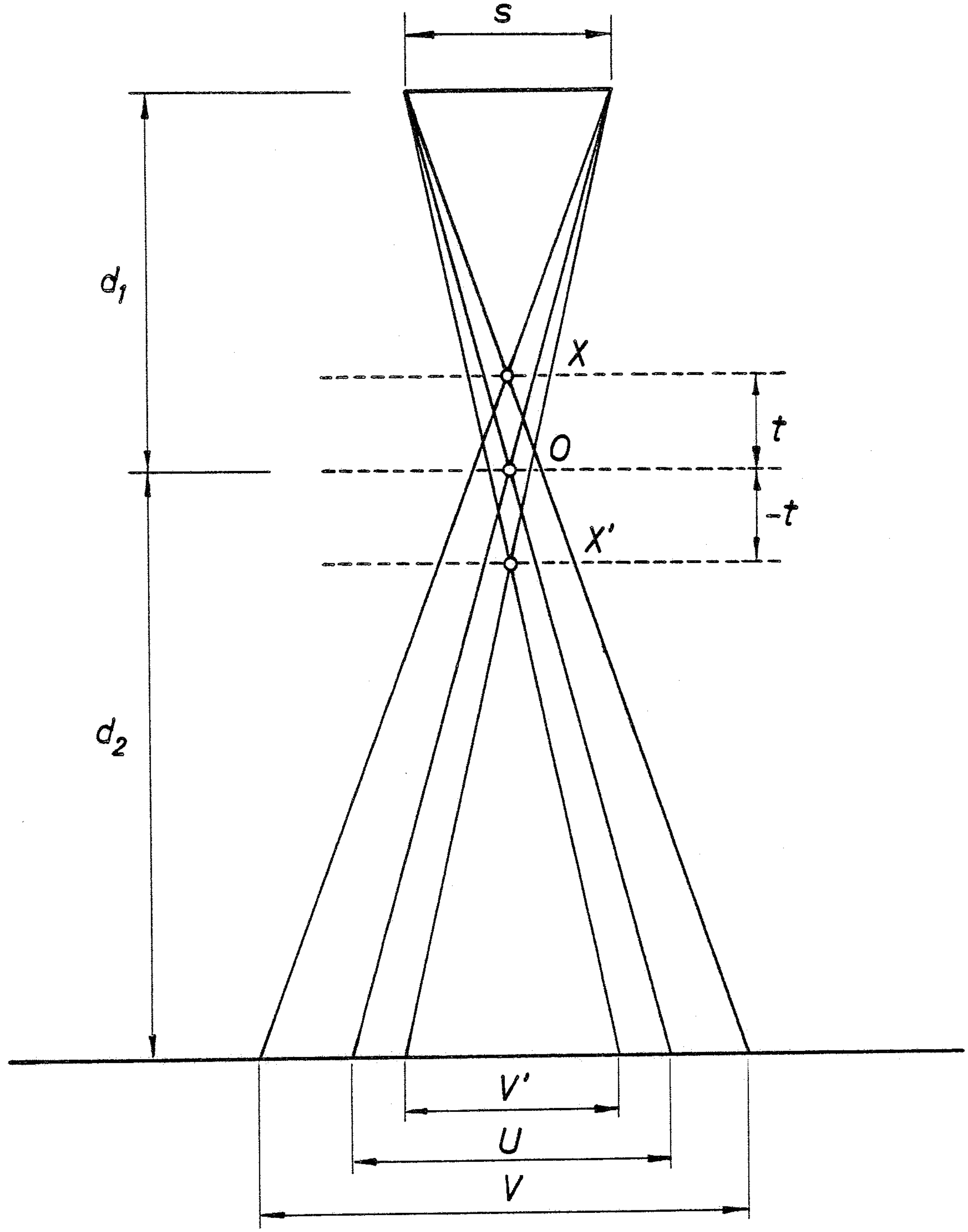

Figure 3.2. Blur formation in the radiologic process.

blur V' of the point X', differ in size and therefore cannot be eliminated simultaneously. An indication of the differential blur that will remain after processing can be expressed as

$$|V-U| = \left| s\cdot\frac{d_2+t}{d_1-t} - s\cdot\frac{d_2}{d_1} \right| = s\left| \frac{(d_1+d_2)\ t}{(d_1-t)\ d_1} \right| \tag{3.10}$$

where s is the size of the focal spot and t is the distance from a layer to the tomographic layer. We see that the tomographic blur $|V-U|$ is proportional to the size of the focal spot. Since a typical size for the focal spot is of the order of 2 mm. while the movement of an X-ray source in standard tomography is of the order of 500 mm. we infer that the results of a TFP cannot be as good as those of standard tomography. Nevertheless, the purpose of a TFP is to improve a radiograph with respect to three-dimensional information and not to produce a complete and accurate three-dimensional reconstruction for which better techniques exist [2], [3]. These facts will be demonstrated experimentally in Chapter V.

Equation (3.10) is shown as an indication only and does not include the shape of the X-ray intensity distribution. A better space-domain characterization is provided by the overall impulse response of the TFP.

Suppose a focal spot with a Gaussian X-ray intensity distribution, namely

$$I_o(x) = e^{-\sigma x^2}$$

If the focal spot to film distance is d, the PSF for a layer (the tomographic layer in this analysis) at a distance d_1 from the focal spot and d_2 from the film is

$$h_T(x) = \exp\left\{ -\sigma \left(\frac{d_1}{d_2}\right)^2 x^2 \right\}$$

and the PSF for another layer at a distance t from the tomographic layer, positive on the focal spot side and negative on the film side, is

$$h(x) = \exp\left\{ -\sigma \left(\frac{d_1-t}{d_2+t}\right)^2 x^2 \right\}$$

The Fourier transforms (cf. Appendix B) of these two PSF's are, respectively:

$$H_T(f) = \sqrt{\frac{\pi}{\sigma}}\ \frac{d_2}{d_1}\ \exp\left\{ -\ \frac{\pi^2}{\sigma}\ \left(\frac{d_2}{d_1}\right)^2 f^2 \right\}$$

and

$$H(f) = \sqrt{\frac{\pi}{\sigma}}\ \frac{d_2+t}{d_1-t}\ \exp\left\{ -\ \frac{\pi^2}{\sigma}\ \left(\frac{d_2+t}{d_1-t}\right)^2 f^2 \right\}$$

Thus, if the transfer function of the tomographic filter is $H_T^{-1}(f)$, the overall transfer function for the other layer is

$$H(f)\ H_T^{-1}(f) = \frac{d_2+t}{d_1-t}\ \frac{d_1}{d_2}\ \exp\left\{ -\ \frac{\pi^2}{\sigma} \left[\left(\frac{d_2+t}{d_1-t}\right)^2 - \left(\frac{d_2}{d_1}\right)^2 \right] f^2 \right\}$$

For t=0 this transfer function is identically equal to one, as expected. The IDFT (cf. Appendix B) was used to determine the corresponding overall impulse responses for $\sigma=2$, d=1000 mm., d_1=500 mm., $-1 < f < 1$ cycles/mm., sampling interval=1/128 cycles/mm., and several values of t (in mm.) as indicated with the plots in Figure 3.3. The overall impulse response for the tomographic layer is obviously an impulse and is not shown. It is readily seen in Figure 3.3 (a)-(d) that between the plane of cut and the focal spot the impulse response is a Gaussian function whose size increases when the distance to the plane of cut increases. On the other hand between the plane of cut and the film, see Figure 3.3 (e)-(h), the impulse response contains sidelobes which increase with the distance to the tomographic layer. In general, the wider the impulse responses and the greater the sidelobes, the better the contrast between the tomographic layer and the overlaying layers. However, the ripples in the impulse responses for the layers on the film side may introduce artifacts which might mask structures in the other layers.

The reason for the distinctive nature of the impulses responses on each side of the tomographic layer is very simple. On the focal spot side ($t > 0$) the transfer function is a Gaussian function whose inverse transform is another Gaussian function, Figure 3.3 (a)-(d). On the film side ($t < 0$), however, the transfer function is an inverse Gaussian function which does not have an inverse transform. It is necessary to truncate this ideal transfer function with a frequency-domain window (that is, a low-pass filter) which introduces the ripples in the space-domain, Figure 3.3 (e)-(h). We have used here a rectangular window (that is, an ideal low-pass filter) with a passband from -1 to 1 cycles/mm.

The analysis presented here could also be applied to investigate the effect of a time or space scaling error in any inverse filtering problem.

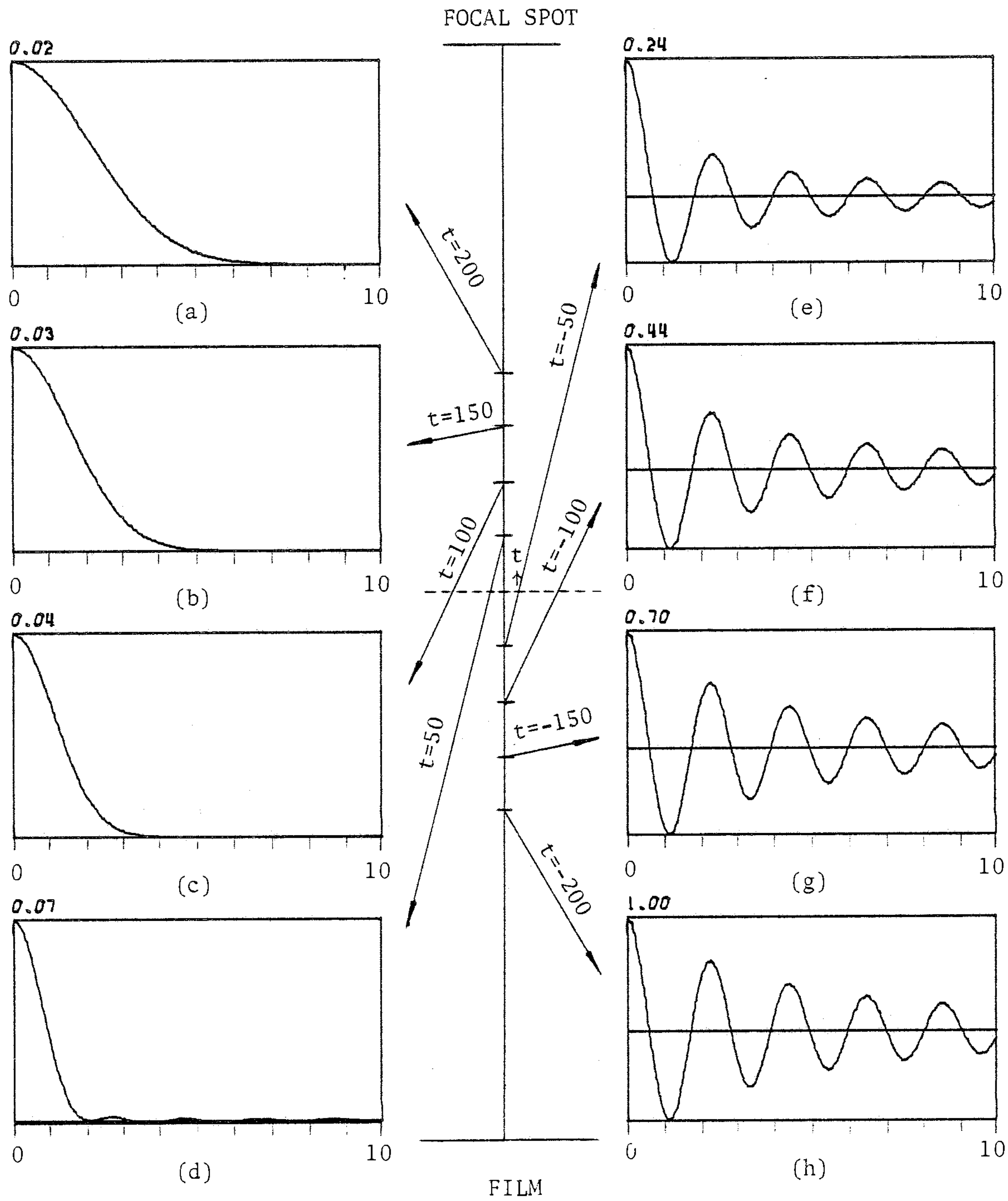

The focal spot to film distance is 1000 mm. (all distances are in mm.)

The tomographic layer (t=0) is at 500 mm. from the film.

Figure 3.3. (a)-(h) Overall impulse responses with a Gaussian focal spot.

3.3.2 Frequency-Domain Analysis

Ideally a tomographic filter should have a frequency response such that in combination with the transfer function of the radiologic system, the resulting overall transfer function would be equal to a constant for the tomographic layer and equal to zero everywhere else. In practice, the second condition cannot be met, not even closely. It is the purpose of this analysis to investigate the overall frequency response at different depths.

The overall transfer function for a particular layer is equal to H/H_t, where H and H_t represent the system transfer functions for that layer and the tomographic layer, respectively. In this example we assume that an ideal inverse filter is used. Evidently, for the tomographic layer, $H/H_t \equiv 1$. The form of H/H_t for other layers is shown in Figure 3.4, for a focal spot with uniform intensity distribution. In Figure 3.5 we show an enlargement of the low-frequency band. Transfer functions for layers on both sides of the plane of cut are shown together for comparison. It is clear that the tomographic filter acts as a low-pass filter for layers between the plane of cut and the focal spot, and as a high-pass filter for layers between the plane of cut and the film.

To fully understand the effects of the process on different layers we must also consider the characteristics of the spectrum of the projected object. Since different layers suffer different magnifications during exposure, the corresponding two-dimensional Fourier transforms of their shadow images are scaled accordingly (see Table B.1). Assuming that each layer has approximately the same spectrum, the relative scalings due to magnification are shown in Figure 3.6.

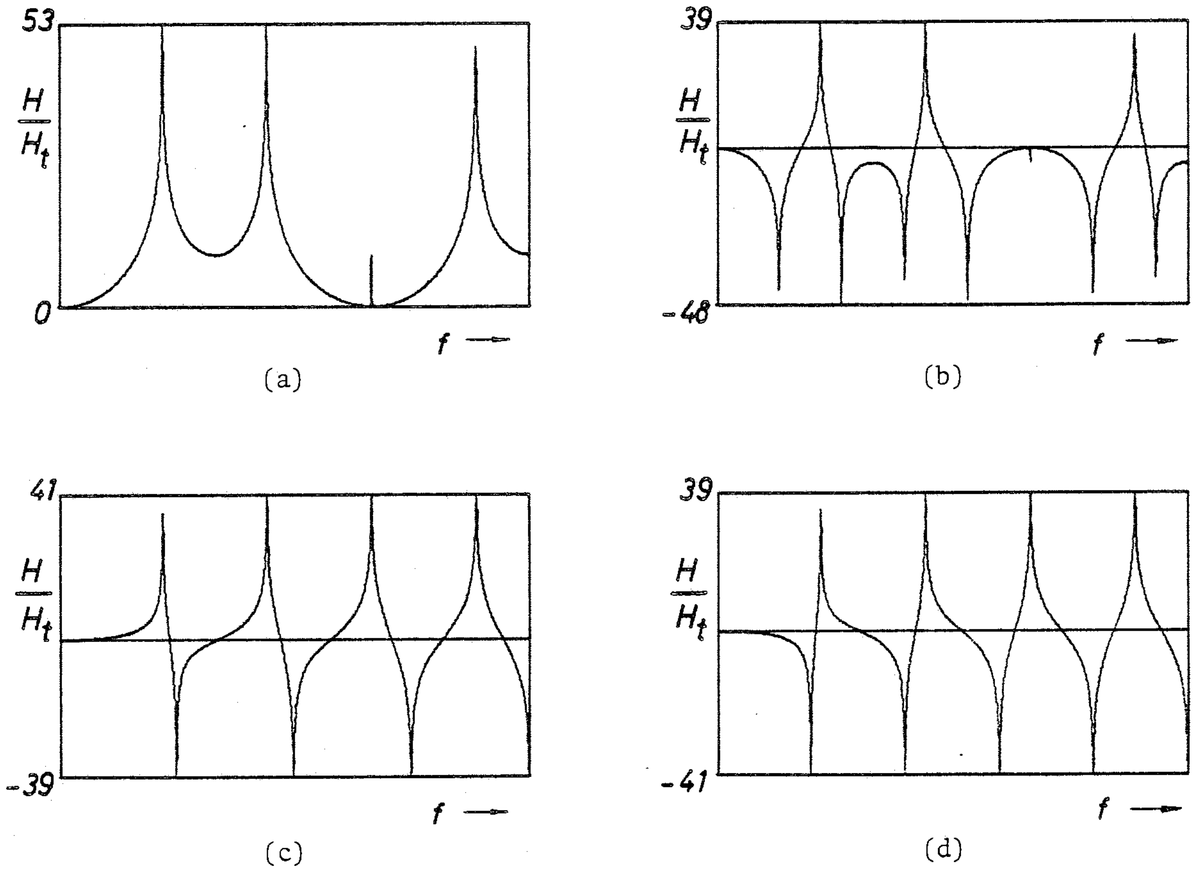

Figure 3.4. Overall frequency response (in dB) of the TFP for several layers. Layers far away from the plane of cut: (a) film side, (b) focal spot side. Layers close to the plane of cut: (c) film side, (d) focal spot side.

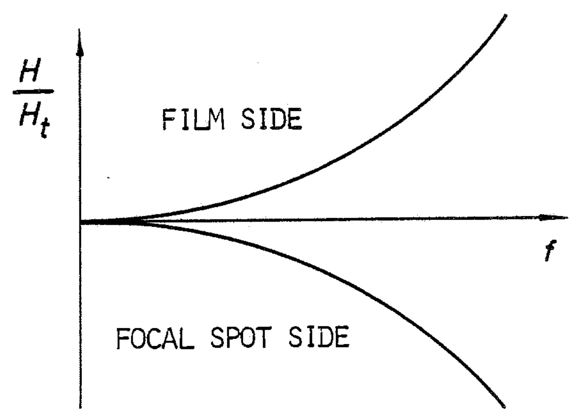

Figure 3.5. Comparison of the overall frequency responses in the low-frequency region for layers on both sides of the plane of cut.

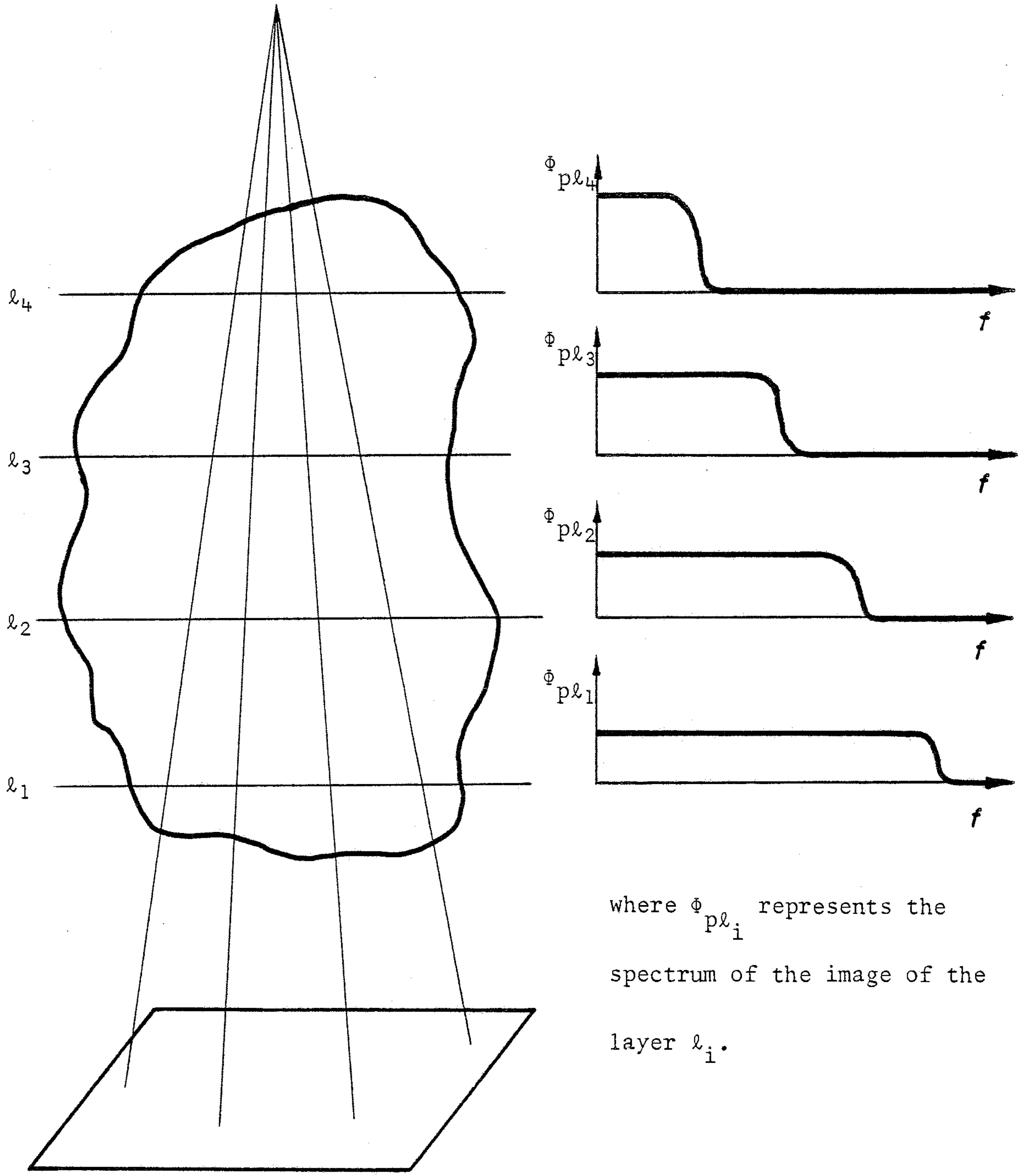

where $\Phi_{p\ell_i}$ represents the spectrum of the image of the layer ℓ_i.

Figure 3.6. Scaling of the spectra of the images of different layers.

These different scalings of the shadow images of the layers in the object is what makes the processing of radiographs interesting. For example, in Section 3.2.2 it is recommended to cascade the inverse filter with a low-pass filter to reduce the noise at high-frequencies. If the cutoff frequency of this filter is within the range of frequencies of interest in the image, it will have a greater effect on the layers closer to the film, which may result in an enhancement of the images of the layers closer to the focal spot.

The previous analyses will help in the interpretations of the experiments in Chapter V, where these issues will be further discussed.

3.4 Effects of Noise

The different sources of noise in the radiologic process were discussed briefly in Section 2.2. The inverse filtering techniques discussed previously do not take into account noise quantitatively. The presence of noise limits the resolution of the restoration. Since some sources of noise are additive and others multiplicative, they are better treated separately. Cole [49] has suggested a method where the multiplicative noise is removed first with a "denoising system" in the density domain followed by a deblurring system which also takes care of the additive noise in the intensity domain.

The presence of noise is handled differently by various filter structures which differ in the fidelity criterion on which the restoration is based. The existing filter structures [8], [37], [49]-[51], most closely related to inverse filtering can be represented by (3.11).

$$H_g(f_x,f_y) = \left(\frac{1}{H(f_x,f_y)}\right)^a \left(\frac{H(f_x,f_y)}{|H(f_x,f_y)|^2 + \gamma C(f_x,f_y)}\right)^{1-a} \qquad (3.11)$$

Table 3.1. Parameters for a family of restoration filters.

Type of filter	a	$C(f_x,f_y)$	γ
Ideal inverse	1	-	-
Wiener	0	$\Phi_R(f_x,f_y)$	1
Constrained least-squares	0	$C\,(f_x,f_y)$	γ
Geometrical mean	a	$\Phi_R(f_x,f_y)$	1
Homomorphic	1/2	$\Phi_R(f_x,f_y)$	1

a	aggressiveness
$\Phi_R(f_x,f_y)$	ratio of the power spectrum of the noise and the power spectrum of the image.
γ	constant

where the values of a, $C(f_x,f_y)$, and γ for different filters are summarized in Table 3.1. For $\gamma=1$, (3.11) constitutes a family of filters with parameter "a" that Cole [49] defines as the "aggressiveness" of the filter.

Thus, the inverse filter is the most aggressive filter and the Wiener filter is the least aggressive filter. The performance of all these filters in the presence of noise has been compared [49], [50], and homomorphic filters produced the restorations with the best visual quality. From (3.11) and Table 3.1 it is seen that the homomorphic filter is the geometric mean between the Wiener filter and the ideal inverse filter. The homomorphic filter is also referred to as the power spectrum equalization filter because it constrains $|H_g(f_x,f_y)|$ such that the power spectrum of the restored image is equal to that of the original, undegraded image.

Many other restoration techniques have been devised. In particular, some good results have been obtained with nonlinear iterative techniques [10] and numerical analysis techniques [51]; however their implementation is slow and presents some data management problems.

Human visual system considerations on the restoration criteria

One of the important processing limitations of the human visual system is its inability to deconvolve images [52]. The restoration of images attempts to solve this problem by producing an estimate of an original image, using all the available *a priori* information about the degradations that the original image has suffered. The lack of total knowledge of the fidelity criteria of the human visual system leaves the criteria by which the goodness of the estimate is to be judged, unspecified. For this reason it is not clear what is the optimum trade-off between resolution and noise.

Stockham [53] has reviewed a specific relationship between some of the current knowledge and thought concerning human vision and the problem of controlling subjective distortion in processed images.

A peculiar characteristic of the human visual process, usually forgotten, is its memory. Indeed, the effect of an image on a human observer depends strongly on his experience in visual interpretation and conclusions from previous views which are stored in the brain. This fact makes the visual fidelity criteria totally variable in space and time; although there are many evident constraints. The variability in space refers to the subjective differences from one human observer to another and the variability in time refers to the life of each human observer. Thus, for example, the reaction to processed radiographs by a radiologist, well-trained with conventional radiographs, may be unfavourable.

To conclude this section, we summarize some well known rudimentary facts on human vision:

1) The human observer is more sensitive to some spatial frequencies than others.

2) The human observer is more sensitive to intensity errors in grey areas than in white areas.

3) The mean square error criterion is in very poor accord with subjective evaluation.

4) The human visual system is not linear; although it seems that after an initial nonlinear transformation, the remainder of the visual system may be considered linear over a moderate range of intensities.

5) The number of grey levels discernible by the human eye is about 20; or even less if the signal-to-noise ratio is small.

3.5 Determination of the System Transfer Function

In Chapter II the PSF of each layer was derived as a function of the X-ray intensity distribution in the focal spot. Many techniques have been developed for accurate focal spot measurements for quality control purposes [22]-[29], [54]. Unfortunately, most of these techniques are slow, cumbersome, and difficult to apply. Furthermore, the characteristics of focal spots may change with time, exposure conditions tube voltage and current, etc.; so that if they had to be measured every time a new radiograph is taken, restorations would be totally impractical. An intermediate solution may consist of using as much *a priori* information as possible from occasional pin-hole images of the focal spot and supplementing that data with information derived directly from the radiograph itself whenever necessary. Indeed, in most cases of image restoration, sufficient information exists in a blurred image to attempt "blind deconvolution" [49], [55]. The magnitude characteristics of the degradation can be estimated without any *a priori* knowledge [49]. The phase characteristics are much more difficult to estimate and an assumption about the possible types of blur is necessary [55], [56].

These blur estimation techniques assume that the image can be represented as a random field with the properties of stationarity and ergodicity; and also, that the blurring process is space-invariant. If these conditions are not met then estimation is not possible. In addition, it is necessary to know the power spectrum of a prototype unblurred image.

To our knowledge, nobody has applied these blur estimation techniques to the restoration of radiographs yet. The apparent problem is that in the radiologic process there are many blurs of different sizes involved, one for each layer. Application of purely "blind deconvolution" techniques to radiographs does not seem possible at present. Nevertheless, with some *a priori* knowledge of the focal-spot characteristics they may be used to advantage to estimate some varying parameters (refer to example in Appendix A, Section A.7).

Some analytical and graphical examples of typical PSF's and their MTF's are shown:

1) Uniform rectangular shape (separable)

$$h(x,y) = \begin{cases} 1.0 & -A \le x \le A \quad \text{and} \quad -B \le y \le B \\ 0.0 & \text{otherwise} \end{cases} \tag{3.12}$$

2) Uniform circular shape

$$h(x,y) = \begin{cases} 1.0 & \sqrt{x^2+y^2} \le R \\ 0.0 & \text{otherwise} \end{cases} \tag{3.13}$$

3) Gaussian (separable)

$$h(x,y) = \exp\{-\sigma_1 x^2 - \sigma_2 y^2\} \tag{3.14}$$

4) Double-peaked Gaussian

$$h(x,y) = \exp\{-\sigma_1 (x-x_0)^2 + \sigma_2 y^2\} + c \exp\{-\sigma_3 (x+x_0)^2 + \sigma_4 y^2\} \tag{3.15}$$

Perspective plots of these functions and their MTF's (in dB) are shown in Figures 3.7 to 3.10, respectively. The Gaussian and double-peaked Gaussian X-ray intensity distributions are more realistic than the uniform ones.

Actual PSF's were obtained using the pin-hole method and the X-ray equipment of the Radiological Research Laboratories, University of Toronto. Contour and perspective plots of these PSF's and their squared MTF's are shown in Figures 3.11 and 3.12. The nominal sizes of the two focal spots involved are 1 mm. and 2 mm. The X-ray film was

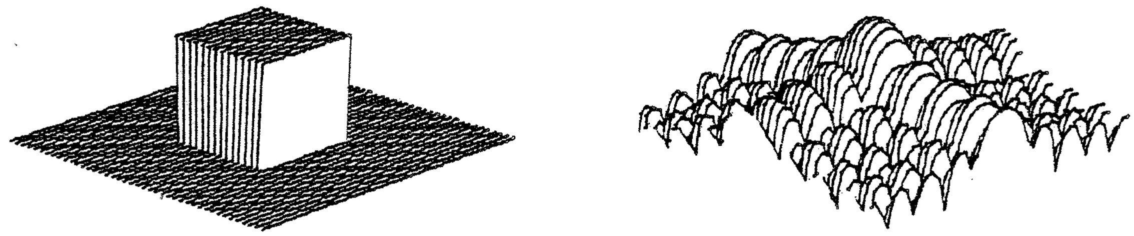

(a) (b)

Figure 3.7. Example of a uniform-square focal spot. (a) PSF. (b) MTF (in dB).

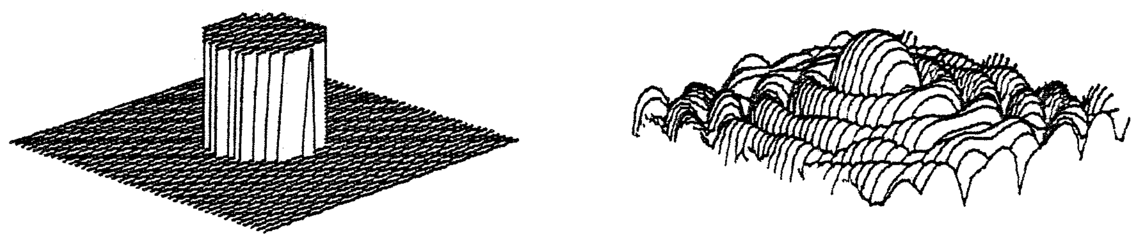

(a) (b)

Figure 3.8. Example of a uniform-circular focal spot. (a) PSF. (b) MTF (in dB).

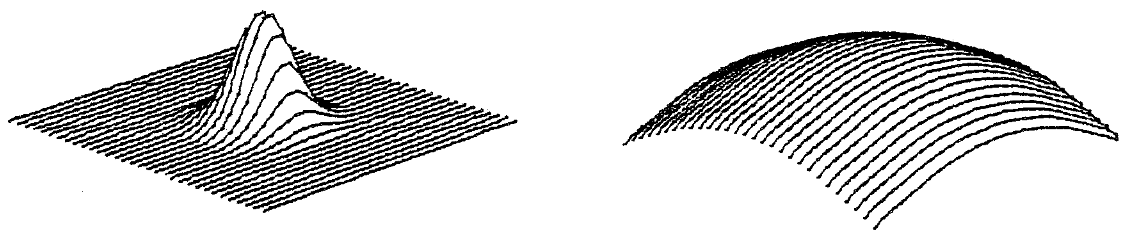

(a) (b)

Figure 3.9. Example of a Gaussian focal spot. (a) PSF (b) MTF (in dB).

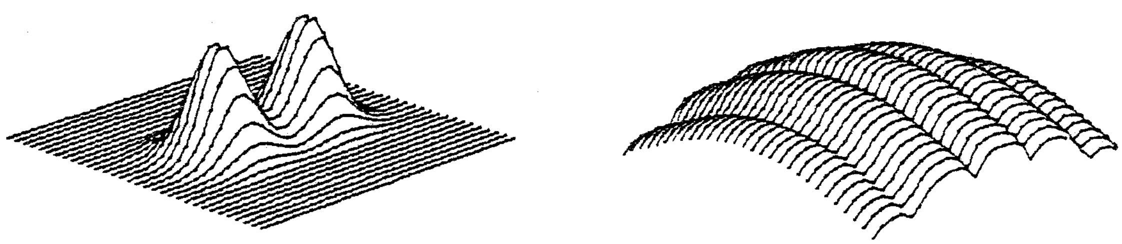

(a) (b)

Figure 3.10. Example of a twin-peaked Gaussian focal spot. (a) PSF. (b) MTF (in dB).

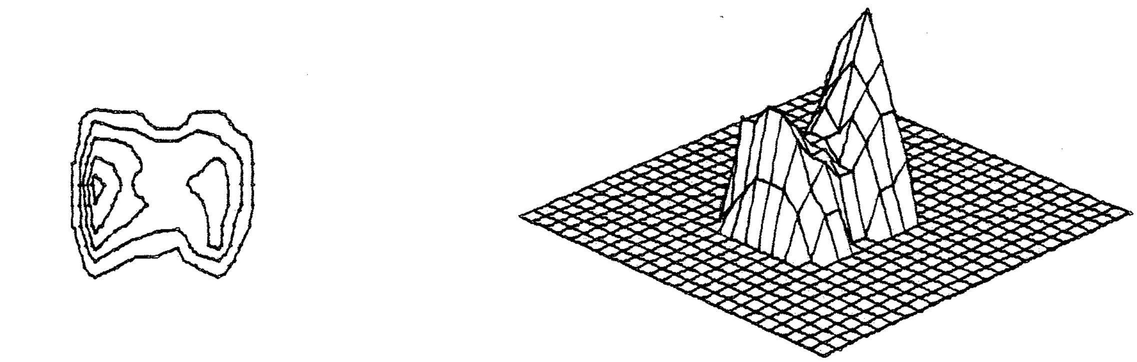

(a)

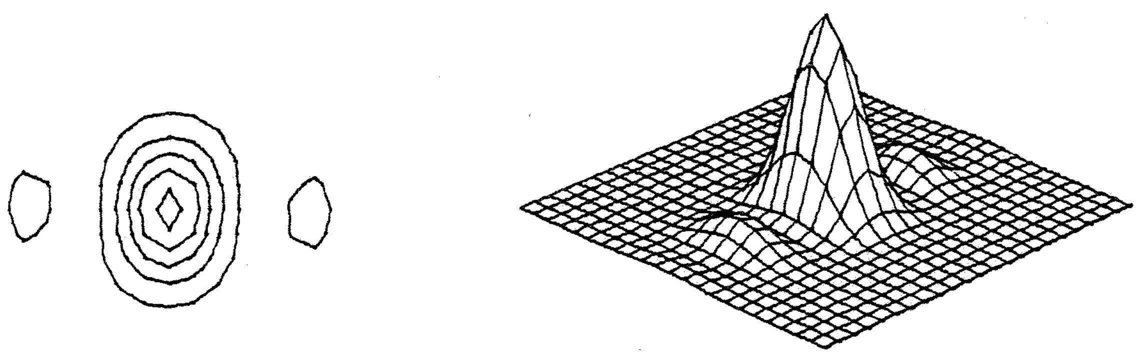

(b)

Figure 3.11. Actual focal spot of 1 mm. nominal size. (a) PSF. (b) Squared MTF.

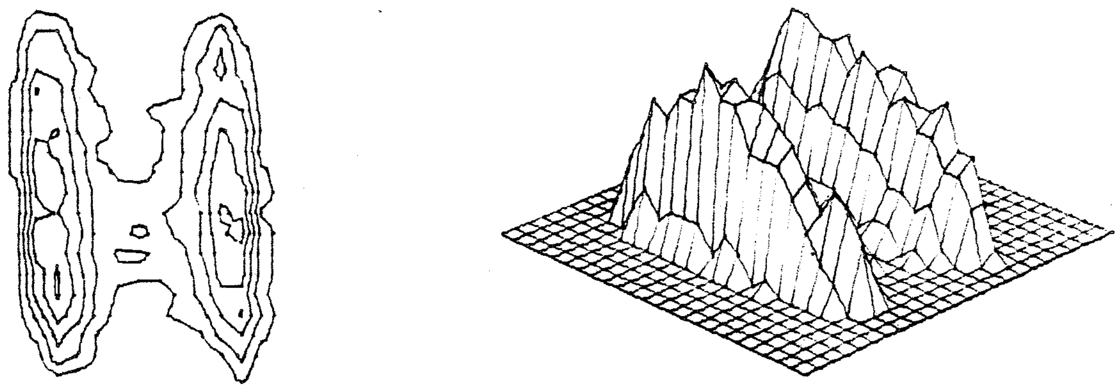

(a)

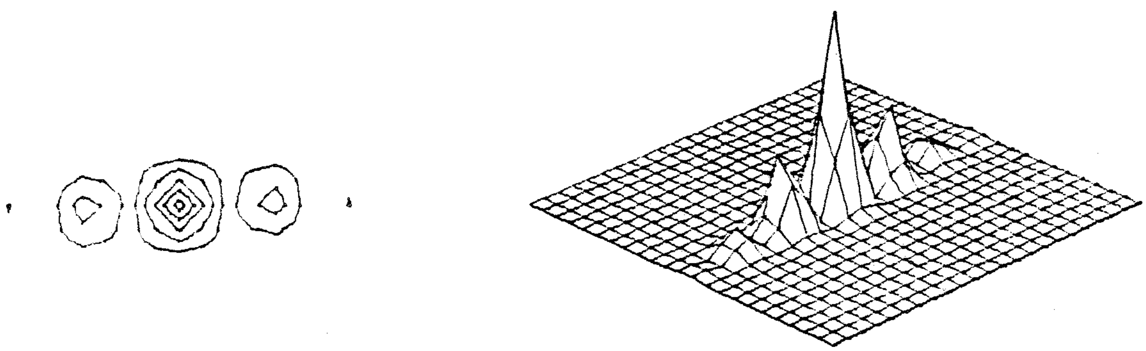

(b)

Figure 3.12. Actual focal spot of 2 mm. nominal size. (a) PSF.
(b) Squared MTF.

digitized using the equipment described in Appendix D.

As it will be shown later, it is convenient to approximate the PSF by a separable function to save computer memory in the design of a tomographic filter.

We have chosen to do the approximation in the frequency domain as follows. Denote the PSF by $h(x,y)$ and its two-dimensional Fourier transform by $H(f_x,f_y)$. Then define a separable PSF $h_s(x,y)$ as

$$h_s(x,y) = h_1(x)\cdot h_2(y) \tag{3.16}$$

where

$$h_1(x) = \mathscr{F}^{-1}\{H_1(f_x)\} \triangleq \mathscr{F}^{-1}\{H(f_x,0)\} \tag{3.17}$$

$$h_2(y) = \mathscr{F}^{-1}\{H_2(f_y)\} \triangleq \mathscr{F}^{-1}\{H(0,f_y)\} \tag{3.18}$$

Thus the separable two-dimensional Fourier transform of $h_s(x,y)$ is

$$H_s(f_x,f_y) = H_1(f_x)\cdot H_2(f_y) = H(f_x,0)\cdot H(0,f_y) \tag{3.19}$$

According to the projection-slice theorem (see Appendix B), this approximation keeps the projections of the PSF along the x-axis and y-axis invariant. This results also in a further advantage, namely a smoothing of the PSF.

The results of this approximation on the PSF's of Figures 3.11 and 3.12 are shown in Figure 3.13 and 3.14, respectively.

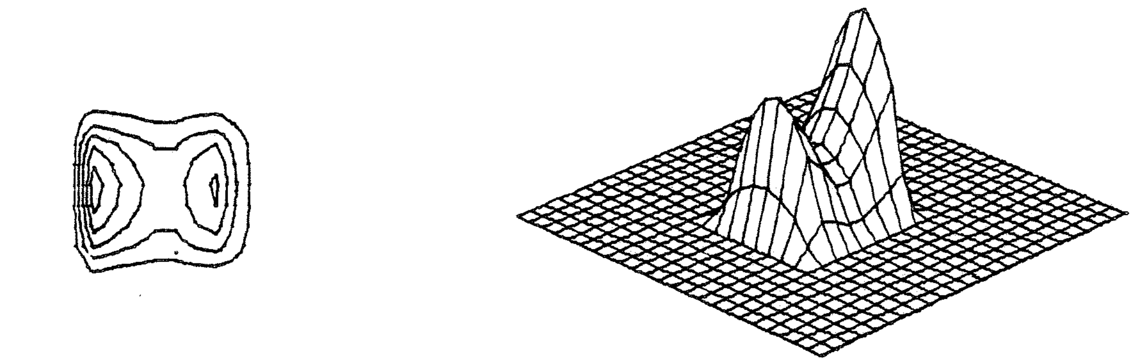

(a)

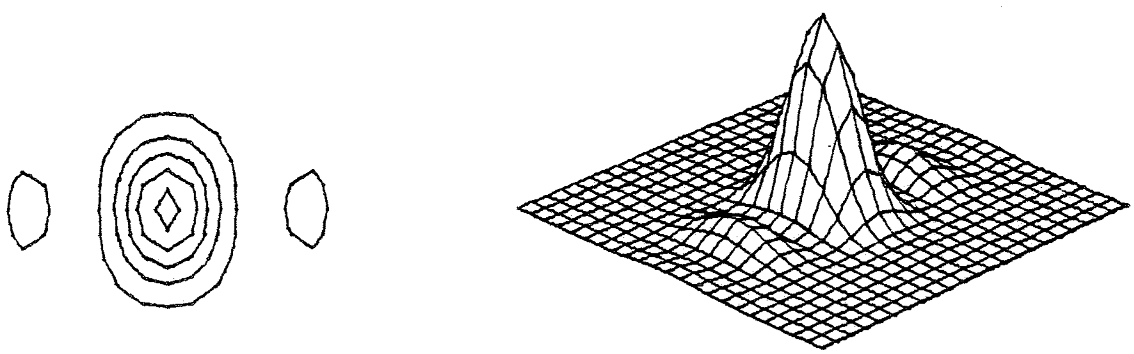

(b)

Figure 3.13. Approximation of the focal spot in Figure 3.11 by a separable function. (a) PSF. (b) Squared MTF.

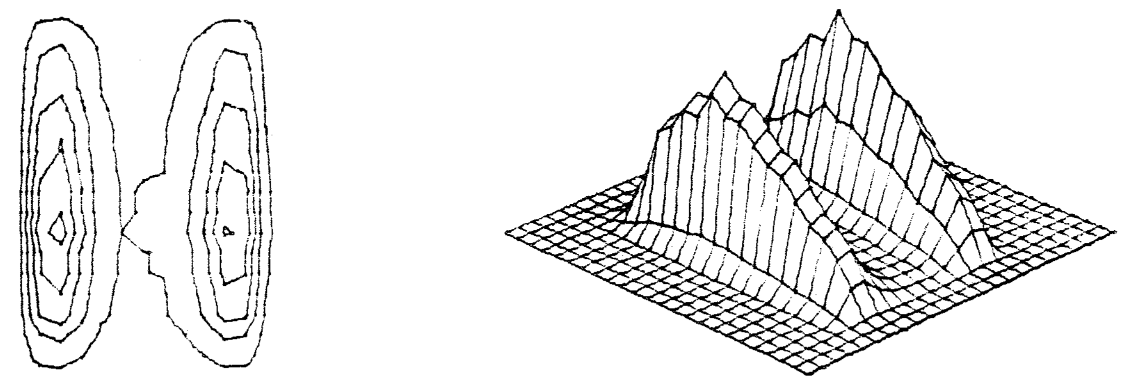

(a)

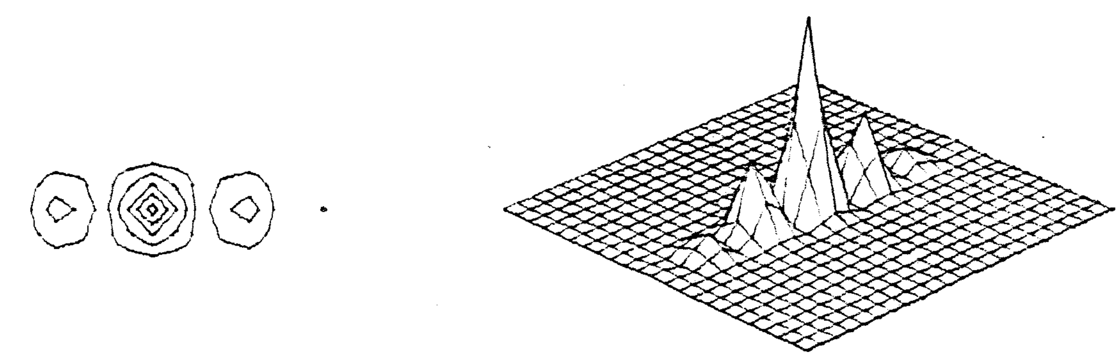

(b)

Figure 3.14. Approximation of the focal spot in Figure 3.12 by a separable function. (a) PSF. (b) Squared MTF.

Chapter IV

DESIGN TECHNIQUES FOR TWO-DIMENSIONAL DIGITAL FILTERS

4.1 Introduction

In the previous chapter the concept of a tomographic filtration process was developed. However, very little was said about the synthesis of tomographic filters in practical applications. A TFP can be implemented optically or digitally. The digital processing of two-dimensional signals offers the following advantages:

1) *Flexibility:* Digital computers can be used to perform linear operations as well as nonlinear operations. Intensity images or density images can be processed. Magnitude and phase filters are readily implemented. The filter characteristics can be changed in an interactive mode (real time) with a dedicated computer or terminal.

2) *Capacity and speed:* The main elements of an optical system such as storage media (film) and parallel processing capabilities result in an enormous capacity and speed. However, experiments in image processing are difficult and time-consuming to set up. The time for developing film must also be considered. Therefore, the throughput using a dedicated digital computer for image processing is usually faster than that of an optical processor, even if the processing speed of the former is considerably slower. With digital systems the result can be displayed in real time on a television monitor.

3) *Accuracy:* In an optical system there are many sources of error due to imperfect components and alignment. In digital processing the accuracy is only limited by the cost of the computer processing and the

precision of the image scanners being used to get the pictures in and out of the computer.

The main disadvantage of using a computer for image processing may be the cost. This is especially true when the required resolution and image size produce large arrays.

In this chapter we present the digital signal processing tools that will be used in the experiments in Chapter V.

4.2 Classification of Two-Dimensional Digital Filters

Two-dimensional digital filters can be classified in terms of their frequency response, impulse response, mathematical form of the transfer function, and the type of implementation.

The frequency response of a two-dimensional digital filter may have a low-pass, band-pass or high-pass characteristics. Generally, in image processing there is no preferred spatial frequency axis. The frequency response of restoration filters may be specified by other filter structures such as those of inverse filtering, homomorphic filtering, etc.

Depending on whether or not the impulse response is of finite extent, digital filters are divided into finite impulse response (FIR) filters or infinite impulse response (IIR) filters. IIR filters have poles in their transfer functions while FIR filters have only zeros.

If the two-dimensional transfer function can be factored into a product of two one-dimensional transfer functions, one in each variable, the filter is said to be separable:

$$H(z_1,z_2) = H_1(z_1)\ H_2(z_2)$$

The great advantage of separable filters is that their implementation is much simpler. Also, the computer memory requirements are reduced enormously.

Direct implementation of FIR filters using convolution is practical only if the impulse response is very short. In general they are implemented using the FFT. Recursive algorithms are used mainly for IIR filters; each output sample is a function of previous output samples, as well as past and present input samples. Since in image processing applications the signal is space-limited, the filter output will be eventually truncated. An IIR filter with a truncated output may be considered as an FIR filter and fast convolution techniques could be used in its implementation. However, the computer memory requirements would be enormous, thus making a recursive implementation more appropriate.

4.3 Design of Two-Dimensional FIR Filters

The current techniques for designing two-dimensional FIR filters are the following: windowing, frequency sampling, linear programming, exchange algorithms, and mappings or projections to convert the two-dimensional problem into a one-dimensional one [62]. All these techniques except the first one, i.e. windowing, are in some sense optimum design techniques (computer-aided design techniques).

Only the windowing technique is discussed here because it is the simplest and most efficient computationally. Due to the current computational constraints in the optimum design techniques, the windowing method is the only one which can be used to approximate a completely arbitrary complex frequency response.

The design of two-dimensional FIR filters using the windowing technique is a direct extension of the one-dimensional case [13], [57]. The desired frequency response is specified either as an analytic function or as a sequence of numbers forming a table of response versus frequency (i.e., the DFT coefficients, see Appendix B). This frequency response must be specified at a large number of points to prevent aliasing in the space domain.

Let $H_d(f_1,f_2)$ be the desired frequency response of the digital filter. Since $H_d(f_1,f_2)$ is periodic in frequency it can be expanded in a two-dimensional Fourier series of the form

$$H_d(f_1,f_2) = \sum_{n_1=-\infty}^{\infty} \sum_{n_2=-\infty}^{\infty} h(n_1,n_2)\ e^{-j2\pi n_1 f_1}\ e^{-j2\pi n_2 f_2} \tag{4.1}$$

where

$$h(n_1,n_2) = \int_0^1 \int_0^1 H_d(f_1,f_2)\ e^{j2\pi n_1 f_1}\ e^{j2\pi n_2 f_2}\ df_1\ df_2 \tag{4.2}$$

The coefficients of the Fourier series $h(n_1,n_2)$, also called filter coefficients, are identical to the filter impulse response or point spread function, which is of infinite extension in the space-domain. Therefore it must be truncated to make the filter realizable. Since simple truncation would produce unacceptable ripple around the discontinuities in the frequency response, the filter coefficients are modified using a finite weighting sequence $w(n_1,n_2)$, called a two-dimensional window, to improve the convergence of the truncated Fourier series. Thus the final approximation to $H_d(f_1,f_2)$ is obtained as:

$$H_r(f_1,f_2) = \sum_{n_1=-\frac{N_1-1}{2}}^{\frac{N_1-1}{2}} \sum_{n_2=-\frac{N_2-1}{2}}^{\frac{N_2-1}{2}} h_r(n_1,n_2)\, e^{-j2\pi n_1 f_1}\, e^{-j2\pi n_2 f_2} \tag{4.3}$$

where

$$h_r(n_1,n_2) = h(n_1,n_2)\, w(n_1,n_2) \tag{4.4}$$

It is easy to show that the respective frequency responses are related by circular convolution, namely

$$H_r(f_1,f_2) = H_d(f_1,f_2)*W(f_1,f_2) \tag{4.5}$$

where

$$W(f_1,f_2) = \sum_{n_1=-\frac{N_1-1}{2}}^{\frac{N_1-1}{2}} \sum_{n_2=-\frac{N_2-1}{2}}^{\frac{N_2-1}{2}} w(n_1,n_2)\, e^{-j2\pi n_1 f_1}\, e^{-j2\pi n_2 f_2} \tag{4.6}$$

The choice of the window function is important. Since the resultant frequency response will be the circular convolution of the desired frequency response with the Fourier transform of the window function, it is necessary to choose a window with a large volume under the main lobe and a small volume under the sidelobes.

Different types of windows provide different trade-offs between the resolution and ripple in the overall frequency response. Here, resolution means the bandwidth of the transitions between discontinuities in the desired frequency response, and the ripple is the maximum deviation from the desired frequency response for frequencies outside the transition regions [57].

In two dimensions, only two types of windows are of interest; separable and circularly symmetric. They are represented mathematically in (4.7) and (4.8), respectively.

$$w(n_1,n_2) = w_1(n_1)\ w_2(n_2) \tag{4.7}$$

$$w(n_1,n_2) = w_1\left\{ \sqrt{n_1^2 + n_2^2} \right\} \tag{4.8}$$

where $w_1(n_1)$ and $w_2(n_2)$ are appropriate one-dimensional (continuous) windows sampled at the proper values. Huang [58] has proved mathematically that good one-dimensional windows produce good circularly-symmetric two-dimensional windows.

There have been many windows proposed that approximate the desired characteristics of an optimal window. We have chosen to use a Kaiser window [59] because it is not only an optimum window in the sense that it is a finite duration sequence that has the minimum spectral energy beyond some specified frequency, but also it contains a parameter that controls the frequency response trade-off between resolution and ripple. The Kaiser window constitutes a relatively simple approximation to a class of functions called prolate spheroidal wave functions which give a closed form solution to the equivalent problem in the continuous case. The one-dimensional Kaiser window is of the form:

$$w_K(n) = \frac{I_o\left(\beta\sqrt{1-\left[\frac{2n}{N-1}\right]^2}\right)}{I_o(\beta)} \qquad -\frac{N-1}{2} \le n \le \frac{N-1}{2} \tag{4.9}$$

where β is a constant that specifies a frequency response trade-off between the peak height of the side lobe ripples and the width or energy of the main lobe, and $I_0(\cdot)$ is the modified Bessel function of the first kind and order zero.

When $H_d(f_1,f_2)$ is not an analytic function and sometimes even when it is, (4.2) may be too difficult to evaluate. Then a summation approximation to the integral as shown in (4.10) can be used.

$$h_a(n_1,n_2) = \frac{1}{M_1M_2} \sum_{k_1=0}^{M_1-1} \sum_{k_2=0}^{M_2-1} H_d(k_1/M_1\ , k_2/M_2)\ e^{j2\pi n_1k_1/M_1}\ e^{j2\pi n_2k_2/M_2} \tag{4.10}$$

Clearly (4.10) may be evaluated efficiently as a $M_1 \times M_2$-point inverse DFT (see Appendix B). It is easy to show that $h_a(n_1,n_2)$ is an aliased version of $h(n_1,n_2)$. Since the window looks only at $N_1 \times N_2$ points of $h_a(n_1,n_2)$, a necessary restriction is that $M_1 \gg N_1$ and $M_2 \gg N_2$. This condition makes the computer memory requirements very large. If the filter is separable the two-dimensional DFT can be evaluated by a sequence of one-dimensional DFT's. In this case the computer memory required is much smaller and is proportional to $M_1 + M_2$ rather than $M_1 \times M_2$.

Another problem with windowing is due to the smearing effect of the convolution, which makes it hard to control the locations of the transition bands of the resulting filter. This may not be a problem in image processing if a smooth transition band is desired and its position is not critical, but the design of narrow-band or wide-band filters may be difficult to achieve.

Figures 4.1 and 4.2 show examples of two-dimensional digital filter designs using the windowing technique. The program listings are included in Appendix C.

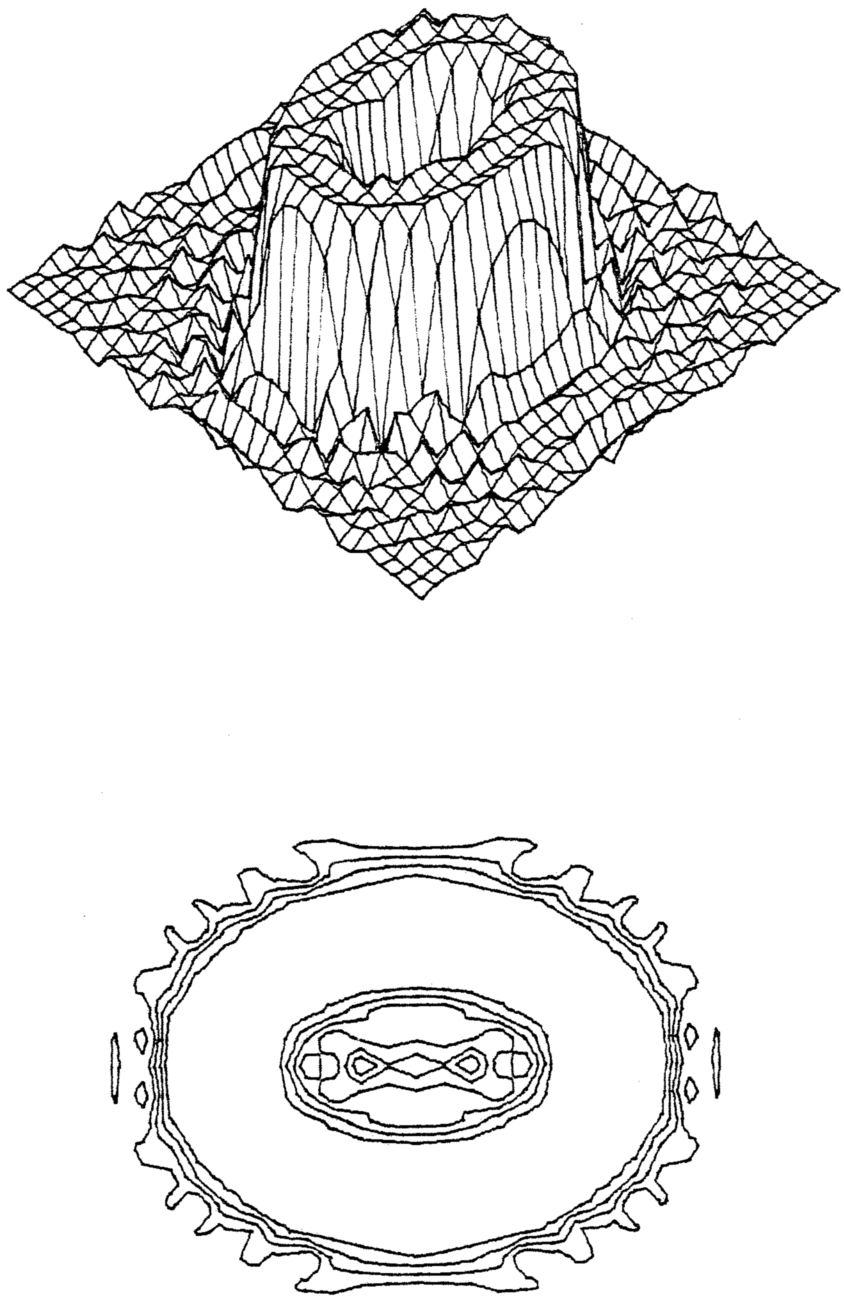

Figure 4.1. Magnitude response (in dB) of a Kaiser-window elliptically-shaped band-pass FIR filter with an impulse response of size 31×31 samples.

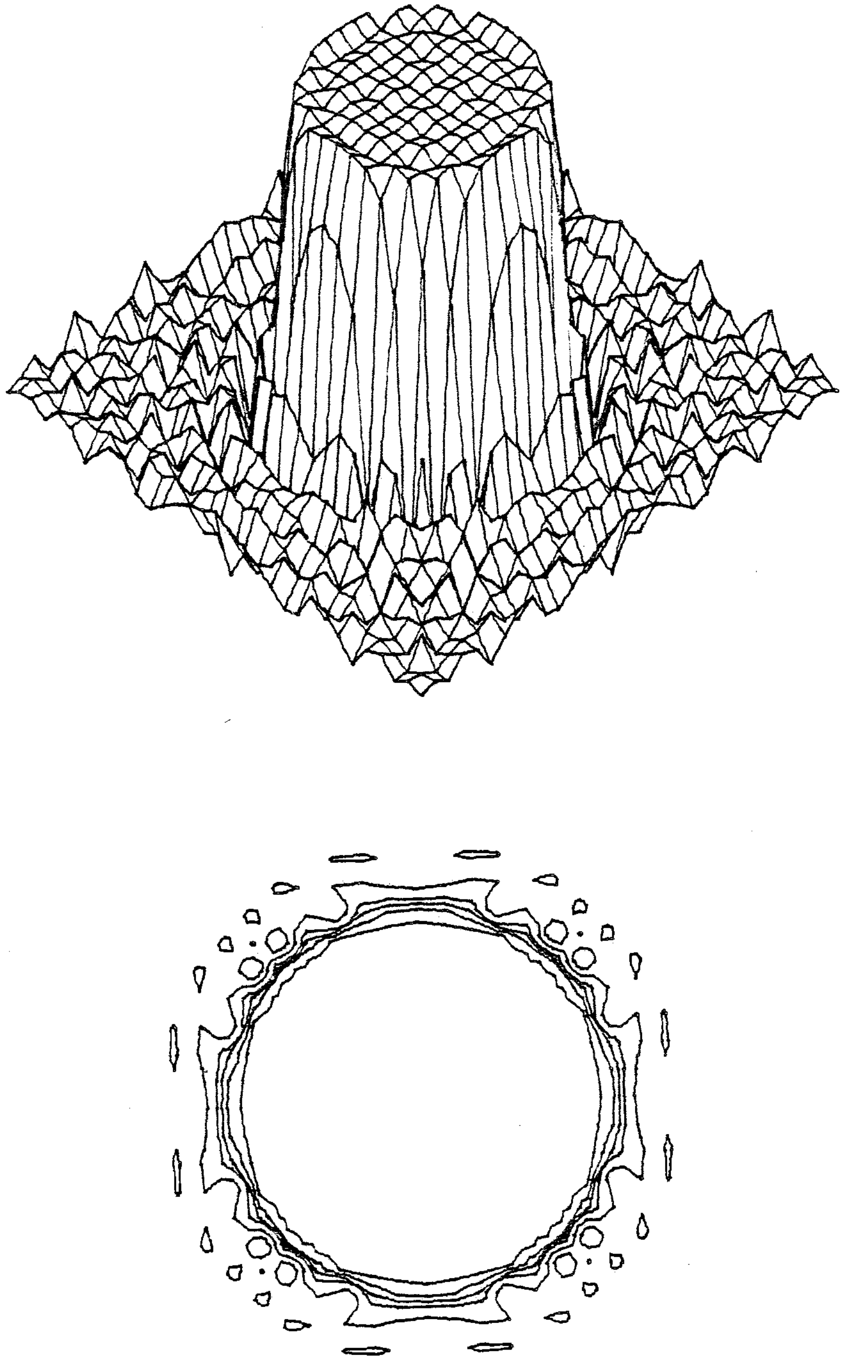

Figure 4.2. Magnitude response (in dB) of a Kaiser-window circularly-symmetric low-pass FIR filter with an impulse response of size 31×31 samples.

The examples shown belong to a class of two-dimensional FIR filters with low-pass, band-pass or high-pass characteristics and elliptical or circular shape. The ideal frequency response of this class of filters is specified by:

$$H_d(f_1,f_2) = \begin{cases} 1 & \text{for} \quad \dfrac{f_1^2}{\ell_1^2} + \dfrac{f_2^2}{\ell_2^2} > 1 \quad \text{and} \quad \dfrac{f_1^2}{\nu_1^2} + \dfrac{f_2^2}{\nu_2^2} < 1 \\ & \quad \text{(lower transition band)} \quad \text{(upper transition band)} \\ 0 & \text{otherwise} \end{cases}$$

In general $H_d(f_1,f_2)$ represents an elliptical annulus (ideal band-pass filter). For low-pass filters the condition for the lower transition band is ignored ($\ell_1=\ell_2=0$) and for high-pass filters the condition for the upper transition band is ignored ($\nu_1=\nu_2=\infty$).

The ideal impulse response for this class of filters is found by evaluating (4.2) and the actual (windowed) impulse response is given by (4.4), (4.8), and (4.9), that is:

$$h_r(n_1,n_2) = h(n_1,n_2)\ w(n_1,n_2) = h(n_1,n_2)\ w_K(\sqrt{n_1^2+n_2^2}) =$$

$$= \left[\frac{\pi\,\nu_1\nu_2 J_1(\pi\sqrt{\nu_1^2n_1^2+\nu_2^2n_2^2})}{\sqrt{\nu_1^2n_1^2+\nu_2^2n_2^2}} - \frac{\pi\,\ell_1\ell_2 J_1(\pi\sqrt{\ell_1^2n_1^2+\ell_2^2n_2^2})}{\sqrt{\ell_1^2n_1^2+\ell_2^2n_2^2}}\right] \times \frac{I_o\left\{\beta\sqrt{1-\dfrac{4(n_1^2+n_2^2)}{(N-1)^2}}\right\}}{I_o(\beta)}$$

$$\text{for} \quad -\frac{N-1}{2} \le n_1 \le \frac{N-1}{2} \quad \text{and} \quad -\frac{N-1}{2} \le n_2 \le \frac{N-1}{2}$$

This equation is evaluated by the subroutine HKWBPF. For the calculation of $I_o(\cdot)$ we have used a function subprogram which is a modification of a subroutine by Kaiser [59]. We did not find a suitable program for the calculation of $J_1(\cdot)$, consequently we developed our own which uses two different algorithms depending on the value of the argument. In this way at least six exact digits are always obtained very quickly.

4.4 Design of Two-Dimensional IIR Filters

The importance of two-dimensional IIR filters is in their potential for saving both computer time and computer memory with respect to FIR filters. However, the design of IIR filters in two dimensions is difficult due to the fact that a polynomial in two variables $P(z_1,z_2)$ cannot in general be factored into first- or second-order polynomials. This implies that many one-dimensional design techniques cannot be readily extended to two dimensions and that a high-order two-dimensional filter cannot in general be synthesized in parallel or cascade form to reduce the effect of quantization noise. It is also difficult to test the stability of two-dimensional IIR filters except in simple cases. Stability is an important issue in the design of IIR filters. If a filter is unstable, any input, including computational noise, can cause the output to grow without bound, obliterating the desired response. The basic theorem for guaranteeing stability with two-dimensional IIR filters is due to Shanks [60]. Application of Shanks' test is conceptually straightforward but computationally involved. Simpler stability tests have been proposed by Huang [61] and others. The state of the art has been reviewed by Mersereau [62].

The frequency domain design techniques for two-dimensional IIR filters can be divided into optimum design techniques and *ad hoc* design techniques.

Optimum filters may be more efficient in terms of the realization but the computation time of the design can become prohibitively large.

The *ad hoc* design techniques proposed so far consist in cascading elementary one- and two-dimensional filters. A class of elementary filters can be obtained with a design method due to Shanks which maps one-dimensional into two-dimensional filters with arbitrary directivity in the two dimensional frequency response plane. These filters are called rotated filters because they are obtained by rotating one-dimensional filters.

In a previous work we used this method to design good approximations to circularly-symmetric filters by cascading rotated filters [63]. We also proved that if the angle of rotation θ lies between 270° and 360° then the filter is marginally stable.To implement filters with angles of rotation not in this range the data transformation techniques to be developed in Section 4.5 are used to achieve the desired frequency response. To measure the goodness of the designed filters, several kinds of shape factors that are suitable for two-dimensional filters were developed [63].

Rotated filters are designed in the s-domain and the the two-dimensional bilinear z-transform is used to obtain a digital filter. Due to the double periodicity of the frequency response of two-dimensional digital filters, the desired frequency response of rotated filters is distorted to an extent which depends on the angle of rotation. We have observed that in the low-frequency region the deviation from the desired frequency response is maximum for a rotation of 315°. The previously mentioned algorithm for designing circularly symmetric filters did not compensate for this effect. The frequency response was approximated iteratively in one direction only and each rotated filter in the cascade was designed with the same cutoff frequency.

We have developed a new algorithm in which the frequency response is approximated in as many directions as the number of rotated filters being cascaded. The cutoff frequency of each rotated filter is adjusted separately and iteratively according to the frequency response obtained when all the filters in the cascade are considered.

This approach has not only the advantage of giving a better circularly-symmetric frequency response but also non-circularly-symmetric filters can be designed by specifying different cutoff frequencies in each direction. Of course, since only low-pass filters are cascaded, the relationships among these cutoff frequencies cannot be arbitrary because the locus of the cutoff frequency of the two-dimensional filter is a smooth path such as a circle or an elipse.

Using this new algorithm problems of convergence may arise if too much accuracy is specified in too many directions. The program takes care of this problem by aborting the iteration as soon as it ceases to converge. An error code is returned which specifies if convergence was attained. There is a compromise between accuracy in the cutoff frequency and the number of directions in which it is specified.

The new algorithm features the following steps:

1) Initialization. Get the poles and zeros of a stable one-dimensional continuous low-pass filter with cutoff frequency normalized to $1/(2\pi)$, (i.e. cutoff angular frequency normalized to unity). Get the N angles of rotation $270^\circ \le \theta(k) \le 360^\circ$, $k=1, \ldots, N$ and the desired cutoff frequencies $f_u(k)$, $k=1, \ldots, N$ of the two-dimensional digital filter in each direction $\theta(k) + 90^\circ$, $k=1, \ldots, N$. The frequencies $f_u(k)$ are given as fractions of the Nyquist frequency $f_N \triangleq 1/(2T)$. If the input arguments are inconsistent, return to the calling program with an error code IERROR=1. Otherwise let i=0 for the first iteration and continue.

2) Let $f_d^i(k) = f_u(k)$, $k=1, \ldots, N$.

3) For $k=1, \ldots, N$ determine the coefficients of the N rotated digital filters derived from the one-dimensional continuous filter by multiplying the poles by $(\pi/2)f_d^i(k)$ or by $\tan[(\pi/2)f_d^i(k)]$ if the frequency axis is to be prewarped (cf. (11) in [63]).

4) With the N rotated filters in cascade find the cutoff frequencies of the resultant two-dimensional filter, $f_c^i(k)$, $k=1, \ldots, N$, in the directions $\theta(k) + 90^\circ$, $k=1, \ldots, N$, respectively. If the algorithm that searches for these cutoff frequencies does not converge, then return to the calling program with IERROR=3.

5) If $|f_u(k)-f_c^i(k)| < \varepsilon$ for $k=1, \ldots, N$ where ε is the specified maximum error of the cutoff frequency in each direction; then return to the calling program with IERROR=0. In this case the execution is completed satisfactorily.

6) If there is no improvement in the last iteration step, that is

if $$\sum_{k=1}^{N} |f_u(k) - f_c^i(k)| \geq \sum_{k=1}^{N} |f_u(k) - f_c^{i-1}(k)|$$

then return with IERROR=4.

7) Let $i \leftarrow i+1$. If i is greater than the maximum allowed number of iterations return with IERROR=2.

8) Let $f_d^i(k) = f_d^{i-1}(k) + f_u(k) - f_c^{i-1}(k)$, $k=1, \ldots, N$.

9) Go back to step 3).

The cutoff frequency of the two-dimensional digital filter in a given direction (cf. step 4) is obtained from a function program that gives the frequency response of the filter at any point in the two-dimensional frequency response plane. This point can be defined either in polar or cartesian coordinates. In addition, since stable rotated filters can be obtained only for angles of rotation between 270° and 360°, a parameter is used which specifies how the filter is to be combined with data transformations to obtain desired symmetries. Thus, the overall system has the required cutoff frequencies.

Additional utility subroutines were written which can be used to normalize, print and punch the filter coefficients, design high-pass filters, evaluate the frequency response in any rectangular region of the two-dimensional frequency plane, determine shape factors, check for stability (not necessary with this technique because stability is guaranteed), synthesize the filter using complex cascade programming, produce contour or perspective plots of the responses, etc.

The source program listing of the new two-dimensional filter design algorithm is given in Appendix C. Examples of filters designed using it are shown in Figures 4.3 and 4.4.

For non-circularly-symmetric filters, it may seem possible to obtain elliptic shapes or other shape types from circularly-symmetric filters by changing the scaling along each axis. However this is not possible in general because the filter would most probably become unstable. On the other hand, the technique that we described previously guarantees stability.

4.5 A Group of Linear Spectral Transformations

In two-dimensional recursive filter design, stability and causality are major requirements. In many cases these requirements impose severe

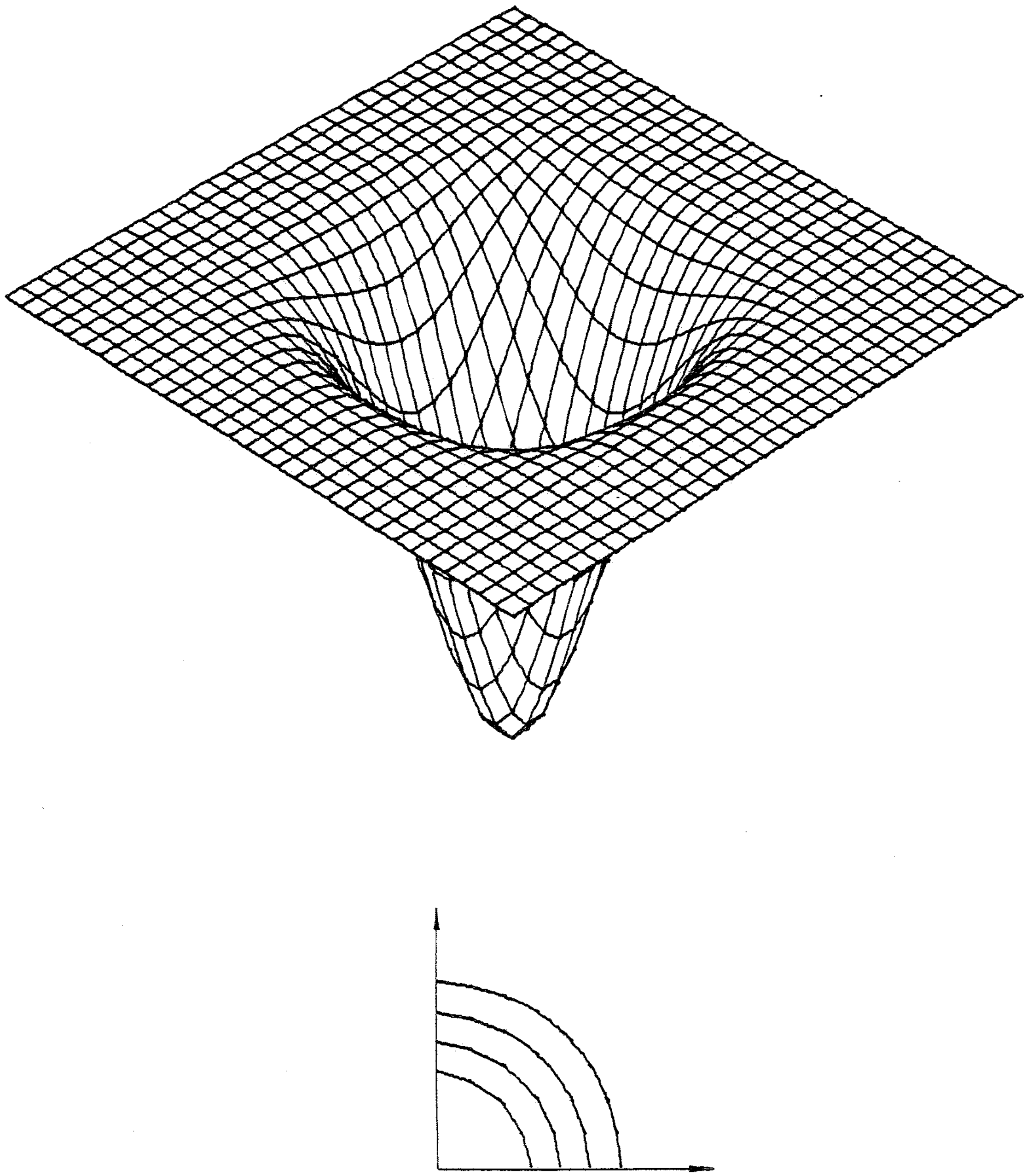

Figure 4.3. Magnitude response of a two-dimensional circularly-symmetric high-pass IIR filter with zero-phase response (derived from a fourth-order Gaussian magnitude approximation continuous filter and rotations by multiples of 30°).

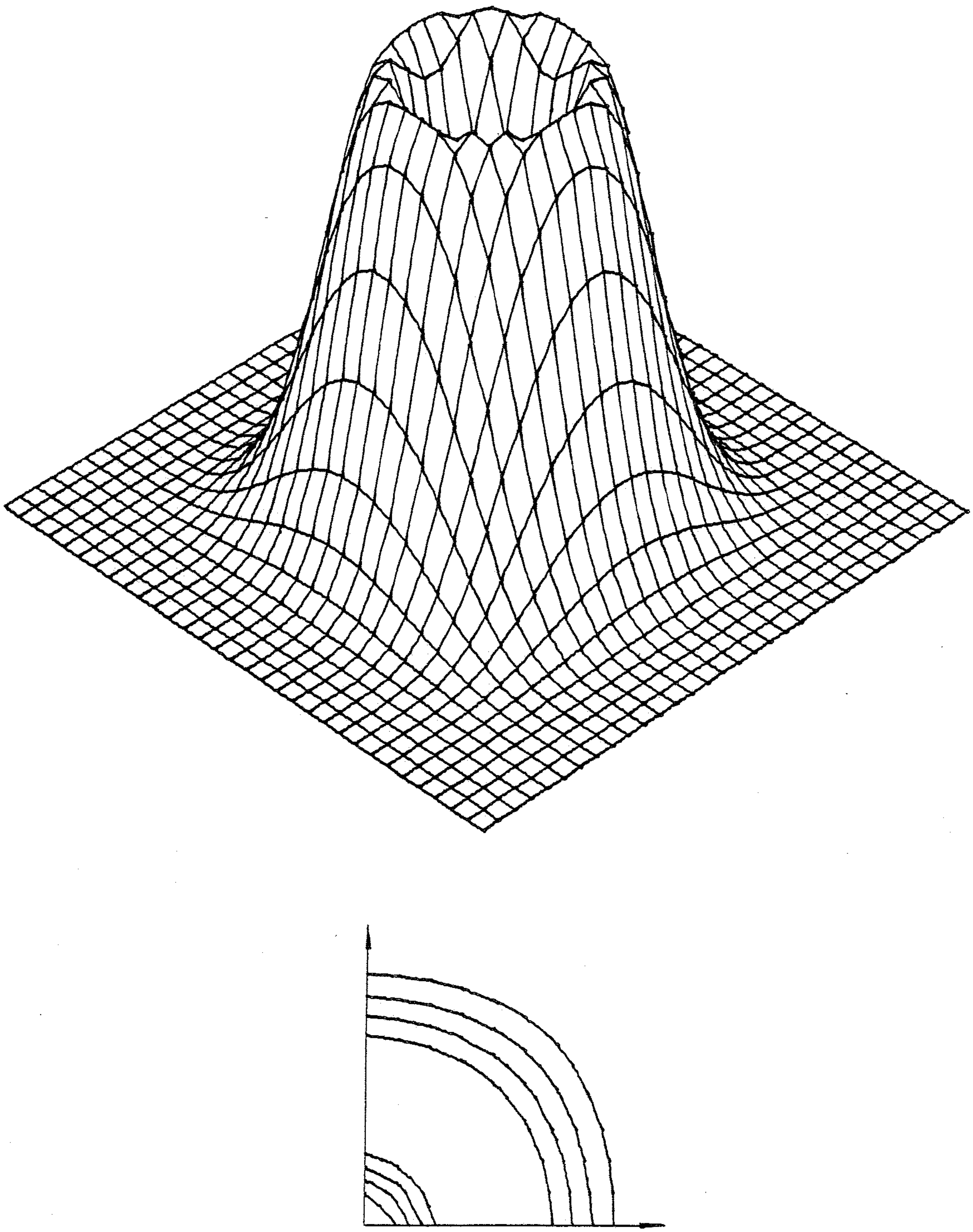

Figure 4.4. Magnitude response of a two-dimensional circularly-symmetric band-pass IIR filter with zero-phase response (derived from a fourth-order Gaussian magnitude approximation continuous filter and rotations by multiples of 30°).

constraints on the filter frequency response which can be attained. When these constraints limit the geometrical shape of the pass and stop regions of the two-dimensional digital filter, something can be done to change that shape. Indeed, instead of modifying the transfer function of the filter, which in most cases would lead to instability, transformations of the input and output data may result in a stable system with the desired transfer function.

Some of the transformations that we consider have already been reported in the literature. Indeed, this section was motivated by the zero-phase technique outlined in [60]. Also, data rotations have been used in the past [63] to design stable recursive filters with circularly-symmetric magnitude response. The purpose of this section is to give a unified presentation with emphasis on the stable realization of the filters by equivalent data transformations. Other spectral transformations for two-dimensional digital filters based on a different approach have been studied elsewhere [64].

The transformations proposed in this section are based on the concept of causality in two dimensions and the fact that the z-transform does not completely specify a sequence unless a region of convergence is associated with it.

Causality, as understood in the time-domain, has no physical meaning in two-dimensional image processing. Nevertheless, since recursive filters process data sequentially, in two dimensions the term causality is conveniently associated with the ordering of the data samples being processed. Huang [61] defines the two-dimensional recursive filter that recurses in the $(+n_1,+n_2)$ direction as causal.

A causal filter has a response in the first quadrant only.

Recursive filters can be described by difference equations. Each difference equation has a unique z-transform (i.e. the transfer function), but depending on which term of the difference equation we solve for, different regions of convergence of the z-transform are specified [61], [12, Chapter 2]. Thus to each region of convergence there corresponds a different unit-sample response. It can be shown that at most one of these unit-sample responses satisfies the BIBO stability condition, that is,

$$\sum_{n_1=-\infty}^{\infty} \sum_{n_2=-\infty}^{\infty} |h(n_1,n_2)| < \infty.$$

The frequency response of all these filters is the same because it only depends on the transfer function. The frequency response is obtained by evaluating the transfer function for $z_1=\exp(-j2\pi f_1 T_1)$ and $z_2=\exp(-j2\pi f_2 T_2)$, where T_1 and T_2 are the sampling intervals.

Suppose that we are given a stable and causal two-dimensional recursive filter with frequency response $H(f_1,f_2)$. Consider all the linear transformations of the spectral plane which map the spectral axes onto themselves. There are eight such possible transformations [65] and they have the algebraic structure of a finite group† under the operation of multiplication [66]. These transformations and their effect on the frequency response of the digital filter are the following (refer to Figure 4.5):

† In the algebraic literature this group is referred to as the dihedral group of order 8.

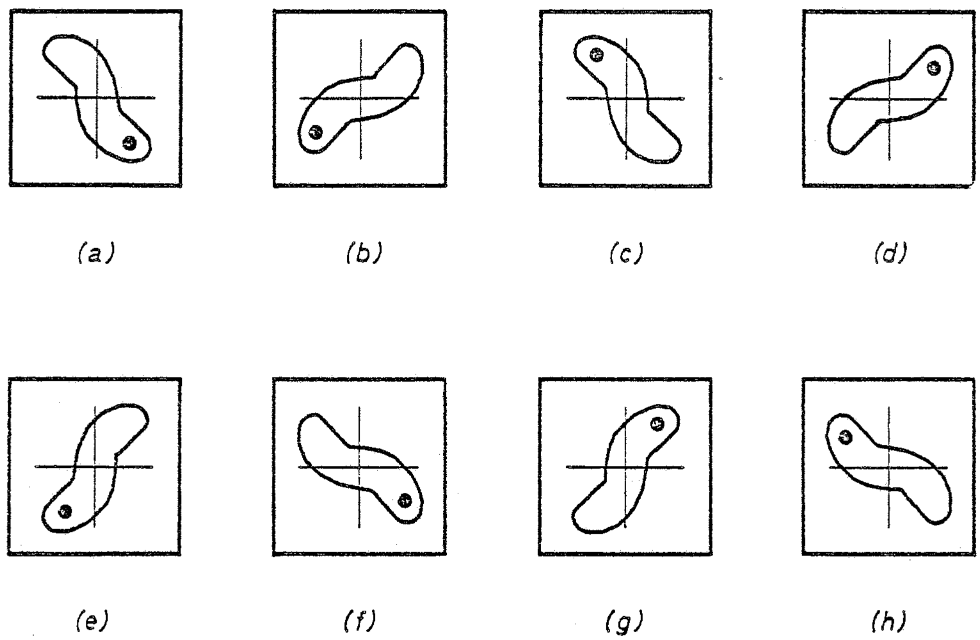

Figure 4.5. (a)-(h) Group of linear spectral transformations.

(a) $H(f_1, f_2)$ identity

(b) $H(f_2, -f_1)$ clockwise 90° rotation

(c) $H(-f_1, -f_2)$ clockwise 180° rotation

(d) $H(-f_2, f_1)$ clockwise 270° rotation

(e) $H(-f_1, f_2)$ vertical mirror image

(f) $H(-f_2, -f_1)$ transpose with respect to the principal diagonal

(g) $H(f_1, -f_2)$ horizontal mirror image

(h) $H(f_2, f_1)$ transpose with respect to the secondary diagonal.

These transformations could equivalently be defined in the (z_1, z_2)-domain by inverting and/or interchanging the complex variables z_1 and z_2 in the filter transfer function, but the transformations are easier to visualize in the frequency domain.

Because of the symmetry of the stability condition [60, Theorem 1], only $H(f_1,f_2)$ and $H(f_2,f_1)$ are causal and stable among these eight transformed filters. All other transformed filters are noncausal and have different stability conditions which are incompatible with those of $H(f_1,f_2)$ and $H(f_2,f_1)$ [61, Theorem 2], [67]; and therefore are unstable. It should also be noted that if the unit-sample response of the filter $H(f_1,f_2)$ is real, both $H(f_1,f_2)$ and $H(-f_1,-f_2)$ have the same magnitude response, which is symmetric with respect to the origin, and opposite phase responses. For this reason, from $H(f_1,f_2)$ only four distinct magnitude responses can be derived by the transformations shown. The other transfer functions may be utilized to obtain filters with zero phase responses. This is achieved by combining in series or in parallel two filters with the same magnitude response and opposite phase responses [60].

As previously mentioned, in some cases a stable filter may be found which has the same frequency response as the unstable filter, by solving the difference equation for a different term. There are two alternatives for synthesizing the equivalent stable filter. The first is to filter the data in a different manner [60] by using an algorithm recursing in another direction. Figure 4.6 shows the direction of recursion, sense of recursion, and the starting point of the input data for each of the transformed filters. A horizontal arrow denotes a recursion by rows and a vertical arrow denotes a recursion by columns. The head of the arrow points in the sense of recursion and the base of the arrow shows the starting point.

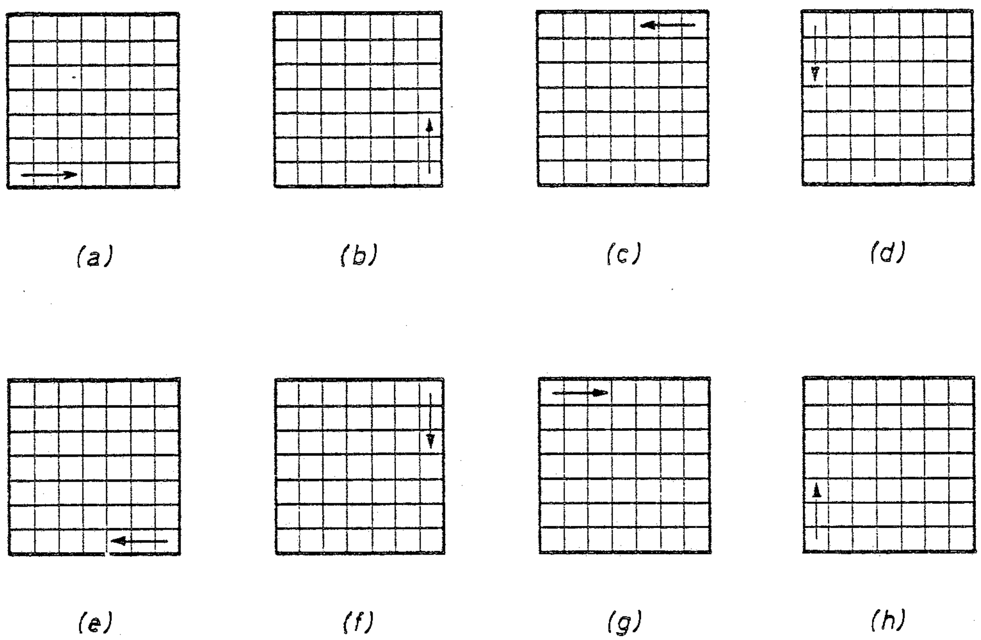

Figure 4.6. (a)-(h) Realization of a transformed filter by changing the direction and sense of recursion of the filter algorithm.

The second alternative is to transform the data [63]. Indeed, it is easily shown that the system described by (4.11) in the frequency domain is equivalent to the system in (4.12). This follows from the fact that the application of a transformation distributes over pointwise multiplication.

$$Y(f_1,f_2) = [\,T\,H(f_1,f_2)\,]\cdot X(f_1,f_2) \tag{4.11}$$

$$= T\{\,H(f_1,f_2)\cdot[\,T^{-1}\,X(f_1,f_2)]\} \tag{4.12}$$

where $X(f_1,f_2)$ and $Y(f_1,f_2)$ are the Fourier transforms of the input and output of the system, respectively, and the transfer function of the system is $H(f_1,f_2)$ operated on by the transformation T, which can be any

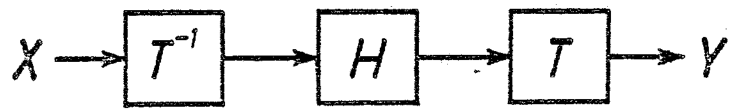

Figure 4.7. Realization of a transformed filter by equivalent data transformations.

of the eight, previously described. In (4.12) the inverse transform is applied to the input data before filtering with $H(f_1,f_2)$, and the transform itself to the output data, after filtering. This process is illustrated in the block diagram of Figure 4.7. This sequence of operations gives the desired transfer function and guarantees stability because the recursive filtering is done with $H(f_1,f_2)$ which is stable by definition. Data transformations do not affect stability because if a filter is stable it will remain so no matter what the (bounded) input is. Also, the data transformations in Figure 4.7 affect neither the linearity nor the space-invariance of the system.

The system (4.12) shown in Figure 4.7 is best realized in the space domain. The transformations are easily applied to the data which are given in the form of a matrix, and they can be done in place if the matrix is square. Here we use the property that an orthogonal change of coordinates in the space domain results in the same change of coordinates in the frequency domain [68].

Systems like that in Figure 4.7 can be cascaded to obtain a system with zero phase or other useful symmetries. In this case it should be noted that, since the set of transformations forms a group under the operation of multiplication, whenever two transformations are cascaded they can be combined together into a single transformation.

A multiplication table for these transformations is given in [66].

One important remark about the use of these techniques is that not only must a filter be stable but also the filter output array must be large enough, so that the effect of truncating the filter output is negligible.

The examples shown in Figures 4.8 through 4.13 illustrate that from a single digital filter other filters with useful symmetries can be obtained. Perspective plots of both the impulse responses and magnitude responses are shown. In every case the impulse response was found by solving the recursive equations using complex cascade programming [68] for a unit-sample input and assuming zero initial conditions. The unit-sample input consists of a 41×41 matrix where the only non-zero value is the sample (21,21) which is equal to one. The filters in Figures 4.8 and 4.9 are first quadrant filters. If we denote by H the transfer function of a first quadrant filter and by R a rotation of 90°, the results of implementing the combination $\rightarrow H \rightarrow R \rightarrow H \rightarrow R^{-1} \rightarrow$ are shown in Figures 4.10 and 4.11. These filters have circular symmetry but not zero phase response. To obtain zero phase response we may implement, for example, $\rightarrow H \rightarrow R \rightarrow H \rightarrow R \rightarrow H \rightarrow R \rightarrow H \rightarrow R \rightarrow$ and the results are shown in Figures 4.12 and 4.13.

4.6 Data Management Techniques in Two-Dimensional Digital Signal Processing

In a digital computer an image is represented by a matrix of real or integer numbers that correspond to intensity or density values at the sample points. The sampling grid is rectangular, usually with the

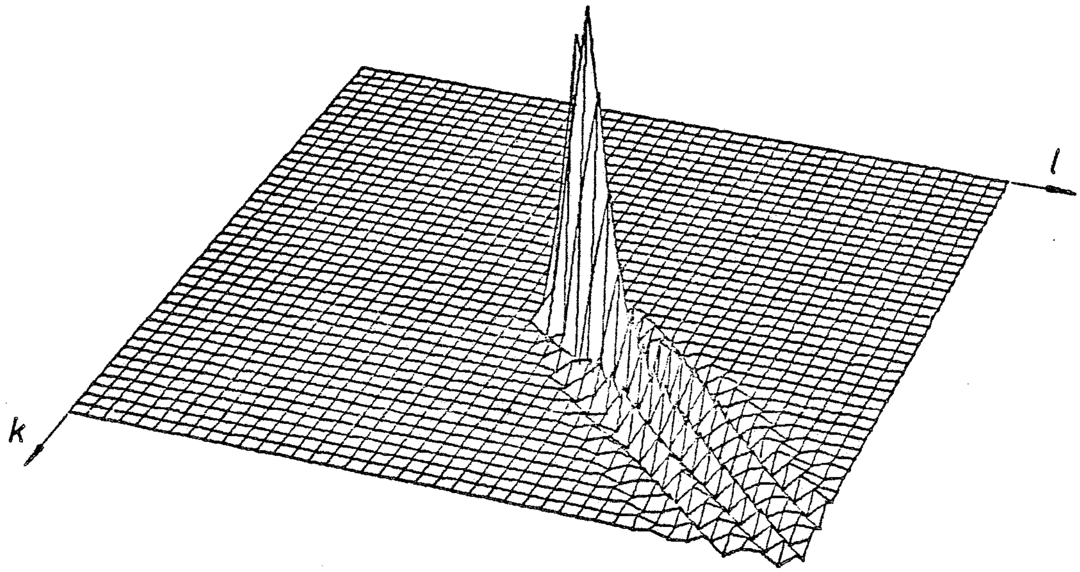

(a)

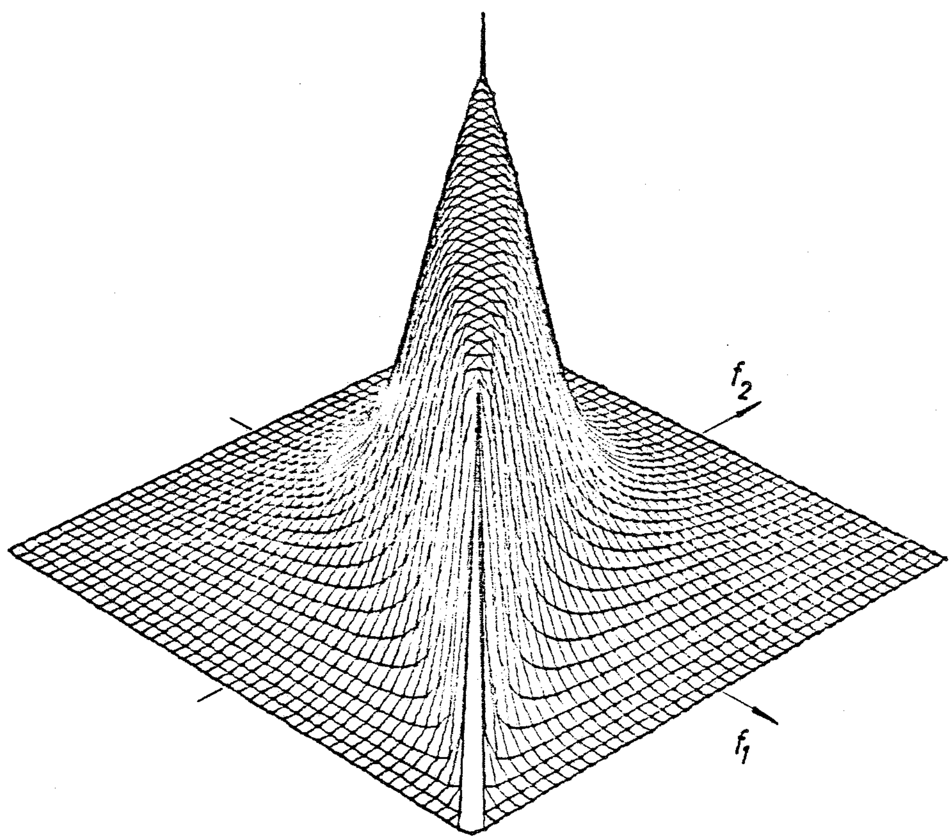

(b)

Figure 4.8. Second-order Butterworth filter rotated 315°. (a) Impulse response. (b) Magnitude response.

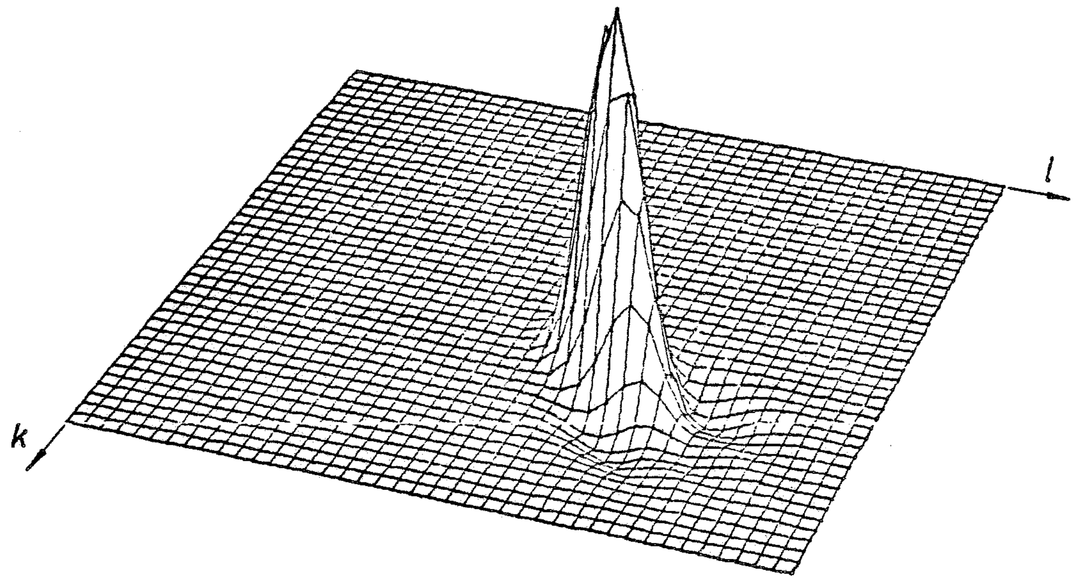

(a)

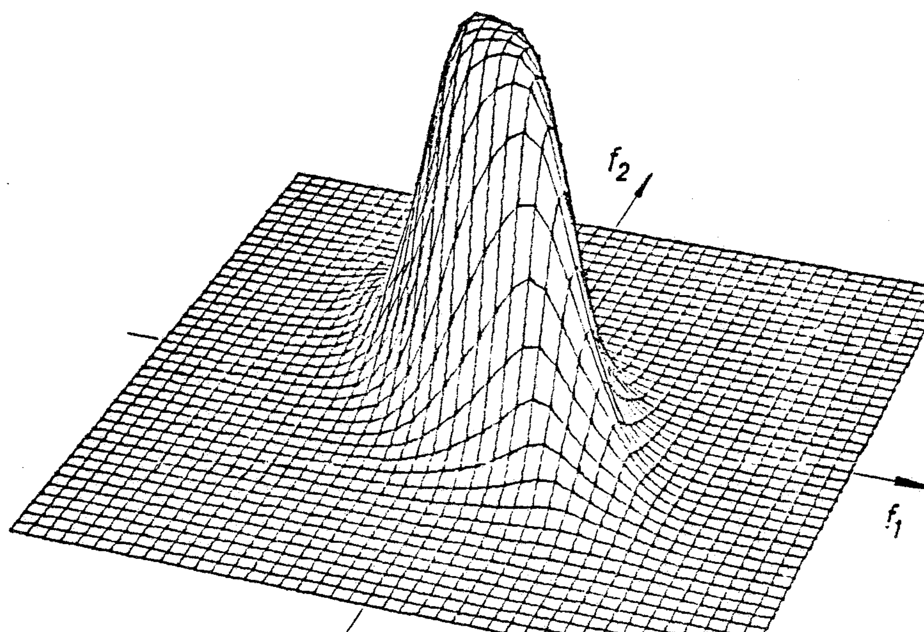

(b)

Figure 4.9. Elliptically-shaped filter formed by cascading three second-order Butterworth filters rotated 285°, 315°, and 345°. (a) Impulse response. (b) Magnitude response.

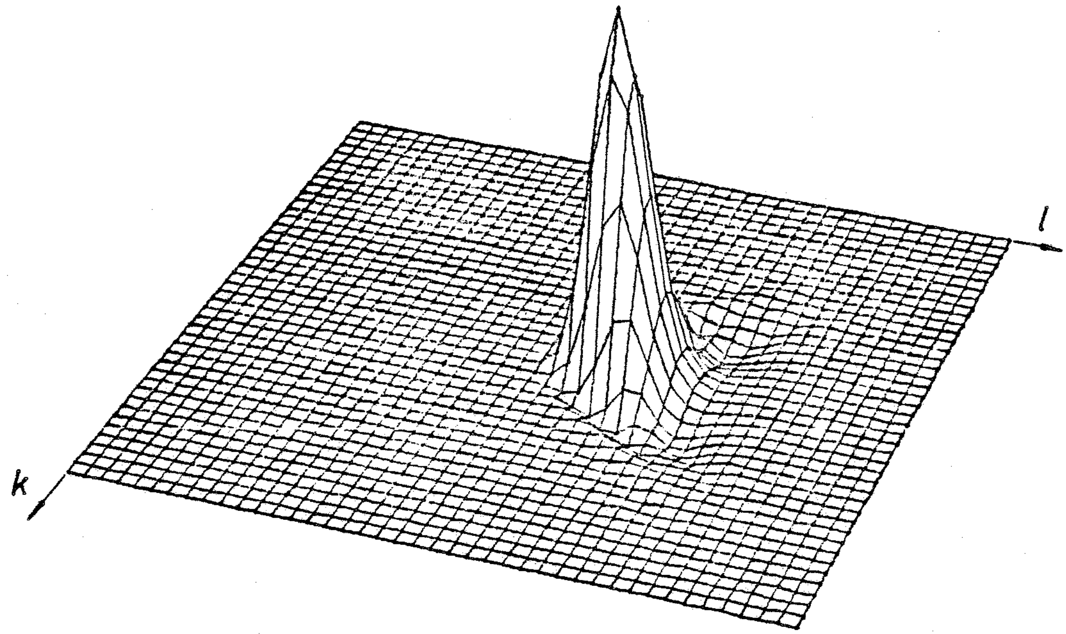

(a)

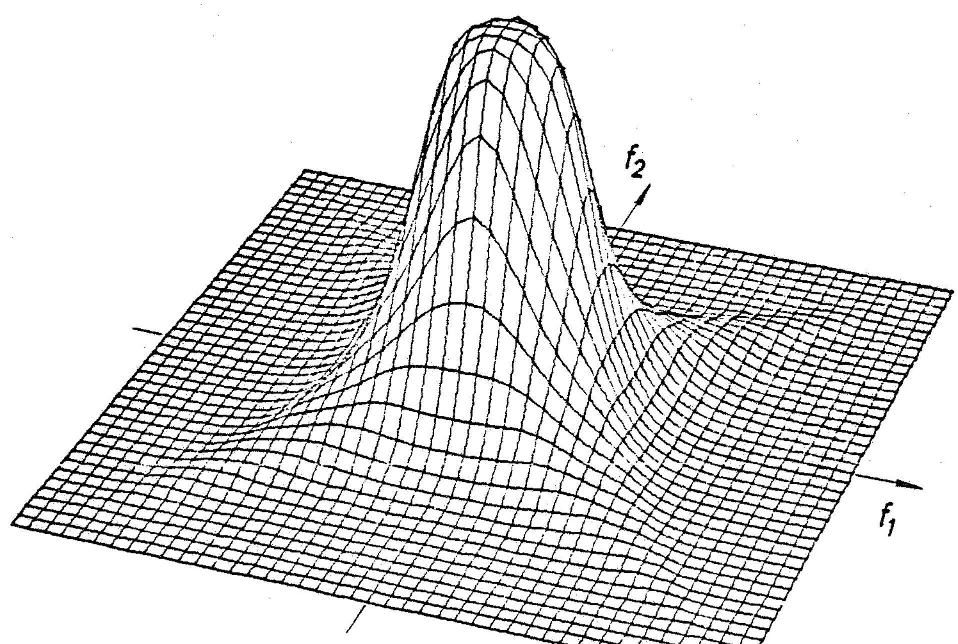

(b)

Figure 4.10. Filter formed by the combination $\rightarrow H \rightarrow R \rightarrow H \rightarrow R^{-1} \rightarrow$, where H is the filter in Figure 4.8 and R is a data rotation of 90°. (a) Impulse response. (b) Magnitude response.

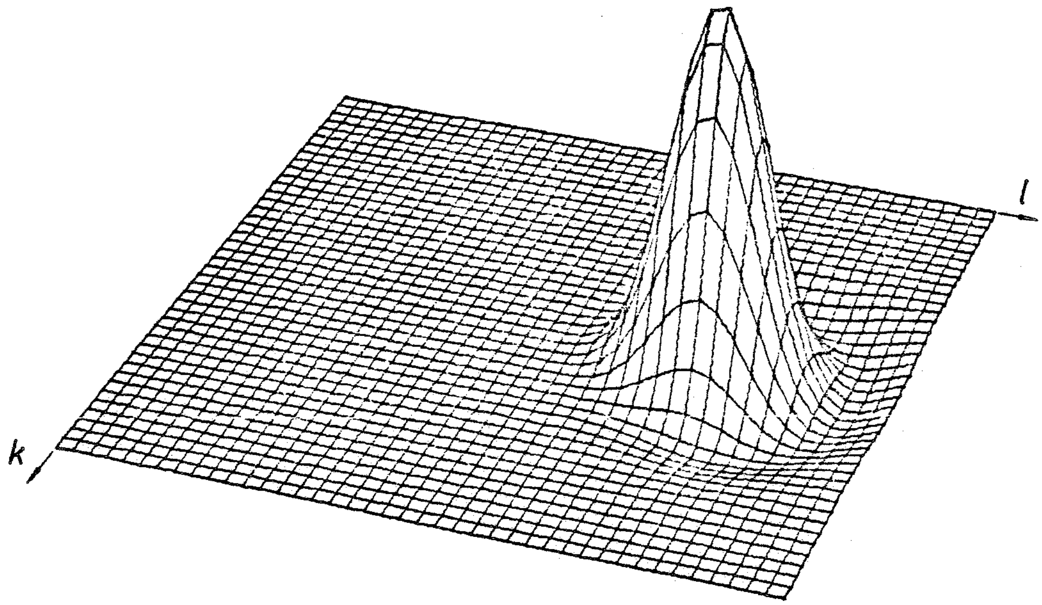

(a)

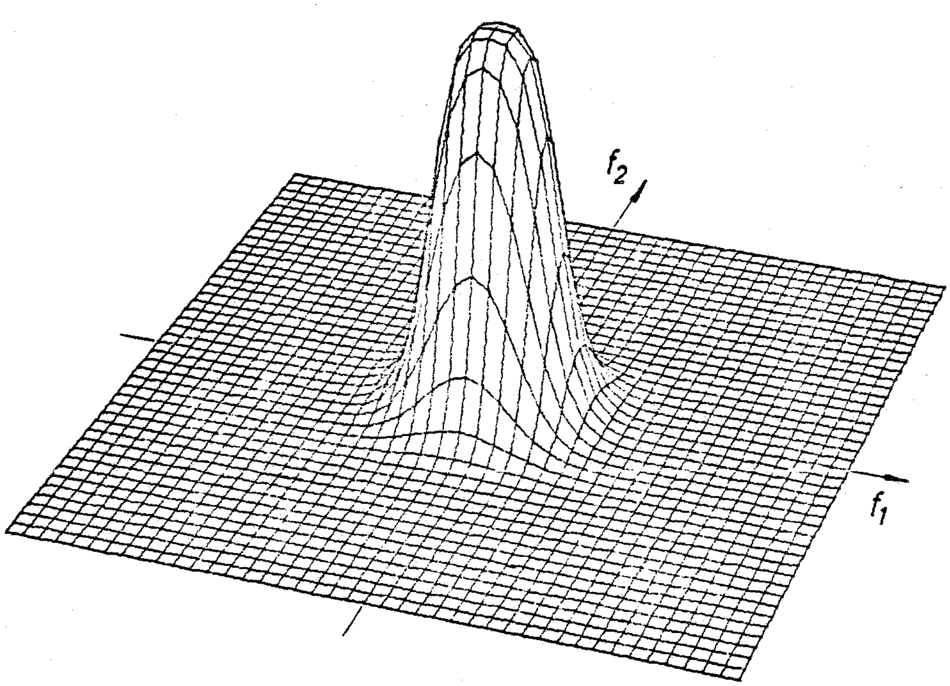

(b)

Figure 4.11. Filter formed by the combination $\rightarrow H \rightarrow R \rightarrow H \rightarrow R^{-1} \rightarrow$, where H is the filter in Figure 4.9 and R is a data rotation of 90°. (a) Impulse response. (b) Magnitude response.

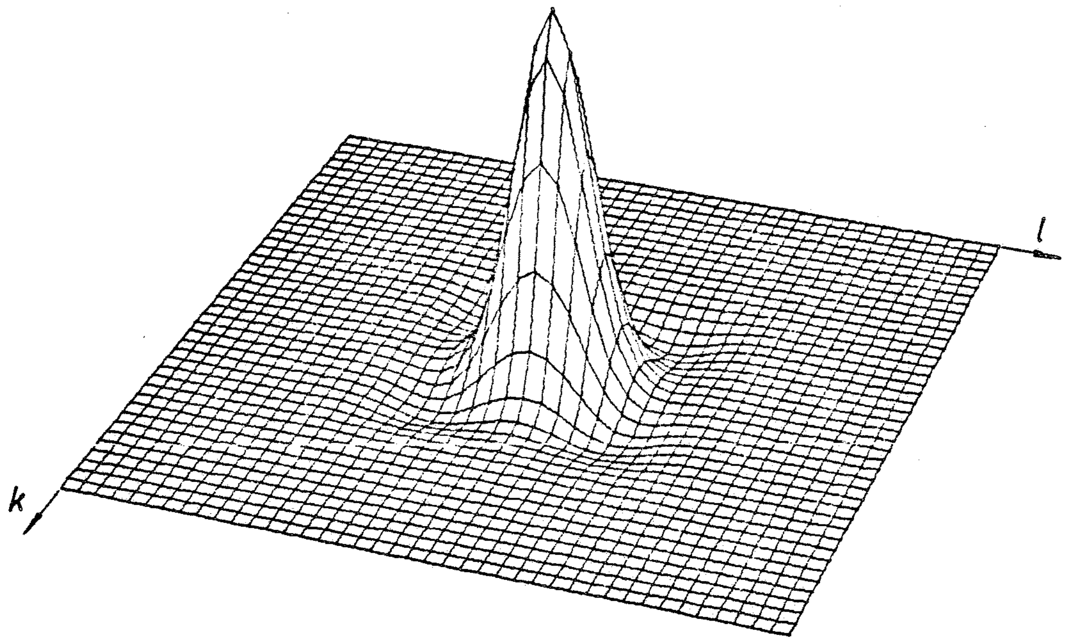

(a)

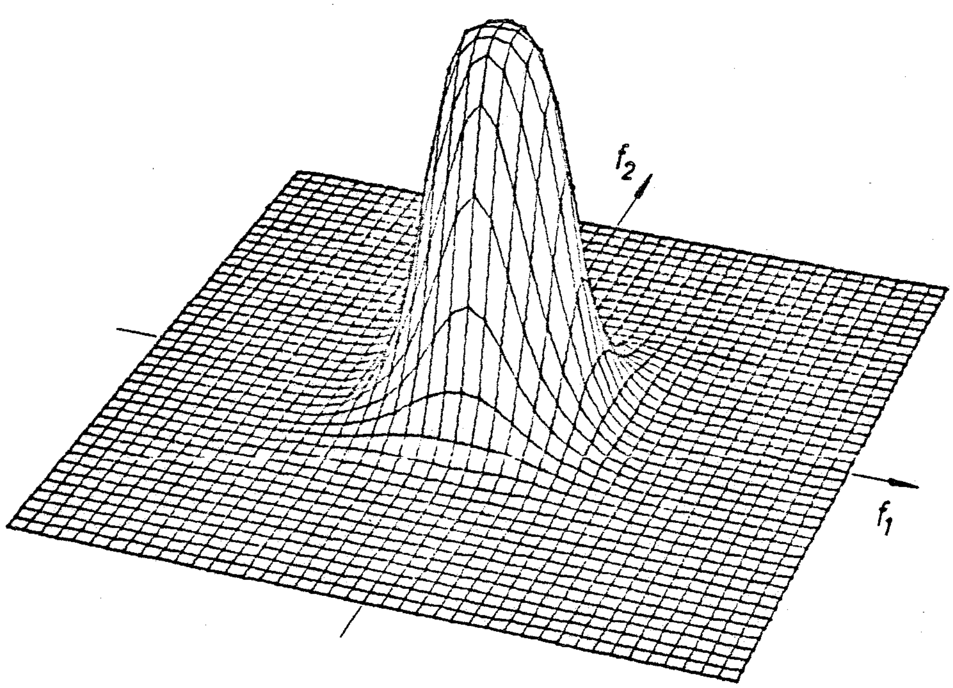

(b)

Figure 4.12. Filter formed by the combination → H → R → H → R → H → R → → H → R →, where H is the filter in Figure 4.8 and R is a data rotation of 90°. (a) Impulse response. (b) Magnitude response.

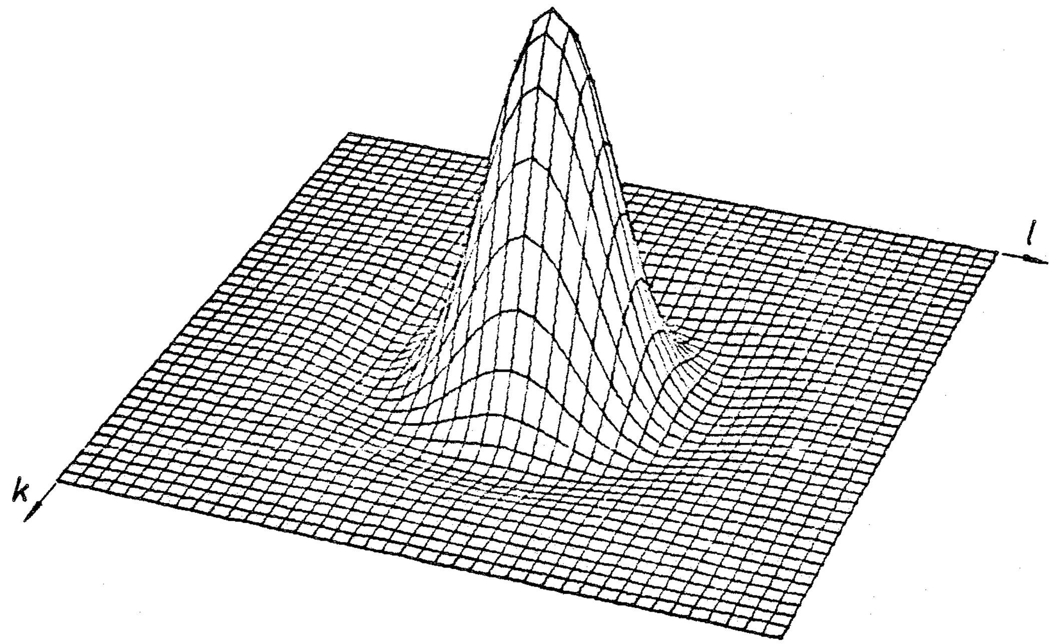

(a)

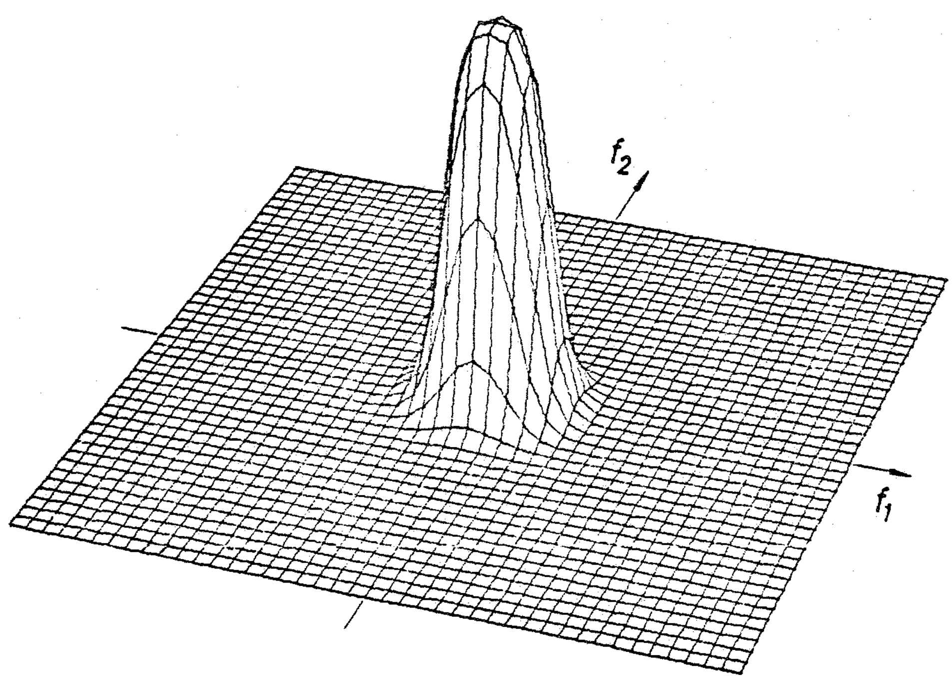

(b)

Figure 4.13. Filter formed by the combination → H → R → H → R → H → R → → H → R →, where H is the filter in Figure 4.9 and R is a data rotation of 90°. (a) Impulse response. (b) Magnitude response.

same sampling intervals in both directions. The Nyquist criterion and the required resolution impose a lower bound on the sampling frequency. The computer memory available imposes an upper bound to the number of samples and thus to the size of the image. If that size is sufficient for a given application or problem the whole data matrix can be stored within the computer random access memory and no special difficulties are encountered in implementing the image processing algorithms, apart from the inconvenience of working in two dimensions.

At the University of Toronto Computer Centre, for example, the machine for general purpose computing used for this research was an IBM SYSTEM/370 MODEL 165-II (OS/MVT with HASP) with 4 megabytes of memory. The dynamic memory pool available to the batch user was slightly under 1400 K total. This allowed direct processing of real matrices of size up to 512x512, single precision. On the other hand,the main memory available in other computer systems is very small. With 28 K of main memory, for example, only matrices of size up to 64×64 can be processed directly. Nevertheless, in any case the usable size for the image data is smaller because additional memory is required for convolution or boundary conditions, depending on the type of realization used: nonrecursive or recursive respectively.

When a datum matrix exceeds the capacity of the computer main memory, the data have to be stored, say row by row in sequential-access storage devices, such as disks or tapes. Rowwise operations are then easily done but columnwise operations are incompatible with the sequential row access storage. This is the principal difficulty in the implementation of two-dimensional digital signal processing algorithms [69].

We are next to propose some solutions for both nonrecursive and recursive realizations.

Nonrecursive realizations

Direct convolution may be easily done by having a few rows in main memory. When a row is no longer needed it is written back into auxiliary storage and a new row is read. However with extensive impulse responses fast convolution techniques must be used.

Fast convolution consists of transforming the matrices to be convolved, multiplying point by point in the transform domain and inverse transforming the result. Since this is really circular convolution, the matrices must be padded with zeros to simulate linear convolution. For example, to convolve a datum matrix of size $M_1 \times N_1$ with a filter impulse response of size $M_2 \times N_2$, transforms of size $(M_1+M_2-1) \times (N_1+N_2-1)$ must be used. In addition, these numbers should be powers of two for an efficient implementation using the FFT programs currently available; if they are not, the matrices should be padded with additional zeros. If the filter impulse response is separable it can be stored in two vectors rather than in a matrix and the two-dimensional convolution can be accomplished by repeated evaluation of one-dimensional convolutions [12, pp.115-120].

Several FFT routines (refer to Table 4.1) were coded in FORTRAN IV to meet the needs of digital image processing. One of the main features of these subroutines is that their source code (see Appendix C) is meaningful and easy to understand.

The subroutine VFFT is a one-dimensional very fast discrete

Table 4.1. FFT routines for digital image processing.

ROUTINE NAME	EXTERNAL ROUTINES NEEDED	INPUT DATA	IN PLACE	AUXILIARY STORAGE	OUTPUT DATA	UNSCRAMBLING
VFFT	-	complex vector	yes	no	complex vector	yes
FFT2	VFFT	complex matrix	yes	no	complex matrix	yes
FFT2R	VFFT RLTR	real matrix	yes	no	half of a hermitian matrix	yes
FFT2D	VFFT	complex matrix	no	yes	complex matrix	optional
FFT2DR	VFFT RLTR	real matrix	no	yes	half of a hermitian matrix	optional

Fourier transform which uses the Sande algorithm, radix 4+2, with unscrambling. This implementation of the FFT recursively calculates the twiddle factors in order to get greater speed at the expense of some loss of precision. The CPU time required to transform 1024 complex datum points (stored in 2 REAL*4 arrays) using VFFT is 47 msec. in the IBM 370-165-II.

Both FFT2 and FFT2R call VFFT to do the transform on the rows and on the columns of the two-dimensional array. FFT2 can transform a matrix of complex numbers stored either in a single complex array or in two separate arrays, one for the real part and one for the imaginary part.

In image processing, due to the large size of the arrays, it is important to use the property that the Fourier transform of a real datum matrix is hermitian (see Appendix B), thus only relevant data are stored. The subroutine FFT2R is for real data and no storage is required for the imaginary part, except for two additional rows or colums. FFT2R can take advantage of the symmetry of the transform either by rows or by columns; if only one option is desired the program size is halved. The CPU time required to transform a 256×256 matrix of real data using FFT2R is 2.7 sec. in the IBM 370-165-II.

Additional utility subroutines to be used in conjunction with FFT2R or FFT2 are also given in Appendix C. They are short and require less than 1 K of computer memory. For example: CMAG2 determines the square magnitude of the transform, COMPLT completes the transform given by FFT2R using symmetries, and CAMOVE rearranges the elements of the transform so that the element at the origin is located at the centre of the array.

When the size of the input data is considerably larger than the size of the impulse response, the ideas of block convolution using either an overlap-add or overlap-save approach can be applied. The input matrix is partitioned into blocks, each one is filtered separately and then the results are appropriately combined [70].

In all other cases the need arises for transforming large datum matrices stored sequentially in auxiliary storage. A conventional approach is to first transform by rows, transpose the intermediate datum matrix and then perform another rowwise transformation. The final result may also be transposed again to have it in normal order. However, transposing requires a separate program and considerable processing time. These fast transposing, in-place algorithms are available for random access storage devices only. Other solutions include storing the rows alternately in as many files as the radix of the FFT structure and then performing sequential operations on the rows. For a transform of length $N = 2^m$, m passes of the data are necessary for the transform plus m-1 passes for unscrambling.

We are to develop here an FFT structure for large datum matrices that requires two auxiliary files only and L passes of the data for a transform of length $N = K^L$, where K must be a power of two. The idea was suggested by Onoe [71] but many details had to be worked out before getting a workable algorithm. Its essence consists in the decomposition of the original transform of size $N = K^L$ into L steps of N/K transforms of size K. At each step the intermediate results are corrected by twiddle factors and regrouped.

We derived the equation of this DFT algorithm which is given in (4.13).

$$X(k) = X(k_o, k_1, \dots, k_{L-2}, k_{L-1}) =$$

$$= \sum_{n=0}^{N-1} x(n) \exp -j2\pi \frac{kn}{N} =$$

$$= \sum_{n_o=0}^{K-1} \sum_{n_1=0}^{K-1} \dots \sum_{n_{L-1}=0}^{K-1} x(n_o, n_1, \dots, n_{L-1}) \times$$

$$\times \exp\left\{-j2\pi \frac{(n_o+n_1K+ \dots +n_{L-1}K^{L-1})(k_o+k_1K+ \dots +k_{L-1}K^{L-1})}{N}\right\} =$$

$$= \sum_{n_o=0}^{K-1} \exp\left\{-j2\pi \frac{(k_o+k_1K+ \dots +k_{L-2}K^{L-2})\, n_o}{K^L}\right\} \exp\left\{-j2\pi \frac{k_{L-1}n_o}{K}\right\} \times$$

$$\times \sum_{n_1=0}^{K-1} \exp\left\{-j2\pi \frac{(k_o+k_1K+ \dots +K_{L-3}K^{L-3})\, n_1}{K^{L-1}}\right\} \exp\left\{-j2\pi \frac{k_{L-2}n_1}{K}\right\} \times$$

$$\vdots$$

$$\vdots$$

$$\times \sum_{n_{L-2}=0}^{K-1} \exp\left\{-j2\pi \frac{k_o n_{L-2}}{K^2}\right\} \exp\left\{-j2\pi \frac{k_1 n_{L-2}}{K}\right\} \times$$

$$\times \sum_{n_{L-1}=0}^{K-1} x(n_o, n_1, \ldots, n_{L-1}) \exp\left\{-j2\pi \frac{k_o n_{L-1}}{K}\right\} \tag{4.13}$$

where the first exponential in each summation is a twiddle factor and the second exponential together with the corresponding summation symbol and a datum sequence is a DFT of size K.

In the implementation of (4.13) the signal flow graph can be arranged in many ways. We need a structure having the same geometry for each stage thereby permitting sequential data accessing and storage. The signal flow graphs shown in Figures 4.14 and 4.15 are examples which satisfy this condition. Generalizing for $N = K^L$, we coded the subroutine FFT2D, whose simplified flow chart is given in Figure 4.16.

In a practical application an appropriate value for K must be chosen. The trade-off between K and L depends on the size N of the transform and the amount of main memory available. The best choice for K is $K = \sqrt{N}$, that is L=2, if that is possible. For L greater than two, records must be skipped with sequential access, which results in an inefficient realization. If direct access devices are available there is no need for skipping.

The unscrambling process takes considerable time; consequently, some options were provided in FFT2D to make it general and save both CPU and I/O time. This means that can take and give the data in either normal order or base-K digit reversed order, at the user's choice.

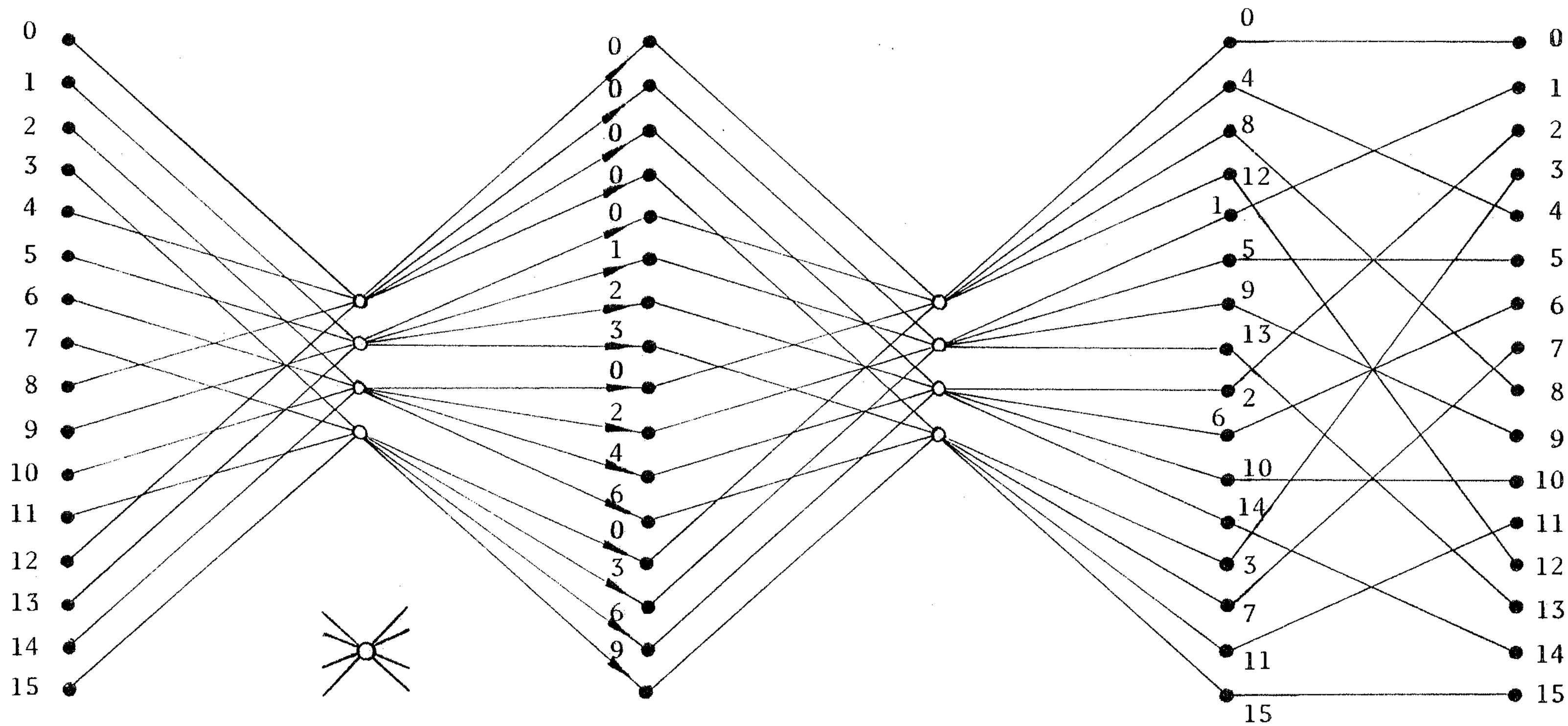

4-point FFT

Figure 4.14. Signal flow graph of a Fourier transform of size 16 decomposed into 2 steps of 4 transforms of size 4, plus unscrambling.

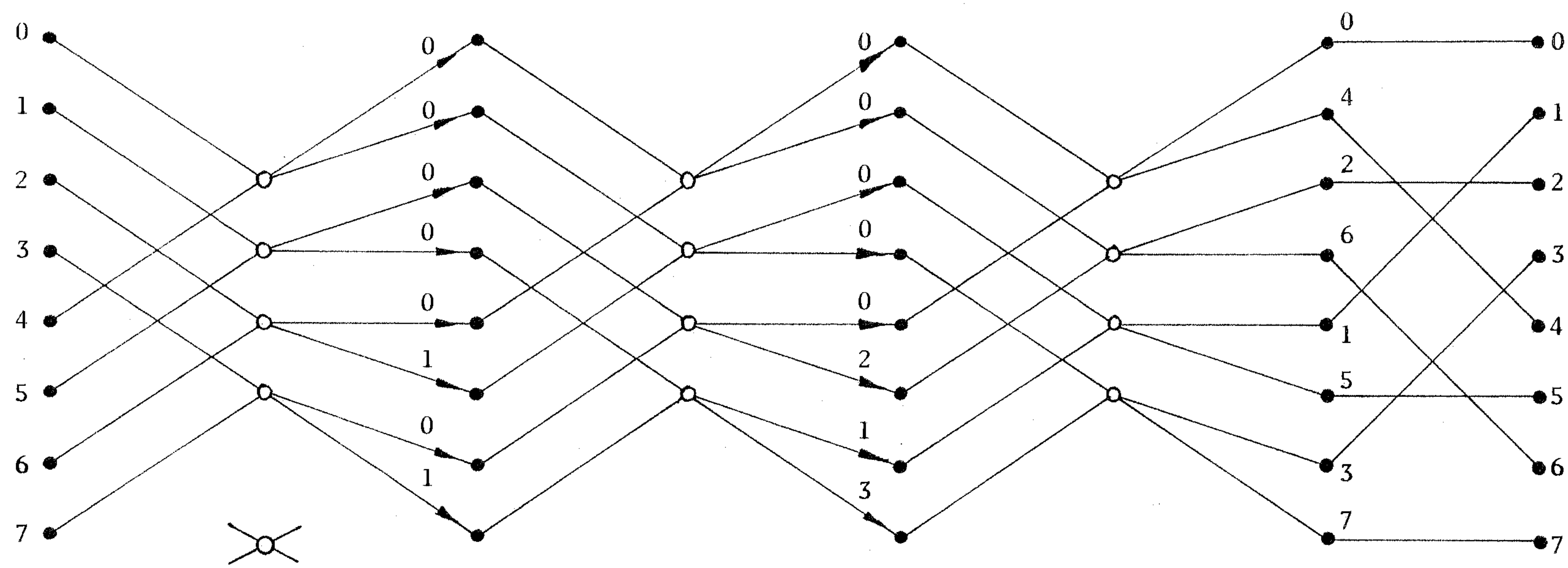

Figure 4.15. Signal flow graph of a Fourier transform of size 8 decomposed into 3 steps of 4 transforms of size 2, plus unscrambling.

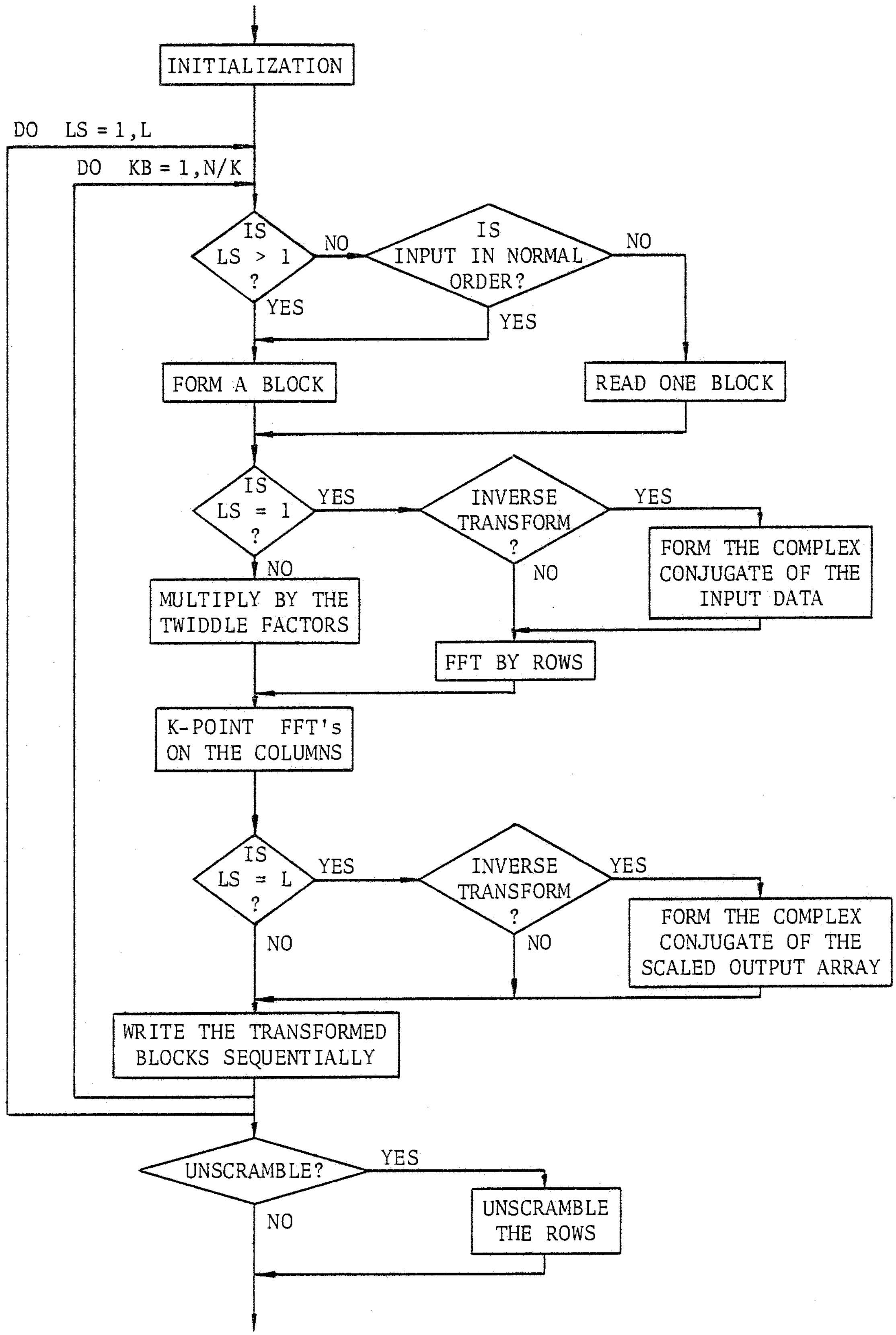

Figure 4.16. Simplified flow chart of the subroutine FFT2D.

To perform fast convolution only, for example, there is no need for unscrambling the transforms because it does not matter in what order the point-by-point multiplications are done. Only the inverse transform of the product should be unscrambled.

The unscrambling procedure for base-K digit reversal is slightly different than for (base-2) bit reversal. A flow chart of a base-K digit-reversed counter is given in Figure 4.17 (cf. Figure 6.1 in [13]).

Recursive realizations

The nature of recursive realizations makes them very suitable for sequentially stored data. Causal filters are readily implemented. Noncausal filters can be synthesized by means of the linear transformations described in the previous section. Some of these transformations (rotations by 90° and 270° and transpositions) must have access to both rows and columns at the same time for interchange operations, not easily done when the data is stored sequentially. We propose an alternative here.

Suppose that we have to implement a filter whose transfer function is a cascade of transfer functions of the type described previously. Assume that the datum matrix is too large to be contained in computer main memory and the data are stored sequentially by rows in auxiliary storage, divided into logical records of K rows each. K is chosen so that each submatrix consisting of K consecutive rows can be stored in main memory.

The key point in this implementation is the ordering of the filter sections corresponding to the cascade of elementary filters. Each filter section in the cascade has a recursive algorithm associated with

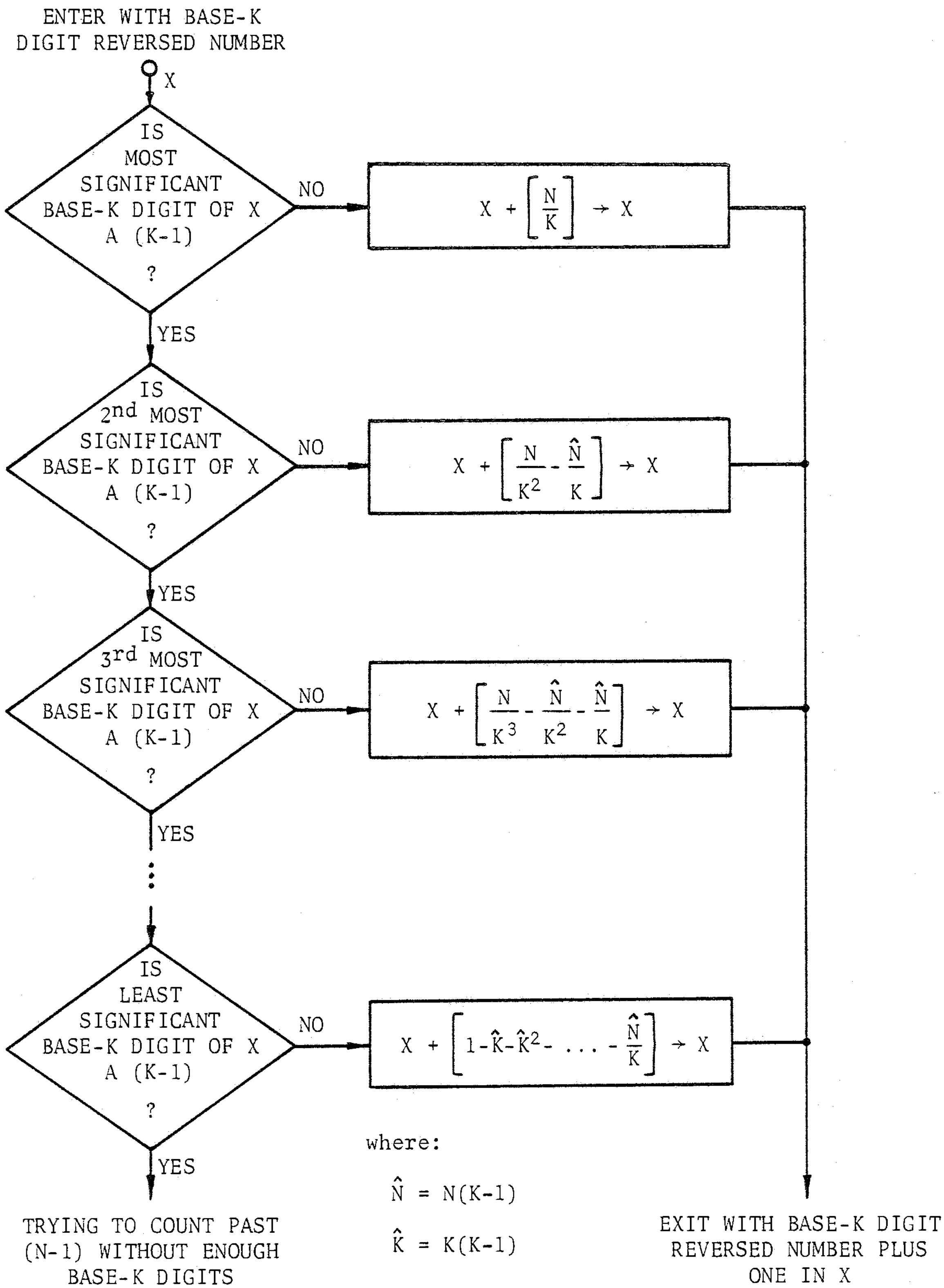

Figure 4.17. Flow chart of a base-K digit reversed counter.

it. Figure 4.6 shows all the possibilities for the direction of recursion, sense of recursion and starting point on the input datum matrix. Since that matrix has been divided into submatrices of K rows each, which will be processed sequentially, the filter sections whose diagrams have arrows originating in the first row and those with arrows originating in the last row cannot be implemented simultaneously. Therefore, we lump together all the filter sections whose diagrams have arrows originating in the bottom row (namely, Figures 4.6 (a), (b), (e), and (h)) followed by a second set of filters whose diagrams have arrows originating in the top row (namely, Figures 4.6 (c), (d), (f), and (g)). Then successively read each record (submatrix of K rows) into the computer main memory and process it with the first set of filters using the technique of datum transformations previously discussed. The result is written back into auxiliary storage. The last output row of each elementary filter must be saved in main memory to serve as the initial conditions for the next record. The same process is done with the remaining records until all the data have been processed. Then the operation is repeated for the second set of filters and with the records in reverse order.

Thus, this technique is compatible with the sequential access of the data and at most two passes of the data through main memory are necessary. It should be noted that two passes are necessary in implementing filters with zero-phase response, only one pass would be required in some cases where the zero-phase response requirement is not necessary.

Chapter V

IMPLEMENTATION OF THE PROPOSED TOMOGRAPHIC FILTERS

5.1 Introduction

In the previous chapters of this thesis we analyzed the problem of recovering three-dimensional information from radiographs, presented a solution, and developed a technique to implement that solution. In this chapter all these elements are combined for the synthesis of tomographic filters in a digital computer. The practical problems associated with the digitization, processing, and reconstruction of pictorial information are considered.

Tomographic filters are tested with computer-generated test patterns. The effect of tomographic filters on radiographs of a test phantom with lesions at different depths is also investigated for several operating conditions of the X-ray system. Finally, we present some suggestions for the implementation of tomographic filters in a clinical environment.

5.2 Synthesis of Tomographic Filters with a Digital Computer

In this section we show how the design and realization of tomographic filters are implemented with the help of a digital computer. The procedure for getting imagery in and out of the computer is discussed. Examples of the magnitude response of typical tomographic filters are given here, but the discussion of actual processing results is done in Sections 5.3 and 5.4.

5.2.1 Preparation and Digitization of Imagery

The data which must first be collected are the characteristics of the radiologic system, a radiograph or set of radiographs, and information on the geometries of the set-ups.

The radiologic system can be characterized by a pin-hole image of the focal spot and the geometry of the set-up. The distances from the pin-hole to the focal spot and to the film plane should be determined. An important piece of information is the relative orientations of the focal-spot pin-hole image and the radiographs. The object magnification for the layers of interest should also be noted.

The pictorial information is on film and must be sampled for processing in a digital computer.

Digitization of pictorial information

The equipment used for the digitization of images is briefly described in Appendix D. It consists basically of a CVI video compressor (model 260) conected to a DEC minicomputer (PDP-11). The input medium to the system is a television camera [72]. This is a cheap, widely available and versatile device, although it does not perform as well as other devices in terms of resolution, signal-to-noise ratio, linearity, and dynamic range [73]. We used a SONY portable television camera with a zoom lens to vary the size of the field. The best resolution that we could obtain was 3 to 4 samples/mm. in an area of approximately 60×60 mm^2. With this system the sampling rate is different in each direction and varies depending on the relative positions of the camera and film, and the zoom lens. Since in our processing the knowledge of the sampling rates is necessary, we used windows made of black cardboard and of known size. The sampling rate in each direction is then given by the number of samples from edge to edge of the window in that direction divided by the distance between edges. We used 50×50 mm^2 windows for the radiographs to be processed with tomographic filters and 10×50 mm^2 windows for the pin-hole images of the focal spot (including a reference point on each of two sides of the pin-hole image).

The film was placed on a portable viewing box which produced a uniform light intensity distribution behind the film. To eliminate unwanted glare, only the portion of the film to be digitized was kept uncovered. Black cardboard was also arranged around the viewing box to provide a shade from light pollution in the room.

Although the full resolution of this system is 256x256 samples. we only used 210x210 to avoid the poorer signal-to-noise ratios in the edges and corners.

The digitized images were quantized to 6 bits (64 grey levels) and stored on magnetic tape for off-line processing.

Image analysis

Some of the digitized radiographs were analyzed by evaluating their power spectra and power cepstra. Welch's method of power spectrum estimation extended to two dimensions [55] was used.

We noted the presence of high frequency side lobes on one of the frequency axes of the power spectra. A visual inspection of the radiographs did not provide a reason for this effect, which did not occur in the power spectra of computer simulated radiographs. It was then suspected that this was an artifact induced by jitter in the scanner itself. Indeed, if the scan lines are not uniformly spaced, an artificial spatial shift of each line results. This shifted line then introduces artificial high frequency edges within the image that are perpendicular to the scan lines [74].

To prove this hypothesis the same region of a radiograph without lesions was digitized three times with three different orientations (0°, 45°, and 90°). Naturally, in the absence of scanner jitter, the spectrum of each digitized radiograph should be rotated by the same amount as the radiograph [68]. In this experiment, rather than applying the costly power spectrum estimation techniques, the two-dimensional DFT was used. The digitized radiographs were multiplied by an appropriate weighting function to reduce other sources of energy aligned with the frequency axes, and then transformed.

We found in each case the presence of high frequency energy on the axis perpendicular to the scan lines. To double check, the digitized radiographs were rotated in the computer and Fourier transformed again. We found that the spectra had also been rotated. Therefore we concluded that the high frequency components were not due to noise asymmetries in the two-dimensional FFT that we used, but were due to jitter in the scanner.

5.2.2 Scaling of the PSF

At the end of Chapter III we already discussed how the PSF can be obtained and approximated by a separable function to save memory in the design of a tomographic filter. However, the sampling intervals of the digitized PSF are not generally equal to those of the digitized radiograph and the size of the focal-spot pin-hole image must be scaled to match the PSF for those layers of interest.

Since we used batch processing, it was decided that the approximation of the PSF by a separable function, the equalization of the sampling intervals with those of the radiograph, and the scaling of the PSF were best done by a separate program prior to processing.

Suppose that the focal-spot pin-hole image was obtained with focal-spot to pin-hole distance Δ_1 and pin-hole to film distance Δ_2 and is digitized with sampling intervals S_x and S_y, thus obtaining $M_x \times M_y$ samples.

Assume that the radiographs were sampled with sampling intervals T_x and T_y. Let d_1 and d_2 denote the distances from the focal spot to the layer of interest and from that layer to the film, respectively.

The PSF for that layer is then obtained (see Fig. 5.1) by scaling the pin-hole image of the focal spot according to (5.1).

$$x = x_o \frac{\Delta_1}{\Delta_2} \frac{d_2}{d_1} \tag{5.1a}$$

$$y = y_o \frac{\Delta_1}{\Delta_2} \frac{d_2}{d_1} \tag{5.1b}$$

where x_o and y_o are distances on the focal-spot pin-hole image and x and y are distances on the radiograph.

The number of samples $N_x \times N_y$ necessary to contain the PSF is given by

$$N_x = M_x \frac{S_x}{T_x} \frac{\Delta_1}{\Delta_2} \frac{d_2}{d_1} \tag{5.2a}$$

$$N_y = M_y \frac{S_y}{T_y} \frac{\Delta_1}{\Delta_2} \frac{d_2}{d_1} \tag{5.2b}$$

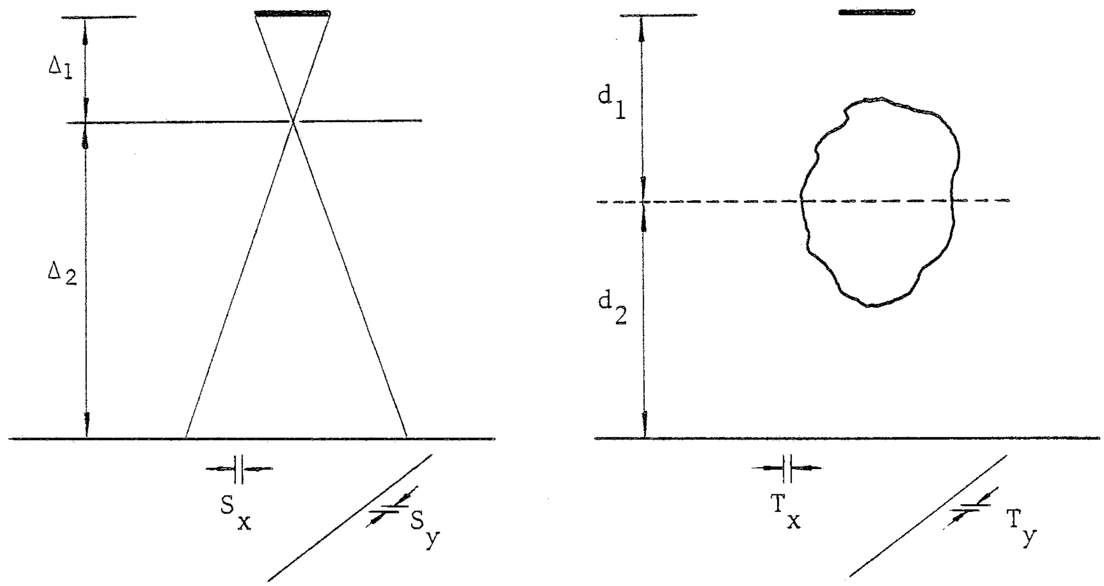

Figure 5.1. Geometries of the set-ups for the focal-spot pin-hole image and for the radiographs.

In certain cases (cf. Section 5.4) the sampling rates in the radiographs are not sufficient to properly define the PSF, so tomographic processing is not possible.

The previously described procedure was not necessary in the simulations of Section 5.3 because we had total control of the sampling frequencies and chose separable focal-spot intensity distributions.

5.2.3 Design of Digital Tomographic Filters

Once the PSF for a layer of interest has been determined, a separate program is used to design digital tomographic filters with certain parameters. These parameters are chosen from a plot of the magnitude response of the ideal inverse filter. From the frequencies at the poles and the magnitude response at critical points, several sets of hard limits and cutoff frequencies can be chosen. Other necessary parameters are the size of the filter impulse response and the parameter

β used in the Kaiser-windowing technique (cf. Chapter IV). The design of the tomographic filter is then straightforward.

The separable PSF is given by two sequences of length N_x and N_y (cf. (5.2)), or only by one if they are identical. The DFT coefficients are then determined with sufficient resolution. The subroutine INVFHL is used to obtain the magnitude response of the tomographic filter with the given hard limit. At this point an ideal low-pass filter is cascaded with the tomographic filter to reduce the high frequency noise.

An FIR digital filter is then designed by transforming the frequency response of the tomographic filter back to the space domain. The impulse response is multiplied by a Kaiser window of appropriate length with parameter β. Normally we use a high β, such as $\beta=9$, in order to obtain low ripples in the stopband and a smooth transition band. The DFT is used once more to obtain the coefficients of the tomographic filter in a form suitable for fast convolution realizations.

To keep the previously described design procedure under control, relevant plots were produced at each step. A typical example of the design of a tomographic filter for a certain layer is shown in Figure 5.2.

Examples of tomographic filters that were actually used are given in Figures 5.3 to 5.5. It can be seen that the high-pass nature of an inverse filter in cascade with a low-pass filter gives band-pass characteristics to tomographic filters.

5.2.4 Filtering the Data

Filtering is the simplest operation in the whole process, although it is the one that requires the most CPU time.

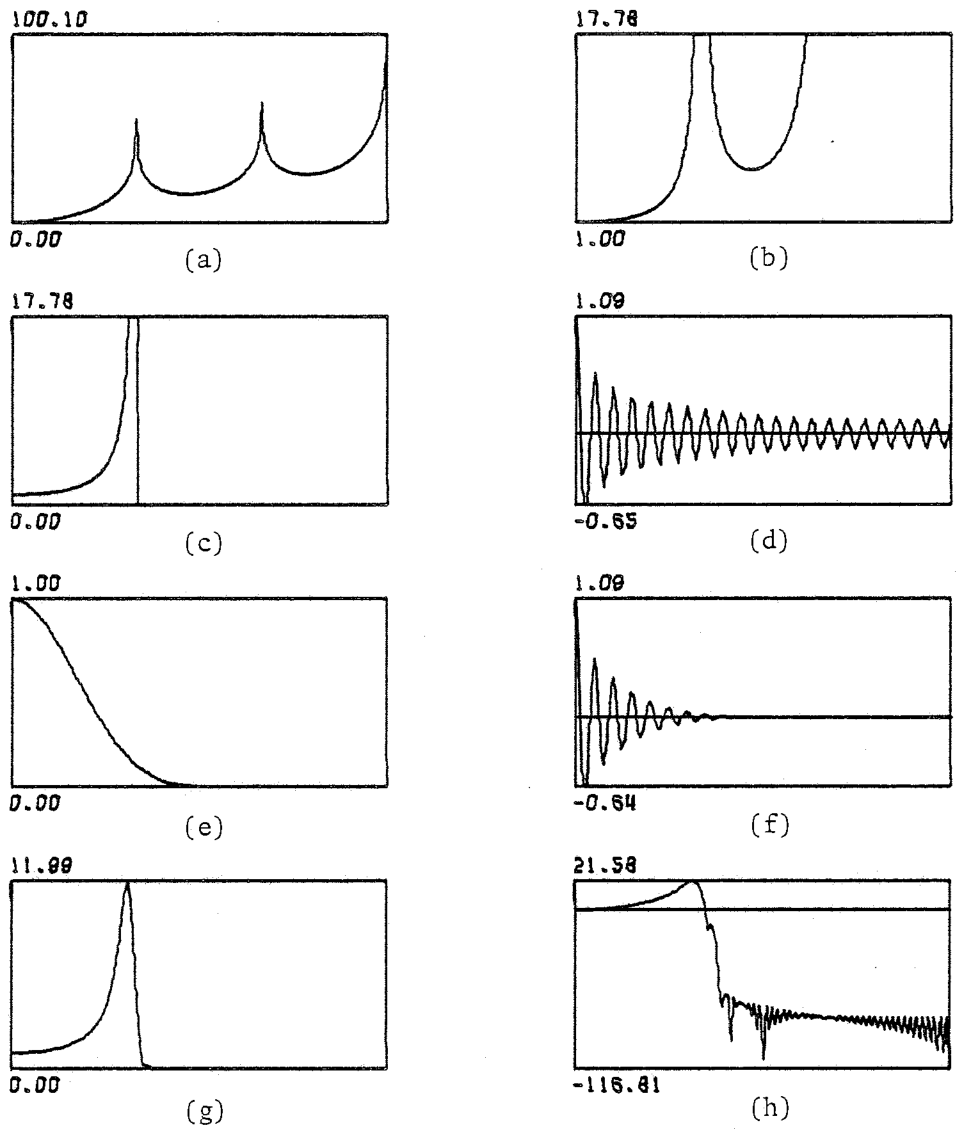

Figure 5.2. Plots of relevant functions in the design of a digital tomographic filter using the windowing technique. (a) Ideal inverse filter (in dB). (b) Inverse filter with hard-limited magnitude response. (c) The filter in b) cascaded with an ideal low-pass filter. (d) Impulse response of the filter in c). (e) Kaiser window with $\beta=9$. (f) Windowed impulse response. (g) Magnitude response of the tomographic filter. (h) Same as g) in dB.

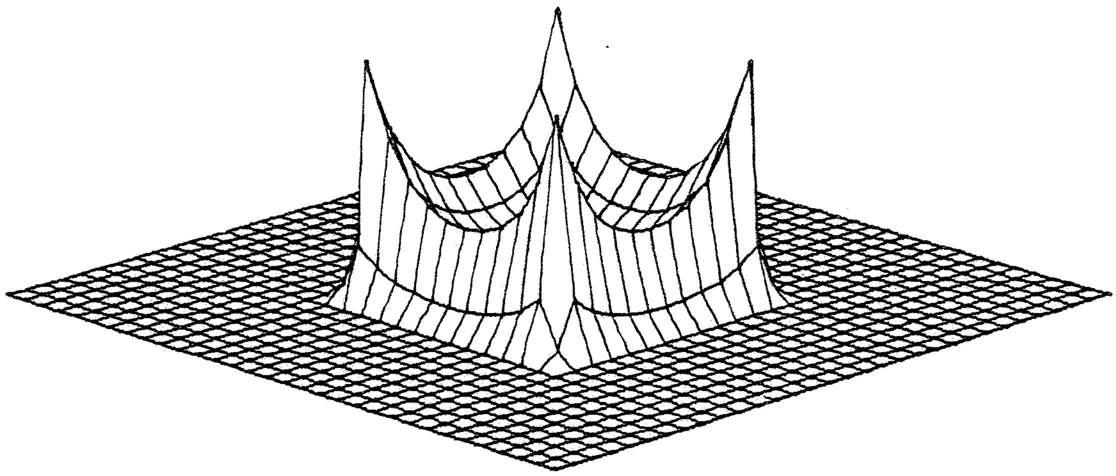

(a)

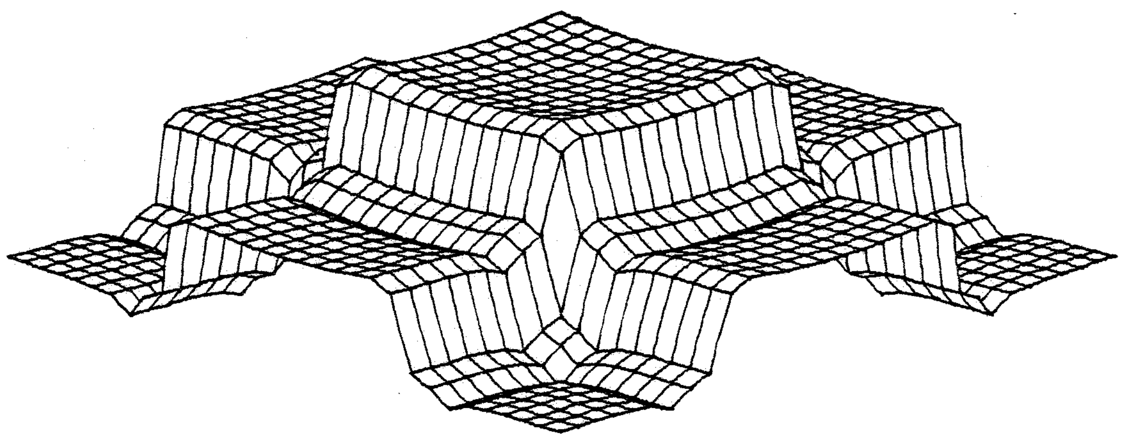

(b)

Figure 5.3. Tomographic filter used to obtain Figure 5.10(c).
(a) Magnitude response. (b) Magnitude response in dB.

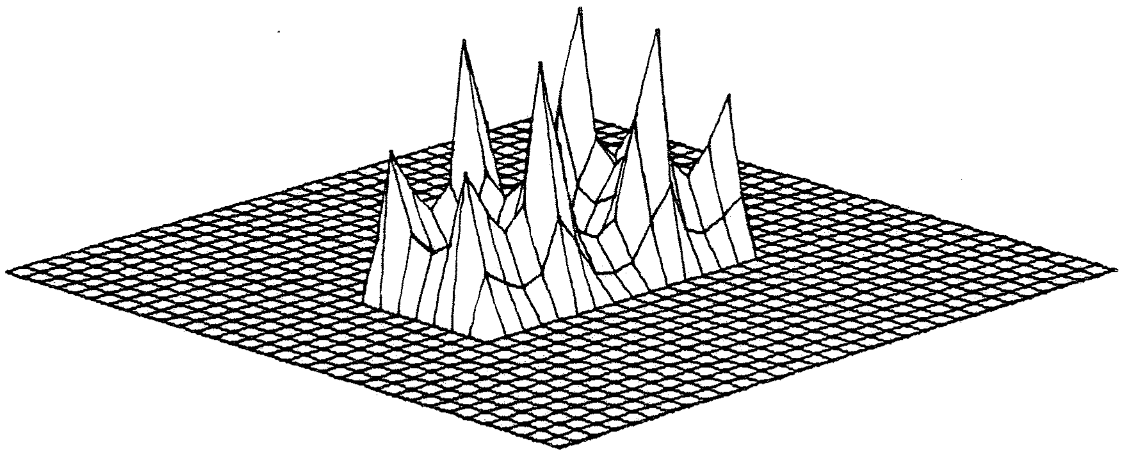

(a)

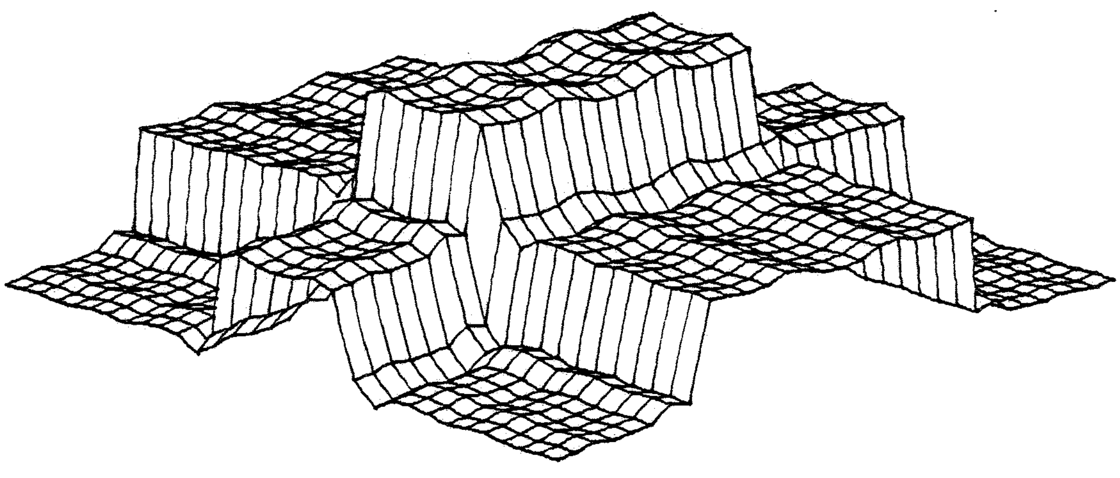

(b)

Figure 5.4. Tomographic filter used to obtain Figure 5.17(b).
(a) Magnitude response. (b) Magnitude response in dB.

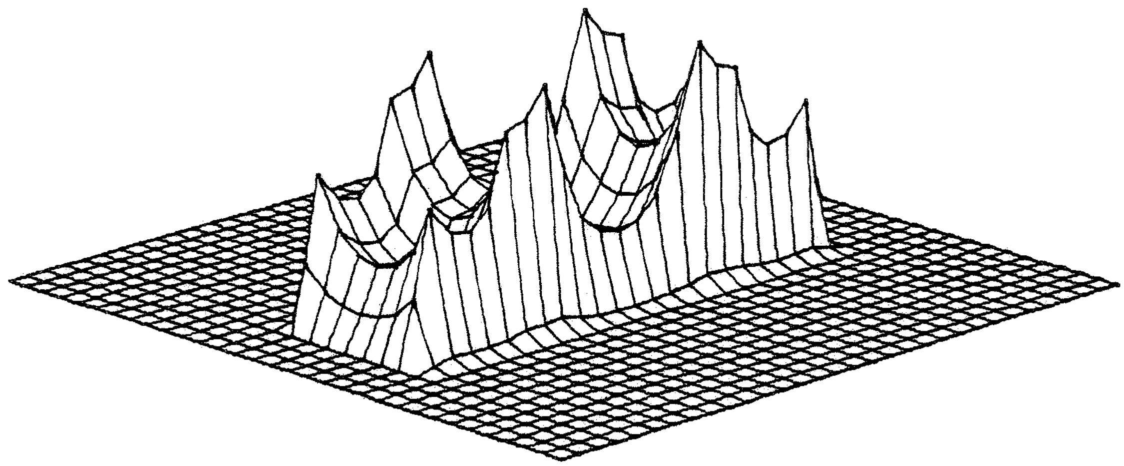

(a)

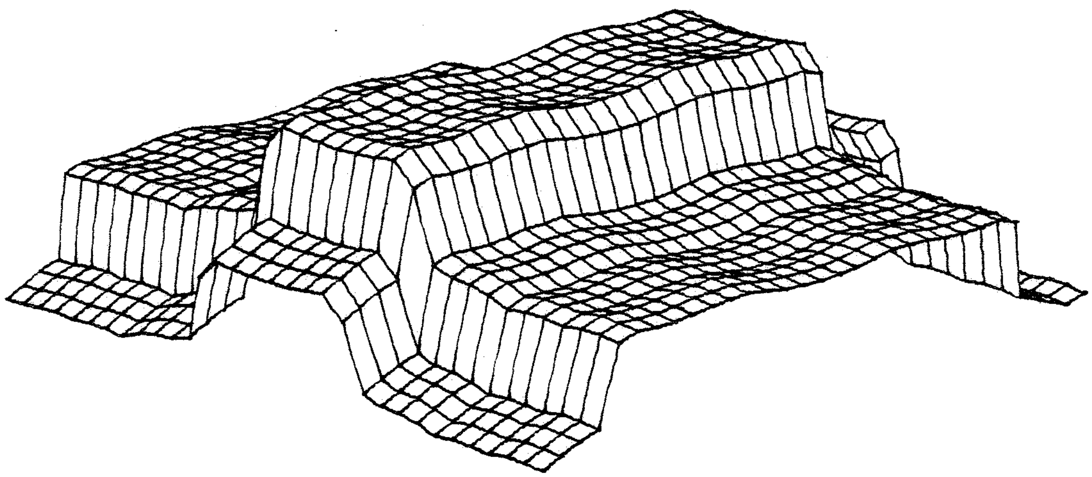

(b)

Figure 5.5. Tomographic filter used to obtain Figure 5.17(c).
(a) Magnitude response. (b) Magnitude response in dB.

A portion of the radiograph is chosen and multiplied by a two-dimensional cosine taper data window to reduce the effects of leakage (see Figure 5.6). It is then Fourier transformed with the subroutine FFT2R. We found the size 256×256 to give a good trade-off between resolution and cost.

The two-dimensional DFT of the radiograph and the filter coefficients are complex multiplied point-by-point. The result is inverse transformed, quantized to 6 bits, and stored on magnetic tape. It may also be displayed in a line printer using the subroutine PICPRT (see Appendix C). The use of the line printer in batch processing to obtain pictorial outputs by overprinting of characters has the advantage of producing an immediate hard copy without distortions which is to some extent quantitative. Nevertheless this type of display is not too appealing to the eye.

5.2.5 Image Reconstruction

The digitized images were displayed off-line on a commercial television monitor using the CVI video expander (model 261A) which is described in Appendix D. Hard copies were obtained with either a 35 mm. photographic camera or an instant camera. A hood was used to shield the display against light pollution. The television system introduces some distortions in size which in general can be tolerated.

Since the sampling intervals are assumed different with this equipment, we precompensated for this by interpolating in the direction of the scan lines, thus reducing the number of samples to obtain a better square ratio. In addition, to improve the visual effect of small images,

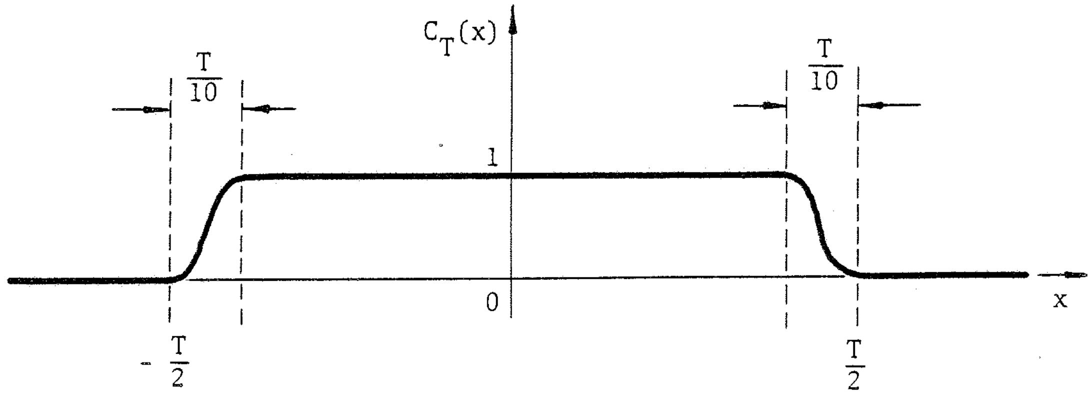

$$C_T(x) = \begin{cases} 1 & |x| < T/2 - T/10 = 2T/5 \\ 0.5[1+\cos\{(|x|-2T/5)10\pi/T\}] & 2T/5 \le |x| \le T/2 \\ 0 & |x| > T/2 \end{cases}$$

(a)

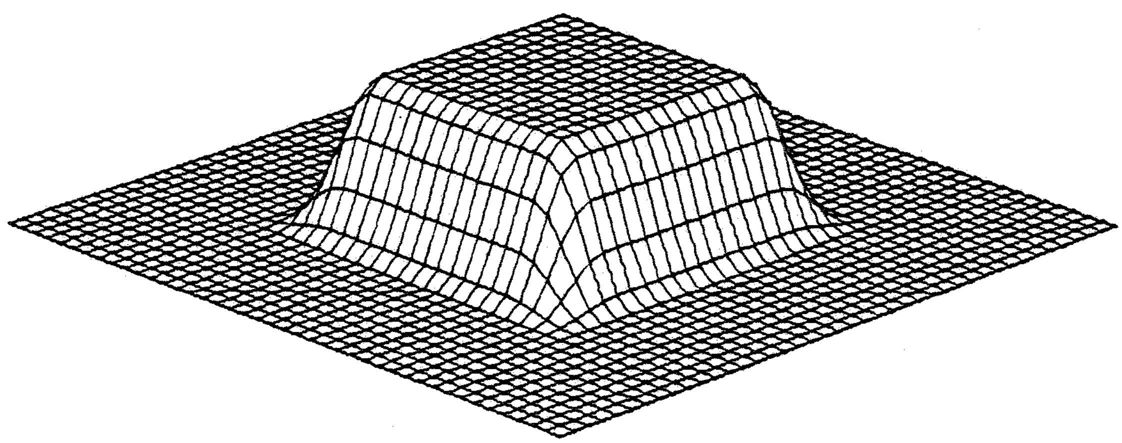

$$\hat{C}_T(x,y) = C_T(x)\ C_T(y)$$

(b)

Figure 5.6. Cosine taper data window. (a) One-dimensional. (b) Two-dimensional.

they were interpolated up to the full resolution of the system.

Any type of simple polynomial interpolation can be used for these purposes. Zero-order interpolation and linear interpolation techniques have been used in the past for similar problems [2]. Recently, a class of interpolation functions, for the purpose of displaying interpolated images with cosmetically pleasing effects have been suggested in the literature [73], [75]. They are the one- and two-dimensional spline functions of order m with continuous derivatives of order 1 to m-1. In all the examples shown in Sections 5.3 and 5.4 we have used bilinear interpolation, to adjust the size of the image to the full resolution of the display. The bilinear interpolation simply interpolates linearly between two samples to generate other samples, in each direction.

5.3 Test of Tomographic Filters with Computer Simulated Radiographs

Before trying to filter actual radiographs, computer simulations were used in order to have more control on the object, focal-spot intensity distribution, noise, etc.

5.3.1 Computer Simulation of Radiographs

For the simulation of radiographs, test patterns were generated in the computer. The basic test pattern consists of a series of converging bars. Assuming an isotropic system there is no need to consider bars in all orientations forming a circule as in a star test pattern. By considering one orientation only, the resolution can be increased. The convergence of the bars provides different spacings among them and therefore the effect of filtering on different frequencies can be examined. In order to have a three-dimensional object we superimposed two flat test patters at two different levels and oriented at 90°, with respect to one another. This superposition of the bars gives a worst case condition kind of test, because of the overlapping of structures from different layers in the projection.

Two focal-spot intensity distributions were used, both separable: uniform-square (Figure 3.7) and Gaussian with $\sigma_1=\sigma_2=2$ (Figure 3.9). The uniform-square intensity distribution constitutes a bad case because of the zeros and phase reversals in the transfer function. The Gaussian intensity distribution constitutes a good case because the Gaussian function is so well behaved.

The details of the simulations (using the subroutine XRAY, see Appendix A) are summarized in Tables 5.1 and 5.2. The pictorial results are shown in Figure 5.7. The difference between Figures 5.7(b) and 5.7(c) is only in the object. In Figure 5.7(c) an object with bars of 50% absorption was used, while in all the other figures the bars in the object had 100% absorption. For comparison purposes and in order to have an ideal image as a reference, Figure 5.7(d) shows a simulation of an X-ray image obtained with a punctual focal spot. In Figure 5.8 magnifications of the central part of the radiographs in Figure 5.7 are shown. They are multiplied by a two-dimensional cosine taper data window and their corresponding two-dimensional Fourier transforms are shown in Figure 5.9.

Figures 5.7(d) and 5.8(d) show a block-like structure not visible in the other simulated radiographs because it is smeared out by the blur. This block-like nature is due to the magnification of the sampling intervals in the object when they are projected on the film (see Tables 5.1 and 5.2 for information about the sampling intervals). The solution

Table 5.1. Completion messages in the simulation of radiographs with a uniform-square focal spot.

XRAY SIMULATION COMPLETED. THE CHARACTERISTICS OF THE SYSTEM ARE AS FOLLOWS:

		FOCAL_SPOT	OBJECT	FILM
DIMENSIONS	X	2.000000	25.50000	60.00000
	Y	2.000000	25.50000	60.00000
NUMBER OF SAMPLES	X	10	100	256
	Y	10	100	256
SAMPLING INTERVALS	X	0.2000000	0.2550000	0.2343750
	Y	0.2000000	0.2550000	0.2343750
FOCAL SPOT TO FILM DISTANCE		1000.000		
ANGLE OF FOCAL SPOT (IN RADIANS)		0.0000000		
NUMBER OF LAYERS IN OBJECT			2	
OBJECT TO FILM DISTANCE	LAYER 1		400.0000	
	LAYER 2		600.0000	
INTENSITY RANGE	AIMAX			0.9999999
	AIMIN			0.0000000

THE SIMULATED RADIOGRAPH HAS BEEN STORED IN UNIT 1

Table 5.2. Completion messages in the simulation of radiographs with a Gaussian focal spot.

XRAY SIMULATION COMPLETED, THE CHARACTERISTICS OF THE SYSTEM ARE AS FOLLOWS:

		FOCAL_SPOT	OBJECT	FILM
DIMENSIONS	X	2.800000	25.50000	60.00000
	Y	2.800000	25.50000	60.00000
NUMBER OF SAMPLES	X	12	100	256
	Y	12	100	256
SAMPLING INTERVALS	X	0.2333333	0.2550000	0.2343750
	Y	0.2333333	0.2550000	0.2343750
FOCAL SPOT TO FILM DISTANCE		1000.000		
ANGLE OF FOCAL SPOT (IN RADIANS)		0.0000000		
NUMBER OF LAYERS IN OBJECT			2	
OBJECT TO FILM DISTANCE	LAYER 1		400.0000	
	LAYER 2		600.0000	
INTENSITY RANGE	AIMAX			0.9999999
	AIMIN			0.0000000

THE SIMULATED RADIOGRAPH HAS BEEN STORED IN UNIT 1

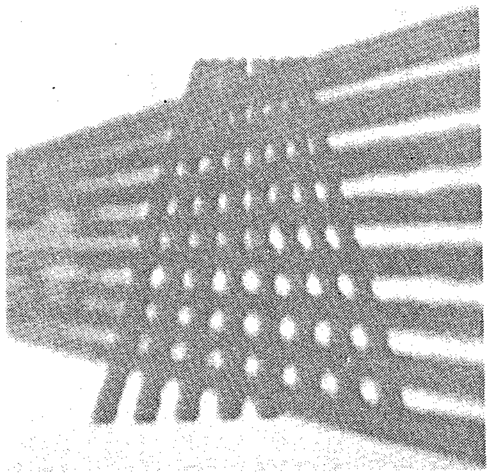

(a)

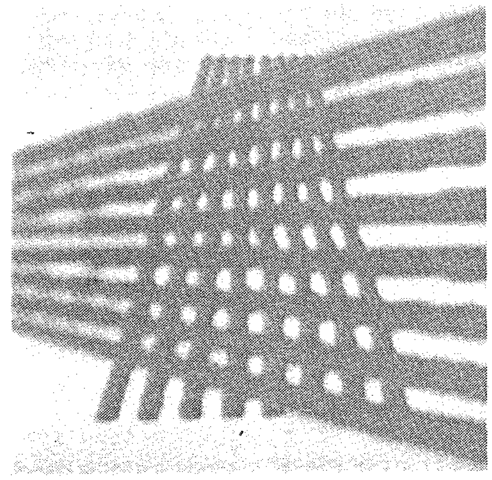

(b)

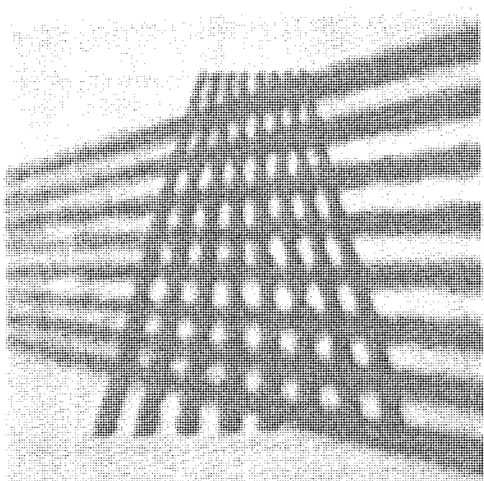

(c)

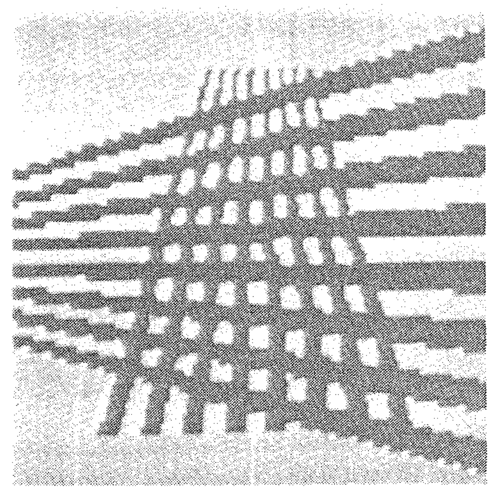

(d)

Figure 5.7. Simulated radiographs with different focal-spot intensity distributions. (a) Uniform-square. (b) Gaussian. (c) Gaussian (50% object absorption). (d) Point source.

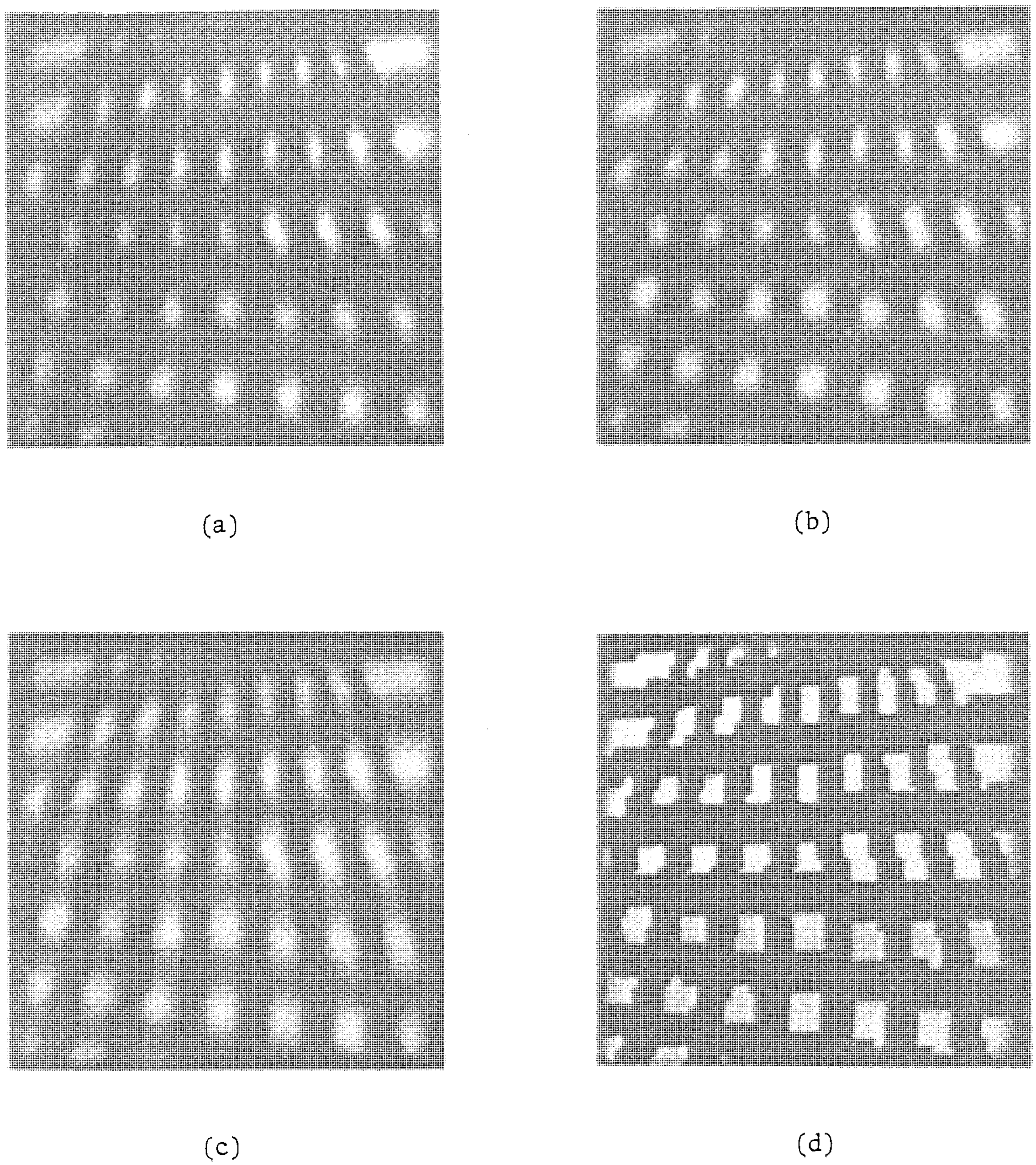

Figure 5.8. (a)-(d) Magnification of the centre parts of the radiographs in Fig. 5.6 [(a)-(d), respectively] multiplied by a two-dimensional cosine taper data window.

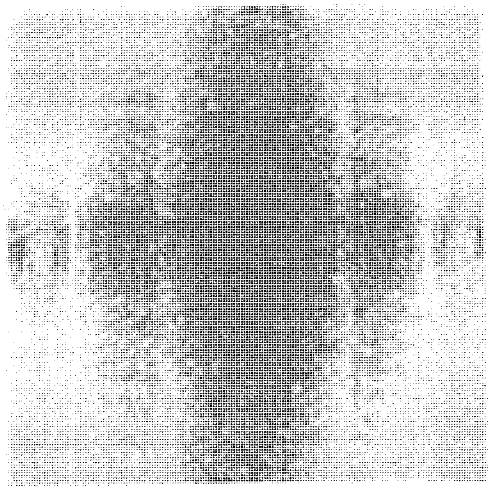

(a)

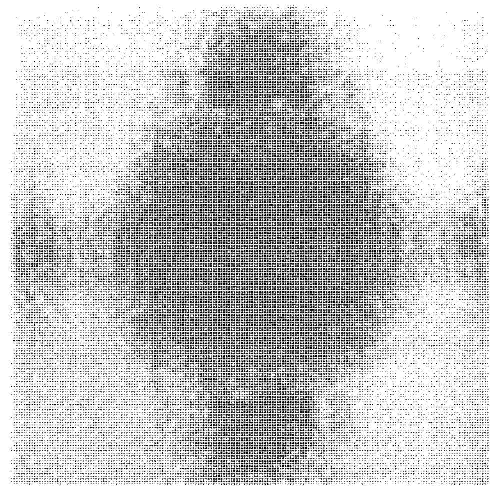

(b)

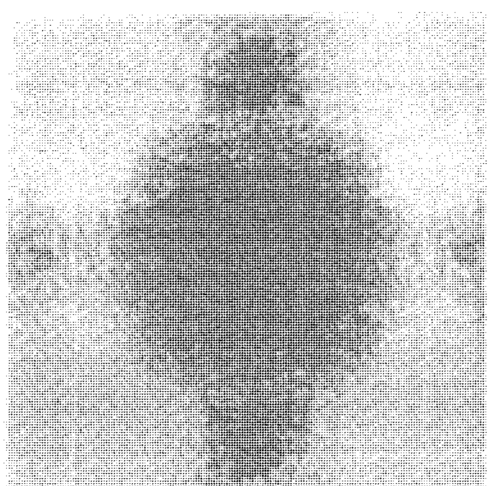

(c)

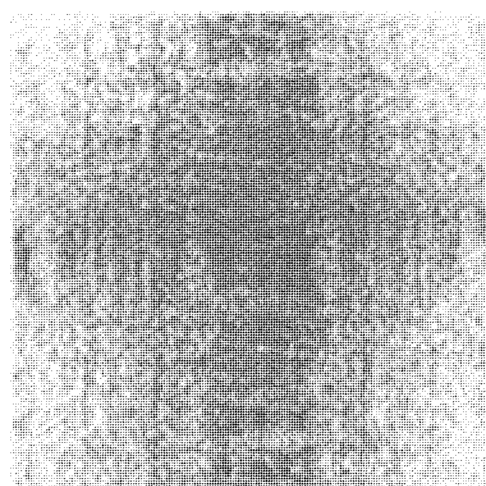

(d)

Figure 5.9. (a)-(d) Two-dimensional Fourier transforms (in dB) of the radiographs in Figure 5.7 (a)-(d), respectively.

that minimizes the error in the staircase approximation is to use sampling intervals in the object equal to the sampling intervals in the film divided by the magnification factor. However, that would result in enormous computer memory requirements. On the other hand, this block-like structure is advantageous in these tests, because it permits the evaluation of the recovery of small details with tomographic filters.

5.3.2 Processing with Tomographic Filters

We tried to keep the simulations and subsequent processing as noiseless as possible so that we could concentrate on the evaluation of tomographic filters. In practical applications noise is the limiting factor to the resolution that can be attained.

Tomographic filters were designed as discussed previously. The impulse response had 129×129 samples and the number of samples to be processed was 128×128, which results in two-dimensional transforms of size 256×256 to implement the convolution.

The results of tomographic filtering are shown in Figures 5.10 to 5.12. The characteristics of the filters used are summarized in Table 5.3. The hard limits and cutoff frequencies were chosen here by trial and error. A discussion of the results follows.

Figures 5.10 to 5.12 should be compared with Figures 5.8 (a)-(c), respectively, and Figure 5.8 (d) to draw the conclusions. In each case we desire to restore the sharpness of the image of one layer and degrade other images. Layers closer to the focal spot have an impulse response of greater extent. Inversely, the magnitude response will be of greater extent for those layers closer to the film; therefore, restoration is

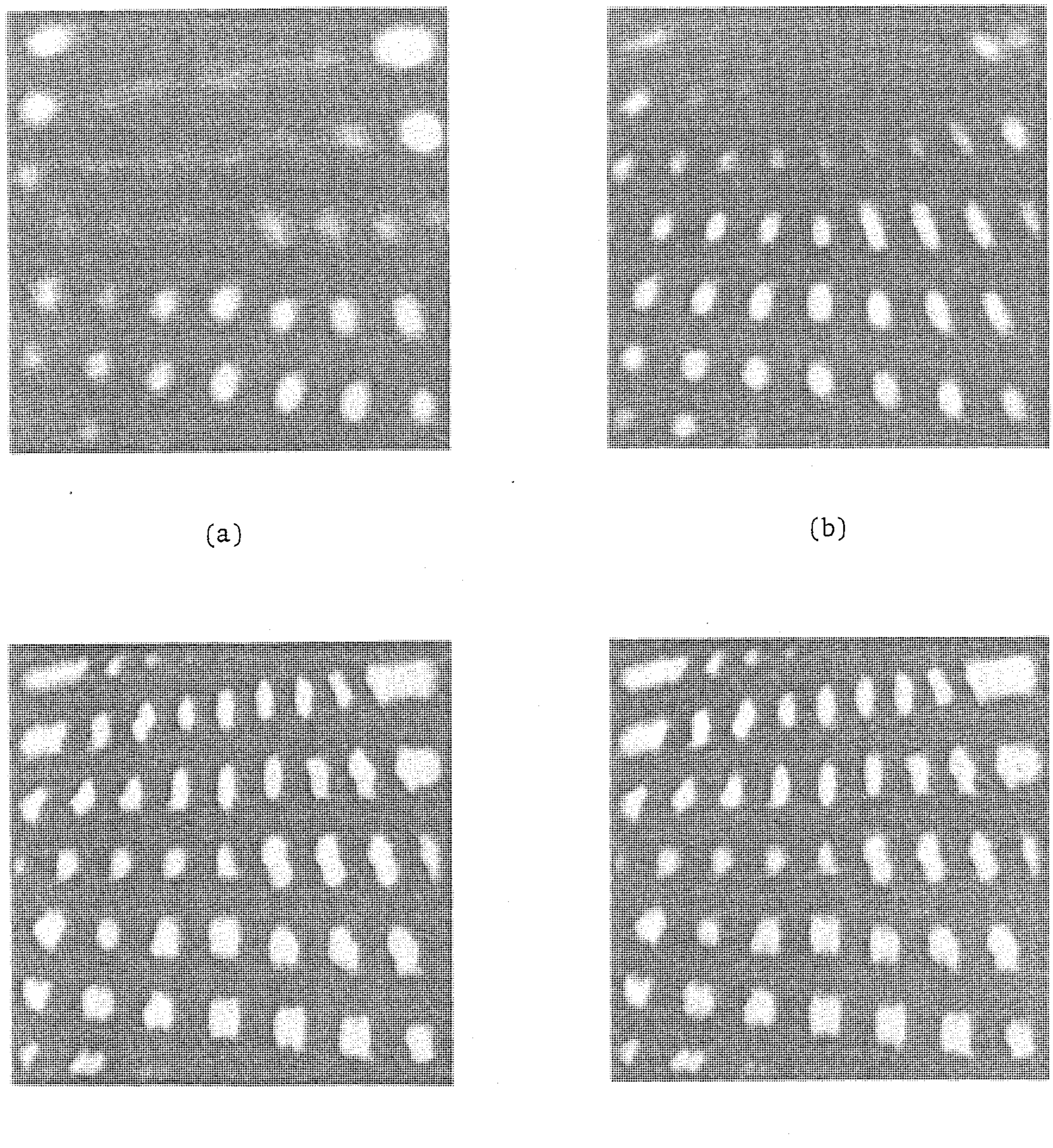

Figure 5.10. Results of filtering Figure 5.7(a) with tomographic filters. For layer 2: (a) h_ℓ=10 dB, (b) h_ℓ=20 dB. For layer 1: (c) h_ℓ=20 dB, (d) h_ℓ=30 dB.

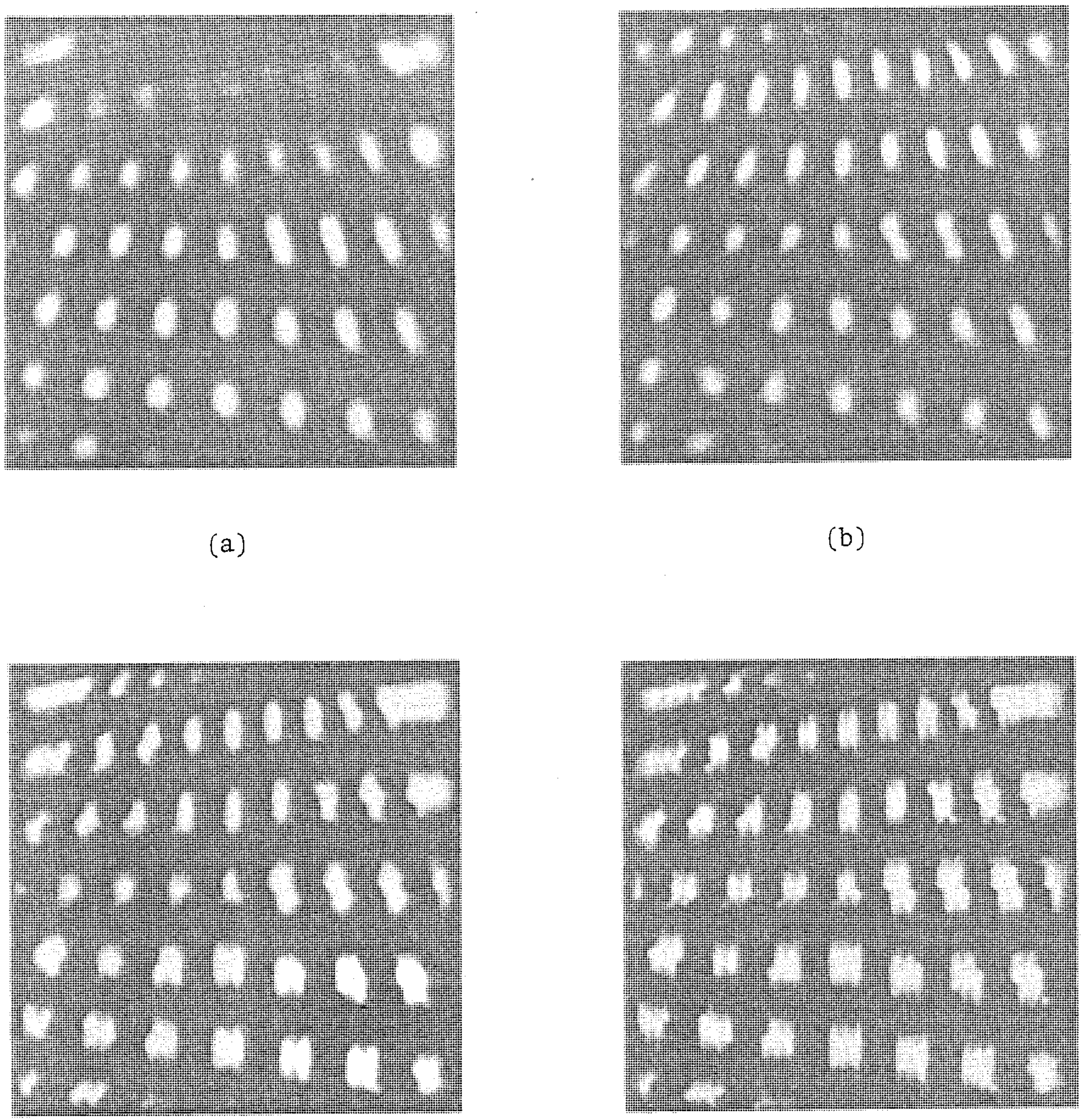

(a) (b) (c) (d)

Figure 5.11. Results of filtering Figure 5.7(b) with tomographic filters. For layer 2: (a) h_ℓ=10 dB, (b) h_ℓ=20 dB. For layer 1: (c) h_ℓ=20 dB, (d) h_ℓ=40 dB.

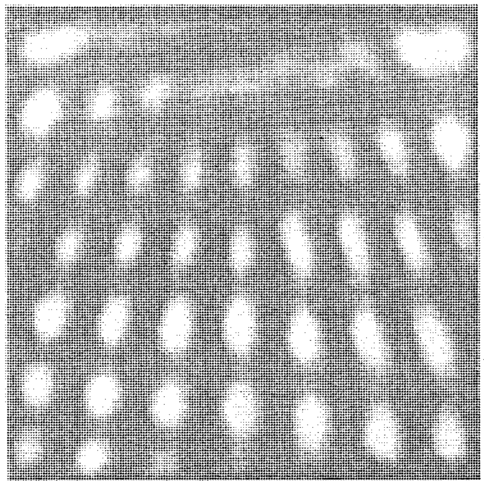

(a)

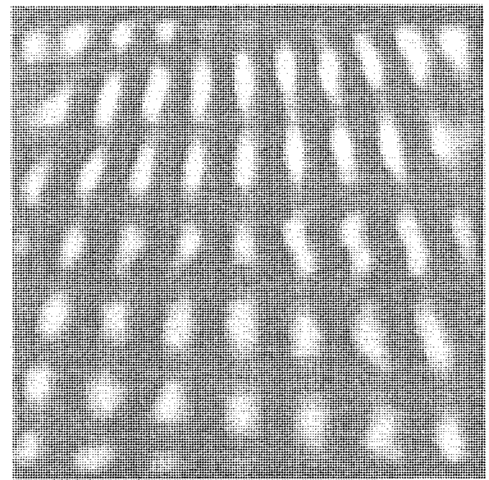

(b)

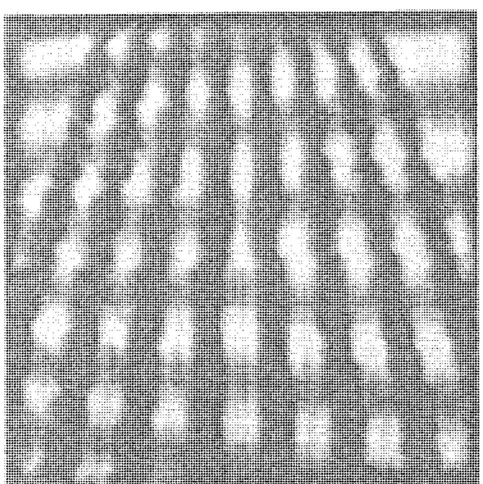

(c)

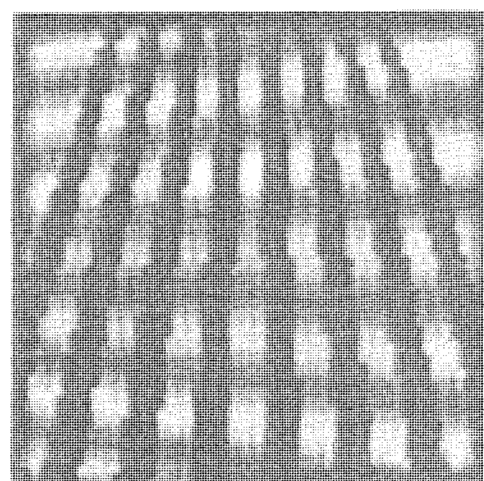

(d)

Figure 5.12. Results of filtering Figure 5.7(c) with tomographic filters. For layer 2: (a) h_ℓ=10 dB, (b) h_ℓ=20 dB. For layer 1: (c) h_ℓ=20 dB, (d) h_ℓ=40 dB.

Table 5.3. Summary of the characteristics of the tomographic filters used to obtain Figures 5.10 to 5.12.

RESULTING FIGURE	ORIGINAL FIGURE	FOCAL SPOT	LAYER TO DEBLUR	h_ℓ (in dB)	LOW-PASS FILTER BANDWIDTH (cycles/mm)	BLUR SIZE (in mm.)
5.10(a)	5.8(a)	Uniform-square	2	10	0.21	3.0
5.10(b)	5.8(a)	"	2	20	0.31	3.0
5.10(c)	5.8(a)	"	1	20	0.78	1.2
5.10(d)	5.8(a)	"	1	30	0.83	1.2
5.11(a) 5.12(a)	5.8(b) 5.8(c)	Gaussian	2	10	0.33	4.5
5.11(b) 5.12(b)	5.8(b) 5.8(c)	"	2	20	0.42	4.5
5.11(c) 5.12(c)	5.8(b) 5.8(c)	"	1	20	0.83	2.1
5.11(d) 5.12(d)	5.8(b) 5.8(c)	"	1	40	1.25	2.1

easier for these layers. This is clearly seen in Figures 5.10 to 5.12.

The second effect which should be observed is that of the filter cutoff frequency. For layers closer to the focal spot it was necessary to use a low-pass filter of lower cutoff frequency to prevent the output from being dominated by noise. The effects of the lower cutoff frequency can be seen, for example, in Figure 5.10(a), where some of the bars in layer 1 have disappeared.

The parameter h_ℓ which was introduced in Section 3.2.2 has served as a valuable tool for preventing images from becoming dominated by noise. If h_ℓ is large, the gain at the peaks (cf. Figures 5.3 to 5.5) may be too high which leads to impulse noise in the image and results in spatial cosine functions of gray levels accross the image.

In conclusion then, since the restoration is easier with a Gaussian focal spot, an X-ray system having this type of intensity distribution should be chosen, if possible, whenever the radiographs are to be processed with an inverse filter.

5.3.3 Positive Restoration Constraints

The main problem encountered in the examples shown previously was that of positive restoration, that is the filter output should be positive. Negative intensities do not have physical meaning and the filters used here do not guarantee a positive result.

A filter that guarantees positive output is the homomorphic filter [53]. The last step in homomorphic filtering is exponentiation which always gives a positive result. However, the filtering is done in the density domain rather than in the intensity domain.

There exist *a priori* techniques applicable to numerical methods of image restoration that introduce constraints in the filtration process and guarantee a positive result [76]. However these techniques cannot be used in our case because we are doing linear filtering.

In linear filtering the Lukosz bound applies. This is an amplitude constraint for the Fourier transform of band-limited non-negative functions [76]. This constraint is of a low-pass nature, which is opposite to the high-pass characteristics of tomographic filters.

The *a posteriori* techniques that have been suggested to deal with negative intensities are the following [77]:

1) Take the absolute value.

2) Square the output.

3) Add a constant to the output.

4) Clip at zero and neglect negative intensities.

All these operations are non-linear and will increase the bandwidth of the result.

After trying some of these options we decided that clipping away the negative intensities would produce a better visual effect. In other situations another type on non-linear intensity mapping may be more convenient.

5.4 Experiments with Actual Radiographs

5.4.1 Characteristics of the Radiographs Used

In order to test the performance of digital tomographic filters with actual radiographs, a complete set was obtained from the Radiological Research Laboratories, University of Toronto. They are radiographs of a mock chest (phantom) with different sets of lesions situated in the top and bottom† layers of the chest. In each case six radiographs were obtained, which correspond to three different magnifications and two focal spot sizes. Nominally, the magnifications are equal to 1, 1.5, and 2; and the focal spot sizes are 1 mm. and 2 mm. (cf. Figures 3.11 and 3.12). Four radiographs were chosen from one set for processing. In order to have sufficient resolution only a small area of 50×50 mm^2 on each radiograph was digitized. These portions of the radiographs are reproduced in Figure 5.13, the corresponding digitized images are shown in Figure 5.14, and the characteristics in Table 5.4.

† The actual system used was oriented with the centre ray vertical.

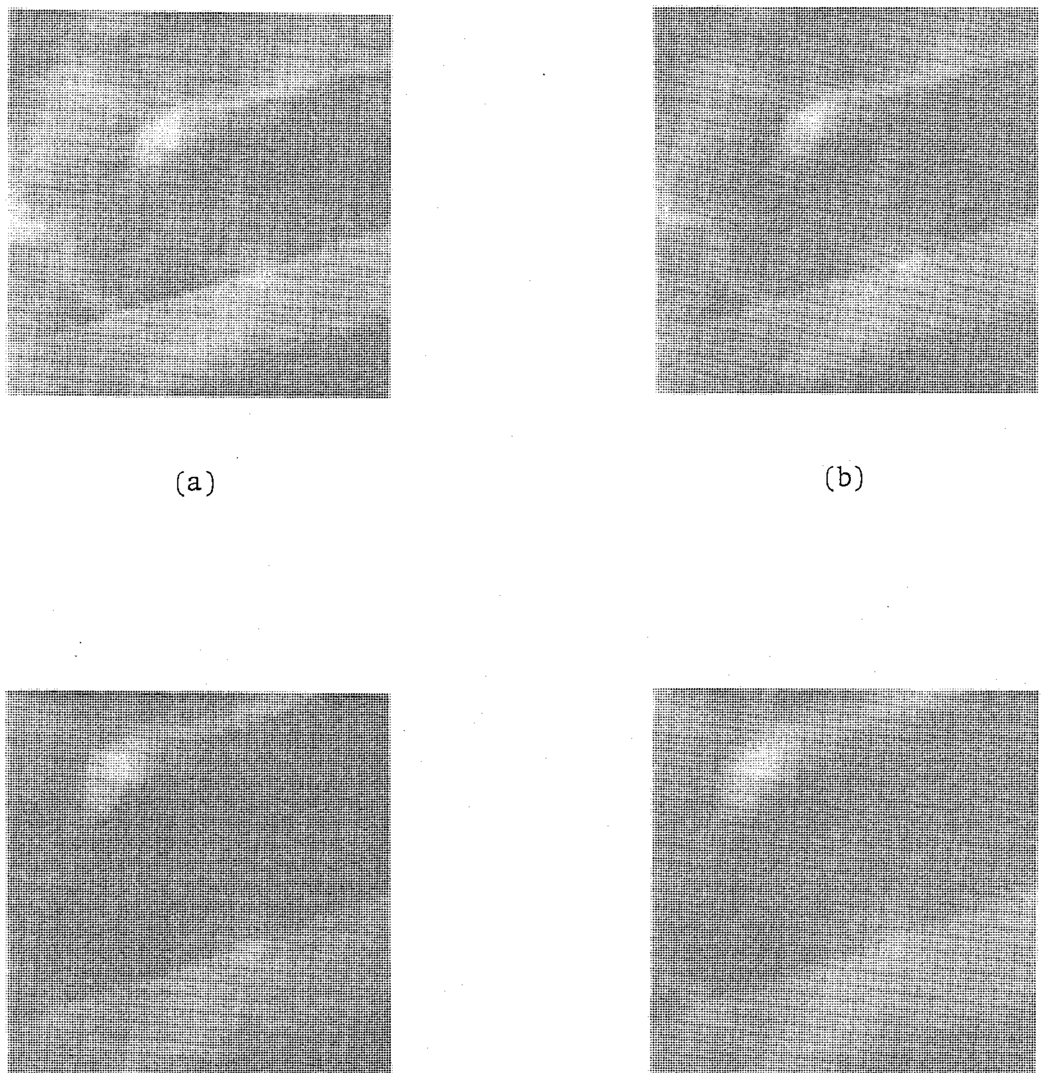

(a) (b) (c) (d)

Figure 5.13. (a)-(d) Portions of the actual radiographs to be processed. The characteristics and geometries of the radiologic system are given in Table 5.4.

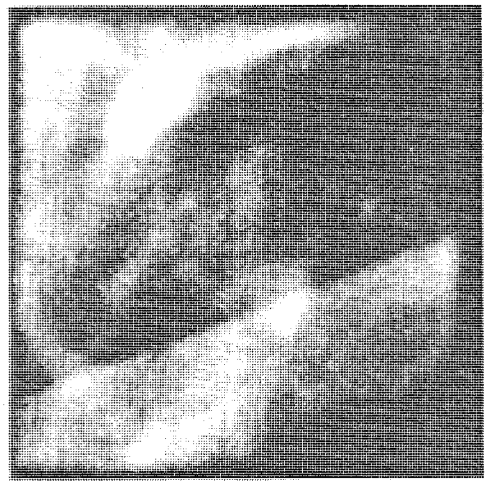

(a)

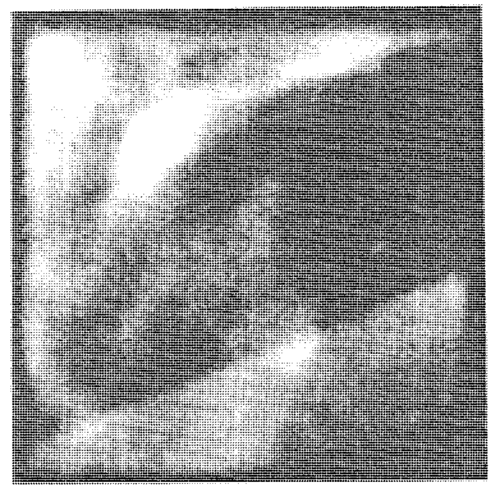

(b)

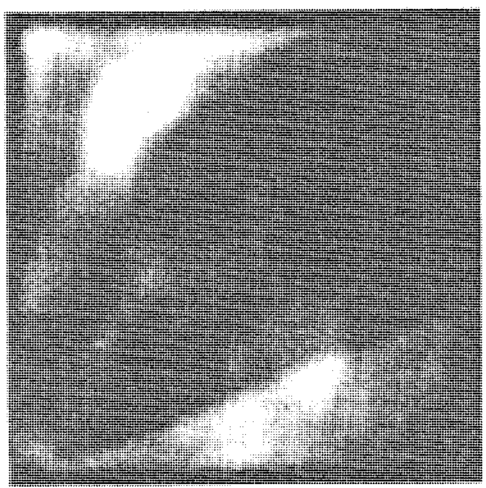

(c)

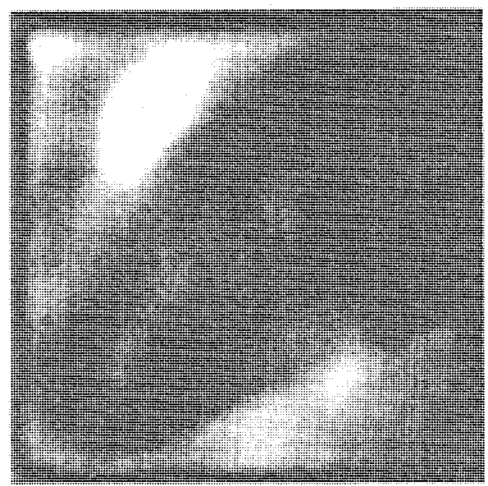

(d)

Figure 5.14. (a)-(d) Magnification of the centre parts of the radiographs in Figure 5.13 [(a)-(d), respectively], digitized, windowed, and reconstructed.

Table 5.4. Information about the portions of the radiographs to be processed.

FIGURE	RADIOGRAPH NUMBER	NOMINAL MAGNIFICATION	NOMINAL FOCAL SPOT SIZE (in mm.)	COORDINATES WITH RESPECT TO THE CENTRE RAY (in inches)
5.13(a)	33	1.5	1	(0.40,2.50)
5.13(b)	34	1.5	2	(0.40,2.50)
5.13(c)	35	2	1	(0.75,2.75)
5.13(d)	36	2	2	(0.75,2.75)

The regions to be processed were carefully chosen to contain two lesions, one in the top layer (small white area in the fourth quadrant) and one in the bottom layer (large white area in the second quadrant). Table 5.5 records relevant data about the geometries of the set-ups.

5.4.2 Processing with Tomographic Filters

The number of samples in the processed radiographs was 140×140 and in the filter impulse responses 117×117 (separable). Consequently, fast convolution was performed by using two-dimensional DFT's of size 256×256. The results are shown in Figures 5.15 to 5.17. The filter parameters are given in Table 5.6, where the subscripts 1 and 2 refer to the directions x and y, respectively, of the separable transfer function.

Only the radiograph in Figure 5.14(a) could not be processed because the small size of the blur did not allow for enough samples to define it.

Table 5.5. Geometric measurements in the set-ups for the actual radiographs and sampling intervals of the digitization (all the distances are given in mm.)

	NOMINAL MAGNIFICATION		
	1×	1.5×	2×
Top layer			
d	1155.7	1460.5	1885.9
d_1	819.8	819.8	819.8
d_2	335.9	640.7	1066.1
m	1.4097	1.7815	2.3005
d_2/d_1	0.4097	0.7815	1.3005
Bottom layer			
d	1155.7	1460.5	1885.9
d_1	1059.8	1059.8	1059.8
d_2	95.9	400.7	826.1
m	1.0905	1.3781	1.7795
d_2/d_1	0.0905	0.3781	0.7795

Pin-hole images	
Δ	1059.8
Δ_1	414.1
Δ_2	645.7
Δ_1/Δ_2	0.6413

Sampling intervals

	Radiographs:	$T_x = 0.3195$	$T_y = 0.2915$
	Pin-hole images:	$S_x = 0.2857$	$S_y = 0.2708$

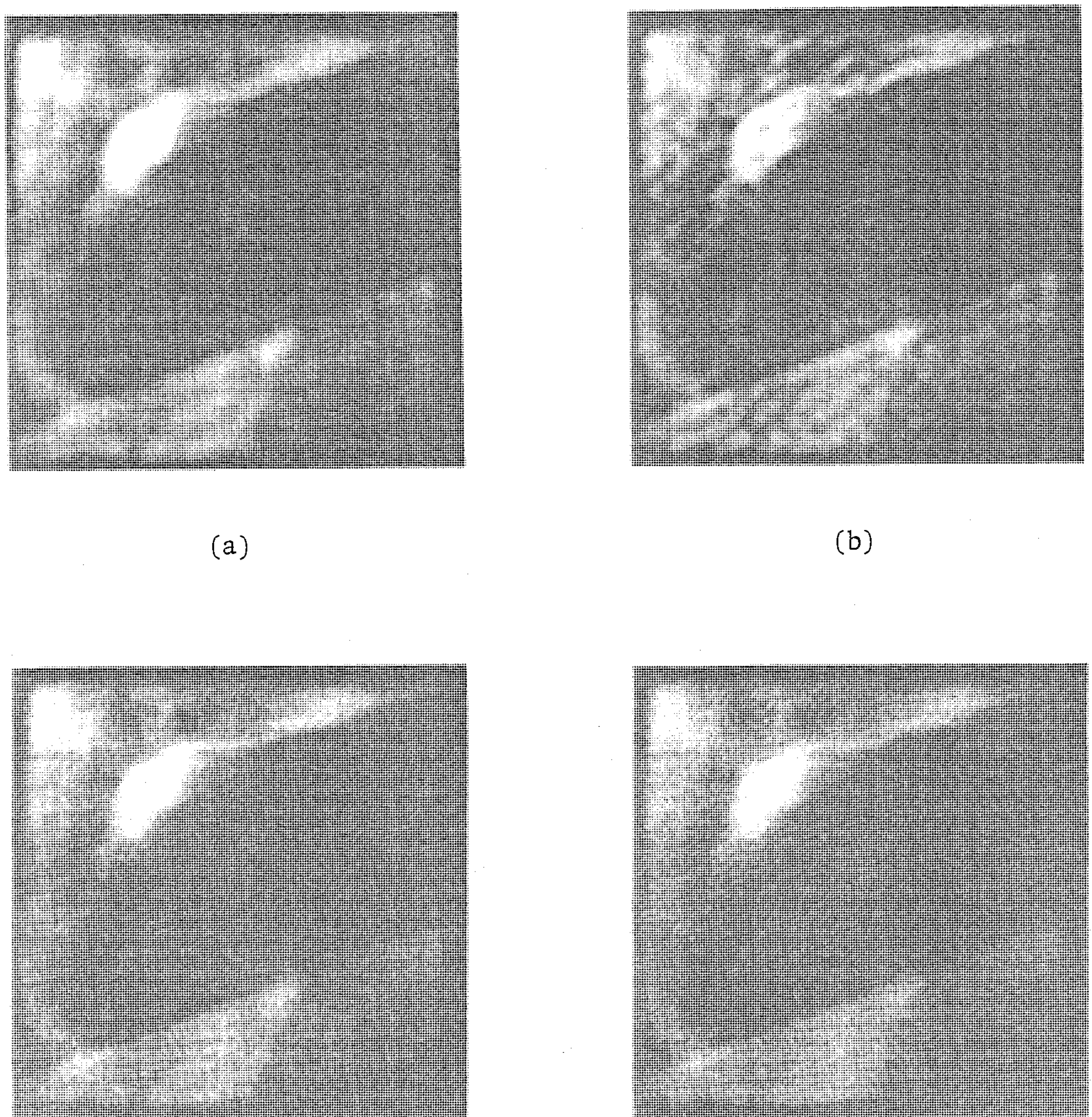

Figure 5.15. (a)-(d) Results of filtering Figure 5.14(b) with tomographic filters. The parameters are given in Table 5.6.

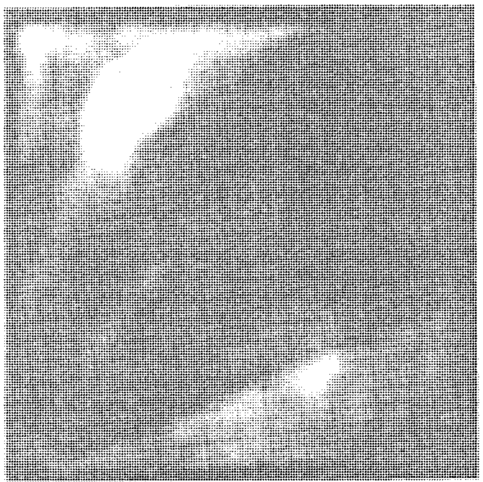

(a)

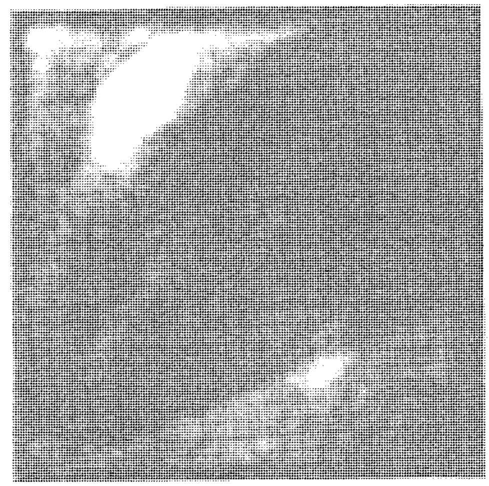

(b)

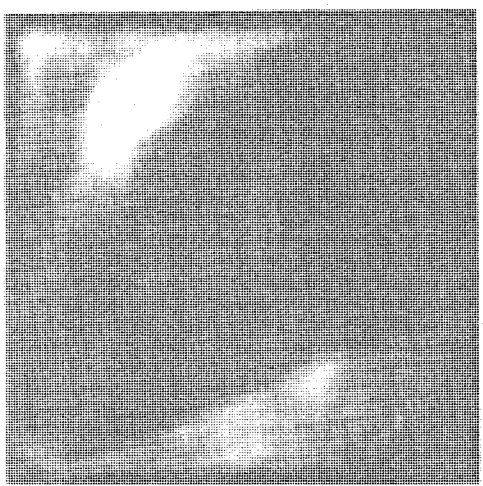

(c)

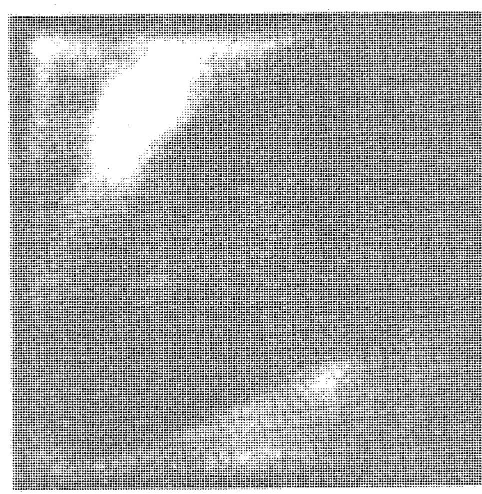

(d)

Figure 5.16. (a)-(d) Results of filtering Figure 5.14(c) with tomographic filters. The parameters are given in Table 5.6.

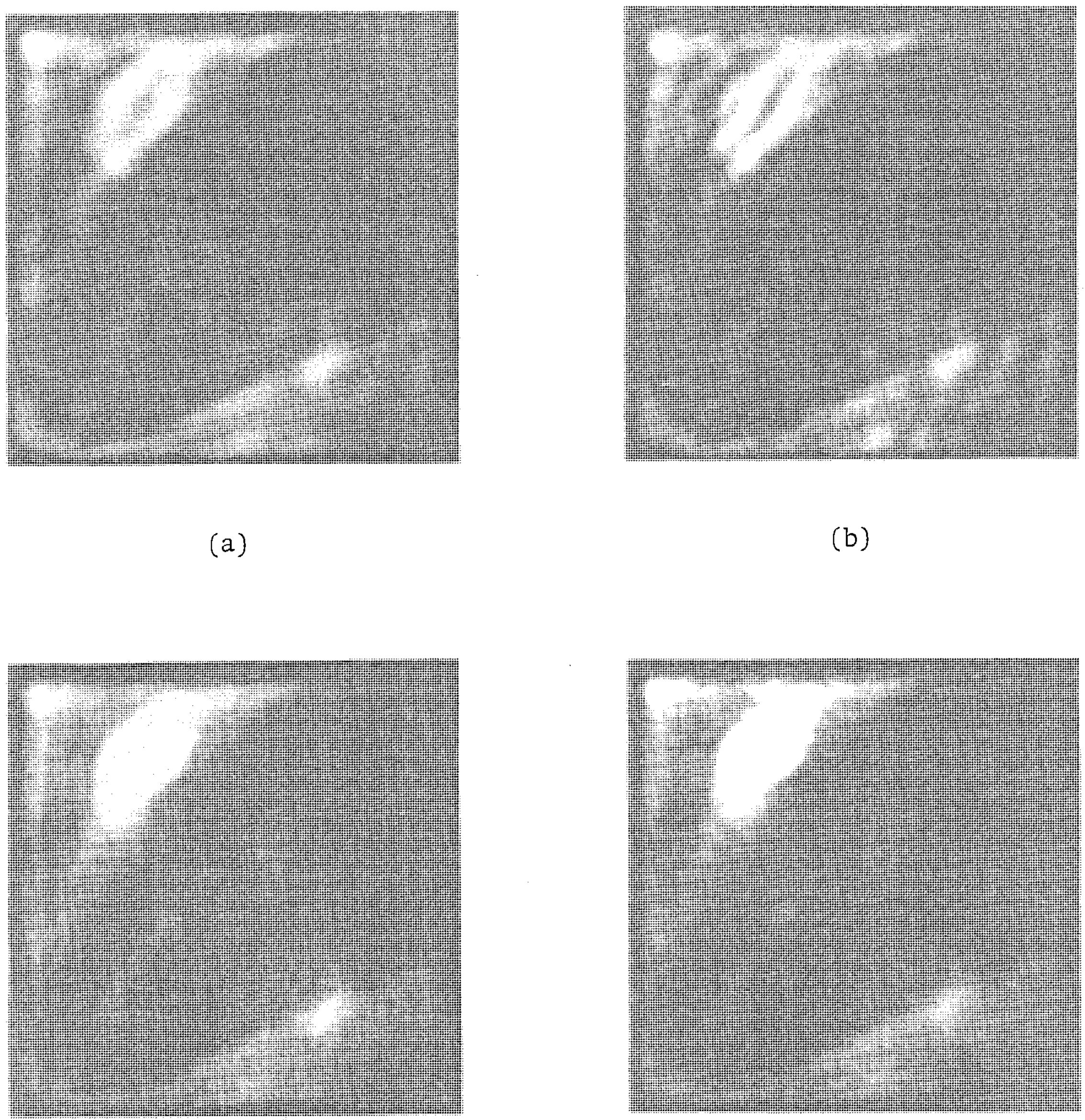

(a) (b) (c) (d)

Figure 5.17. (a)-(d) Results of filtering Figure 5.14(d) with tomographic filters. The parameters are given in Table 5.6.

Table 5.6. Summary of the characteristics of the tomographic filters used to obtain Figures 5.15 to 5.17.

RESULTING FIGURE	ORIGINAL FIGURE	LAYER TO DEBLUR	HARD-LIMITS (in dB) h_{ℓ_1}	h_{ℓ_2}	LOW-PASS FILTER BANDWIDTHS (cycles/mm) f_{c_1}	f_{c_2}
5.15(a)	5.14(b)	top	10	10	0.34	0.37
5.15(b)	5.14(b)	top	20	20	0.41	0.51
5.15(c)	5.14(b)	bottom	15	15	1.32	0.94
5.15(d)	5.14(b)	bottom	20	20	1.48	1.11
5.16(a)	5.14(c)	top	10	10	0.40	0.39
5.16(b)	5.14(c)	top	20	20	0.49	0.53
5.16(c)	5.14(c)	bottom	10	10	0.71	0.64
5.16(d)	5.14(c)	bottom	20	20	0.86	0.84
5.17(a)	5.14(d)	top	20	20	0.24	0.30
5.17(b)	5.14(d)	top	20	20	0.70	0.30
5.17(c)	5.14(d)	bottom	10	10	1.07	0.39
5.17(d)	5.14(d)	bottom	20	20	0.40	0.53

There is an effect that prevents full appreciation of the quality of the restorations. It is the blurring due to the object itself, because the lesions do not have sharp corners.

In general, the reconstruction of the top layer of the phantom produces a sharper image of the lesion in that layer and also an apparent reduction of its size. The same filter degrades the large lesion in the bottom layer by filling it with gray levels. On the other hand the reconstruction of the bottom layer degrades the lesion above it by smearing its image in the background.

The problems of positive restoration that we had with the processing of computer simulated radiographs were not noticed in the processing of actual radiographs. This was probably due to the higher degree of randomness in the energy distribution of actual radiographs.

Enhancement techniques can be used after the reconstruction with a tomographic filter to produce radiographic images more appealing to the human eye.

5.4.3 Enhancement Techniques

Enhancement techniques can increase dramatically the visual appearance of an image, especially in images with low contrasts. However, enhancement techniques need *a priori* knowledge of the features that we want to enhance and usually some iteration is needed before the viewer is satisfied. A summary of enhancement techniques follows [41]:

1) *Intensity mappings:* Nonlinear operations on a point-by-point basis to map one gray scale into another. They are used for film gamma correction, histogram equalization, stretching of intensity regions, etc.

2) *Eye modelling:* Consists of precompensating for the response of the visual system [53].

3) *Spectral shaping:* Use of low-pass, high-pass, band-pass, and high-emphasis filters in the frequency domain [43]. If there is no preferred spatial frequency axis these filters will possibly be circularly-symmetric and recursive filters can be used in their implementation.

4) *Pseudo-colour:* Mapping of a particular gray scale to a given intensity, hue and saturation defining a colour scale. Thus, the

effective dynamic range of the original gray scale is increased by appealing to the human's visual response in colour.

We have developed programs to perform intensity mappings interactively using a minicomputer and the CVI equipment at the CRF (see Appendix D). Some facilities for pseudo-colour also exist at the CRF.

Tomographic enhancement

In this work we have been concerned with the tomographic restoration of radiographs. It is also possible to do some tomographic enhancement of radiographs using only the properties of magnification rather than the focal spot blur. This form of enhancement is done with spectral shaping filters (cf. Section 2.2.5).

Assume that all the layers in the object have the same bandwidth. After being projected their spectra will be scaled differently depending on the magnification of each layer (cf. Figure 3.6). A low-pass filter will eliminate more high frequency components for those layers closer to the film, therefore enhancing structures closer to the focal spot (cf. Figures 5.10 to 5.12). On the other hand a high-pass filter will enhance the layers closer to the film. Finally, with a band-pass filter selected frequency bands can be enhanced for layers between a certain depth and the film.

5.5 Experiments with Thin Objects

The examples shown in Sections 5.3 and 5.4 have the drawback that the superposition of the various layers makes it difficult to see the effects of tomographic filtering on each layer. To avoid this problem some experiments were made with thin objects located at several levels and filtered with tomographic filters.

Six simulations were performed, see Figures 5.18 to 5.23. Two simple shapes were chosen, an annulus and a square-like annulus, which were located at three different levels: 400, 500, and 600 mm. from the film. The characteristics of the simulated radiologic system were the same as those of the previous tests with a Gaussian focal spot, namely

$$I_o(x,y) = \exp\{-2(x^2+y^2)\} \qquad -1.4 < x,y < 1.4$$

and the focal spot to film distance was also 1000 mm.

Each simulated radiograph was filtered 24 times. The variables were the parameters h_ℓ and f_c (the magnitude hard-limit and the cutoff frequency) and the distance from the plane of cut to the film. Four different pairs of parameters h_ℓ and f_c were used, the same as shown in Table 5.3 for the Gaussian focal spot. Since the results are similar for all of them, only the radiographs filtered with h_ℓ=40 dB and f_c=1.25 cycles/mm. are shown. The tomographic filters were designed for the following distances from the plane of cut to the film: 600, 550, 500, 450, 400, and 350 mm.

In Figures 5.18 and 5.19 the thin object is exactly in the middle between the focal spot and the film. In either case (annulus or square-like annulus) the sharpest image is obtained obviously when the plane of cut coincides with the thin object at 500 mm. from the film. When the object is between the plane of cut and the film (Figures 5.18 (b)-(c) and 5.19 (b)-(c)) the effects of a high-pass filter (cf. Section 3.3) are manifest. On the other hand, when the object is between the plane of cut and the focal spot (Figures 5.18 (e)-(g) and 5.19 (e)-(g)) the

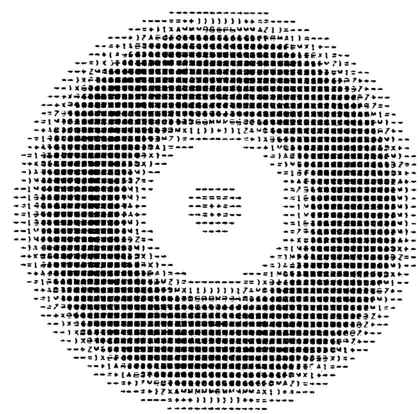

(a)

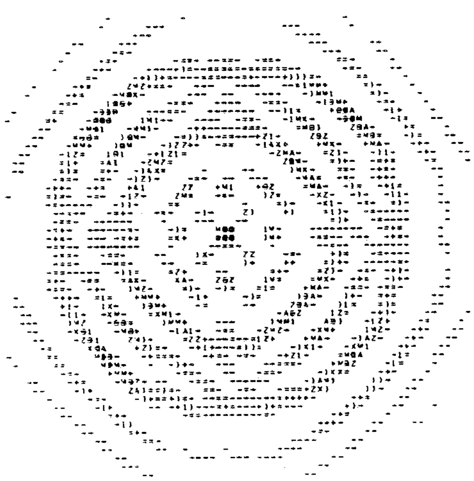

(b)

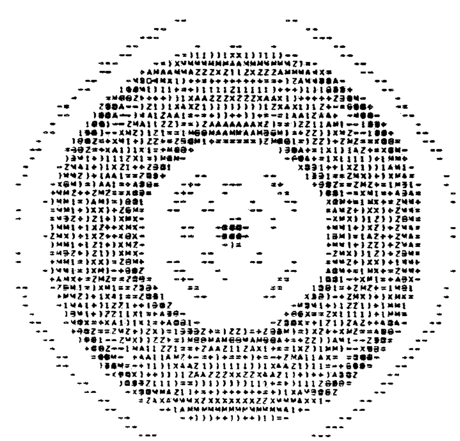

(c)

Figure 5.18. (a) Simulated radiograph of an annulus located 500 mm. from the focal spot and 500 mm. from the film. This image was processed with tomographic filters designed for layers at the following distances from the film: (b) 600 mm. (c) 550 mm.

- continues -

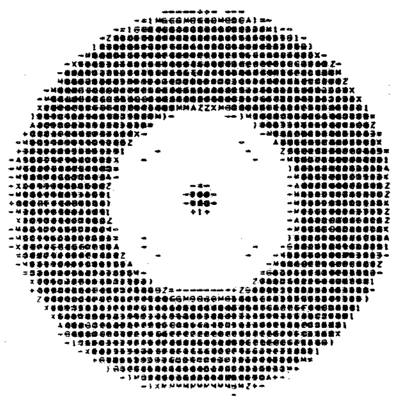

(d)

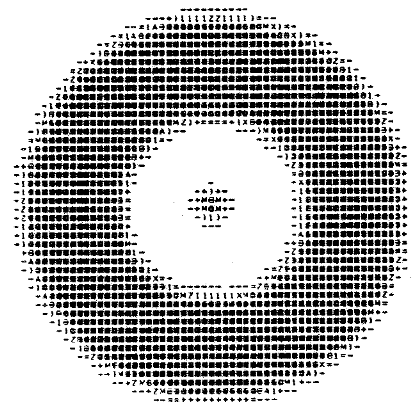

(e)

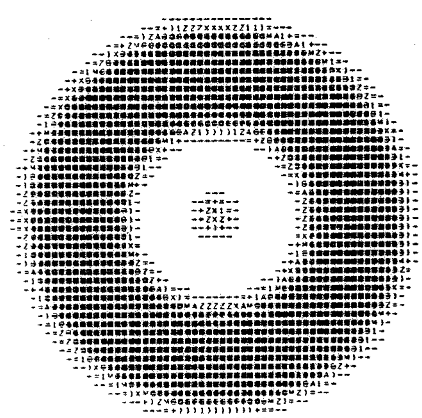

(f)

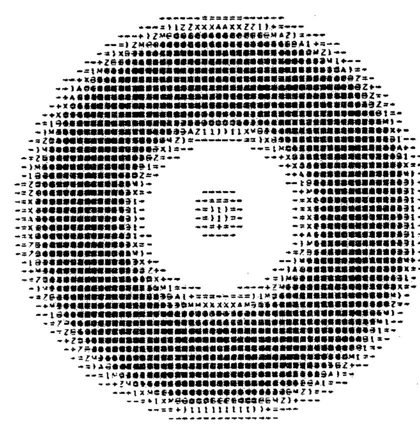

(g)

Figure 5.18. - continued -

(d) 500 mm. (e) 450 mm. (f) 400 mm. (g) 350 mm.

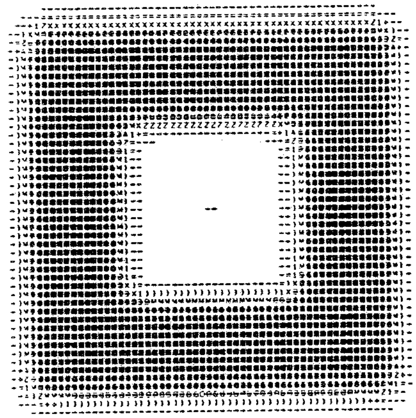

(a)

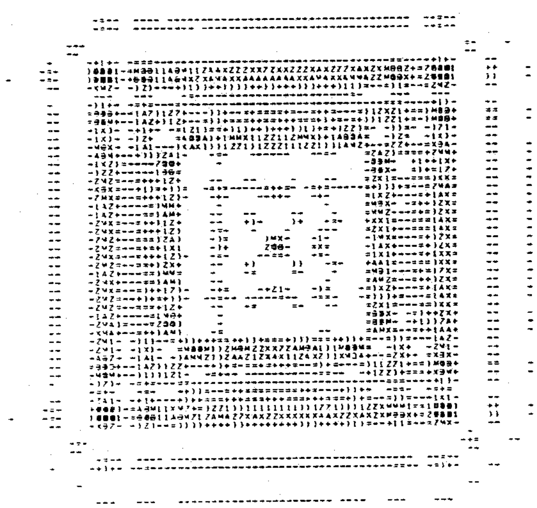

(b)

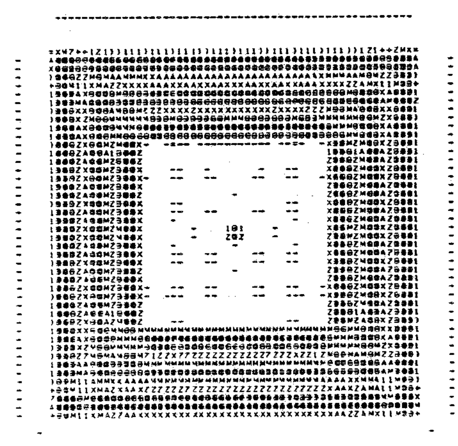

(c)

Figure 5.19. (a) Simulated radiograph of a square-like annulus located 500 mm. from the focal spot and 500 mm. from the film. This image was processed with tomographic filters designed for layers at the following distances from the film: (b) 600 mm. (c) 550 mm.

- continues -

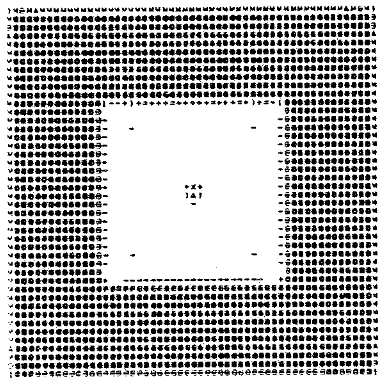

(d)

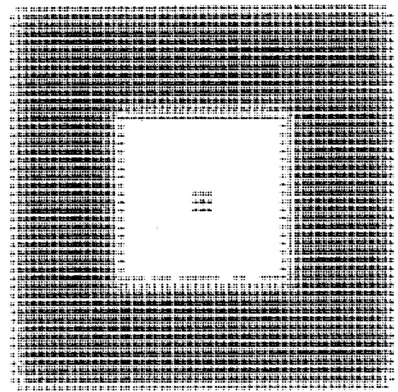

(e)

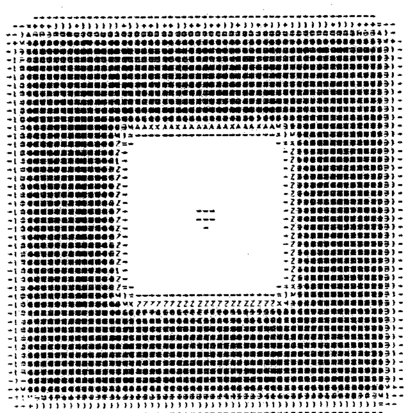

(f)

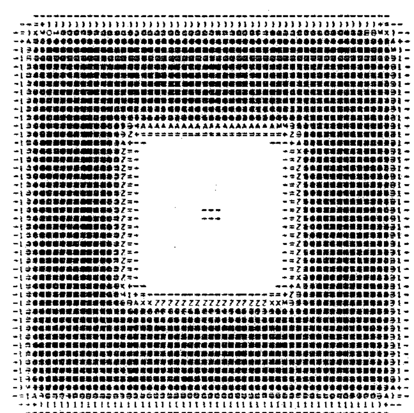

(g)

Figure 5.19. - continued -

(d) 500 mm. (e) 450 mm. (f) 400 mm. (g) 350 mm.

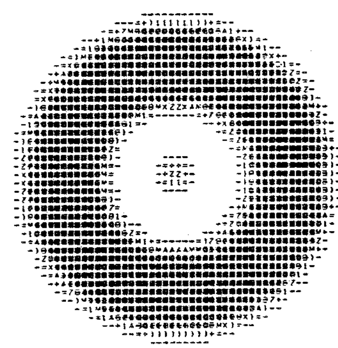

(a)

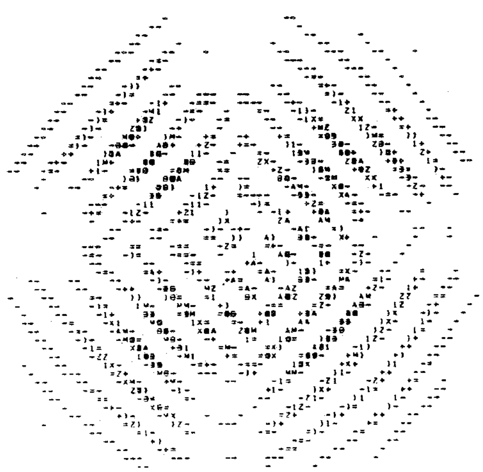

(b)

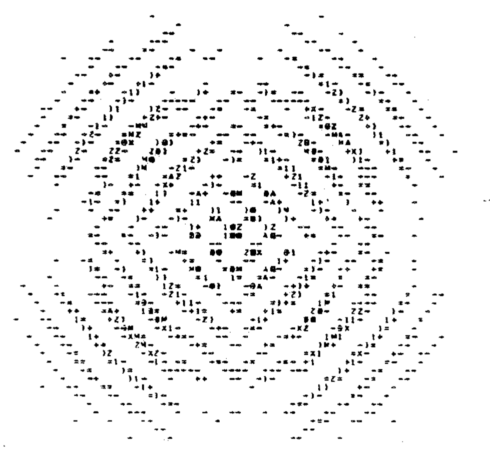

(c)

Figure 5.20. (a) Simulated radiograph of an annulus located 600 mm. from the focal spot and 400 mm. from the film. This image was processed with tomographic filters designed for layers at the following distances from the film: (b) 600 mm. (c) 550 mm.

- continues -

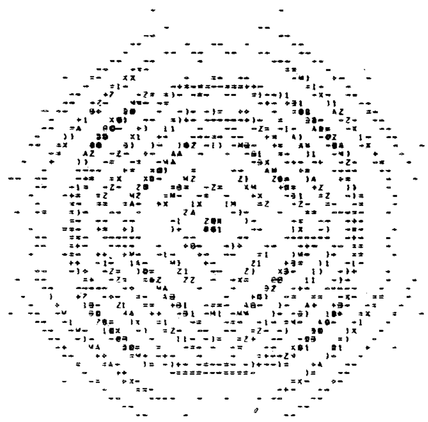

(d)

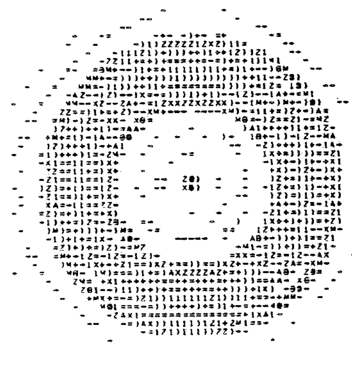

(e)

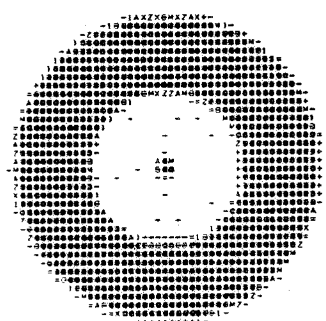

(f)

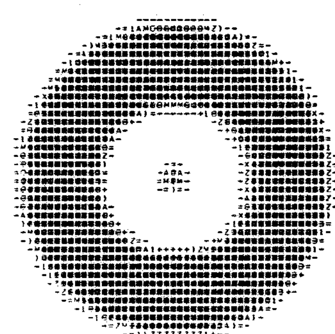

(g)

Figure 5.20. - continued -

(d) 500 mm. (e) 450 mm. (f) 400 mm. (g) 350 mm.

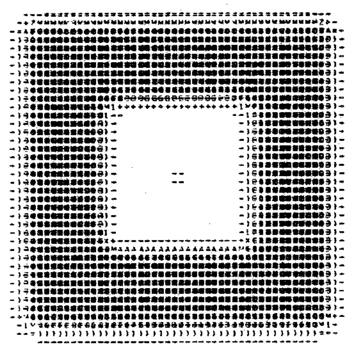

(a)

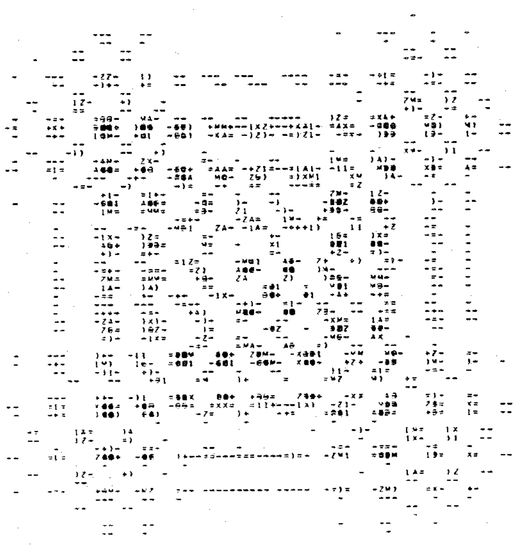

(b)

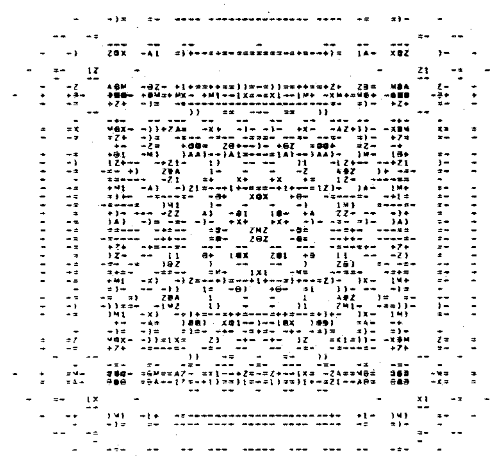

(c)

Figure 5.21. (a) Simulated radiograph of a square-like annulus located 600 mm. from the focal spot and 400 mm. from the film. This image was processed with tomographic filters designed for layers at the following distances from the film: (b) 600 mm. (c) 550 mm.

- continues -

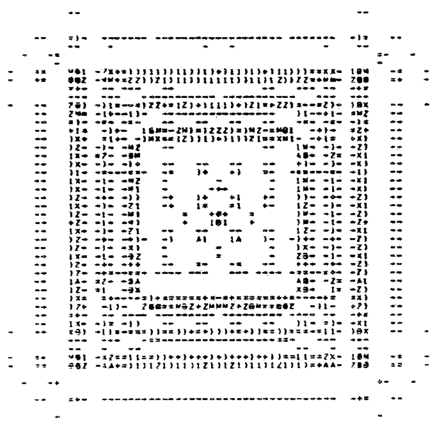

(d)

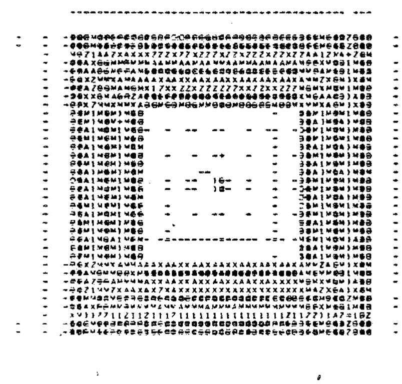

(e)

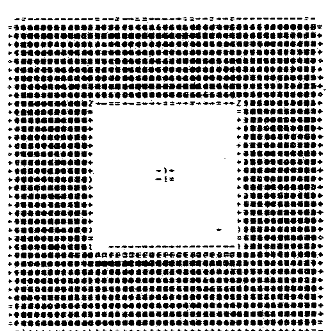

(f)

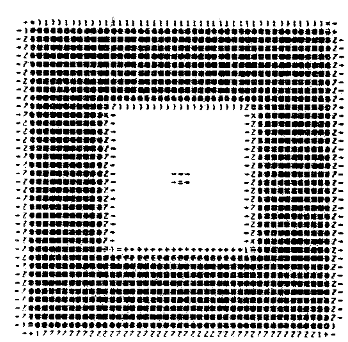

(g)

Figure 5.21. - continued -

(d) 500 mm. (e) 450 mm. (f) 400 mm. (g) 350 mm.

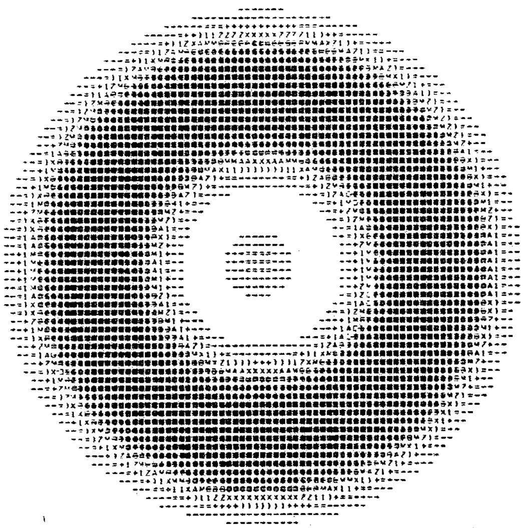

Figure 5.22. Simulated radiograph of an annulus located 400 mm. from the focal spot and 600 mm. from the film.

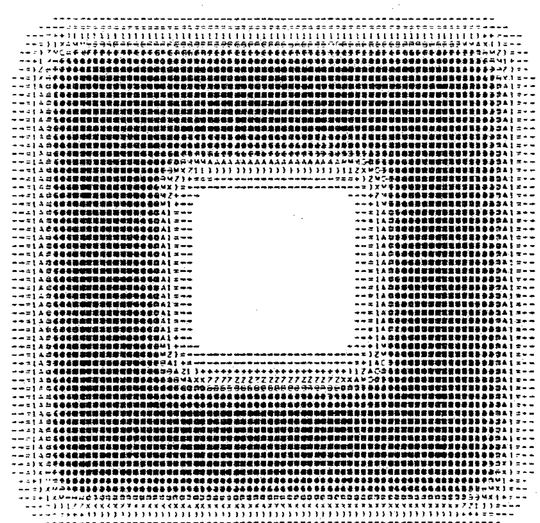

Figure 5.23. Simulated radiograph of a square-like annulus located 400 mm. from the focal spot and 600 mm. from the film.

low-pass characteristics of the overall transfer function are clearly seen. These results are also in accordance with the impulse responses shown in Figure 3.3 for the same system configuration.

In Figures 5.20 and 5.21 the thin object was closer to the film, at 400 mm. from it. The effect of the ripples in the impulse response (cf. Figure 3.3 (e)-(h)) for the layers between the plane of cut and the film is very evident here.

Figures 5.22 and 5.23 were also processed but since the results of tomographic filtering in this case were similar to to those of Figures 5.18 (d)-(g) and 5.19 (d)-(g) to a greater scale, it was decided not to include these images here.

In summary, the experiments in this section have corroborated the theoretical evaluations in Section 3.3. By considering thin objects the problems associated with the superposition of images of overlaying layers, which mask the image of the tomographic layer, have been avoided.

5.6 Simulation of an Actual System and General Discussion

A final experiment was prepared for the simulation of an actual system with a double-peaked focal spot and a simple object of low absorption (10%), consisting of two rectangles at 826.1 and 1066.1 mm. from the film. The focal spot to film distance was 1885.9 mm.
The actual system being simulated was the one described in Section 5.4 with 2× nominal magnification. The two rectangles were located in the same layers where the lesions were. The focal spot is the one shown in Figure 3.12. To test the consequences of the asymmetries in the

focal spot X-ray intensity distribution, two simulations were performed with the object rotated 90°. These two simulations are shown in Figures 5.24 and 5.25. Each of these two simulated radiographs was filtered with the same filters used to obtain Figure 5.17. The filter parameters are shown in Table 5.6. The results are shown in Figures 5.26 and 5.27.†

These images are characterized by the ripples which have been introduced. They are due to the peaks in the filter transfer function (cf. Figures 5.4 and 5.5). Note for example in Figures 5.26 (b) and 5.27 (b) how the ripples appear consistently in the larger rectangle which corresponds to the layer with the larger magnification. Notice also that the orientation of the ripples is always the same because they depend on the focal spot X-ray intensity distribution, which was fixed in this experiment, only the object was rotated.

The effects of the radiologic system and tomographic filtration can be measured and explained when the object is known; but in practical applications the success and value of a tomographic filtration process will depend on the characteristics of the relevant features inside the object being examined. These characteristics are determined by the distribution of absorption coefficients. In the remainder of this section we discuss briefly some factors in the object that affect the quality of the results.

When the X-ray absorption in overlaying layers is large, the visibility of the tomographic layer is reduced; but no additional problems

---

† Cross-sections of each one of these images were also generated, but since they did not offer any additional insight to the evaluation of tomographic filters, they are not reproduced here.

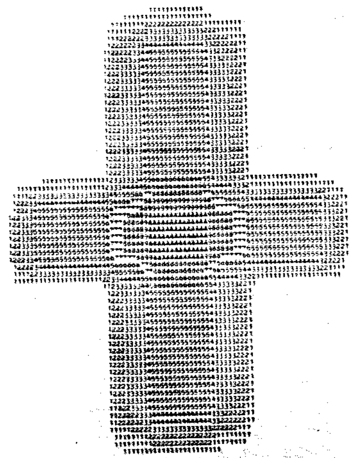

Figure 5.24. Simulated radiograph of a low-absorption object (the characters 1-9,A represent intensity levels).

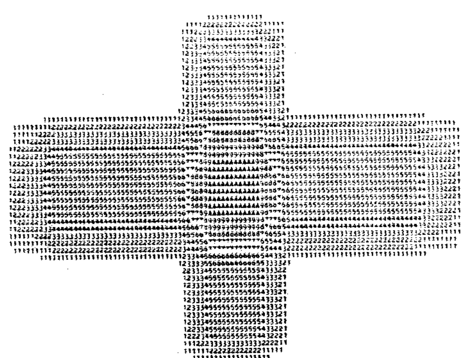

Figure 5.25. Simulated radiograph of the same object as in Figure 5.24 rotated 90° (the characters 1-9,A represent intensity levels).

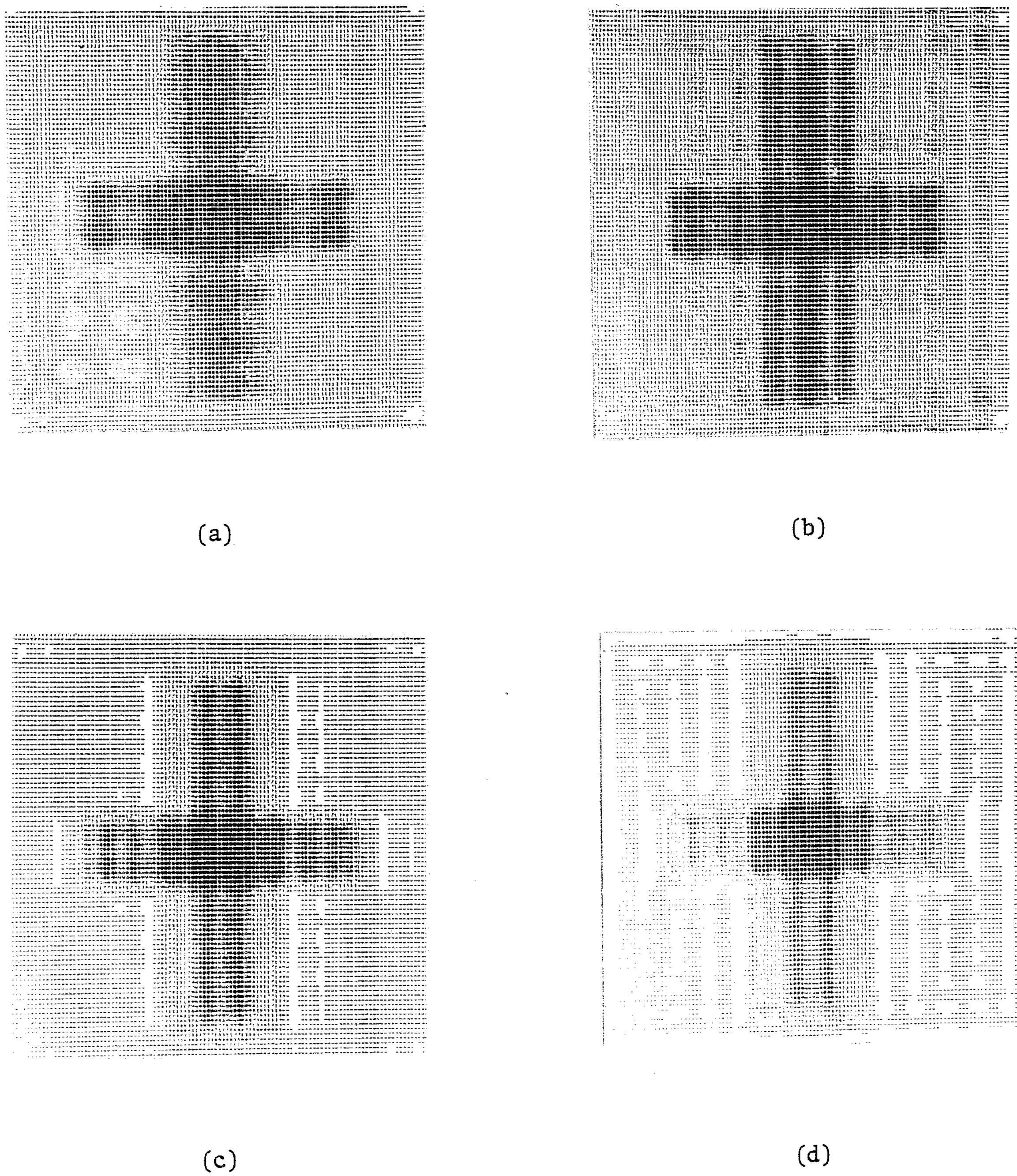

(a) (b) (c) (d)

Figure 5.26. (a)-(d) Results of filtering Figure 5.24 with the same tomographic filters used to obtain Figure 5.17 (a)-(d), respectively.

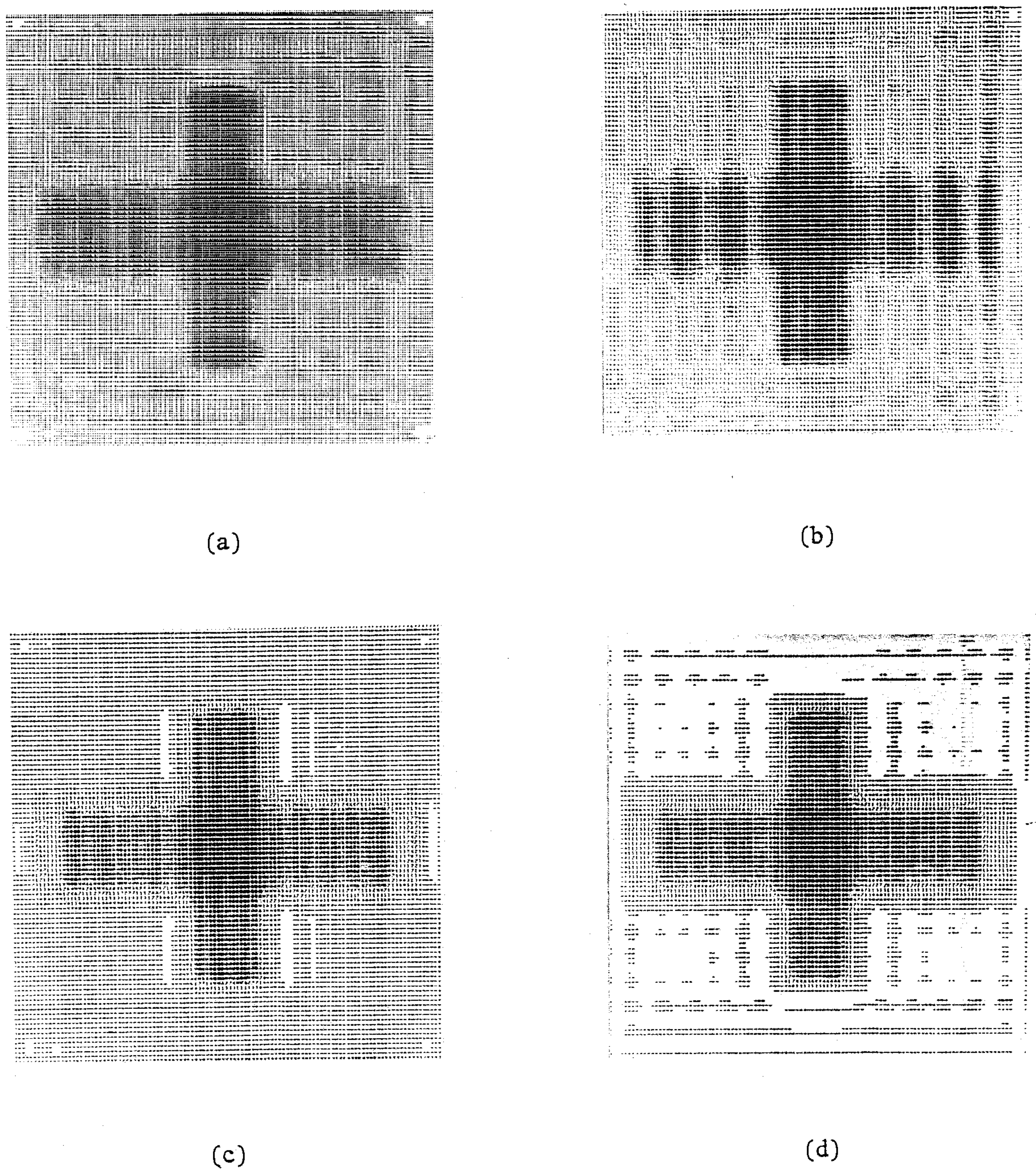

Figure 5.27. (a)-(d) Results of filtering Figure 5.25 with the same tomographic filters used to obtain Figure 5.17 (a)-(d), respectively.

seem to be introduced by the filtration process due to this higher absorption, in spite of the fact that tomographic filters were derived assuming small variations in the absorption coefficients in the object.

Another factor to consider is the size, shape and distribution of structures in the object, which can be visualized in terms of frequency components. We have seen that at very low frequencies tomographic filtering does not have any capabilities to differenciate among layers and furthermore the filter output may become very noisy, thus decreasing the quality of the image. To do tomographic filtering we need structures with edges, that is structures which have high-frequency components. Fortunately, in radiologic applications there is interest for small particles such as lesions, blood vessels, etc. Even when these particles are readily seen in the form of a white spot or line on the film, some help is needed in their interpretation.

Finally, another factor that affects the quality of filtered radiographs is due to the ripples in the impulse responses for the layers on the side of the film when the plane of cut is close to the focal spot. In some cases this is an advantage if it makes disappear unwanted details from overlaying layers, but on the other hand the ripples may lead to false interpretations.

A possible approach to learn how to deal with all these factors which depend on the (unknown) object is to do a series of filtrations of the same radiograph starting with "harmless" tomographic filters whose transfer function is close to unity and continuing processing with more "aggressive" tomographic filters until the image is dominated by noise. This series can be repeated for different depths. By comparing the successive outputs like in a movie, the changes in the structures can be examined in detail. Of course, doing this on a routine basis may not be practical but it could be useful in future experimentations with tomographic filters. This technique could also be applied in certain cases when a new radiograph cannot be obtained or a better radiologic technique is not available (e.g. old radiographs from archives, remote diagnosis, etc.).

5.7 Suggestions for the Implementation of Tomographic and Enhancement Filters in a Clinical Environment

The digital tomographic filtering in this thesis was done off-line on a large-scale multiprogramming computer using batch processing. This certainly is not a convenient realization for image processing. Except for well established procedures, image processing should always be done interactively, which requires a dedicated computer or terminal. The necessary hardware can now be developed for real-time processing [78]. If a minicomputer is used, its limited capacity implies the use of auxiliary storage devices and longer processing time. However, the throughput of a minicomputer is usually better than that of batch processing.

The equipment for the digitization and display of radiographs should be carefully chosen according to the requirements. Enhancement techniques for example, do not generally require as much resolution as tomographic filtering.

Digitally refreshed displays should be used whenever possible. Indeed, the digital refresh of a display has far superior stability and signal-to-noise ratios than traditional commercial analog systems.

From the economic point of view it might be more appropriate to design a system with limited memory and display resolution, but designed around a user scenario in which zooming, interpolation, magnification, minification, panning, rolling, etc. provide an interactive facility equal to if not more powerful for analysis purposes than a higher resolution system [73].

Pattern recognition algorithms could be incorporated after the tomographic filtration process. A data communication link could be provided to permit the transmission of radiographs to and from other instalations for remote consultation or diagnosis (telemedicine), for teaching purposes, or for a better distribution of the computation power. The tendency nowadays is to employ high resolution in the transmission of radiographs [79].

Chapter VI

COMPARATIVE EVALUATION OF TOMOGRAPHIC FILTERING

6.1 Introduction

In this chapter an objective performance assessment of tomographic filtering is produced by comparing system transfer functions and various quantitative performance parameters relevant to tomography, such as the thickness of the tomographic layer, the rate of change of the Modulation Transfer Function (MTF), and the signal to noise ratio.

6.2 Objective Performance Assessment of Tomographic Filtering

The performance of tomographic filters was evaluated theoretically in Chapter III and practically in Chapter V; the results were already discussed. Here we produce a comparative assessment of tomographic filtering taking as benchmarks two well established radiologic procedures: standard tomography and conventional radiology; tomographic filtering stands between these two, as shown in Figure 6.1. We will quantify more that relative standing as well as the trade-offs among these methods. We will be as much objective as possible without going into details of clinical value and operational procedures (man-machine interaction) which tend to be subjective.

First we discuss qualitatively the mathematical and physical similarities and differences among the radiologic procedures in terms of their transfer functions. Quantitative differences and trade-offs are then examined by considering three fundamental parameters in

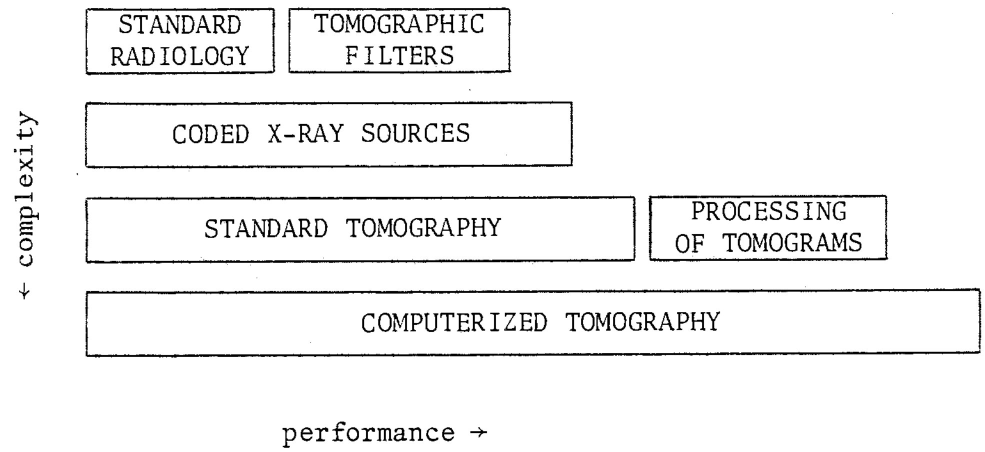

Figure 6.1. Relative standing of several radiologic procedures (not to scale).

tomography: the exposure angle, the thickness of the cut, and the radiation dose.

6.2.1 The Transfer Function

The frequency-domain equation of image formation in radiology (6.1) is derived in Appendix A (cf. (A.16)).

$$G(f_x,f_y) = I_B\ \delta(f_x,f_y) - \int_0^d H_i(f_x,f_y,z_i)\ F_\mu(f_x,f_y,z_i)\ dz_i \qquad (6.1)$$

where $G(f_x,f_y)$ is the Fourier transform of the resulting image, I_B is a constant, $H_i(f_x,f_y,z_i)$ is the overall transfer function of the i^{th} layer at a depth z_i, and $F_\mu(f_x,f_y,z_i)$ is the Fourier transform of the (scaled) distribution of linear absorption coefficients in the i^{th} layer (cf. (A.15)).

Equation (6.1) applies to standard tomography, conventional radiology, or tomographic filtering by using the transfer function given in (6.2), (6.3), or (6.4), respectively (cf. (A.14), (A.21), and (A.22)).

Standard Tomography

$$H_i(f_x,f_y,z_i) = \left[\frac{z_i-d}{z_i-\Delta_2}\,\frac{\Delta_1}{d}\right]^2 \iint I_o\left\{\frac{z_i-d}{z_i-\Delta_2}\,\frac{\Delta_1}{d}\,x\ ,\ \frac{z_i-d}{z_i-\Delta_2}\,\frac{\Delta_1}{d}\,y\right\} \times$$

$$\times\ e^{-j2\pi(f_x x+f_y y)}\ dx\ dy \tag{6.2}$$

Conventional Radiology

$$H_i(f_x,f_y,z_i) = \left[\frac{z_i-d}{z_i}\right]^2 \iint I_o\left\{\frac{z_i-d}{z_i}\,x\ ,\ \frac{z_i-d}{z_i}\,y\right\} e^{-j2\pi(f_x x+f_y y)}\ dx\ dy \tag{6.3}$$

Tomographic Filtering

$$H_i(f_x,f_y,z_i) = \frac{\left[\frac{z_i-d}{z_i}\right]^2 \iint I_o\left\{\frac{z_i-d}{z_i}\,x\ ,\ \frac{z_i-d}{z_i}\,y\right\} e^{-j2\pi(f_x x+f_y y)}\ dx\ dy}{\left[\frac{z_t-d}{z_t}\right]^2 \iint I_o\left\{\frac{z_t-d}{z_t}\,x\ ,\ \frac{z_t-d}{z_t}\,y\right\} e^{-j2\pi(f_x x+f_y y)}\ dx\ dy} \tag{6.4}$$

where the depth of the tomographic layer is $z_t=\Delta_2$, as usual.

In spite of the fact that the equations of image formation in standard tomography, conventional radiology, and tomographic filtering are similar, there are fundamental physical differences among these methods. A good objective indication of performance of a radiologic system is given by the overall transfer functions of the layers in the object. The qualitative differences among these transfer functions are discussed next, while various quantitative performance parameters will be examined in the following sections.

The function $I_o(\cdot,\cdot)$: The function $I_o(\cdot,\cdot)$ in (6.2) is substantially different from the function $I_o(\cdot,\cdot)$ in (6.3) and (6.4). In conventional radiology $I_o(\cdot,\cdot)$ is defined over an area called the focal spot and the edges of this intensity distribution are not sharp; examples of typical focal-spot intensity distributions were shown in Chapter III. On the other hand, in tomography $I_o(\cdot,\cdot)$ defines the movement of a point-like X-ray source which is turned on and off over a line which can be straight, circular, elliptical, spiral, hypocycloidal, etc. This means that the blur in conventional radiology is more uniform in all directions than in standard tomography. The uniformity of the blur is the reason why the more complicated X-ray source movements are preferred in tomography; the scanning of an area by an X-ray source has also been considered in tomography, it has been referred to as areal tomography [80, p.63]. Of course, the source of X-rays in tomography is also of finite size but the blur that this produces is generally negligible compared to the blur due to its movement.

Nature of the process: The transfer functions in (6.2), (6.3), and in the numerator of (6.4) correspond to radiologic procedures, while the transfer function in the denominator of (6.4) corresponds to an image processing operation (inverse filtering). This means that the errors and noise are of different nature in each case. In standard tomography additional blur and/or errors occur if the patient moves during the exposure and/or there are mechanical misadjustments. On the other hand, in a tomographic filtration process the effect of a patient moving is not so critical because the exposure time is shorter, but the filtering process is not ideal in practice and noise is amplified by the inverse filter, especially at high frequencies where the gain is greater.

Transfer function of the tomographic layer: The transfer functions in (6.2) and (6.4) are equal to a constant when $z_i=z_t(=\Delta_2)$ while the transfer function in (6.3) cannot be identically equal to a constant (except in the limiting case that $z_i=0$ or $I_o(x,y)$ is an impulse). This is the basic point in the analogy between tomographic filtering and standard tomography, which has been studied elsewhere in this dissertation (cf. Chapter III and Appendix A).

Transfer functions of the out-of-focus layers: Even assuming an identical $I_o(\cdot,\cdot)$ in every case (which is not practically possible) generally the transfer functions in (6.2), (6.3), and (6.4) for the out-of-focus layers are not equal. The characteristics of the overall transfer functions of the out-of-focus layers in a tomographic filtration process have been studied in Chapter III. For an analysis of the transfer functions in standard tomography see for example [48].

Quantitative performance parameters

The transfer functions contain all the information necessary to compare the various systems. However, they are inconvenient to calculate and compare. The first simplification is to ignore the phase transfer function and consider only the magnitude transfer function, usually referred to as the modulation transfer function (MTF). Nevertheless, for easyness of comparison single number parameters are commonly used in radiology. Those relevant to tomography are considered next.

6.2.2 The Exposure Angle

The most evident quantitative difference between a tomographic filtration process and standard tomography is the size of the focal spot in radiology as opposed to the extension of the movement of the X-ray source in tomography. They have a direct effect on the extension of the blur and therefore on the thickness of the tomographic layer. A typical size for a focal spot is of the order of 1 or 2 mm. while the movement of an X-ray source varies from a few mm. in zonography† up to 500 mm. and more in standard tomography.

In tomography it is more usual to give the exposure angle rather than the extension of the movement of the X-ray source. The exposure angle is defined as the angle through which the projecting ray of a central point of the plane of cut moves during the exposure.

In conventional radiology and therefore in a tomographic filtration process the exposure angle is determined by the size of the focal spot. With a typical focal spot size of 2 mm. and focal spot to plane of cut distance of 1000 mm., the exposure angle is 2 arctan 0.001 = 0.002 radians. The following table gives the range of exposure angles for various tomographic procedures:

Tomographic filtration process	5' - 15'
Zonography	1° - 5°
Standard tomography	10° - 60°
Transversal tomography	120° - 170°

Thus, in terms of the exposure angle, a tomographic filtration process is closer to zonography than to any other tomographic technique.

---

† Zonography is essentially standard tomography using smaller movements of the X-ray source [5, p.360], [81, chapter 14], [82], [83]. Other narrow-angle tomographic techniques are the following [81, pp. 7-8 and 300-311]: Stereozonography, narrow-angle stratigraphy, and orthotomography.

6.2.3 The Thickness of the Cut

Conventionally, in tomography the thickness of the cut is defined as the distance between the two levels which have a tomographic blurring $B \geq B_m$ that is insufficiently large to be noticeable in the presence of the usual radiographic blurrings B_m [5, p.355]. In standard tomography a reasonable choice for B_m is 0.7 mm. [5, p.355]. This is a subjective definition† and it depends on the amount of other blurrings such as those due to the focal-spot intensity distribution and patient movement. In a tomographic filtration process the tomographic blur is based on the focal-spot intensity distribution, and the blur due to patient movement is negligible because the exposure time is short. Therefore the threshold B_m in a tomographic filtration process should be chosen to be less than 0.7 mm. Since the definition of 'thickness of cut' is already so fuzzy, here we neglect the effects of the focal-spot intensity distribution and the high-pass filter characteristics on layers on the film side. Hence, from (3.10), the thickness of the tomographic layer is given by:

$$2t = \frac{2\ B_m\ d_1^2}{s\ (d_1+d_2)\ +\ B_m\ d_1}$$

or in terms of the exposure angle Θ_m:

$$2t = \frac{2\ B_m\ d_1}{\Theta_m\ (d_1+d_2)\ +\ B_m} \tag{6.5}$$

In standard tomography the thickness of the cut is of the order of a few millimetres, in zonography it is of the order of a few centimetres

† A more objective definition has been proposed in [48] in terms of the amount of attenuation desired and the spatial frequencies of interest. A plot of the transfer function is required to make this calculation easy.

and in a tomographic filtration process even larger. However for a fair comparison the value of B_m should be changed accordingly, as previously discussed. Indeed the minimum discernible blur in standard tomography has a fixed component due to focal spot size and patient movements, which are practically nonexistent in tomographic filtering. Therefore, let the minimum discernible blur in tomographic filtered radiographs be B_m/K_f where B_m is 0.7 mm. as usual in standard tomography and K_f is an appropriate constant greater than one. Because of the lack of experimental evidence we can only make an educated guess about the value of K_f: we assume that a realistic value is at least K_f=2. Furthermore, computer processed radiographs can readily be manipulated, magnified, contrast enhanced, etc. In particular, magnification is important here because it is inversely proportional to the minimum discernible blur, namely $B_m/K_f/K_m$, where K_m is the magnification of the processed radiograph (not the radiologic magnification but the display magnification). Since only a small portion of the radiograph, say 1 to 4 square inches, will be processed at a time by the tomographic filter, this area can be displayed at full resolution and thus magnification can be as high as 20; nevertheless in this calculation we will assume a lower value, say K_m = 10.

Consequently, taking into account the constants K_m and K_f, (6.5) becomes (6.6) for tomographic filtering.

$$2t = \frac{2B_m d_1}{K_f K_m \theta_m (d_1+d_2) + B_m} \qquad (6.6)$$

Hence, assuming B_m = 0.7 mm., d_1= d_2= 1000 mm., K_f= 2, K_m= 10, and θ_m= 10', the thickness of the cut is 2t = 12 mm. for the tomographic filtration process. On the other hand in zonography, with $K_f = K_m = 1$ and $\theta_m = 3°$ we obtain $2t = 13$ mm. and in standard tomography with $\theta_m = 35°$ we obtain $2t = 1$ mm. Of course, the display magnification of standard tomograms and zonograms would also further reduce the apparent thickness of cut, however this technique would not work so well in these cases because there are other blurrings present (due to focal spot and patient movement).

It may seem that the thinner the cut the better, nevertheless there are cases where a thick cut is preferred. Each special tomographic technique has its own predilective applications [81, Chapter 14]. Interactive tomographic filtering offers the advantage that by computer manipulation the apparent thickness of the cut can be changed by magnification at the expense of reducing the field of view.

6.2.4 The Rate of Change of the Transfer Function

To further quantify the difference between tomographic filtering and standard tomography we propose a new measure based on the contrast between layers. Indeed, we will calculate and compare the rates of change of the transfer functions in (6.2) and (6.4) from layer to layer for a specific type of exposure function $I_o(\cdot,\cdot)$.

Equations (6.2) to (6.4) can be simplified by introducing $F_{I_o}(f_x,f_y)$, the two-dimensional Fourier transform of $I_o(x,y)$, and using the scaling property (cf. Table B.1); thus we obtain (6.7) to (6.9), respectively.

$$H_i(f_x,f_y,z_i) = F_{I_o}\left(\frac{z_i - \Delta_2}{z_i - d}\,\frac{d}{\Delta_1}\,f_x\,,\ \frac{z_i - \Delta_2}{z_i - d}\,\frac{d}{\Delta_1}\,fy\right) \qquad (6.7)$$

$$H_i(f_x,f_y,z_i) = F_{I_o}\left(\frac{z_i}{z_i - d}\,f_x\,,\ \frac{z_i}{z_i - d}\,f_y\right) \qquad (6.8)$$

$$H_i(f_x,f_y,z_i) = \frac{F_{I_o}\left(\frac{z_i}{z_i - d}\,f_x\,,\ \frac{z_i}{z_i - d}\,f_y\right)}{F_{I_o}\left(\frac{z_t}{z_t - d}\,f_x\,,\ \frac{z_t}{z_t - d}\,f_y\right)} \qquad (6.9)$$

where (6.9) is valid in a finite region around the origin in the frequency plane.

We have now reached the point where to proceed with the comparison we must make some assumption about the function $I_o(x,y)$, or equivalently, its Fourier transform. We discussed in Chapter II that a Gaussian function is a good approximation to the intensity distribution in actual focal spots. In standard tomography $I_o(x,y)$ is not Gaussian in general because it represents the movement of the X-ray source whose intensity is usually constant during the exposure. Nevertheless, for the purpose of this comparison we will assume identical functions $I_o(x,y)$ leading to (6.7), (6.8) and (6.9), because what we want to compare is the rate of change of the transfer function with respect to the mode of operation (i.e. movement or filtering) rather than with respect to $I_o(x,y)$. Thus, in the specific case the $I_o(x,y)$ is a circularly-symmetric Gaussian function (see (6.10)), $F_{I_o}(f_x,f_y)$ is also a Gaussian function (see (6.11)).

$$I_o(x,y) = \exp\{-\sigma^2 x^2 - \sigma^2 y^2\} \tag{6.10}$$

$$F_{I_o}(f_x,f_y) = \frac{\pi}{\sigma^2} \exp\left\{-\left(\frac{f_x}{\sigma/\pi}\right)^2 - \left(\frac{f_y}{\sigma/\pi}\right)^2\right\} \tag{6.11}$$

Substituting (6.11) into (6.7), (6.8) and (6.9) we obtain (6.12), (6.13) and (6.14) respectively.

$$H_i(f_x,f_y,z_i) = \frac{\pi}{\sigma^2} \exp\left\{-\left[\frac{\pi}{\sigma} \frac{z_i - \Delta_2}{z_i - d} \frac{d}{\Delta_1}\right]^2\left(f_x^{\,2} + f_y^{\,2}\right)\right\} \tag{6.12}$$

$$H_i(f_x,f_y,z_i) = \frac{\pi}{\sigma^2} \exp\left\{-\left[\frac{\pi}{\sigma} \frac{z_i}{z_i - d}\right]^2\left(f_x^{\,2} + f_y^{\,2}\right)\right\} \tag{6.13}$$

$$H_i(f_x,f_y,z_i) = \exp\left\{-\left(\frac{\pi}{\sigma}\right)^2\left[\left(\frac{z_i}{z_i - d}\right)^2 - \left(\frac{z_t}{z_t - d}\right)^2\right]\left(f_x^{\,2} + f_y^{\,2}\right)\right\} \tag{6.14}$$

These formulae clearly show the low pass nature of the transfer functions of standard tomography (6.12) and conventional radiology (6.13). On the other hand the overall transfer function of a tomographic filtration process (6.14) can be low-pass (if $z_i > z_t$) or high pass (if $z_i < z_t$) depending on the layer concerned.

The rate of change of the transfer function with respect to z_i is given by the first derivative of $H_i(f_x, f_y, z_i)$ with respect to z_i. However, since the transfer functions in (6.12) and (6.14) are both exponential functions we will use as a measure of the rate of change of the transfer function from layer to layer the derivative of the coefficient of $f_x^2 + f_y^2$ with respect to z_i. The derivative of the coefficient in (6.12) is given in (6.15) and the derivative of the coefficient in (6.14) is given in (6.16).

$$y_{ST}(z_i) = 2\left(\frac{\pi}{\sigma}\right)^2 \frac{d^2}{\Delta_1} \frac{z_i - \Delta_2}{(d - z_i)^3} \tag{6.15}$$

$$y_{TF}(z_i) = 2\left(\frac{\pi}{\sigma}\right)^2 d \frac{z_i}{(d - z_i)^3} \tag{6.16}$$

Therefore, in standard tomography the slope $y_{ST}(z_i)$ is negative if $z_i < \Delta_2$ (i.e. between the film and the tomographic layer) and positive if $z_i > \Delta_2$ (i.e. between the tomographic layer and the focal spot). This change of sign of the slope is due to the fact that the coefficient itself stays positive when the tomographic layer is crossed and it is zero at the tomographic layer (i.e. the function has a minimum). On the other hand in tomographic filtering the slope $y_{TF}(z_i)$ is always positive because it is the coefficient that changes sign when crossing the tomographic layer. The ratio of the two slopes is given in (6.17).

$$\Gamma(z_i) = \frac{y_{TF}(z_i)}{y_{ST}(z_i)} = \frac{\Delta_1}{d} \frac{z_i}{z_i - \Delta_2} \tag{6.17}$$

Hence, whenever $|\Gamma(z_i)| > 1$ the rate of change of the transfer function from layer to layer is greater in a tomographic filtration process than in the equivalent system using standard tomography, and viceversa when $|\Gamma(z_i)| < 1$. The ranges of z_i in each case are easily calculated:

$$0 < z_i < \frac{d\Delta_2}{2d - \Delta_2} \qquad |\Gamma(z_i)| < 1 \tag{6.18}$$

$$\frac{d\Delta_2}{2d - \Delta_2} < z_i < d \qquad |\Gamma(z_i)| > 1 \tag{6.19}$$

Consequently for the layers between the focal spot and the layer at a distance $d\Delta_2/(2d - \Delta_2)$ from the film, the transfer function in a tomographic filtration process varies faster from layer to layer than in the equivalent system using standard tomography. It can be shown that the interval $d\Delta_2/(2d - \Delta_2) < z_i < d$ always contains the tomographic layer $z_i = \Delta_2$, hence in a region around the tomographic layer tomographic filtering gives better contrast between layers than standard tomography.

Examples (all distances in mm.)

d	Δ_2	$d\Delta_2/(2d - \Delta_2) < z_i < d$	$\frac{200\ \Delta_1}{d + \Delta_1}$ %
1000	500	333.3 $< z_i <$ 1000	66%
1000	400	250 $< z_i <$ 1000	75%
1000	600	428.6 < zi < 1000	57%

where the last column represents the percentage of the space between the focal spot and the film where tomographic filtering gives better contrast.

Specific values of the slopes can be obtain by substituting values in (6.15) and (6.16). Indeed, assuming $\sigma = 2$, $d = 1000$, and $\Delta_1 = \Delta_2 = 500$ we obtain the following results:

z_i	$y_{ST}(z_i)$	$y_{TF}(z_i)$
0	-0.49%	0
100	-0.54%	0.07%
200	-0.58%	0.15%
300	-0.57%	0.43%
400	-0.46%	0.91%
500	0	1.97%
600	1.5%	4.6%
700	7.3%	12.8%
800	37%	49%
900	395%	444%
1000	∞	∞

The previous analysis has assumed identical exposure functions $I_o(x,y)$ in each case as defined in (6.10). We are now going to repeat the analysis assuming different σ's in (6.10) both for tomographic filtering and standard tomography, but the shape of $I_o(x,y)$ is still the same in both cases, a Gaussian function. Equations (6.15) and (6.16) thus become (6.20) and (6.21) respectively.

$$y_{ST}(z_i) = 2\left(\frac{\pi}{\sigma_{ST}}\right)^2 \frac{d^2}{\Delta_1} \frac{z_i - \Delta_2}{(d - z_i)^3} \tag{6.20}$$

$$y_{TF}(z_i) = 2\left(\frac{\pi}{\sigma_{TF}}\right)^2 d \frac{z_i}{(d - z_i)^3} \tag{6.21}$$

Their ratio is

$$\Gamma(z_i) = \frac{y_{TF}(z_i)}{y_{ST}(z_i)} = \left(\frac{\sigma_{ST}}{\sigma_{TF}}\right)^2 \frac{\Delta_1}{d} \frac{z_i}{z_i - \Delta_2} \tag{6.22}$$

and $|\Gamma(z_i)| > 1$ whenever the following inequality is satisfied:

$$\frac{\sigma_{TF}^2 d \Delta_2}{\sigma_{TF}^2 d + \sigma_{ST}^2 \Delta_1} < z_i < \frac{\sigma_{TF}^2 d \Delta_2}{\sigma_{TF}^2 d - \sigma_{ST}^2 \Delta_1} \tag{6.23}$$

Assuming $\sigma_{TF} = 2$ and $\sigma_{ST} = 0.005$, $d = 1000$ and $\Delta_1 = \Delta_2 = 500$, we obtain

$499.9 < z_i < 500.1$

Thus now the region where the rate of change of the transfer function of a tomographic filtration process is greater than that of standard tomography is very narrow indeed, practically negligible; however it always includes the plane of cut. This suggest that the use of the term "thickness of the cut" may not be as relevant in tomographic filtering as it is in standard tomography.

The absolute values of the slopes $y_{ST}(z_i)$ and $y_{TF}(z_i)$ in the examples given previously now differ by an additional factor

$$\left(\frac{\sigma_{TF}}{\sigma_{ST}}\right)^2 = \left(\frac{2}{0.005}\right)^2 = 160,000$$

in favour of standard tomography because of the different size (scalings) used in this example.

Hence the percentage of the space between focal spot and film in favour of tomographic filtering is now

$$\frac{200\ \sigma_{TF}^2\ \sigma_{ST}^2\ \Delta_1\Delta_2}{\sigma_{TF}^4\ d^2 - \sigma_{ST}^4\ \Delta_1^2}\ \% \qquad (6.24)$$

If $\sigma_{TF} >> \sigma_{ST}$ (6.24) can be approximated by (6.25).

$$\frac{200\ \sigma_{ST}^2\ \Delta_1\Delta_2}{\sigma_{TF}^2\ d^2}\ \% \qquad (6.25)$$

which in the previous example amounts only to 0.003%.

In conclusion then, the operation of tomographic filtering gives better layer contrast than standard tomography in an interval around the plane of cut. However, if the normal sizes of the exposure function are taken into consideration, the performance of standard tomography is by far better because that interval is negligible.

6.2.5 The Signal to Noise Ratio

In this section tomographic filtering is evaluated further by studying the effects that system parameters such as focal spot size have on the results; thus allowing comparisons between systems. This evaluation is done in terms of the signal to noise ratio which is defined as the ratio of the power of the signal from the plane of cut if it was the only one present in the object and the power of the noise contributed by all other planes. The signal to noise ratio, as defined here, provides another measure of the contrast of the image of the plane of cut with respect to the others.

In this analysis the object, represented by the distribution of linear attenuation coefficients $\mu(x_i, y_i, z_i)$, is considered to be a random process with parameter space x_i, y_i, z_i. It is convenient to express $\mu(x_i, y_i, z_i)$ as a function of the coordinates on the film plane, that is (cf. (A.15)): $\quad x_i = \frac{d - z_i}{d} x$ and $y_i = \frac{d - z_i}{d} y$

Therefore:

$$\mu(x_i, y_i, z_i) = \mu\left(\frac{d - z_i}{d} x, \frac{d - z_i}{d} y, z_i\right) .$$

Let the two-dimensional correlation function of this random process with respect to the first two parameters be

$$R_\mu\left(\frac{d - z_i}{d} x, \frac{d - z_i}{d} y, z_i\right) \tag{6.26}$$

The two-dimensional power spectral density function of this random process is given by the two-dimensional Fourier transform of (6.26), which is given in (6.27).

$$\begin{aligned} S_{\mu_i}(f_x, f_y, z_i) &= \iint R_\mu\left(\frac{d - z_i}{d} x, \frac{d - z_i}{d} y, z_i\right) \times \\ &\qquad \times e^{-j2\pi(f_x x + f_y y)} \, dx \, dy \\ &= \left(\frac{d}{d - z_i}\right)^2 S_\mu\left(\frac{d}{d - z_i} f_x, \frac{d}{d - z_i} f_y, z_i\right) \end{aligned} \tag{6.27}$$

where S_μ is the two-dimensional Fourier transform of R_μ.

For example, if the random process is white noise S_{μ_i} is given by (6.28).

$$S_{\mu_i}(f_x, f_y, z_i) = \left(\frac{d}{d - z_i}\right)^2 S_o \tag{6.28}$$

where S_o is a constant for all f_x, f_y and z_i. If this noise is bandlimited between -W and W, the power spectral density function is:

$$S_{\mu_i}(f_x,f_y,z_i) = \begin{cases} \left(\dfrac{d}{d - z_i}\right)^2 S_o & \text{for } -W_i \le f_x,\ f_y \le W_i \\ 0 & \text{otherwise} \end{cases} \tag{6.29}$$

where $W_i = \dfrac{d - z_i}{d} W$

Following a derivation similar to that in Section A.2 (ch.(A.16), Appendix A), it can be shown that imagining the random process $\mu(x_i,y_i,z_i)$ results in an image which is also a random process with power spectral density $S_g(f_x,f_y)$ given by (6.30).

$$S_g(f_x,f_y) = I_B^2\ \delta(f_x,f_y) - \int_o^d \left| H_i(f_x,f_y,z_i) \right|^2 S_{\mu_i}(f_x,f_y,z_i)\ dz_i \tag{6.30}$$

where I_B is a constant and $H_i(f_x,f_y,z_i)$ is the overall two-dimensional transfer function of the i^{th} layer at a depth z_i.

I_B is given by (A.8a) divided by the DC gain of the tomographic filter if present, H_i is given by (6.2), (6.3) or (6.4) depending on the type of radiologic process considered and S_{μ_i} is given by (6.29).

We can now determine the power in the image which is given by (6.31).

$$P = \iint S_g(f_x,f_y)\ df_x\ df_y \tag{6.31}$$

To determine the signal to noise ratio we separate the power component due to the image of the tomographic layer (P_t) and the noise power due to the other layers (P_n). It is also useful to separate the noise power due to layers between the anode and the plane of cut (P_a) and the noise power due to layers between the plane of cut and the film (P_f). These powers are related as follows:

$$P = P_t + P_n = P_t + P_a + P_f \tag{6.32}$$

If z_t is the depth of the plane of cut and 2t is its thickness, expressions for these powers can be obtained from (6.30) as indicated in (6.33) to (6.36)

$$P = p(z_f, z_a) \tag{6.33}$$

$$P_t = p(z_t - t, z_t + t) \tag{6.34}$$

$$P_a = p(z_t + t, z_a) \tag{6.35}$$

$$P_f = p(z_f, z_t - t) \tag{6.36}$$

where the function $p(z_1,z_2)$ is defined in (6.37) and the depths z_a and z_f determine the limits of the object $(0 \le z_f \le z_a \le d)$.

$$p(z_1,z_2) = \int_{z_1}^{z_2} \left[\iint \left| H_i(f_x,f_y,z_i) \right|^2 S_{\mu_i}(f_x,f_y,z_i)\,df_x\,df_y \right] dz_i \tag{6.37}$$

The corresponding signal to noise ratios (SNR) can then be calculated as follows:

$$\mathrm{SNR} = \frac{P_t}{P_n} = \frac{P_t}{P_a + P_f} = \frac{p(z_t - t,\ z_t + t)}{p(z_t + t,\ z_a) + p(z_f,\ z_t - t)} \tag{6.38}$$

$$SNR_a = \frac{P_t}{P_a} = \frac{P(z_t - t,\ z_t + t)}{p(z_t + t,\ z_a)} \tag{6.39}$$

$$SNR_f = \frac{P_t}{P_f} = \frac{p(z_t - t,\ z_t + t)}{p(z_f,\ z_t - t)} \tag{6.40}$$

It is easy to show that

$$\frac{1}{SNR} = \frac{1}{SNR_a} + \frac{1}{SNR_f} \tag{6.41}$$

or

$$SNR = \frac{SNR_a \times SNR_f}{SNR_a + SNR_f} \tag{6.42}$$

To proceed with the evaluation we consider the case where the intensity distribution in the focal spot is a Gaussian function, as justified in Section 6.2.4 (recall (6.10)), and the object is bandlimited white noise (recall (6.29)) with S_o small, to conform with the approximation in (A.6). Therefore:

$$\iint I_o(x_o,y_o)\ dx_o\ dy_o = \iint \exp\{-\sigma^2 x_o^2 - \sigma^2 y_o^2\}\ dx_o\ dy_o = \frac{\pi}{\sigma^2} \tag{6.43}$$

Although the SNR does not depend on the energy in the focal spot, we consider the case where this energy is a constant indepent of σ to allow a more meaningful comparison of powers when σ varies. Consequently:

$$I_o(x_o,y_o) \triangleq \frac{\sigma^2}{\pi} \exp\{-\sigma^2 x_o^2 - \sigma^2 y_o^2\}$$

and

$$\iint I_0(x_0,y_0)\ dx_0\ dy_0 = 1$$

And if the DC gain of the tomographic filter is also normalized to unity, then $I_B=1$ in all cases. Hence,

$$H_i(f_x,f_y,z_i) = \exp\{-(\frac{\pi}{\sigma})^2 B_i(f_x^2 + f_y^2)\} \tag{6.44}$$

where (6.44) is derived from (6.12), (6.13) and (6.14) and B_i is given by the following table:

Procedure	B_i	
Standard tomography	$(\frac{z_i - \Delta_2}{z_i - d}\ \frac{d}{\Delta_1})^2$	(6.45)
Conventional radiology	$(\frac{z_i}{z_i - d})^2$	(6.46)
Tomographic filtering	$(\frac{z_i}{z_i - d})^2 - (\frac{z_t}{z_t - d})^2$	(6.47)

and finally:

$$S_{\mu_i}(f_x,f_y,z_i) = \left(\frac{d}{d - z_i}\right)^2 S_o \qquad \text{for } -W_i \le f_x,f_y \le W_i \tag{6.48}$$

where $W_i = \frac{d - z_i}{d} W$

Also, to make the results more general, lets assume that the tomographic filter is bandlimited between $-f_c$ and f_c, as discussed in Section 3.2.2 (recall the low-pass filter $H_o(f_x,f_y)$).

Now we can calculate the following integral (refer to (6.37))

$$p(z_1,z_2) = \int_{z_1}^{z_2} \left[\iint \; | H_i(f_x,f_y,z_i) |^2 \; S_{\mu_i}(f_x,f_y,z_i) \; df_x \; df_y \right] dz_i \tag{6.49}$$

Substituting (6.44) and (6.48) into (6.49) we obtain:

$$p(z_1,z_2) = \int_{z_1}^{z_2} \left[\int_{-f_m}^{f_m} \int_{-f_m}^{f_m} \exp\{-2(\tfrac{\pi}{\sigma})^2 \; B_i \; (f_x^2 + f_y^2)\} \left(\frac{d}{d - z_i}\right)^2 S_o \; df_x \; df_y \right] dz_i \tag{6.50}$$

$$= \frac{S_o}{2} (\frac{d\sigma}{\pi})^2 \int_{z_1}^{z_2} \frac{1}{(d - z_i)^2} \; \frac{1}{|B_i|} \; \Phi^2 \{2(\tfrac{\pi}{\sigma})^2 \; B_i \; f_m^2\} \; dz_i \tag{6.51}$$

where $f_m = \min(f_c,W_i)$ and $\Phi(x)$ is a generalized form of the error function to include positive exponentials, as defined in (6.52)

$$\Phi(x) \triangleq \frac{2}{\sqrt{\pi}} \int_0^{\sqrt{|x|}} e^{-\mathrm{sgn}(x)u^2} \; du \tag{6.52}$$

$$= \frac{2}{\sqrt{\pi}} \left[\sum_{n=o}^{\infty} \frac{(-\mathrm{sgn}(x)\;)^n \; |x|^{\frac{2n+1}{2}}}{n!\,(2n + 1)} \right] \tag{6.53}$$

When $x>o$, the function $\Phi(x)$ is the well known error function for the square root of the argument, that is

$$\Phi(x) = \mathrm{erf}(\sqrt{x}) \text{ for } x>o \tag{6.54}$$

When $x<o$, the function $\Phi(x)$ is calculated here using the power series in (6.53) which is absolutely convergent for all real values of x.

Therefore, (6.51) can be calculated to determine the signal to noise ratios in (6.38), (6.39) and (6.40). Since the SNR is a function of several parameters characteristic of the radiologic process such as S_o, σ, d, z_t, W and f_c, whose influence over the SNR is not obvious, equations (6.38), (6.39) and (6.40) were evaluated for more than 4000 cases using (6.51). The integral in (6.51) was calculated using Simpson's rule with 1 mm intervals. The value of d was 1000 mm in all cases. The size of the focal spot, determined by σ (the larger σ is, the smaller the focal spot is), was varied between $\sigma=2$ and $\sigma=10$ (in mm^{-1}) for all combinations of the other parameters. The total thickness of the object was 264 mm in all cases (assumed to be the thickness of a typical chest). The plane of cut was always in the center of the object but the position of the object was varied to observe the effect its position would have on the SNR. Thus, three cases were considered: z_t = 500 mm (object is exactly in the middle between the focal spot and the film), z_t = 520 mm (object is closer to the focal spot) and z_t = 480 mm (object is closer to the film). The thickness of the tomographic layer (2t) was varied between 4 mm and 240 mm (t = 2, 10, 20, 50, 100 and 120 mm).

Two types of object power spectra were considered: white noise ($W = \infty$) and bandlimited white noise (two different bandwidths: W = 4 and 5 cycles/mm), with $S_o = 10^{-2}$, 10^{-5} and 10^{-8} (recall 6.48). The image given by each type of object was bandlimited by the low-pass filter $H_o(f_x,f_y)$ using two cut-off frequencies f_c = 3 and 4 cycles/mm.

The correspondence between object bandwidth and filter bandwidth was as follows (all units in cycles/mm):

W	f_c
∞	3
∞	4
4	3
5	4

These frequencies were chosen so that when the object is bandlimited white noise, the low-pass filter has no effect, that is the image is only bandlimited by the bandwidth of the object itself.

Since it is impractical to include here all the results obtained only sufficient summary tables are produced to support the conclusions.

The following data were selected from the results to show the effect on the SNR by parameters such as the nominal thickness of the cut, the position of the object between focal spot and film, the size of the focal spot, and the bandwidth of the object and the low pass filter. These selected results are given in Tables 6.1 to 6.5.

Table 6.1 shows the variation of the SNR with the thickness of what is considered to be the tomographic layer. It is clear that the SNR (also SNR_a and SNR_f) increases with the thickness of the tomographic layer, as expected, because of the definition of the SNR (recall (6.38), (6.39) and (6.40)).

Table 6.2 shows the variations of the SNR with respect to the position of the object between the focal spot and the film. When the object moves closer to the focal spot the SNR increases in standard tomography but in conventional radiology and tomographic

Table 6.1. The signal to noise ratios versus the thickness of the cut

Fixed parameters: $d = 1000$ mm, $z_t = 500$ mm, $\sigma = 10$, $W = 5$ cycles/mm

$f_c = 4$ cycles/mm.

t(mm) =	2	10	20	50	100	120
Standard tomography						
SNR	0.017	0.089	0.19	0.67	3.6	11.
SNR_a	0.033	0.18	0.39	1.3	7.1	23.
SNR_f	0.033	0.18	0.39	1.3	7.1	23.
Conventional radiology						
SNR	0.015	0.081	0.18	0.60	3.1	9.8
SNR_a	0.036	0.19	0.43	1.5	8.3	27.
SNR_f	0.026	0.14	0.3	0.99	4.9	15.
Tomographic filtering						
SNR	0.013	0.068	0.15	0.48	2.3	7.4
SNR_a	0.045	0.24	0.55	2.1	13.	47.
SNR_f	0.018	0.093	0.2	0.62	2.8	8.7

Table 6.2. The signal to noise ratios versus the position of the object

Fixed parameters: d = 1000 mm, σ = 10, t = 20 mm, W = 5 cycles/mm, f_c = 4 cycles/mm

z_t (mm) =	480	500	520
Standard tomography			
SNR	0.193	0.194	0.195
SNR_a	0.386	0.388	0.391
SNR_f	0.386	0.388	0.391
Conventional radiology			
SNR	0.177	0.176	0.176
SNR_a	0.426	0.427	0.428
SNR_f	0.301	0.300	0.299
Tomographic filtering			
SNR	0.150	0.145	0.140
SNR_a	0.536	0.551	0.567
SNR_f	0.209	0.197	0.185

filtering the SNR decreases. To explain this effect we look more closely at the variations of SNR_a and SNR_f. In conventional radiology and tomographic filtering SNR_a increases and SNR_f decreases when the object is moved towards the focal spot. Since SNR_f dominates over SNR_a ($SNR_f < SNR_a$) SNR also decreases.

A similar argument is in order with regard to the size of the focal spot, as shown in Table 6.3. Indeed, increasing the size of the focal spot causes an increase in size of the system impulse response and moving the object (or the plane of cut) closer to the focal spot also causes an increases in the extent of the impulse response. Consequently, an increase of the impulse response size causes an increase of SNR in standard tomography and a decrease of SNR in conventional radiology and tomographic filtering, where SNR_a increases but SNR_f decreases, resulting in a decrease of SNR. These results are in agreement with the conclusions drawn from the practical results in Chapter 5, where the difficulty of filtering for layers closer to the focal spot was recognized (cf. Section 5.3.2). One might be tempted to conclude here that a smaller focal spot would be preferred for tomographic filtering. Although this may be true with respect to noise in the image, it is important to recognize that the 'noise' due to the presence of other layers is highly structured and not white noise as assumed here. Consequently, larger focal spots may still be preferred (recall (6.16)). Since in practice the focal spot is given, the best results will be obtained by adjusting the filter parameters such as the magnitude hard-limit and cutoff frequency.

Table 6.3. The signal to noise ratios versus the size of the focal spot

Fixed parameters: $d = 1000$ mm, $z_t = 500$ mm, $t = 20$ mm, $W = 5$ cycles/mm

σ =	2	4	6	8	10
Standard tomography					
SNR	0.490	0.270	0.221	0.203	0.194
SNR_a	0.980	0.541	0.442	0.406	0.388
SNR_f	0.980	0.541	0.442	0.406	0.388
Conventional radiology					
SNR	0.164	0.165	0.168	0.173	0.176
SNR_a	0.470	0.470	0.465	0.447	0.427
SNR_f	0.253	0.254	0.264	0.283	0.300
Tomographic filtering					
SNR	$7.7\ 10^{-23}$	$9.5\ 10^{-5}$	$3.5\ 10^{-2}$	0.11	0.15
SNR_a	$1.3\ 10^{+2}$	2.1	0.96	0.67	0.55
SNR_f	$7.7\ 10^{-23}$	$9.5\ 10^{-5}$	$3.5\ 10^{-2}$	0.13	0.20

Similar results are obtained with variations of the bandwidth of the object (Table 6.4) or the bandwidth of the low-pass filter (Table 6.5). In standard tomography the SNR increases when the object bandwidth or the cutoff frequency increase. On the other hand in conventional radiology and tomographic filtering the SNR decreases because it is dominated by SNR_f which decreases. Note also that when the object is bandlimited white noise (i.e. when $H_0(f_x,f_y)$ has no effect) in standard tomography SNR_a is equal to SNR_f.

When the system parameters are the same (that is, any column in Tables 6.1 to 6.5) the signal to noise ratios compare as follows (the arrows denote how they increase):

	SNR_a	SNR_f	SNR
Standard tomography			
Conventional radiology	$\downarrow$	$\uparrow$	$\uparrow$
Tomographic filtering			

Therefore, the SNR is largest for standard tomography and smallest for tomographic filters. From this we cannot conclude that tomographic filters are useless because with real objects the noise is structured and the SNR may be perceived differently by the eye. On the other hand, SNR_a is always largest for tomographic filters, which shows that the tomographic filtering technique performs better for layers in the object closer to the film.

6.2.6 The Radiation Dose

The goal in diagnostic radiology is to obtain as much relevant information as possible from inside a patient's body, while keeping the total radiation dose to a minimum to reduce any possible danger to the patient.

Table 6.4. The signal to noise ratios versus the bandwidth of the object

Fixed parameters: $d = 1000$ mm, $z_t = 500$ mm, $\sigma = 10$, $t = 20$ mm.

W(cycles/mm) =	4	5
Standard tomography		
SNR	0.189	0.194
SNR_a	0.377	0.388
SNR_f	0.377	0.388
Conventional radiology		
SNR	0.178	0.176
SNR_a	0.408	0.430
SNR_f	0.316	0.300
Tomographic filtering		
SNR	0.164	0.145
SNR_a	0.478	0.550
SNR_f	0.250	0.200

Table 6.5. The signal to noise ratios versus the cutoff frequency.

Fixed parameters: d = 1000 mm, z_t = 500 mm, σ = 10, t = 20 mm,

W = ∞ (100 cycles/mm)

f_c (cycles/mm) =	3	4
Standard tomography		
SNR	0.192	0.211
SNR_a	0.308	0.349
SNR_f	0.508	0.537
Conventional radiology		
SNR	0.186	0.177
SNR_a	0.428	0.460
SNR_f	1.176	0.288
Tomographic filtering		
SNR	0.180	0.124
SNR_a	0.571	0.841
SNR_f	0.262	0.146

Each radiologic procedure represents a compromise between dose, and image and diagnostic qualities [84]. Standard tomography must be regarded as a relatively high exposure-dose procedure and it is used only when there are specific indications which outweight the risks [81, p.314]. The radiation dose per exposure, typically 1-2 rad., is comparable to conventional radiology, but the total dose is usually greater since multiple exposures are the rule. Indeed, since the location of the relevant structures is not usually known, various tomograms have to be obtained until their positions are known; this is especially true in the case that the details are small. It was formerly believed that the dose in standard tomography could be kept low using a simultaneous multisection technique: Instead of using just one film, several films (typically five or six) are contained in a multicassette box and spaced at about 1 cm. apart. However the total dose to the patient is not reduced if intensifying screens are used, in which case the patient dose is comparable to the one with the same number of single section exposures [85].

Here the advantage of a tomographic filtration process is clear. With a single radiograph and tomographic filtering operations an indication of the positions of the structures can be obtained. Once they are known, a subsequent thin-section tomogram at the proper depth using standard techniques may give a more accurate representation. Indeed, it has been suggested [84] that a diagnostic hierarchy could be formulated which would significantly reduce the total radiation levels to which specific types of patients are exposed. A tomographic filtration process would fit well in such a hierarchy, especially when on-line image processing and communication systems [86] are available in hospitals which will facilitate the storage, retrieval, processing, and display of the pictorial data.

Chapter VII

CONCLUSIONS AND RECOMMENDATIONS

7.1 Summary and Conclusions

In this dissertation we have introduced, analyzed and implemented a new class of filters for tomographic deblurring of conventional radiographs. Initially we proposed and studied a detailed model for the radiologic process, which revealed the physics and mathematics of the formation of the X-ray images. The salient feature of this model and the analyses throughout this dissertation has been the consideration of what happens when three-dimensional objects are imaged by X-rays. Problems of non-linearities and space-variance were disclosed and a number of solutions and approximations were discussed to make the system tractable. The model was used to determine the characteristics of tomographic filters for selective deblurring of the images of the layers in the object. Tomographic filters have inverse filter characteristics. Although the transfer functions of different layers have the same shape, selective deblurring is possible because they differ by a scaling factor. The effect of tomographic filtering on overlaying layers was investigated. It was found that the overall transfer functions have lowpass characteristics between the tomographic layer and the focal spot and highpass characteristics between the tomographic layer and the film.

Interactive optical, electro-optical, or digital signal processing facilities are necessary for the implementation of tomographic filters. We have developed a realization using two-dimensional digital signal processing techniques because of the advantages over optical processing previously discussed. In addition, digital computers can be used to perform operations of pattern recognition or artifical intelligence, either fully-automated or semi-automated, interacting with a radiologist. The growing interest in digital techniques for image processing has resulted in the appearance of some very recent books on the subject by leading researchers in this field [77], [87]-[90].

The two types of digital filtering techniques, recursive and non-recursive have been considered. The windowing design technique and non-recursive implementations using the FFT were chosen for this application. Indeed, although recursive realizations may be faster than non-recursive filters and require less memory, the design of recursive filters to approximate arbitrary magnitude and phase responses requires a fair amount of computational power. Since the filters designed in this dissertation were used only a few times it was not advisable to decrease the execution time at the expense of increasing the design time. For the same reason no attempts were made to optimize the length of the impulse response. The data management problems associated with the processing of large matrices in a digital computer were discussed and solutions proposed. Some of the digital signal processing techniques developed in this dissertation have already made an impact in the literature. Indeed the IIR filter design techniques presented in Section 4.4 have been applied by Harrison [99] to the processing of geophysical data for the point determinations of ore grade from a Canadian copper mine. An alternate extension of this design method which facilitates frequency response optimization via nonlinear programming has been published by Goodman [100]. Goodman's filters also make use of the spectral transformations introduced in Section 4.5 (published in [65]). O'Connor and Huang [101] have generalized the result in Section 4.5 [65] and presented a stability preserving mapping theorem which allows most recursive filters of a particular type to be mapped into another type of recursive filter.

The theoretical and practical evaluations of the performance of tomographic filters have shown that the image quality results cannot be as good as those of standard tomography or three-dimensional radiographic reconstruction techniques in terms of the thickness of the tomographic layer. Nevertheless, a tomographic filtration process allows the image analyst to interact with the system to exploit its capabilities, rather than being a passive observer of an image. A tomographic filtration process has also the advantage that it can be implemented without the use of any special purpose X-ray hardware and while other tomographic procedures use moving parts during the exposure and depend on multiple exposures to obtain additional information from a patient's body with the consequent increase in radiation dose to the patient, a tomographic filtration process uses instead multiple filtrations of a single radiograph without endangering the patient.

A measure of the rate of change of the transfer function from layer to layer in a special case (i.e. with a Gaussian exposure function $I_o(x,y)$) has shown that in an interval around the plane of cut tomographic filtering offers a higher rate of change than standard tomography but that interval becomes negligible when actual distances are used. Examples of the size of that interval in various cases have been given.

Finally, the SNR has served as a valuable tool in providing a better understanding of the mathematical behavior of the various radiologic procedures such as standard tomography, conventional radiology and tomographic filtering, as well as allowing comparisons between systems.

In conclusion then, tomographic filtering is a new technique that may find practical applications in diagnostic radiology, especially when used interactively. Its main advantage is that it can be used with conventional radiology equipment and its main drawback is the noise generated by the high-pass filter effect on the layers in the film side.

7.2 Recommendations for Future Research

The work presented in this dissertation constitutes a first approach to the problem of recovering three-dimensional information from a single radiograph. We have concentrated on proving the feasibility of tomographic filters from a technical point of view and we have developed methods for their digital implementation. Both analytical and experimental evaluations were performed; however the usual limitations of time and cost precluded the possibility of more extensive tests. There are both short term and long term possibilities and both are considered here.

- development of the appropriate image processing hardware (including image acquisition, storage, retrieval and display).

- development of the appropriate utility functions in software (e.g. magnification, minification, intensity mappings, etc.)
- development of information quality standards so that the results of experiments can be judged accordingly and rules can be set for calibration of experiments.
- evaluation of different methods to overcome the problems of inverse filtering.
- evaluation of other filter structures for tomographic filtering (e.g. homomorphic, Wiener, etc.).
- investigate the use of recursive filters for image restoration (e.g. "recursive tomographic filters").
- effects of the order of the tomographic filter on the quality of the results.
- effects of computer wordlength, mode of arithmetic, roundoff errors, etc., specifically to the application.
- study further the fact that tomographic filtering produces a high-pass overall transfer function between the tomographic layer and the film. Is that really a disadvantage or an advantage?
- investigate the "tomographic filtering of tomograms", that is change the plane of cut of a tomogram by means of tomographic filtering.
- investigate what shape and size of focal spot X-ray intensity distribution (i.e. the exposure function $I_o(x,y)$) are more desirable taking into account the trade-offs: e.g. larger focal spots give better depth resolution but restoration is difficult.

- medical evaluation of tomographic filtering taking into account the variables dependent on the human body such as position and size of lesions, overlaying structures (e.g. ribs), exposure, geometry, direction of the projection, etc., in order to find out for what applications (e.g. type of disease, organ, lesions, etc.) would tomographic filtering be preferred over other methods in the medical imaging hierarchy.
- investigate the use of tomographic filtering as a pre-processing technique for automated pattern recognition processes.
- investigate the problem of identifying the blur characteristics from the radiograph itself, using the techniques of power spectrum and power cepstrum estimation (refer to example in Appendix A, Section A.7).
- investigate other areas of application of the tomographic filtering concept (e.g. geophysics, astronomy, image analysis, etc.)
- study the man-machine interaction human factors, in particular the novel image perception and analysis methods required by interactive tomographic filtering and investigate the possibility of a new profession: "medical image analyst" and/or "medical image specialist" [98] which would require backgrounds in engineering, psychology and medicine.

Considering all the previous variables, the medical evaluation of processed radiographs is left for the experts in this field, such as a panel of radiologists with the appropriate interactive image processing facilities.

Our hypothesis about the future of computers in X-ray diagnosis is the following: Interactive systems should be developed to combine the judgement of a human specialist with computation power in solving the problem of the diagnoses of radiographs. The development of more intelligent algorithms would alleviate the tasks of radiologists and improve the accuracy of the diagnoses. The processing of images by computer and the availability of visual terminals throughout hospitals would facilitate the storage, transmission and retrieval of radiographs and other medical imagery.

APPENDICES

Appendix A

THE MATHEMATICS OF TOMOGRAPHIC FILTERING

A.1 Introduction

In this appendix the mathematics of standard tomography, conventional radiology, and tomographic filtering are studied in depth and compared. The analogy between standard tomography and tomographic filtering is further clarified by this analysis.

First a mathematical model of standard tomography is derived. It is shown that a tomogram can be filtered to change the depth of the plane of cut and the transfer function of such a filter is derived. A mathematical model of conventional radiology is then obtained by considering conventional radiology as a special case of standard tomography, in which the plane of cut coincides with the film and the movement of the point source is replaced by a finite-size source. Again it is shown how tomographic filtering can convert a radiograph into a tomogram. Finally, the algorithm used to simulate the radiologic process in a digital computer is described.

A.2 A Mathematical Model of Standard Tomography

The derivation of an equation describing the image formation process in standard tomography will serve to derive the equation of image formation in conventional radiology and to compare tomographic filtering with standard tomography.

This derivation was motivated by that in [48]. We have removed some of the constraints in [48] (namely, the linear movement of a constant-intensity X-ray source), while we have added others relevant to this application (namely, small displacements of the X-ray source). Nevertheless, none of these constraints imply a lack of generality in the derivation. The notation has been kept consistent with that of Chapter II. Readers without a background in linear system theory will find this derivation more clear than that of conventional radiology in Chapter II, although the result is essentially the same, as it will be shown in the following sections.

Consider the diagram of standard tomography shown in Figure A.1. In our model, the punctual X-ray source can move anywhere in a plane parallel to the film. This movement can be linear, circular, spiral, etc., even the scanning of an area may be considered. Generally the intensity I_o of the X-ray source may change with its location. In standard tomography the film also moves in synchronism with the X-ray source to keep the desired plane of cut in focus.

Suppose a reference coordinate system x,y,z with origin at O. The coordinates of a point in a plane at a depth z_i are denoted by (x_i,y_i). Let Δ_1 and d be the distances from the X-ray source to the plane of cut and to the film, respectively. Thus, $\Delta_2 \triangleq d-\Delta_1$ is the distance from the plane of cut to the film.

When the source of X-rays is at (x_o,y_o), the coordinates of the centre of the film (x_c,y_c) are given in (A.1).

$$x_c = K\, x_o \tag{A.1a}$$

$$y_c = K\, y_o \tag{A.1b}$$

where

$$K = -\,\Delta_2/\Delta_1 \tag{A.2}$$

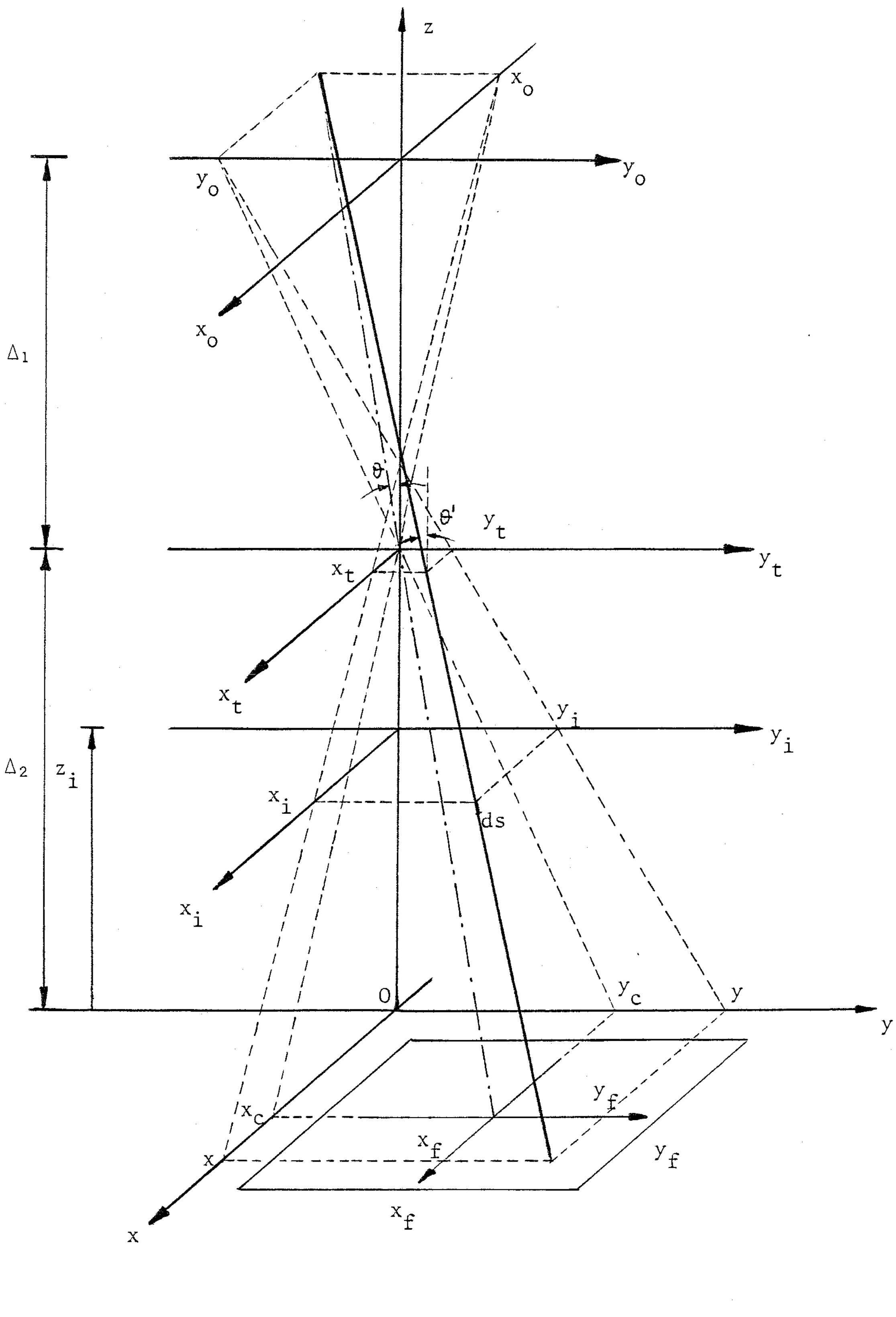

Figure A.1. Diagram of standard tomography.

Thus, the relationship between the absolute coordinates (x,y) on the film plane and the coordinates (x_f,y_f) of a point in the film with respect to the centre of the film is given by:

$$x = x_c + x_f = K\, x_o + x_f \tag{A.3a}$$

$$y = y_c + y_f = K\, y_o + y_f \tag{A.3b}$$

The coordinates (x_i,y_i,z_i) of any point in the space between the film and the focal spot can be expressed as a function of (x_o,y_o) — the point of origin of the X-ray passing through (x_i,y_i,z_i), and (x_f,y_f) — the point of impact of that X-ray on the film:

$$x_i = \frac{(z_i-\Delta_2)x_o}{\Delta_1} + \frac{d-z_i}{d}\, x_f \tag{A.4a}$$

$$y_i = \frac{(z_i-\Delta_2)y_o}{\Delta_1} + \frac{d-z_i}{d}\, y_f \tag{A.4b}$$

For a punctual source of X-rays at (x_o,y_o) emitting an intensity $I_o(x_o,y_o;x_f,y_f)$ towards the point (x_f,y_f) on the film, the intensity $I(x_f,y_f;x_o,y_o)$ reaching that point is (cf. (2.2)):

$$I(x_f,y_f;x_o,y_o) = I_o(x_o,y_o;x_f,y_f)\ \exp\left\{-\int_s \mu(x_i,y_i,z_i)\, ds\right\} \tag{A.5}$$

where $\mu(x_i,y_i,z_i)$ is the function representing the distribution of linear attenuation coefficients and s denotes the path between (x_o,y_o) and (x_f,y_f).

Approximations

1) $I_o(x_o,y_o;x_f,y_f)$ can be assumed with good approximation independent of (x_f,y_f) [48]. Thus, $I_o(x_o,y_o;x_f,y_f) \simeq I_o(x_o,y_o)$.

2) ds is replaced by dz_i

$$ds = \frac{dz_i}{\cos\theta'} \simeq \frac{dz_i}{\cos\theta} = \sqrt{1 + \tan^2\theta}\ dz_i = \sqrt{1 + \frac{x_o^2+y_o^2}{\Delta_i^2}}\ dz_i$$

If the displacements of the X-ray source are small compared to the distance from the X-ray source to the plane of cut, then $x_o, y_o << \Delta_1$, in which case $ds \simeq dz_i$.

3) Since the values of the linear attenuation coefficients, or at least their variations from point to point, are small, the exponential in (A.5) can be approximated by the linear terms of its Taylor series expansion [48].

Therefore, taking into account all these approximations, (A.5) becomes:

$$I(x_f,y_f;x_o,y_o) = I_o(x_o,y_o) \left[1 - \int_0^d \mu(x_i,y_i,z_i)\ dz_i \right] \qquad (A.6)$$

When the source of X-rays moves and its intensity is given by $I_o(x_o,y_o)$ while the film also moves simultaneously as defined in (A.3), the total intensity after the exposure at any point (x_f,y_f) on the film is

$$\begin{aligned} I(x_f,y_f) &= \iint I(x_f,y_f;x_o,y_o)\ dx_o\ dy_o = \\ &= \iint I_o(x_o,y_o) \left[1 - \int_0^d \mu(x_i,y_i,z_i)\ dz_i \right] dx_o\ dy_o = \\ &= I_B - \int_0^d I_i(x_f,y_f,z_i)\ dz_i \end{aligned} \qquad (A.7)$$

where

$$I_B = \iint I_o(x_o,y_o)\ dx_o\ dy_o \qquad (A.8a)$$

$$I_i(x_f,y_f,z_i) = \iint I_o(x_o,y_o)\ \mu(x_i,y_i,z_i)\ dx_o\ dy_o \qquad (A.8b)$$

and the values of x_i and y_i are given in (A.4) as a function of x_o, y_o, x_f, y_f, and z_i.

Replacing (A.4) into (A.8b) we obtain

$$I_i(x_f,y_f,z_i) = \iint I_o(x_o,y_o) \times$$

$$\times \mu\left(\frac{(z_i-\Delta_2)x_o}{\Delta_1} + \frac{d-z_i}{d} x_f \; , \; \frac{(z_i-\Delta_2)y_o}{\Delta_1} + \frac{d-z_i}{d} y_f \; , \; z_i\right) dx_o \; dy_o \quad \text{(A.9)}$$

Make the following change of variables:

$$\frac{(z_i-\Delta_2)x_o}{\Delta_1} = -\frac{d-z_i}{d}\xi; \quad x_o = \frac{z_i-d}{z_i-\Delta_2}\frac{\Delta_1}{d}\xi; \quad dx_o = K_i \; d\xi \quad \text{(A.10a)}$$

$$\frac{(z_i-\Delta_2)y_o}{\Delta_1} = -\frac{d-z_i}{d}\eta; \quad y_o = \frac{z_i-d}{z_i-\Delta_2}\frac{\Delta_1}{d}\eta; \quad dy_o = K_i \; d\eta \quad \text{(A.10b)}$$

where

$$K_i = \frac{z_i-d}{z_i-\Delta_2}\frac{\Delta_1}{d} \quad \text{(A.10c)}$$

Thus, by replacing (A.10) into (A.9) we obtain (A.11).

$$I_i(x_f,y_f,z_i) = K_i^2 \iint I_o(K_i\xi,K_i\eta) \; \mu\left(\frac{d-z_i}{d}(x_f-\xi), \; \frac{d-z_i}{d}(y_f-\eta), z_i\right) d\xi \; d\eta \quad \text{(A.11)}$$

Since (A.11) is a convolution, in the frequency domain it becomes a product (cf. Table B.1):

$$G_i(f_x,f_y,z_i) = H_i(f_x,f_y,z_i) \; F_\mu(f_x,f_y,z_i) \quad \text{(A.12)}$$

where

$$G_i(f_x,f_y,z_i) = \iint I_i(x,y,z_i) \; e^{-j2\pi(f_x x+f_y y)} \; dx \; dy \quad \text{(A.13)}$$

$$H_i(f_x,f_y,z_i) = K_i^2 \iint I_o\left(\frac{z_i-d}{z_i-\Delta_2}\frac{\Delta_1}{d}x, \frac{z_i-d}{z_i-\Delta_2}\frac{\Delta_1}{d}y\right) e^{-j2\pi(f_x x+f_y y)}\, dx\, dy \tag{A.14}$$

$$F_\mu(f_x,f_y,z_i) = \iint \mu\left(\frac{d-z_i}{d}x, \frac{d-z_i}{d}y, z_i\right) e^{-j2\pi(f_x x+f_y y)}\, dx\, dy \tag{A.15}$$

Replacing (A.12) into the Fourier transform† of (A.7) we obtain (A.16).

$$\begin{aligned} G(f_x,f_y) &= I_B\, \delta(f_x,f_y) - \int_0^d G_i(f_x,f_y,z_i)\, dz_i \\ &= I_B\, \delta(f_x,f_y) - \int_0^d H_i(f_x,f_y,z_i)\, F_\mu(f_x,f_y,z_i)\, dz_i \end{aligned} \tag{A.16}$$

where $G(f_x,f_y)$ is the Fourier transform of the tomogram $I(x_f,y_f)$ (cf. (A.7)) and $H_i(f_x,f_y,z_i)$ is the transfer function of the i^{th} layer, at a distance z_i from the film, as given in (A.14).

Equation (A.16) is the equation of standard tomography in the frequency domain. This result agrees with that in [48], with the appropriate changes of notation, of course.

A.3 Change of the Plane of Cut by Filtering the Tomogram

In our model of standard tomography the depth of the plane of cut is $z_i=\Delta_2$ (cf. Figure A.1). As $z_i\to\Delta_2$, $I_o\left(\frac{z_i-d}{z_i-\Delta_2}\frac{\Delta_1}{d}x, \frac{z_i-d}{z_i-\Delta_2}\frac{\Delta_1}{d}y\right)$ in (A.14) approaches an impulse whose Fourier transform is a constant.

---

† The linearity property of the Fourier transform (cf. Table B.1) is used to find the Fourier transform of (A.7).

Thus, the transfer function of the plane of cut is a constant and its impulse response is an impulse, as expected by intuition (cf. Figure A.1).

Equation (A.16) suggests that we can change the plane of cut by filtering the tomogram. Indeed, suppose we are interested in the plane at a depth $z_i = z_t$. Dividing both sides of (A.16) by $H(f_x,f_y) \overset{\Delta}{=} H_t(f_x,f_y,z_t)$ we obtain:

$$\frac{G(f_x,f_y)}{H(f_x,f_y)} = I_B \frac{\delta(f_x,f_y)}{H(f_x,f_y)} - \int_0^d \frac{H_i(f_x,f_y,z_i)}{H(f_x,f_y)} F_\mu(f_x,f_y,z_i)\, dz_i \qquad \text{(A.17)}$$

After filtering the tomogram with $H^{-1}(f_x,f_y)$, the overall transfer function for the layer at a depth z_t is a constant; thus this layer has become the new plane of cut. The overall transfer function of the previous plane in focus ($z_i = \Delta_2$) is now $H^{-1}(f_x,f_y)$, namely the filter transfer function. The overall transfer function for any other layer is $H_i(f_x,f_y,z_i)\, H^{-1}(f_x,f_y)$.

A.4 A Mathematical Model of Conventional Radiology

Consider a radiologic system with focal-spot intensity distribution $I_o(x_o,y_o)$ and film to focal-spot distance d. The diagram in Figure A.1 still applies if we let $\Delta_2=0$ and the movement of the punctual source of X-rays in standard tomography is replaced by the intensity distribution of the finite-size focal spot. Under these conditions all the equations derived previously are still valid with $\Delta_2=0$.

The intensity on the film is given by (A.7):

$$I(x_f,y_f) = I_B - \int_0^d I_i(x_f,y_f,z_i)\, dz_i \qquad \text{(A.7)}$$

with I_B as previously defined and $I_i(x_f,y_f,z_i)$ as given in (A.20) (cf. (A.11)).

$$I_i(x_f,y_f,z_i) = K_i^2 \iint I_o\left(\frac{z_i-d}{z_i}\,\xi,\ \frac{z_i-d}{z_i}\,\eta\right) \times$$

$$\times\ \mu\left\{\frac{d-z_i}{d}\,(x_f-\xi),\ \frac{d-z_i}{d}\,(y_f-\eta), z_i\right\}\ d\xi\ d\eta \qquad (A.20)$$

By letting $\mu(x,y)=\delta(x,y)$, an impulse, we obtain the impulse response of the i^{th} layer, which of course, agrees with that derived in Chapter II.

In the frequency domain (A.12) and (A.16) are equally valid, but in conventional radiology the transfer function $H_i(f_x,f_y,z_i)$ of each layer is (cf. (A.14) and let $\Delta_2=0$):

$$H_i(f_x,f_y,z_i) = K_i^2 \iint I_o\left(\frac{z_i-d}{z_i}\,x,\frac{z_i-d}{z_i}\,y\right)\ e^{-j2\pi(f_x x+f_y y)}\ dx\ dy \qquad (A.21)$$

where

$$K_i = \frac{z_i-d}{z_i}$$

Therefore, the mathematical models of standard tomography and conventional radiology are similar but with different transfer functions. In radiology none of the transfer functions is identically equal to a constant except in the limiting case that $z_i=0$ (film plane).

A.5 Tomographic Filtering of Radiographs

As we did in (A.17) we can filter a radiograph so that the transfer function of one of the layers is equal to a constant, thus converting a radiograph into a tomogram. Indeed, consider (A.22).

$$\frac{G(f_x,f_y)}{H(f_x,f_y)} = I_B \frac{\delta(f_x,f_y)}{H(f_x,f_y)} - \int_0^d \frac{H_i(f_x,f_y,z_i)}{H(f_x,f_y)} F_\mu(f_x,f_y,z_i)\, dz_i \qquad (A.22)$$

where $H_i(f_x,f_y,z_i)$ is defined in (A.21) and

$$H(f_x,f_y) = H_i(f_x,f_y,z_i)\Big|_{i=t} = H_t(f_x,f_y,z_t) =$$

$$= \left(\frac{z_t-d}{z_t}\right)^2 \iint I_o\left[\frac{z_t-d}{z_t}\, x,\ \frac{z_t-d}{z_t}\, y\right] e^{-j2\pi(f_x x+f_y y)}\, dx\, dy \qquad (A.23)$$

Consequently, we have shown that by comparing the movement of a punctual X-ray source with a finite size focal spot and replacing the movement of the film in standard tomography by the filtration of a conventional radiograph, we can establish a conceptual analogy between standard tomography and tomographic filtering.

A.6 Computer Simulation of the Radiologic Process

In this section we describe the procedure used to obtain the computer simulated X-ray images for some of the experiments in Chapter V. For this purpose we coded the routine XRAY in FORTRAN IV. A brief description of the assumptions made and the work performed by this routine follows.

In order to simulate an actual system as closely as possible, the linear model was not used in this approximation, but rather the exponentials were calculated. Thus, the routine XRAY implements a discretization of (2.4). The film plane and the focal spot plane are divided into rectangular cells and the object is devided into thin layers parallel to the film, which are also divided into cells.

The film and focal spot cells have an X-ray intensity with them that is stored in computer memory in the form of two-dimensional arrays. The intensity within each cell is assumed to be uniform. The cells in the object have attenuation factors associated with them which are stored in computer memory in the form of a three-dimensional array. All these arrays are assumed to be centred with respect to the centre ray.

Thus, there is an elementary beam of X-rays from each cell in the focal spot to each cell in the film plane. For each film cell the contributions from all the cells in the focal spot are added up taking into account the attenuation experienced by each beam within the object. Each beam has the shape of a truncated pyramid, and its attenuation is calculated as follows:

$$I = I_o \prod_{k=1}^{K} \frac{\sum_{i=1}^{N_k} [E_i a_i + a_o]}{A_k} \tag{A.24}$$

where:

- I attenuated intensity that reaches a cell in the film.
- I_o intensity of the X-rays emitted from a cell in the focal spot.
- K number of layers in the object.
- N_k number of cells in the k^{th} layer that intercept the X-ray beam.
- E_i attenuation factor of each cell intercepted by the X-ray beam.
- a_i area of the portion of each cell intercepted by the X-ray beam.
- a_o area of the cross-section of the beam which does not intercept the k^{th} layer.
- A_k area of the cross-section of the beam with the plane of the k^{th} layer.

It should be noted that $\sum_{i=0}^{N_k} a_i = A_k$ and in the simplest cases we may have $a_i = A_k$ if the beam crosses the k^{th} layer within one cell only.

The calculation of (A.24) is repeated for all cells in the focal spot and in the film. This is similar to convolution but not quite, due to the presence of more than one layer interacting multiplicatively. That is why we have not used fast convolution techniques in this simulation.

Since the object is defined by layers of attenuation factors rather than attenuation coefficients, some correction may be necessary to take into account the different apparent thicknesses of the cells in a layer depending on the position in the field. This would not be necessary if the layers were spherical with centres in the focal spot.

Space-variant radiologic systems can also be simulated with XRAY because the angle of the focal spot is taken into account.

The source listing of XRAY is given in Appendix C.

A.7 Example of Focal-spot Parameter Estimation in Radiographs

The techniques of power spectrum and power cepstrum estimation might be used to obtain from a radiograph some of the characteristics of the focal spot.

We have shown that typical focal spots have a twin-peaked intensity distribution (see Figures 3.10 to 3.14). The parameter that we want to estimate in this example is the distance between peaks and their orientation. This information is useful in determining the phase characteristics of the transfer function. The given data is a radiograph of an object obtained with a twin-peaked focal spot. For simplicity we assume that the system is space-invariant (i.e., the focal spot is parallel to the film) and the object is planar with similar statistics anywhere in the field.

The first step is to estimate the power spectrum of the radiograph. Since the power spectrum is the result of an averaging process, it retains little of the flavor of the original image, while the characteristics of the blur due to the focal spot intensity distribution are strongly manifested.

Consider how the distance 2d between peaks of the PSF will show up in the power spectrum. The twin peaks of the PSF may be described by a Gaussian-shaped single peak at the origin convolved with a pair of impulses at the distance 2d. In the frequency domain this corresponds to the product of the transform of a single peak with a cosine function of frequency d. Therefore the power spectrum has periodic zeros in a certain direction at intervals 1/d.

A direct search for zero crossings usually fails because they are obscured in practice by the randomness of the object and noise. A better approach is to compute the power cepstrum, which is the Fourier transform of the logarithm of the power spectrum. It has been shown [56] that periodic zeros in the power spectrum at intervals 1/d result in large negative spikes in the power spectrum at a distance d from the origin. The orientation of the spikes determines also the orientations of the peaks of the PSF. This technique has been used successfully [55] in the case of motion blur and out of focus blur in photographic images.

Appendix B

THE TWO-DIMENSIONAL FOURIER TRANSFORM

B.1 Introduction

In this appendix we study some aspects of the two-dimensional Fourier transform that are not readily available in the literature. The definitions and properties which are straightforward extensions from one dimension are only summarized for reference. We emphasize those properties which do not have counterparts in one dimension.

In Section B.2 the two-dimensional Fourier transform is defined and some manipulations, such as changing the reference coordinate system and transforming circularly-symmetric functions are considered. In Section B.3 some properties inherent in the two-dimensional Fourier transform are presented, including the projection-slice theorem for the case of parallel projection rays. In Section we study the possibility of extending the projection-slice theorem to the case of divergent projection rays. Finally, in Section B.4 the two-dimensional discrete Fourier transform and its fast implementation by a digital computer are considered.

B.2 Definitions

The two-dimensional Fourier transform of a complex function of two independent real variables, x and y, is defined [7] as

$$G(f_x,f_y) = \mathscr{F}\{g(x,y)\} = \iint g(x,y)\ \exp\{-j2\pi(f_x x+f_y y)\}\ dx\ dy \qquad (B.1)$$

The two-dimensional inverse Fourier transform of a function $G(f_x,f_y)$ is defined in (B.2).

$$g(x,y) = \mathscr{F}^{-1}\{G(f_x,f_y)\} = \iint G(f_x,f_y)\ \exp\{j2\pi(xf_x+yf_y)\}\ df_x\ df_y \quad (B.2)$$

In (B.1) and (B.2) we have used a rectangular coordinate system as reference. The coordinate system may be changed, in which case the Jacobian of the transformation appears in the integrands of (B.1) or (B.2) in order to maintain the differential area constant. In the case of circularly symmetric functions sometimes it is very convenient to use a polar coordinate system. The equations which define the transformation and inverse transformation from rectangular to polar coordinates in both the xy and $f_x f_y$ planes are the following:

$$\left.\begin{aligned} r &= \sqrt{x^2+y^2} & x &= r\cos\theta \\ \theta &= \arc\tan\frac{y}{x} & y &= r\sin\theta \\ \rho &= \sqrt{f_x^2+f_y^2} & f_x &= \rho\cos\phi \\ \phi &= \arc\tan\frac{f_y}{f_x} & f_y &= \rho\sin\phi \end{aligned}\right\} \quad (B.3)$$

Applying the coordinate transformations (B.3) to (B.1), the Fourier transform of $\lambda(r,\theta) \triangleq g(r\cos\theta\ ,\ r\sin\theta)$ can be written as

$$\Lambda(\rho,\phi) = \int_0^{2\pi}\left[\int_0^{\infty} r\ \lambda(r,\theta)\ \exp[-j2\pi r\rho\cos(\theta-\phi)]\ dr\right] d\theta \quad (B.4)$$

If $\lambda(r,\theta)$ is circularly symmetric, i.e. $\lambda_o(r) \triangleq \lambda(r,\theta)$, the Fourier transform of $\lambda_o(r)$ is

$$\Lambda(\rho,\phi) = \int_0^{\infty} r\ \lambda_o(r)\left[\int_0^{2\pi} \exp[-j2\pi r\rho\cos(\theta-\phi)]\ d\theta\right] dr \quad (B.5)$$

which can be written as a function of the zeroth-order Bessel function of the first kind $J_o(\cdot)$, as in (B.6).

$$\Lambda_o(\rho) \stackrel{\Delta}{=} \mathscr{F}\{\lambda_o(r)\} = 2\pi \int_0^\infty r\ \lambda_o(r)\ J_o(2\pi r\rho)\ dr \tag{B.6}$$

Thus the Fourier transform of a circularly symmetric function is itself circularly symmetric and can be found by performing the one-dimensional manipulation in (B.6). This expression is referred to as the Fourier-Bessel transform, or alternatively, as the Hankel transform of order zero. By means of arguments identical with those used previously, similar results can be derived for the inverse transform.

B.3 Properties

Since all the properties of the one-dimensional Fourier transform can be extended directly to two dimensions, they are only summarized in Table B.1 and we will not discuss them here. Rather, we consider those properties in two dimensions which do not have counterparts in one dimension.

1) *Separable functions:* A function separable in rectangular coordinates, $g(x,y) = g_1(x)\ g_2(y)$ has the particularly simple property that its two-dimensional Fourier transform can be found as a product of one-dimensional Fourier transforms [7]:

$$\begin{aligned} G(f_x,f_y) &= \iint g(x,y)\ \exp[-j2\pi(f_x x+f_y y)]\ dx\ dy \\ &= \int g_1(x)\ \exp[-j2\pi f_x x]\ dx \int g_2(y)\ \exp[-j2\pi f_y y]\ dy \end{aligned} \tag{B.7}$$

Table B.1. Properties of the Two-Dimensional Fourier Transform

LINEARITY	$\mathcal{F}\{ag(x,y)+bh(x,y)\} = aG(f_x,f_y)+bH(f_x,f_y)$
CONVOLUTION	$\mathcal{F}\{g(x,y) * h(x,y)\} = G(f_x,f_y)\ H(f_x,f_y)$
SCALING	$\mathcal{F}\{g(ax,by)\} = (1/\lvert ab\rvert)\ G(f_x/a,f_y/b)$
SHIFTING	$\mathcal{F}\{g(x-a,y-b)\} = G(f_x,f_y)\ \exp[-j2\pi(af_x,bf_y)]$
AUTOCORRELATION	$\mathcal{F}\{\int\int g(\xi,\eta)g^*(\xi-x,\eta-y)d\xi d\eta\} = \lvert G(f_x,f_y)\rvert^2$
PARCEVAL'S THEOREM	$\mathcal{F}\{\int\int g(x,y)h^*(x,y)dxdy\} = \int\int G(f_x,f_y)H^*(f_x,f_y)df_x df_y$
HERMITIAN	$G(f_x,f_y) = G^*(-f_x,-f_y)$ if $g(x,y)$ is a real function
INVERSION	$\mathcal{F}\{\mathcal{F}^{-1}\{g(x,y)\}\} = \mathcal{F}^{-1}\{\mathcal{F}\{g(x,y)\}\} = g(x,y)$

2) *Spatial frequencies:* The two-dimensional Fourier transform may be regarded as a decomposition of a function $g(x,y)$ into a linear combination of elementary functions of the form $\exp\{j2\pi(f_x x+f_y y)\}$. Such functions have a number of interesting properties [7]. Note that for any particular frequency pair (f_x,f_y) the corresponding elementary function has zero phase along lines described by

$$y = -\frac{f_x}{f_y}\ x + \frac{n}{f_y} \quad \text{(n an integer)} \tag{B.8}$$

The Fourier transform in two dimensions can be interpreted as the spatial frequency components of the signal. Thus, the frequency components of the signal in a certain direction constitute a "slice" of the two-dimensional Fourier transform. This is proved by the projection-slice theorem.

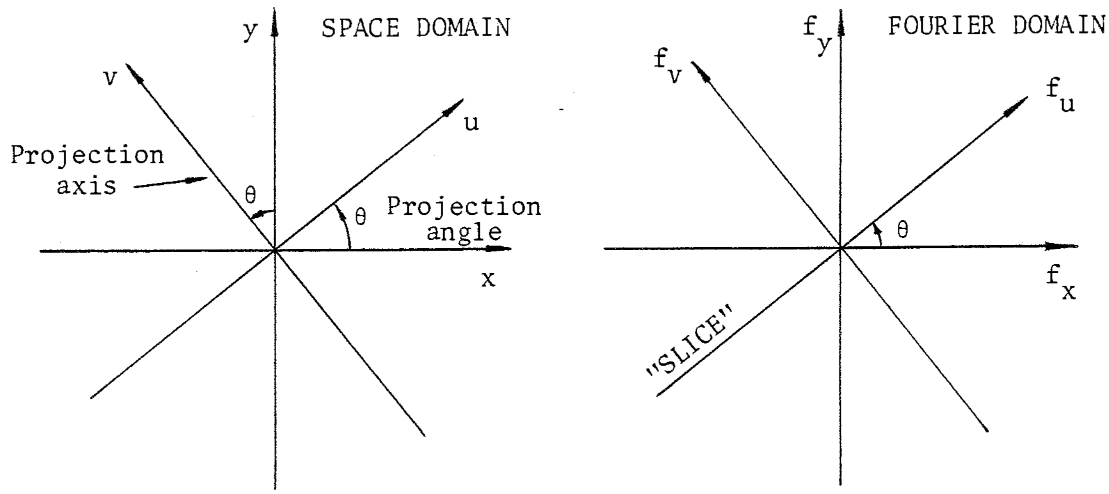

$$p_v(u) = \int g(u,v)\, dv \qquad P_v(f_u) = G(f_u, f_v)\Big|_{f_v=0} = G(f_u, 0)$$

Figure B.1. The projection-slice theorem.

3) *Projection-slice theorem:* The one-dimensional Fourier transform of a projection is a "slice" of the two-dimensional Fourier transform. This is illustrated in Figure B.1 and the proof may be found in [2]. The projection-slice theorem is the basis for many algorithms for computerized tomography.

This theorem can also be used as an alternative to the Henkel transform for computing the Fourier transform of circularly-symmetric functions without the need for Bessel functions. Indeed, the frequency-domain slice $\Lambda_o(\rho)$ in (B.6) can be calculated by doing a projection of the circularly-symmetric function followed by a one-dimensional Fourier transform.

B.4 Radial Projection-Slice Theorem

The projection-slice theorem introduced previously assumes that the projection rays are parallel. This is not always the case; in radiology for example, there is a point-like source of diverging X-rays and the projection-slice theorem is no longer valid. To our knowledge, an equivalent theorem considering diverging projection rays has not been proposed yet. With diverging rays the theorem may still be true but with a more complicated type of slice.

We have studied this hypothesis in depth from different points of view but we were not able to prove it.

B.5 The DFT and FFT in Two Dimensions

A discretization of (B.1) and (B.2) results in the two-dimensional discrete Fourier transform (DFT) and the two-dimensional inverse discrete Fourier transform (IDFT), respectively, as shown in (B.9) and (B.10), where the subscripts p indicate that the signals are periodic [13].

$$X_p(k_1,k_2) = \sum_{n_1=0}^{N_1-1} \sum_{n_2=0}^{N_2-1} x_p(n_1,n_2) \exp[-j\frac{2\pi}{N_1}n_1k_1] \exp[-j\frac{2\pi}{N_2}n_2k_2] \tag{B.9}$$

$$x_p(n_1,n_2) = \frac{1}{N_1N_2} \sum_{k_1=0}^{N_1-1} \sum_{k_2=0}^{N_2-1} X_p(k_1,k_2) \exp[j\frac{2\pi}{N_1}n_1k_1] \exp[j\frac{2\pi}{N_2}n_2k_2] \tag{B.10}$$

The properties of the two-dimensional DFT are similar to those of the two-dimensional Fourier transform, given in Table B.1.

Equations (B.9) and (B.10) can be evaluated as a series of one-dimensional DFT's and therefore the fast Fourier transform (FFT) may be used. This is clear if we rewrite (B.9) as

$$X_p(k_1,k_2) = \sum_{n_1=0}^{N_1-1} \exp[-j\frac{2\pi}{N_1} n_1 k_1] \left[\sum_{n_2=0}^{N_2-1} x_p(n_1,n_2) \exp[-j\frac{2\pi}{N_2} n_2 k_2] \right] \quad (B.11)$$

Since $x_p(n_1,n_2)$ is usually given in the form of a matrix, (B.11) can be evaluated by performing N_1 FFT's on the columns of $x_p(n_1,n_2)$ thus obtaining another matrix that we call $y_p(n_1,k_2)$. We then perform N_2 FFT's on the rows of $y_p(n_1,k_2)$. Since computers store data sequentially, to operate on the rows of a matrix we must either transpose it and operate on the columns, or use a FFT program capable of processing every N_2-th element of the sequentially stored matrix (e.g. subroutine FFT2 in Appendix C).

Appendix C

SOURCE PROGRAM LISTINGS

This appendix contains the source listings of the principal computer programs developed during the course of this work. These programs were selected because of their generality, shortness, and possible usefulness to other researchers. Consequently, no main programs or subprograms that were too specific or too long are included here.

The programs are written in FORTRAN IV and run on an IBM 370/165-II computer using both the WATFIV and IBM FORTRAN (G1 and H Extended) compilers. In order to save compilation time and number of cards read, a load-module library (USER.COMMLIB) was created on-line. The subprograms used more frequently were optimized, compiled, and stored in USER.COMMLIB.

The programs are organized here into functional groups and presented in the following order:

1) *Fast Fourier Transform Programs*

VFFT - Calculates the DFT or IDFT of a set of complex numbers.

RLTR - Completes the transform when VFFT is used with real data.

FFT2 - Calculates the two-dimensional DFT or IDFT of a complex matrix (calls VFFT).

FFT2R - Calculates the two-dimensional DFT of a real matrix or the IDFT of a hermitian matrix (calls VFFT and RLTR).

FFT2D - Calculates the DFT or IDFT of a complex matrix stored in auxiliary storage (calls VFFT).

2) *Two-Dimensional FIR Filter Design Programs*

HKWBPF - Calculates the impulse response of a two-dimensional Kaiser-window band-pass or low-pass filter (calls BFJ1, BFI0, and HMI).

BFJ1 - Generates the first-order Bessel function of the first kind.

BFI0 - Generates the modified zeroth-order Bessel function of the first kind.

HMI - Copies one half of a matrix into the other half.

3) *Two-Dimensional IIR Filter Design and Realization Programs*

CDFILT - Determines the coefficients of a circularly-symmetric low-pass, high-pass, or band-pass two-dimensional IIR filter (calls DFILT and PTPHCC).

DFILT - Determines the coefficients of a two-dimensional low-pass IIR filter (calls RTMI and FRESIN).

FRESIN - Calculates the magnitude response of a two-dimensional IIR filter at any spatial frequency.

PTPHCC - Normalizes, prints and punches the coefficients of a two-dimensional IIR filter.

GFRES - Evaluates the magnitude response of a two-dimensional IIR filter in any rectangular region of spatial frequencies (calls FRESIN).

FILTER - Implements a two-dimensional high-pass or band-pass IIR filter (calls CCP2 and ASCALE).

CCP2 - Implements a two-dimensional low-pass IIR filter using the technique of complex cascade programming (calls TRANSF).

4) *Programs Related to Radiologic Systems*

XRAY - Simulates a radiologic process of given characteristics.

INVFHL - Calculates the magnitude response of an inverse filter with a given hard-limit.

The programs developed and used in this dissertation for the design and realization of tomographic filters, power-spectrum estimation, histogram equalization, etc. are not included here because they are too long and specific. They are also computer-instalation dependant because they use disk and tape files and the plotting system.

5) *Utility Programs*

PICPRT - Produces a pictorial output using the line printer.

ASCALE - Scales the elements of an array.

DBS - Transforms an array of numbers to decibels.

CMAG2 - Calculates the squared magnitude of the two-dimensional DFT given by FFT2R.

COMPLT - Completes the array given by CMAG2 using symmetries.

CAMOVE - Produces a two-dimensional circular shift of the elements of a matrix.

CTDW2 - Multiplies a matrix by a two-dimensional cosine taper data window.

TRANSF - Implements all linear transformations which map a square matrix onto itself.

Other powerful utility subroutines were used and are not included here because of space limitations. These are:

RTMI - Finds the roots of a given function using Mueller's iteration scheme (IBM System/360, Scientific Subroutine Package, Version III, Programmer's Manual, IBM publication GH20-0205-4, 1970, pp. 217-219).

CONTUR - Plots a set of contour lines by interpolating in a matrix [68].

PERSP - Plots a perspective view of a surface defined by a matrix with hidden line elimination (available from the author).

NGRAPH - Plots multiple graphs of one-dimensional arrays (available from the author).

WINDOW - Generates several types of window functions (available from the author).

CALCSIM - Package of subroutines which require little memory space and simulate the Gould or Calcomp plotting system using a line printer (available from the author).

The source listings of the previously mentioned programs start in the following page.

1) Fast Fourier Transform Programs

```
      SUBROUTINE VFFT (X, Y, NT, IFN)
C                                J.M. COSTA  1976 0512 1810  VER 01.01
C  THIS SUBROUTINE CALCULATES THE DISCRETE FOURIER TRANSFORM OR THE
C  INVERSE DISCRETE FOURIER TRANSFORM OF A SET OF COMPLEX NUMBERS USING
C  THE FAST FOURIER TRANSFORM ALGORITHM DEVELOPED BY G. SANDE (MIXED
C  RADIX 4 AND RADIX 2, SEE W.M. GENTLEMAN AND G. SANDE, FAST FOURIER
C  TRANSFORMS - FOR FUN AND PROFIT, 1966 FALL JOINT COMPUTER
C  CONFERENCE). THE CALCULATION IS DONE IN PLACE, THAT IS THE OUTPUT
C  DATA REPLACES THE INPUT DATA. THE M-TH COMPLEX OUTPUT DATA POINT
C  OF THE N POINT DISCRETE FOURIER TRANSFORM IS
C
C              N            -(K-1)
C     CO(M) = SUM  CI(K) * W       ,  WHERE W = EXP(J*2*PI*(M-1)/N),
C             K=1
C
C  J IS THE IMAGINARY OPERATOR, AND CI(K) IS THE K-TH COMPLEX INPUT
C  DATA POINT. SIMILARLY, THE K-TH COMPLEX OUTPUT DATA POINT OF THE N
C  POINT INVERSE DISCRETE FOURIER TRANSFORM IS
C
C                    N             (K-1)
C     CO(K) = (1/N) SUM  CI(M) * W       .
C                   M=1
C
C  THIS IMPLEMENTATION OF THE FAST FOURIER TRANSFORM RECURSIVELY
C  CALCULATES THE EXPONENTIAL FUNCTION IN ORDER TO GET GREATER
C  SPEED AT THE EXPENSE OF SOME LOSS OF PRECISION.
C  THE SUBROUTINE PARAMETERS ARE AS FOLLOWS.
C
C  X       - ARRAY OF LENGTH N CONTAINING THE REAL PART OF THE DATA.
C  Y       - ARRAY OF LENGTH N CONTAINING THE IMAGINARY PART OF THE DATA.
C  NT      - NUMBER OF ELEMENTS IN EACH OF THE ARRAYS X AND Y.
C            NT/IABS(IFN) MUST BE A POWER OF TWO NOT GREATER THAN 8192.
C  IFN     - INPUT PARAMETER, EQUAL TO +INC FOR THE TRANSFORM,
C                             EQUAL TO -INC FOR THE INVERSE TRANSFORM.
C            INC REPRESENTS THE INCREMENT BETWEEN DATA ELEMENTS
C            (NORMALLY 1).  IT ALLOWS THE USE OF MULTI-DIMENSIONAL
C            OR SPECIAL (E.G. COMPLEX) ARRAYS.  IF INC IS EQUAL TO 1,
C            EVERY ELEMENT OF THE ARRAYS X AND Y IS USED.  WHEN INC IS
C            GREATER THAN 1, ONLY EVERY INC-TH ELEMENT OF EACH ARRAY
C            IS USED.  THE NUMBER OF COMPLEX POINTS USED IN THE
C            TRANSFORM IS NT/INC.  THIS NUMBER MUST BE A POWER OF TWO
C            NOT GREATER THAN 8192.
C
      DIMENSION X(NT),Y(NT),KE(13),KI(13),CA(6),SA(6)
      EQUIVALENCE (KE( 1),KE01), (KE( 2),KE02), (KE( 3),KE03),
     *            (KE( 4),KE04), (KE( 5),KE05), (KE( 6),KE06),
     *            (KE( 7),KE07), (KE( 8),KE08), (KE( 9),KE09),
     *            (KE(10),KE10), (KE(11),KE11), (KE(12),KE12),
     *            (KE(13),KE13)
      EQUIVALENCE (KI( 1),KI01), (KI( 2),KI02), (KI( 3),KI03),
     *            (KI( 4),KI04), (KI( 5),KI05), (KI( 6),KI06),
     *            (KI( 7),KI07), (KI( 8),KI08), (KI( 9),KI09),
     *            (KI(10),KI10), (KI(11),KI11), (KI(12),KI12),
     *            (KI(13),KI13)
      DATA NP/-999/,INCP/-999/,IOUT/6/,LG2NMX/13/,PI2/6.283185/
C
C  CHECK TO SEE IF THE INITIALIZATION HAS BEEN DONE
      INC=IABS(IFN)
      IF (NT.EQ.NP .AND. INC.EQ.INCP) GO TO 250
C
C  FIND THE LOGARITHM (BASE 2) OF THE NUMBER OF POINTS
      INCP=INC
      INCT2=INC+INC
      NP=INCT2
      DO 100 LOG2N=1,LG2NMX
        IF (NP.EQ.NT) GO TO 120
        NP=NP+NP
  100 CONTINUE
C
      NP=-999
      IF (NT.NE.INC) WRITE(IOUT,1000) NT,INC
 1000 FORMAT(18H0***ERROR IN VFFT,,I8,29H DATA POINTS AT INCREMENTS OF,
     -       I6,26H IS NOT A POWER OF TWO ***)
      RETURN
C
C  SET UP THE UNSCRAMBLING LOOP PARAMETERS (NOTE THAT THE VARIABLES
C  KE-J AND KI-J ARE EQUIVALENCED TO KE(J) AND KI(J) RESPECTIVELY)
  120 KE01=NT
      KI01=NT/2
      DO 200 J=2,LG2NMX
        KE(J)=KI(J-1)
        KI(J)=MAX0(KE(J)/2,INC)
```

```
  200 CONTINUE
C
C  SET UP THE INITIAL VALUES FOR THE RECURSIVE CALCULATION OF
C  THE TWIDDLE FACTORS
      AN=1.0/FLOAT(NT/INC)
      IF (LOG2N.EQ.1) GO TO 250
      FM4=PI2*AN
      LOG4N=LOG2N/2
      DO 230 K=1,LOG4N
        CA(K)=COS(FM4)
        SA(K)=SIN(FM4)
        FM4=4.0*FM4
  230 CONTINUE
C
  250 IF (IFN.GE.0) GO TO 320
C
C  FOR THE INVERSE TRANSFORM ONLY,
C  FORM THE COMPLEX CONJUGATE OF THE INPUT DATA
      DO 300 I=1,NT,INC
  300 Y(I)=-Y(I)
C
  320 IF (LOG2N.EQ.1) GO TO 650
C
C
C  CALCULATE THE RADIX 4 FAST FOURIER TRANSFORM
      M4=NT
      DO 600 K=1,LOG4N
        M=M4/4
        CC=CA(K)
        SS=SA(K)
        C1=1.0
        S1=0.0
C
        DO 500 J=1,M,INC
          IF(J.EQ.1) GO TO 340
C
C  CALCULATE THE TWIDDLE FACTORS
          C2=C1*C1-S1*S1
          S2=C1*S1+C1*S1
          C3=C2*C1-S2*S1
          S3=C2*S1+S2*C1
  340     JMM4=J-M4
C
          DO 400 I=M4,NT,M4
            J0=I+JMM4
            J1=J0+M
            J2=J1+M
            J3=J2+M
            AR0=X(J0)+X(J2)
            AR1=X(J0)-X(J2)
            AI0=Y(J0)+Y(J2)
            AI1=Y(J0)-Y(J2)
            AR2=X(J1)+X(J3)
            AR3=X(J1)-X(J3)
            AI2=Y(J1)+Y(J3)
            AI3=Y(J1)-Y(J3)
            X(J0)=AR0+AR2
            Y(J0)=AI0+AI2
            IF (J.EQ.1) GO TO 360
C
C  MULTIPLY BY THE TWIDDLE FACTORS
            X(J2)=C1*(AR1+AI3)+S1*(AI1-AR3)
            Y(J2)=C1*(AI1-AR3)-S1*(AR1+AI3)
            X(J1)=C2*(AR0-AR2)+S2*(AI0-AI2)
            Y(J1)=C2*(AI0-AI2)-S2*(AR0-AR2)
            X(J3)=C3*(AR1-AI3)+S3*(AI1+AR3)
            Y(J3)=C3*(AI1+AR3)-S3*(AR1-AI3)
            GO TO 400
C
C  TWIDDLE FACTORS ARE ONE AND ZERO
  360       X(J2)=AR1+AI3
            Y(J2)=AI1-AR3
            X(J1)=AR0-AR2
            Y(J1)=AI0-AI2
            X(J3)=AR1-AI3
            Y(J3)=AI1+AR3
  400     CONTINUE
C
C  CALCULATE THE NEXT SET OF TWIDDLE FACTORS RECURSIVELY
          TMP=C1*CC-S1*SS
          S1=C1*SS+S1*CC
          C1=TMP
  500   CONTINUE
        M4=M
  600 CONTINUE
C
C
C  PICK UP ANY EXTRA FACTORS OF TWO TO COMPLETE THE TRANSFORM
      IF (LOG2N.EQ.2*LOG4N) GO TO 750
  650 DO 700 I=1,NT,INCT2
```

```
      J=I+INC
      AR0=X(I)+X(J)
      AI0=Y(I)+Y(J)
      X(J)=X(I)-X(J)
      Y(J)=Y(I)-Y(J)
      X(I)=AR0
      Y(I)=AI0
  700 CONTINUE
C
C  UNSCRAMBLE THE OUTPUT ARRAYS
  750 JJ=1
      DO 800 K13= 1 ,KE13,KI13
      DO 800 K12=K13,KE12,KI12
      DO 800 K11=K12,KE11,KI11
      DO 800 K10=K11,KE10,KI10
      DO 800 K09=K10,KE09,KI09
      DO 800 K08=K09,KE08,KI08
      DO 800 K07=K08,KE07,KI07
      DO 800 K06=K07,KE06,KI06
      DO 800 K05=K06,KE05,KI05
      DO 800 K04=K05,KE04,KI04
      DO 500 K03=K04,KE03,KI03
      DO 800 K02=K03,KE02,KI02
      DO 800 K01=K02,KE01,KI01
        IF (JJ.LE.K01) GO TO 800
        TEMP=X(JJ)
        X(JJ)=X(K01)
        X(K01)=TEMP
        TEMP=Y(JJ)
        Y(JJ)=Y(K01)
        Y(K01)=TEMP
  800 JJ=JJ+INC
C
C  FOR THE INVERSE TRANSFORM ONLY,
C  FORM THE COMPLEX CONJUGATE OF THE SCALED OUTPUT ARRAY
      IF (IFN.GE.0) RETURN
      DO 900 I=1,NT,INC
        X(I)=AN*X(I)
        Y(I)=-AN*Y(I)
  900 CONTINUE
      RETURN
C
      END
```

```
      SUBROUTINE RLTR (X,Y,NT,IFN)
C                                   J.M. COSTA   1976 0312 1360   VER 01.01
C  POSITIVE IFN CASE:
C  IF IFN IS GREATER THAN ZERO, THIS SUBROUTINE COMPLETES THE DISCRETE
C  FOURIER TRANSFORM OF N+N REAL DATA VALUES, WHERE THE ORIGINAL DATA
C  VALUES ARE STORED ALTERNATELY IN THE ARRAYS X AND Y, THAT IS
C  X(1),Y(1),X(INC+1),Y(INC+1), ... ,X(INC*(N-1)+1),Y(INC*(N-1)+1),
C  AND ARE FIRST TRANSFORMED BY A COMPLEX FOURIER TRANSFORM OF LENGTH N.
C  AFTER CALLING RLTR THE REAL PART OF THE COEFFICIENTS OF THE DISCRETE
C  FOURIER TRANSFORM IS STORED IN X(1),X(INC+1), ... ,X(INC*N+1), AND
C  THE IMAGINARY PART IN Y(1),Y(INC+1), ... ,Y(INC*N+1).  THE OTHER HALF
C  OF THE COEFFICIENTS CAN BE OBTAINED BY COMPLEX CONJUGATION.
C  A TYPICAL CALLING SEQUENCE IS:
C                                         CALL VFFT (X,Y,N*INC,+INC)
C                                         CALL RLTR (X,Y,(N+1)*INC,+INC)
C
C  NEGATIVE IFN CASE:
C  IF IFN IS LESS THAN ZERO, THE INVERSE TRANSFORM IS DONE, THE FIRST
C  STEP IN EVALUATING A REAL FOURIER SERIES.  THE TIME DOMAIN RESULTS
C  ALTERNATE IN ARRAYS X AND Y, THAT IS X(1),Y(1),X(INC+1),Y(INC+1), ...
C  X(INC*(N-1)+1),Y(INC*(N-1)+1).
C  A TYPICAL CALLING SEQUENCE IS:
C                                         CALL RLTR (X,Y,(N+1)*INC,-INC)
C                                         CALL VFFT (X,Y,N*INC,-INC)
C
C  THE SUBROUTINE PARAMETERS ARE AS FOLLOWS.
C  X    - ARRAY OF LENGTH N CONTAINING THE ODD NUMBERED ELEMENTS OF AN
C         ARRAY OF REAL DATA OR THE REAL PART OF AN ARRAY OF COMPLEX DATA
C  Y    - ARRAY OF LENGTH N CONTAINING THE EVEN NUMBERED ELEMENTS OF AN
C         ARRAY OF REAL DATA OR THE IMAGINARY PART OF AN ARRAY OF COMPLEX
C         DATA.
C  NT   - NUMBER OF DATA POINTS IN EACH OF THE ARRAYS X AND Y PLUS INC.
C  IFN  - INPUT PARAMETER, EQUAL TO +INC FOR THE TRANSFORM,
C                          EQUAL TO -INC FOR THE INVERSE TRANSFORM.
C           INC REPRESENTS THE INCREMENT BETWEEN DATA ELEMENTS
C           (NORMALLY 1).  IT ALLOWS THE USE OF MULTI-DIMENSIONAL
C           OR SPECIAL (E.G. COMPLEX) ARRAYS.  IF INC IS EQUAL TO 1,
C           EVERY ELEMENT OF THE ARRAYS X AND Y IS USED.  WHEN INC IS
C           GREATER THAN 1, ONLY EVERY INC-TH ELEMENT OF EACH ARRAY
C           IS USED.  THE NUMBER OF COMPLEX POINTS USED IN THE
```

```
C            TRANSFORM IS (NT-INC)/INC.  THIS NUMBER MUST BE A POWER OF
C            TWO.
C
      DIMENSION X(NT),Y(NT)
C
C   INITIALIZATION
      INC=IABS(IFN)
      NK=NT-INC
      N=NK/INC
      NK=NK+2
      NH=NK/2
      SS=3.14159265358979/FLOAT(N)
      CC=COS(SS)
      SS=SIN(SS)
      C=-1.0
      S=0.0
      IF(IFN.LT.0) GO TO 20
      C=-C
      SS=-SS
      X(NK-1)=X(1)
      Y(NK-1)=Y(1)
C
C   COMPLETE THE TRANSFORM OR INVERSE TRANSFORM
   20 DO 30 J=1,NH,INC
      K=NK-J
      AA=X(J)+X(K)
      AB=X(J)-X(K)
      BA=Y(J)+Y(K)
      BB=Y(J)-Y(K)
      XX=C*BA+S*AB
      YY=S*BA-C*AB
      Y(K)=0.5*(YY-BB)
      Y(J)=0.5*(YY+BB)
      X(K)=0.5*(AA-XX)
      X(J)=0.5*(AA+XX)
      AA=CC*C-SS*S
      S=SS*C+CC*S
      C=AA
   30 CONTINUE
      RETURN
C
      END
```

```
      SUBROUTINE FFT2 (X, Y, M, N, MX, IFN)
C                                               J.M. COSTA   1975 1128 0125
C   THIS SUBROUTINE CALCULATES THE TWO-DIMENSIONAL DISCRETE FOURIER
C   TRANSFORM OR THE INVERSE TWO-DIMENSIONAL DISCRETE FOURIER TRANSFORM
C   OF A MATRIX OF COMPLEX NUMBERS.  THE TWO-DIMENSIONAL TRANSFORM IS
C   DECOMPOSED INTO A SERIES OF ONE-DIMENSIONAL TRANSFORMS, BY ROWS AND
C   BY COLUMNS, FOR WHICH THE SUBROUTINE VFFT IS CALLED.
C   THE TRANSFORMATION IS DONE IN PLACE, THAT IS THE OUTPUT DATA REPLACES
C   THE INPUT DATA.
C   THE SUBROUTINE PARAMETERS ARE AS FOLLOWS.
C   X        - MATRIX CONTAINING THE REAL PART OF THE DATA.
C   Y        - MATRIX CONTAINING THE IMAGINARY PART OF THE DATA.
C   M        - FIRST DIMENSION OF X AND Y.
C   N        - SECOND DIMENSION OF X AND Y.
C   MX       - INPUT PARAMETER THAT ALLOWS PROCESSING SUBMATRICES OF
C              X AND Y.  NORMALLY SET MX=M TO PROCESS ENTIRE MATRICES.
C              TO PROCESS THE MX BY NX SUBMATRICES OF X AND Y WITH UPPER
C              LEFT HAND CORNER (I,J) USE THE FOLLOWING CALL
C                        CALL FFT2 (X(I,J),Y(I,J),M,NX,MX,IFN)
C   IFN      - INPUT PARAMETER, EQUAL TO +INC FOR THE TRANSFORM,
C                               EQUAL TO -INC FOR THE INVERSE TRANSFORM.
C              INC REPRESENTS THE INCREMENT BETWEEN DATA ELEMENTS
C              (NORMALLY 1).  IT ALLOWS THE USE OF MULTI-DIMENSIONAL
C              OR SPECIAL (E.G. COMPLEX) ARRAYS.  IF INC IS EQUAL TO 1,
C              EVERY ELEMENT OF THE ARRAYS X AND Y IS USED.  WHEN INC IS
C              GREATER THAN 1, ONLY EVERY INC-TH ELEMENT OF EACH ARRAY
C              IS USED.  THE NUMBER OF COMPLEX POINTS USED IN THE
C              TRANSFORM IS MX/INC IN THE FIRST DIMENSION AND N IN THE
C              SECOND DIMENSION.  THESE NUMBERS MUST BE POWERS OF TWO.
C
      DIMENSION X(M,N),Y(M,N)
C
C   FFT BY ROWS
      DO 3 I=1,N
    3 CALL VFFT(X(1,I),Y(1,I),MX,IFN)
C
C   FFT BY COLUMNS
      INC=IABS(IFN)
      MN=M*N
      IFN1=ISIGN(M,IFN)
```

```
      DO 6 I=1,MX,INC
    6 CALL VFFT(X(I,1),Y(I,1),MN,IFN1)
C
      RETURN
      END
```

```
      SUBROUTINE FFT2R (X,MT,NT,ISN)
C                                             J.M. COSTA   1976 0312 1135
C  THIS SUBROUTINE CALCULATES THE TWO-DIMENSIONAL DISCRETE FOURIER
C  TRANSFORM OF A MATRIX OF REAL NUMBERS OR THE INVERSE TWO-DIMENSIONAL
C  DISCRETE FOURIER TRANSFORM OF A HERMITIAN MATRIX.
C  SINCE THE TRANSFORM AF A REAL MATRIX IS A HERMITIAN MATRIX THIS
C  SUBROUTINE GIVES ONE HALF OF THE TRANSFORMED MATRIX ONLY.  THE OTHER
C  HALF CAN BE OBTAINED BY COMPLEX CONJUGATION.  THE TRANSFORMATION IS
C  DONE IN PLACE.  SPACE FOR AN ADDITIONAL COMPLEX ROW OR COLUMN MUST
C  BE PROVIDED.  SIMILARLY, FOR THE INVERSE TRANSFORM SUPPLY ONE HALF
C  OF A HERMITIAN MATRIX ONLY AND THE RESULT WILL BE A REAL MATRIX.
C  SUBROUTINES NEEDED: VFFT AND RLTR.
C  THE SUBROUTINE PARAMETERS ARE AS FOLLOWS.
C  X   - TWO-DIMENSIONAL ARRAY OF DIMENSIONS MT BY NT.
C  MT  - FIRST DIMENSION OF X.
C  NT  - SECOND DIMENSION OF X.
C  ISN - INPUT PARAMETER, POSITIVE FOR THE TRANSFORM, NEGATIVE FOR THE
C        INVERSE TRANSFORM. IN ADDITION, ISN DETERMINES IF AN EXTRA
C        ROW OR AN EXTRA COLUMN HAS BEEN SUPPLIED FOR THE HERMITIAN
C        MATRIX. THE DIMENSIONS OF X SHOULD BE INTERPRETED AS FOLLOWS.
C        IF IABS(ISN)=1, THEN X(MT,NT) = X(M+2,N)
C        IF IABS(ISN)=2, THEN X(MT,NT) = X(M,N+2)
C        WHERE M AND N MUST BE POWERS OF TWO.
C
      DIMENSION X(MT,NT)
      MTXNT=MT*NT
      IF(IABS(ISN).GT.1) GO TO 60
C
C
C  THE DIMENSIONS OF X ARE X(M+2,N)
      M=MT-2
      IF (ISN.LT.0) GO TO 30
C
C  TRANSFORM
      DO 10 I=1,NT
      CALL VFFT (X(1,I),X(2,I),M,2)
   10 CALL RLTR (X(1,I),X(2,I),MT,2)
      DO 20 I=1,MT,2
   20 CALL VFFT (X(I,1),X(I+1,1),MTXNT,MT)
      RETURN
C
C  INVERSE TRANSFORM
   30 DO 40 I=1,MT,2
   40 CALL VFFT (X(I,1),X(I+1,1),MTXNT,-MT)
      DO 50 I=1,NT
      CALL RLTR (X(1,I),X(2,I),MT,-2)
   50 CALL VFFT (X(1,I),X(2,I),M,-2)
      RETURN
C
C
C  THE DIMENSIONS OF X ARE X(M,N+2)
   60 N=NT-2
      MTXN=MT*N
      MPM=MT+MT
      IF(ISN.LT.0) GO TO 90
C
C  TRANSFORM
      DO 70 I=1,MT
      CALL VFFT (X(I,1),X(I,2),MTXN,MPM)
   70 CALL RLTR (X(I,1),X(I,2),MTXNT,MPM)
      DO 80 I=1,NT,2
   80 CALL VFFT (X(1,1),X(1,I+1),MT,+1)
      RETURN
C
C  INVERSE TRANSFORM
   90 DO 100 I=1,NT,2
  100 CALL VFFT (X(1,I),X(1,I+1),MT,-1)
      DO 110 I=1,MT
      CALL RLTR (X(I,1),X(I,2),MTXNT,-MPM)
  110 CALL VFFT (X(I,1),X(I,2),MTXN,-MPM)
      RETURN
C
      END
```

```
      SUBROUTINE FFT2D (X,Y,M,N,K,IFN,BUFFER,MK)
C
C                                            JOSEP M. COSTA  1975 0523 1429
C   THIS SUBROUTINE CALCULATES THE 2D DISCRETE FOURIER TRANSFORM OR THE
C   INVERSE 2D DISCRETE FOURIER TRANSFORM OF A 2D ARRAY OF COMPLEX
C   NUMBERS STORED IN AUXILIARY STORAGE.
C   THE 2DARRAY OF DIMENSIONS M BY N IS DIVIDED INTO N/K BLOCKS OF M BY K
C   ELEMENTS SO THAT THE STORAGE REQUIRED IN THE COMPUTER MAIN MEMORY IS
C   3*M*K WORDS ONLY.  THE AVERAGE NUMBER OF READ AND WRITE OPERATIONS
C   IS 2*K*(2*K+3).
C   A NUMBER OF OPTIONS FOR THE INPUT AND OUTPUT OF THE DATA ARE
C   AVAILABLE TO SAVE BOTH CPU AND I/O TIME.  THE ARGUMENT IFN CONTROLS
C   THIS OPTIONS.
C   THE VALUES OF IUX AND IUY ARE INTERCHANGED IN THE SUBROUTINE WITH THE
C   VALUES OF JUX AND JUY, RESPECTIVELY.  IN THIS WAY, AT ANY TIME IUX
C   AND IUY POINT TO THE UNITS CONTAINING THE DATA AND JUX AND JUY REFER
C   TO THE UNITS USED AS WORKING FILES.
C
C   THE SUBROUTINE PARAMETERS ARE AS FOLLOWS.
C   X       - WORK ARRAY OF LENGTH MK FOR THE REAL PART OF THE DATA.
C   Y       - WORK ARRAY OF LENGTH MK FOR THE IMAGINARY PART OF THE DATA.
C   M       - NUMBER OF ROWS IN THE 2D ARRAY
C   N       - NUMBER OF COLUMNS IN THE 2D ARRAY
C   K       - NUMBER OF ROWS IN EACH BLOCK
C   BUFFER  - WORK ARRAY OF LENGTH MK
C   MK      - M*K.  MUST BE SUPPLIED FOR DIMENSIONING.
C   IFN     - SIGNED TWO DIGIT INTEGER NUMBER
C             =0 DO NOTHING (RETURN)
C             >0 TRANSFORM
C             <0 INVERSE TRANSFORM
C             FIRST DIGIT OF IFN (CONTROLS THE INPUT)
C             =1  READ NORMAL INPUT FROM UNITS IUX AND IUY
C             =2  READ SCRAMBLED INPUT FROM UNITS IUX AND IUY
C             SECOND DIGIT OF IFN (CONTROLS THE OUTPUT)
C             =1  UNSCRAMBLE THE OUTPUT AND STORE RESULTS IN UNITS IUX
C                 AND IUY
C             =2  GIVE SCRAMBLED OUTPUT IN UNITS IUX AND IUY
C
C   FOR MOST EFFICIENCY, CODE IFN=12 FOR THE TRANSFORM AND IFN=-21 FOR
C   THE INVERSE TRANSFORM.
C
      DIMENSION X(MK), Y(MK), BUFFER(MK)
      COMMON /TIMING/ ITIME(5,10),ITT
      COMMON /FILES/ IUX,IUY,JUX,JUY
      DATA PI/3.141593/
      DATA LMAX/20/
C
C   INITIALIZATION
      IF(MK.NE.M*K) GO TO 2
      KP=1
      DO 1 L=1,LMAX
      KP=KP*K
      IF(KP.EQ.N) GO TO 5
    1 CONTINUE
    2 WRITE(6,6000) M,N,K,MK,IFN
      RETURN
 6000 FORMAT('-*** ERROR IN FFT2D, INCONSISTENT DIMENSIONS:   M=',
     -         I6,'   N=',I6,'   K=',I6,'   MK=',I6,'   IFN=',I6,'  ***')
    5 IF(IFN.EQ.0) RETURN
      IFNP=IABS(IFN)
      IF(IFNP.GT.22) GO TO 2
      IFNIN=IFNP/10
      IFNOUT=IFNP-IFNIN*10
      PHI=-2.0*PI
      AMN=1.0/FLOAT(M*N)
      MP1=M+1
      MM1=M-1
      NBYK=N/K
      NBYKK=NBYK/K
      KM1=K-1
      KLIM=NBYKK*KM1
      NSKIP1=NBYKK-1
      KP=1
C
C   L STEPS
      ITT=ITT+1
      CALL UTTIME(ITIME(1,ITT))
      DO 60 LSTEP=1,L
      KP=KP*K
      AKP=FLOAT(KP)
      REWIND IUX
      REWIND IUY
      REWIND JUX
      REWIND JUY
      I1=1
      I2=M
      JU=1
      JUP=0
C
C   NBYK BLOCKS OF K VECTORS EACH
```

```
      DO 30 KBLOCK=1,NBYK
      KBM1=KBLOCK-1
      NSKIP0=KBM1/K
      IF(IFNIN.LT.2 .OR. LSTEP.GT.1) GO TO 6
C
C  READ A BLOCK IN BASE-K DIGIT REVERSED ORDER
      NSKIP=JU-1
      IF(NSKIP.GE.JUP) GO TO 106
      REWIND IUX
      REWIND IUY
      GO TO 107
  106 NSKIP=NSKIP-JUP
  107 IF(NSKIP.LE.0) GO TO 109
      DO 108 I=1,NSKIP
      READ(IUX)
  108 READ(IUY)
  109 READ(IUX) X
      READ(IUY) Y
C
C  GENERATE NEXT BLOCK NUMBER IN BASE-K DIGIT REVERSED ORDER
      IF(KBLOCK.EQ.NBYK) GO TO 7
      JUP=JU
      KV=KLIM
  110 IF(KV.GE.JU) GO TO 111
      JU=JU-KV
      KV=KV/K
      GO TO 110
  111 JU=JU+KV/KM1
      GO TO 7
C
C  READ EVERY NBYK'TH ROW FROM UNITS IUX AND IUY
    6 IX=1
      IY=1
      NSKIP=NSKIP0
      DO 4 J=1,K
      IF(NSKIP.LE.0) GO TO 42
      DO 47 I=1,NSKIP
      READ(IUX)
   47 READ(IUY)
   42 CONTINUE
      READ(IUX) BUFFER
      DO 3 I=I1,I2
      X(IX)=BUFFER(I)
    3 IX=IX+1
      READ(IUY) BUFFER
      DO 44 I=I1,I2
      Y(IY)=BUFFER(I)
   44 IY=IY+1
    4 NSKIP=NSKIPI
      I1=I1+M
      IF((KBLOCK/K)*K.EQ.KBLOCK) I1=1
      I2=I1+MM1
      REWIND IUX
      REWIND IUY
C
    7 CONTINUE
      IF (LSTEP.GT.1) GO TO 12
      IF(IFN.GT.0) GO TO 75
C
C  FOR THE INVERSE TRANSFORM ONLY,
C  FORM THE COMPLEX CONJUGATE OF THE INPUT DATA.
      DO 73 I=1,MK
   73 Y(I)=-Y(I)
C
C  FFT BY ROWS
   75 DO 8 I=1,MK,M
    8 CALL VFFT (X(I),Y(I),M,1)
      GO TO 28
C
C  MULTIPLY BY THE TWIDDLE FACTORS
   12 KM=KBM1
      KF=K**(LSTEP-2)
      KBMODK=0
      DO 122 I=2,LSTEP
      KBMODK=KBMODK+MOD(KM,K)*KF
      KF=KF/K
  122 KM=KM/K
      ALPHA=-6.283185307*FLOAT(KBMODK)/AKP
      CC=COS(ALPHA)
      C=CC
      SS=SIN(ALPHA)
      S=SS
      DO 15 J=MP1,MK,M
      IJEND=J+MM1
      DO 14 IJ=J,IJEND
      T=X(IJ)*C-Y(IJ)*S
      Y(IJ)=X(IJ)*S+Y(IJ)*C
   14 X(IJ)=T
      T=C*CC-S*SS
      S=C*SS+S*CC
```

```
   15 C=T
C
C  FFT BY COLUMNS
   28 DO 13 I=1,M
   13 CALL VFFT (X(I),Y(I),MK,M)
      IF(LSTEP.LT.L .OR. IFN.GT.0) GO TO 29
C
C  FOR THE INVERSE TRANSFORM ONLY,
C  FORM THE COMPLEX CONJUGATE OF THE SCALED OUTPUT ARRAY.
      DO 543 I=1,MK
      X(I)=X(I)*AMN
  543 Y(I)=-Y(I)*AMN
C
C  WRITE RESULT OF THIS STEP ON UNITS JUX AND JUY
   29 WRITE(JUX) X
   30 WRITE(JUY) Y
      ENDFILE JUX
      ENDFILE JUY
C
C  SWOP THE FILE POINTERS
      I=IUX
      IUX=JUX
      JUX=I
      I=IUY
      IUY=JUY
      JUY=I
   60 CONTINUE
      ITT=ITT+1
      CALL UTTIME(ITIME(1,ITT))
      IF(IFNOUT.GT.1) RETURN
C
C  UNSCRAMBLE
      REWIND JUX
      REWIND JUY
      KM1=K-1
      KLIM=NBYKK*KM1
      J=1
      DO 90 I=1,NBYK
      NSKIP=(J-1)/K
      I1=(J-NSKIP*K)*M-MM1
      I2=I1+MM1
      REWIND IUX
      REWIND IUY
      IX=1
      IY=1
      DO 69 II=J,N,NBYK
      IF(NSKIP.LE.0) GO TO 62
      DO 63 IV=1,NSKIP
      READ(IUX)
   63 READ(IUY)
   62 READ(IUX) BUFFER
      DO 65 IV=I1,I2
      X(IX)=BUFFER(IV)
   65 IX=IX+1
      READ(IUY) BUFFER
      DO 66 IV=I1,I2
      Y(IY)=BUFFER(IV)
   66 IY=IY+1
   69 NSKIP=NSKIPI
      WRITE(JUX) X
      WRITE(JUY) Y
      IF(I.EQ.NBYK) GO TO 91
      KV=KLIM
   80 IF(KV.GE.J) GO TO 90
      J=J-KV
      KV=KV/K
      GO TO 80
   90 J=J+KV/KM1
   91 ENDFILE JUX
      ENDFILE JUY
C
C  SWOP THE FILE POINTERS
      I=IUX
      IUX=JUX
      JUX=I
      I=IUY
      IUY=JUY
      JUY=I
      RETURN
      END
```

2) Two-Dimensional FIR Filter Design Programs

```
      SUBROUTINE HKWBPF (H,M,N,MX,FCX1,FCY1,FCX2,FCY2,KR,B)
C                                              JOSEP M. COSTA   1976 1129 1130
C   THIS SUBROUTINE GENERATES THE IMPULSE RESPONSE OF A TWO-DIMENSIONAL
C   KAISER WINDOW BANDPASS OR LOWPASS FILTER, WITH CIRCULAR OR ELLIPTIC
C   SHAPE IN THE PASS BAND.
C   EXTERNAL SUBROUTINES NEEDED: BFIO, BFJ1, HMI, AND VMI.
C
C   H   -    SQUARE MATRIX OF DIMENSIONS M BY N THAT ON OUTPUT WILL CONTAIN
C            THE IMPULSE RESPONSE OF THE DIGITAL FILTER
C            ARRANGED IN A FORM SUITABLE FOR TAKING THE TWO-DIMENSIONAL
C            FAST FOURIER TRANSFORM.  THE SUBROUTINE CAMOVE MAY BE CALLED
C            TO REARRANGE THE DATA IF DESIRED.
C   M   -    FIRST DIMENSION OF H
C   N   -    SECOND DIMENSION OF H
C   MX  -    NUMBER OF POINTS IN THE FIRST DIMENSION
C   FCX1 -LOWER CUTOFF FREQUENCY OF THE PASS BAND IN THE X DIRECTION
C   FCY1 -LOWER CUTOFF FREQUENCY OF THE PASS BAND IN THE Y DIRECTION
C   FCX2 -UPPER CUTOFF FREQUENCY OF THE PASS BAND IN THE X DIRECTION
C   FCY2 -UPPER CUTOFF FREQUENCY OF THE PASS BAND IN THE Y DIRECTION
C            ALL THESE CUTOFF FREQUENCIES ARE GIVEN AS FRACTIONS OF HALF
C            THE SAMPLING FREQUENCY, THAT IS  0 < F < 1.
C   KR  -    NUMBER OF SAMPLES OF THE IMPULSE RESPONSE OVER THE RADIUS
C   B   -    BETA, THE DESIGN PARAMETER FOR THE KAISER WINDOW THAT CONTROLS
C            THE TRANSITION BAND AND THE RIPPLE.
C
      LOGICAL LP
      DIMENSION H(M,N)
C
C   INITIALIZATION
      PI=3.141592653
      IF(KR.LT.1 .OR. KR.GT.((MINO(MX,N)+1)/2)-1) GO TO 9
      IF(FCX2.LE.0.0 .OR. FCX2.GE.1.0 .OR.
     -   FCY2.LE.0.0 .OR. FCY2.GE.1.0        ) GO TO 9
      LP=.TRUE.
      IF(FCX1.GE.FCX2 .OR.  FCY1.GE.FCY2) GO TO 10
      LP=.FALSE.
      IF(FCX1.GT.0.0 .AND. FCY1.GT.0.0) GO TO 10
    9 WRITE(6,8000) M,N,MX,FCX1,FCY1,FCX2,FCY2,KR,B
 8000 FORMAT('0 *** ERROR IN HKWBPF, WRONG INPUT ARGUMENTS: ',/,'0',
     -   24X,3I10,4G14.4,2I10)
      STOP
   10 IEND=(MX+3)/2
      JEND=(N+3)/2
      DO 30 J=1,JEND
      DO 30 I=1,IEND
   30 H(I,J)=0.0
      BFIOBI=1.0/BFIO(B)
      KEND=KR+1
      KR2=KR*KR
      AN=1.0/FLOAT(KR2)
      X1=FCX1*FCX1
      X2=FCX2*FCX2
      Y1=FCY1*FCY1
      Y2=FCY2*FCY2
      XY1=PI*FCX1*FCY1
      XY2=PI*FCX2*FCY2
C
C   TWO LOOPS OVER THE FIRST QUADRANT
      DO 60 KY=1,KEND
      KYY=(KY-1)*(KY-1)
      Y1KY=Y1*FLOAT(KYY)
      Y2KY=Y2*FLOAT(KYY)
      DO 60 KX=1,KEND
      KXX=(KX-1)*(KX-1)
      K=KXX+KYY
C
C   VALUE OF THE IMPULSE RESPONSE AT THE ORIGIN
      IF(K.NE.0) GO TO 40
      T=XY2
      IF(.NOT.LP) T=T-XY1
      H(KX,KY)=0.5*PI*T
      GO TO 60
C
C   VALUE OF THE IMPULSE RESPONSE OUTSIDE A CIRCLE OF RADIUS KR
   40 IF(K.GT.KR2) GO TO 60
C
C   GENERATE THE COEFFIENTS OF THE IDEAL FILTER USING THE FUNCTION BFJ1
      SFC=SQRT(X2*FLOAT(KXX)+Y2KY)
      S2=FLOAT(K)
      S=SQRT(S2)
      T=XY2*BFJ1(PI*SFC)/SFC
      IF(LP) GO TO 50
```

```
      SFC=SQRT(X1*FLOAT(KXX)+Y1KY)
      T=T-(XY1*BFJ1(PI*SFC)/SFC)
C
C   MULTIPLY THE COEFFICIENTS OF THE IDEAL FILTER BY THE COEFFICIENTS OF
C   A CIRCULARLY-SYMMETRIC KAISER WINDOW
 50 H(KX,KY)=T*BFI0(SQRT(1.0-S2*AN))*BFI0BI
 60 CONTINUE
C
C   COPY THE RESULTS INTO THE OTHER QUADRANTS BY SYMMETRIES
      CALL VMI(H(1,2),M,N-1,IEND)
      CALL HMI(H(2,1),M,N,MX-1)
      RETURN
      END




      FUNCTION BFJ1 (X)
                                               J.M. COSTA  1975 1114 0113
C
C   THIS FUNCTION GENERATES THE FIRST-ORDER BESSEL FUNCTION OF THE FIRST
C   KIND, J1(X), TO WITHIN SPECIFIED ACCURACY USING THE FOLLOWING POWER
C   SERIES EXPANSION.
C                          N
C   BFJ1(X) = (X/2) + SUM  ((-X/2)**(2*K+1))/((FCT(K)**2)*(K+1))
C                         K=1
C   FOR X BETWEEN 0.0 AND 25.0, AND WHERE FCT(K) DENOTES THE FACTORIAL
C   OF K, I.E., FCT(K)=K*(K-1)* ... *3*2*1.
C   IF X IS GREATER THAN 25.0 THE FOLLOWING ASYMPTOTIC SERIES IS USED,
C   WHICH GIVES AT LEAST SIX EXACT DECIMAL PLACES (SEVEN IF X IS GREATER
C   THAN 100.0).
C
C   BFJ1(X) = (1./SQRT(PI*X))*((P1(X)+Q1(X))*SIN(X)-(P1(X)-Q1(X)*COS(X))
C
C   WHERE:
C                PI    = 3.14159265358979323846
C                P1(X) = 1.0 + 0.1171875/(X**2)
C                Q1(X) = 0.375/X-0.1025390625/(X**3)
C
C   ALL CALCULATIONS ARE DONE USING DOUBLE PRECISION.
C   REFERENCE:  S.M. SELBY (EDITOR), STANDARD MATHEMATICAL TABLES, 21ST
C               EDITION, CLEVELAND, OHIO: CRC, THE CHEMICAL RUBBER CO.,
C               1973, PP. 534-535.
C
      DOUBLE PRECISION DBLE,DFLOAT,DABS,DSQRT,DCOS,DSIN,
     -                 DT,DBFJ1,DPT,DFACT,DX,DX2,DPI,P1,Q1
      DATA DPI/Z413243F6A8885A30/, DT/1.0 D-08/
C
C   DETERMINE WHICH ASYMPTOTIC SERIES WILL BE USED
      IF(X.LE.25.0) GO TO 3
C
C   THE ARGUMENT IS GREATER THAN 25.0
      DX=DBLE(X)
      DX2=DX*DX
      P1=1.0 D0+0.1171875 D0/DX2
      Q1=0.375 D0/DX-0.1025390625 D0/(DX2*DX)
      BFJ1=SNGL((1.0 D0/DSQRT(DPI*DX))*
     -         ((P1+Q1)*DSIN(DX)-(P1-Q1)*DCOS(DX)) )
      RETURN
C
C   THE ARGUMENT IS LESS THAN OR EQUAL TO 25.0
  3 DBFJ1=0.5 D0*DBLE(X)
      DPT=DBFJ1
      DFACT=-DPT*DPT
C
C   AT EACH STAGE OF THE DO-LOOP A NEW TERM OF THE POWER SERIES
C   EXPANSION IS GENERATED AND ADDED TO THE RESULT
      DO 6 K=1,100
      DPT=DPT*DFACT/DFLOAT(K*K+K)
      DBFJ1=DBFJ1+DPT
C
C   EXIT THE DO-LOOP UPON REACHING THE DESIRED ACCURACY
      IF(DABS(DPT).LT.DT) GO TO 9
  6 CONTINUE
      WRITE(6,10) X,BFJ1
 10 FORMAT('0 DESIRED ACCURACY NOT OBTAINED, BFJ1(',F9.4,') = ',F9.4)
C
C   THE FINAL RESULT IS GIVEN IN SINGLE PRECISION
  9 BFJ1=SNGL(DBFJ1)
      RETURN
C
      END
```

```
      FUNCTION BFI0 (X)
C                                                J.M. COSTA   1975 1113 1921
C   THIS FUNCTION GENERATES THE MODIFIED ZEROTH-ORDER BESSEL FUNCTION
C   OF THE FIRST KIND, I0(X), TO WITHIN SPECIFIED ACCURACY USING THE
C   FOLLOWING POWER SERIES EXPANSION,
C
C                        N
C   BFI0(X)  =  1  +  SUM    ((X/2)**(2*K))/(FCT(K)**2)
C                       K=1
C
C   FOR X BETWEEN 0.0 AND 20.0. AND WHERE FCT(K) DENOTES THE FACTORIAL
C   OF K, I.E., FCT(K)=K*(K-1)* ... *3*2*1.
C   REFERENCE:   S.M. SELBY (EDITOR), STANDARD MATHEMATICAL TABLES, 21ST
C                EDITION, CLEVELAND, OHIO: CRC, THE CHEMICAL RUBBER CO.,
C                1973, PAGE 537.
C
      DATA T/1.0E-08/
C
C   INITIALIZATION
      FACT=0.25*X*X
      PT=1.0
      BFI0=PT
C
C   AT EACH STAGE OF THE DO-LOOP A NEW TERM OF THE POWER SERIES
C   EXPANSION IS GENERATED AND ADDED TO THE RESULT
      DO 6 K=1,25
      PT=PT*FACT/FLOAT(K*K)
      BFI0=BFI0+PT
C
C   RETURN UPON REACHING THE DESIRED ACCURACY
      IF(BFI0*T.GT.PT) RETURN
    6 CONTINUE
C
      WRITE(6,10) X,BFI0
   10 FORMAT('0 DESIRED ACCURACY NOT OBTAINED, BFI0(',F7.4,') = ',F9.4)
      RETURN
C
      END
```

```
      SUBROUTINE HMI (X,M,N,MX)
C                                         JOSEP M. COSTA   1976 1129 1130
C   THIS SUBROUTINE COPIES THE UPPER HALF OF A MATRIX INTO THE LOWER HALF
C
      DIMENSION X(M,N)
      MXP1=MX+1
      MXBY2=MX/2
      DO 6 I=1,MXBY2
      IC=MXP1-I
      DO 6 J=1,N
    6 X(IC,J)=X(I,J)
      RETURN
C
      ENTRY VMI (X,M,N,MX)
C
C   THIS ENTRY COPIES THE LEFT HALF OF A MATRIX INTO THE RIGHT HALF
C
      NP1=N+1
      NBY2=N/2
      DO 9 J=1,NBY2
      JC=NP1-J
      DO 9 I=1,MX
    9 X(I,JC)=X(I,J)
      RETURN
      END
```

3) Two-Dimensional IIR Filter Design and Realization Programs

```
      SUBROUTINE CDFILT (ZP,NZPNP,NZ,WORK,NROT,CC,NF,IFILT,LHBP,BW,
     -                   CUTOFF,MODE)
C                                         JOSEP M. COSTA  1975 0707 1459
C   THIS SUBROUTINE PREPARES THE CALL TO DFILT FOR CIRCULARLY-SYMMETRIC
C   TWO-DIMENSIONAL DIGITAL FILTERS.
C   THE ARGUMENT LIST IS SIMILAR TO THAT OF DFILT WITH THE FOLLOWING
C   EXCEPTIONS.
C
C   WORK   - WORK ARRAY DIMENSIONED AT LEAST 3*NROT.
C   NF     - MUST BE SUPPLIED FOR DIMENSIONING
C            NF = MAX0(NZPNP-NZ,NZ)*NROT*MAX0(1,LHBP-1).
C   BW     - BANDWIDTH OF A CIRCULARLY-SYMMETRIC BAND-PASS FILTER
C            (IF LHBP.NE.3 THE VALUE OF BW IS IGNORED).
C   CUTOFF - CUTOFF FREQUENCY OF THE CIRCULARLY-SYMMETRIC 2-D FILTER.
C   MODE   - IF MODE=1 THE POLYGONAL WHICH APPROXIMATES THE CIRCULARLY-
C            SYMMETRIC FILTER HAS A VERTEX ON EACH AXIS, OTHERWISE
C            ZERO-DEGREE AND 270-DEGREE ROTATED FILTERS WILL RESULT.
C   LHBP   - INPUT PARAMETER WHICH DETERMINES THE TYPE OF FILTER
C            =1  LOW-PASS DESIGN
C            =2  HIGH-PASS DESIGN
C            =3  BAND-PASS DESIGN.
C
      DIMENSION ZP(2,NZPNP), CC(16,NF), WORK(3,NROT)
C
C   INITIALIZATION
      DATA ZCRH,ZCRL/ .7071068, .2928932/
      DATA DFMAX/1.0E-2/, NITMAX/50/
      DBETA=90.0/FLOAT(NROT)
      BETA0=270.0
      IF(MODE.EQ.1) BETA0=BETA0+0.5*DBETA
      NP=NF
      IF(LHBP.EQ.3) NP=NP/2
      ZCR=ZCRH
      IF(LHBP.EQ.2) ZCR=ZCRL
C
C   DETERMINE THE EQUALLY-SPACED ANGLES OF ROTATION
      DO 6 J=1,NROT
      WORK(1,J)=BETA0+FLOAT(J-1)*DBETA
    6 WORK(2,J)=CUTOFF
C
C   FILTER DESIGN
      CALL DFILT (ZP,NZPNP,NZ,WORK,NROT,CC,NP,IFILT,ZCR,DFMAX,NITMAX,IE)
      NTOT=NF
      IF(LHBP.LT.3) GO TO 10
C
C   COMPLETE THE DESIGN FOR BAND-PASS FILTERS
C   (AN ITERATIVE ALGORITHM COULD BE INCORPORATED HERE TO HAVE MORE
C    CONTROL ON THE CUTOFF FREQUENCIES OF THE BAND-PASS FILTER)
C
      DO 9 J=1,NROT
    9 WORK(2,J)=CUTOFF-BW
      CALL DFILT(ZP,NZPNP,NZ,WORK,NROT,CC(1,NP+1),NP,IFILT,ZCR,DFMAX,
     -           NITMAX,IE)
C
C   NORMALIZE, PRINT, AND PUNCH THE FILTER COEFFICIENTS
   10 CALL PTPHCC(CC,NF,1)
      RETURN
C
      END
```

```
      SUBROUTINE DFILT (ZP,NZPNP,NZ,PARM,NROT,CC,NF,IFILT,ZEROCR,
     -                  DFMAX,NITMAX,IERROR)
C
C                                         JOSEP M. COSTA  1975 0707 1452
C   *  THIS ROUTINE CONVERTS A ONE-DIMENSIONAL CONTINUOUS FILTER INTO A
C   *  TWO-DIMENSIONAL RECURSIVE DIGITAL FILTER WITH SPECIFIED
C   *  CUT-OFF FREQUENCIES IN A GIVEN SET OF DIRECTIONS IN THE 2-D
C   *  FOURIER PLANE.  IT CALLS THE SUBPROGRAMS RTMI AND FRESIN.
C
C   ZP      - COMPLEX VECTOR OF LENGTH NZPNP CONTAINING THE COMPLEX ZERO
C             AND POLE LOCATIONS OF THE CONTINUOUS FILTER.  ALL THE ZEROS
C             FIRST FOLLOWED BY THE POLES.
C   NZPNP   - DIMENSION OF ZP (NUMBER OF FINITE ZEROS PLUS NUMBER OF
C             FINITE POLES IN THE 1-D CONTINUOUS FILTER).
C   NZ      - NUMBER OF FINITE ZEROS IN THE 1D CONTINUOUS FILTER.
```

```
C   PARM     - 2D ARRAY OF DIMENSIONS 3 BY NROT CONTAINING THE ANGLES OF
C              THE ROTATED FILTERS IN THE FORTH QUADRANT AND THE CUTOFF
C              FREQUENCIES IN THE DIRECTIONS PERPENDICULAR TO THE
C              ORIENTATIONS OF THE ROTATED FILTERS.
C              PARM(1,I), I=1,...,NROT, CONTAIN THE ANGLES OF ROTATION.
C              PARM(2,I), I=1,...,NROT, CONTAIN THE CUTOFF FREQUENCIES.
C              PARM(3,I), I=1,...,NROT, WORK ARRAY.
C   NROT     - SECOND DIMENSION OF PARM.  NUMBER OF ROTATED FILTERS TO BE
C              CASCADED TO FORM THE ELLIPTICALLY-SHAPED FILTER.
C   CC       - COMPLEX ARRAY OF DIMENSIONS 8 BY NF, WHICH ON OUTPUT WILL
C              CONTAIN THE COEFFICIENTS OF THE 2D DIGITAL FILTER.
C   NF       - SECOND DIMENSION OF CC, NUMBER OF ELEMENTARY FILTERS IN THE
C              CASCADE.  IT MUST BE CALCULATED OUTSIDE THIS SUBROUTINE.
C   IFILT    - FILTER PARAMETER THAT DETERMINES HOW THE ELLIPTICALLY-SHAPED
C              FILTER WILL BE COMBINED WITH DATA TRANSFORMATIONS TO FORM A
C              FILTER WITH QUADRANTAL SYMMETRIES.  SEE SUBROUTINE CCP2.
C   ZEROCR   - NORMALIZED MAGNITUDE RESPONSE AT THE CUTOFF FREQUENCY.
C   DFMAX    - INPUT VALUE WHICH SPECIFIES THE UPPER BOUND OF THE ERROR OF
C              THE RESULTANT CUTOFF FREQUENCY.
C   NITMAX   - MAXIMUM NUMBER OF ITERATION STEPS SPECIFIED.
C   IERROR   - RESULTANT ERROR PARAMETER CODED AS FOLLOWS
C              =0 - NO ERROR,
C              =1 - WRONG INPUT ARGUMENTS,
C              =2 - NO CONVERGENCE AFTER NITMAX ITERATION STEPS,
C              =3 - NO CONVERGENCE IN RTMI,
C              =4 - NO IMPROVEMENT IN THE LAST ITERATION STEP.
C
      EXTERNAL FRESI
      LOGICAL LCONV,PREWRP
      DIMENSION ZP(2,NZPNP), PARM(3,NROT), CC(16,NF)
      DATA SHIFT/0.0/,XLI/0.0/,XRI/0.999/,SCMIN/0.01745/
      DATA DEG/.5729577E 02/, PI/.3141593E 01/, RAD/.1745329E-01/
      DATA MINUS/'-'/, BLANK/' '/,NERMAX/10/
      DATA PREWRP/.TRUE./
C
C  *  INITIALIZE THE ITERATION
      NP=NZPNP-NZ
      NORDR1=MAX0(NZ,NP)
      NG=NORDR1*NROT
      IF(NG.EQ.NF) GO TO 5
      WRITE(6,8000) NF
      IERROR=1
      GO TO 950
    5 WRITE(6,6004)
      EPS=DFMAX
      IEND=NITMAX
      PDF=FLOAT(NROT)
      IERROR=0
      NERROR=0
      K=0
      DO 6 J=1,NROT
      DO 6 IZ=1,NORDR1
      K=K+1
    6 WRITE(6,6010) K,IZ,PARM(1,J)
      PIB2=0.5*PI
      PFR2=0.0
      DO 10 J=1,NROT
   10 PARM(3,J)=PARM(2,J)
C
C  *  ITERATION BEGINS
      DO 900 NIT=1,NITMAX
      LCONV=.TRUE.
      K=0
      DO 600 J=1,NROT
      BETA=PARM(1,J)
      SB=SIN(BETA*RAD)
      CB=COS(BETA*RAD)
      DELTA2=PIB2*PARM(3,J)
      IF(PREWRP) DELTA2=TAN(DELTA2)
      DO 600 IZ=1,NORDR1
      IP=NZ+IZ
      K=K+1
C
C  *  CALCULATE THE COEFFICIENTS OF THE FILTER
      IF(IZ.GT.NZ) GO TO 110
      ZPR=DELTA2*ZP(1,IZ)
      ZPI=DELTA2*ZP(2,IZ)
      CC(1,K)= CB-SB-ZPR
      CC(3,K)= CB+SB-ZPR
      CC(5,K)=-CB-SB-ZPR
      CC(7,K)=-CB+SB-ZPR
      DO 105 L=2,8,2
  105 CC(L,K)=-ZPI
      GO TO 115
  110 DO 112 L=1,7,2
      CC(L,K)=1.0
  112 CC(L+1,K)=0.0
  115 IF(IP.GT.NZPNP) GO TO 117
      ZPR=DELTA2*ZP(1,IP)
      ZPI=DELTA2*ZP(2,IP)
```

```
      CC( 9,K)= CB-SB-ZPR
      CC(11,K)= CB+SB-ZPR
      CC(13,K)=-CB-SB-ZPR
      CC(15,K)=-CB+SB-ZPR
      DO 116 L=10,16,2
  116 CC(L,K)=-ZPI
      GO TO 140
  117 DO 118 L=9,15,2
      CC(L,K)=1.0
  118 CC(L+1,K)=0.0
  140 IF(ABS(SB).GT.SCMIN) GO TO 145
      CC( 3,K)=1.0
      CC( 4,K)=0.0
      CC(11,K)=1.0
      CC(12,K)=0.0
      GO TO 150
  145 IF(ABS(CB).GT.SCMIN) GO TO 400
      CC( 5,K)=0.0
      CC( 6,K)=0.0
      CC(13,K)=0.0
      CC(14,K)=0.0
  150 CC( 7,K)=0.0
      CC( 8,K)=0.0
      CC(15,K)=0.0
      CC(16,K)=0.0
  400 IF(SHIFT.EQ.0.0) GO TO 600
      DO 500 L=1,4
      CC(L,K)=CC(L,K)+SHIFT*CC(L+4,K)
  500 CC(L+8,K)=CC(L+8,K)+SHIFT*CC(L+12,K)
  600 CONTINUE
      IF(NIT.EQ.1) WRITE(6,6011)
C
C  *  CHECK THE CUTOFF FREQUENCY
      FF=FRESIN(CC,NG,IFILT,ZEROCR)
      ICARR=MINUS
      ADF=0.0
      DO 700 J=1,NROT
      AA=ANGLE(PARM(1,J)+90.0)
      CALL RTMI (FRC,FRES,FRES1 ,XLI,XRI,EPS,IEND,IER)
      IF(IER.EQ.0) GO TO 650
      IERROR=3
      LERROR=650
      NERROR=NERROR+1
      WRITE(6,6012) IER,LERROR
      IF(NERROR.GT.NERMAX) GO TO 950
  650 DF=PARM(2,J)-FRC
      ABSDF=ABS(DF)
      ADF=ADF+ABSDF
      IF(ABSDF.GE.DFMAX) LCONV=.FALSE.
      WRITE(6,6015) ICARR,NIT,PARM(2,J),FRC,DF,PARM(3,J),FRES,ADF
      ICARR=BLANK
  700 PARM(3,J)=PARM(3,J)+DF
      IF(LCONV) GO TO 950
      IF(ADF.LT.PDF) GO TO 800
      IERROR=4
      GO TO 950
  800 PDF=ADF
  900 CONTINUE
C
C  *  END OF ITERATION
      LERROR=950
      IERROR=2
      WRITE(6,6012) NITMAX,LERROR
  950 WRITE(6,8001) IERROR
      RETURN
C
 6004 FORMAT('1','TWO-DIM FILTER #',10X,'ONE-DIM FILTER #',10X,'ROTATION
     - (DEGREES)')
 6010 FORMAT('0',13X,I3,23X,I3,17X,F10.3)
 6011 FORMAT('1','NIT',10X,'CUTOFF',19X,'FRC',18X,'DF',16X,'FRD',
     -           16X,'FRES',16X,'ADF',/,'0')
 6012 FORMAT(' ','*** ERROR ***  VALUE OF IER OR NIT IS ',I3,' AT ',I4)
 6015 FORMAT(A1 ,I3,6(5X,G16.7))
 8000 FORMAT('0','*** ERROR *** DIMENSIONS OF CC DO NOT MATCH WITH THE N
     -UMBER OF BILINEAR FILTERS THAT WILL BE GENERATED ***',2I6)
 8001 FORMAT('0 IERROR= ',I4)
      END
```

```
      FUNCTION FRESIN (CC,NF,IFILT,ZEROCR)
                                               JOSEP M. COSTA   1975 0726 0513
C
C   THIS FUNCTION CALCULATES THE MAGNITUDE RESPONSE OF A 2D DIGITAL
C   FILTER AT A POINT GIVEN IN CARTESIAN COORDINATES OR IN POLAR
C   COORDINATES.
C   FRESIN SUPPLIES THE FILTER COEFFICIENTS AND DETERMINES THE SCALE
C   FACTOR FOR A RESPONSE OF 1.0 AT THE ORIGIN.
C
C   CC      - 2D ARRAY OF DIMENSIONS 16 BY NF CONTAINING THE FILTER
C             COEFFICIENTS.
C   NF      - SECOND DIMENSION OF CC (NUMBER OF BILINEAR FILTERS IN THE
C             CASCADE).
C
C   ENTRIES
C             COORD  - TO SUPPLY THE COORDINATE FR2 BEFORE CALLING FRESO.
C             FRESO  - MAGNITUDE RESPONSE AT A POINT DEFINED BY THE
C                      CARTESIAN COORDINATES IN THE FREQUENCY PLANE,
C                      FR1 AND FR2.
C             ANGLE  - TO SUPPLY THE COORDINATE THETA BEFORE CALLING FRES1
C             FRES1  - MAGNITUDE RESPONSE AT A POINT DEFINED BY THE
C                      POLAR COORDINATES IN THE FREQUENCY PLANE,
C                      RFR AND THETA.
C
      LOGICAL IN, ROT90, COMPLX(20)
      DIMENSION CC(16,NF)
      DATA PI/.3141593E 01/, RAD/.1745329E-01/
      DATA PBOUND,STEP/1.0 E50,1.0E20/
C
C   INITIALIZATION
      JFILT=MOD(IABS(IFILT),5)
      ROT90=.TRUE.
      IF(JFILT.NE.3) GO TO 10
      JFILT=JFILT-1
      ROT90=.FALSE.
   10 DO 30 K=1,NF
      COMPLX(K)=.TRUE.
      DO 20 J=2,16,2
      IF(CC(J,K).NE.0.0) GO TO 30
   20 CONTINUE
      COMPLX(K)=.FALSE.
   30 CONTINUE
      SCALE=1.0
      DELTA=0.0
      NP=NF
      IN=.FALSE.
      ER21=1.0
      ER12=1.0
      ER22=1.0
      EI21=0.0
      EI12=0.0
      EI22=0.0
      GO TO 50
C
C   CARTESIAN COORDINATES.
      ENTRY COORD (FR2)
      PIFR2=PI*FR2
      RETURN
      ENTRY FRESO (FR1)
      PIFR1=PI*FR1
      GO TO 40
C
C   POLAR COORDINATES.
      ENTRY ANGLE (THETA)
      PICT=PI*COS(THETA*RAD)
      PIST=PI*SIN(THETA*RAD)
      RETURN
      ENTRY FRES1 (RFR)
      PIFR1=PICT*RFR
      PIFR2=PIST*RFR
C
   40 ER21=COS(PIFR1)
      EI21=SIN(PIFR1)
      ER12=COS(PIFR2)
      EI12=SIN(PIFR2)
      ER22=ER21*ER12-EI21*EI12
      EI22=ER21*EI12+EI21*ER12
   50 F2R=1.0
      F2I=0.0
      DO 90 J=1,JFILT
      DO 60 K=1,NP
      P1=CC( 1,K)+CC( 3,K)*ER21+CC( 5,K)*ER12+CC( 7,K)*ER22
      P2=          CC( 4,K)*EI21+CC( 6,K)*EI12+CC( 8,K)*EI22
      P3=CC( 9,K)+CC(11,K)*ER21+CC(13,K)*ER12+CC(15,K)*ER22
      P4=          CC(12,K)*EI21+CC(14,K)*EI12+CC(16,K)*EI22
      P5=          CC( 3,K)*EI21+CC( 5,K)*EI12+CC( 7,K)*EI22
      P6=CC( 2,K)+CC( 4,K)*ER21+CC( 6,K)*ER12+CC( 8,K)*ER22
      P7=          CC(11,K)*EI21+CC(13,K)*EI12+CC(15,K)*EI22
      P8=CC(10,K)+CC(12,K)*ER21+CC(14,K)*ER12+CC(16,K)*ER22
      ANR=P1-P2
      ADR=P3-P4
```

```
      ANI=P5+P6
      ADI=P7+P8
      ADM=ADR*ADR+ADI*ADI
      TEMPR=(ANR*ADR+ANI*ADI)/ADM
      TEMPI=(ANI*ADR-ANR*ADI)/ADM
      TEMP=F2R*TEMPR-F2I*TEMPI
      F2I=F2R*TEMPI+F2I*TEMPR
      F2R=TEMP
      IF(.NOT.COMPLX(K)) GO TO 55
      ANR=P1+P2
      ADR=P3+P4
      ANI=P5-P6
      ADI=P7-P8
      ADM=ADR*ADR+ADI*ADI
      TEMPR=(ANR*ADR+ANI*ADI)/ADM
      TEMPI=(ANI*ADR-ANR*ADI)/ADM
      TEMP=F2R*TEMPR-F2I*TEMPI
      F2I=F2R*TEMPI+F2I*TEMPR
      F2R=TEMP
C
C  CHECK FOR POSSIBLE OVERFLOWS AND SCALE IF NECESSARY
   55 IF(F2R.LT.PBOUND .AND. F2I.LT.PBOUND) GO TO 60
      SCALE=SCALE*STEP
      WRITE(6,1000) SCALE,F2R,F2I
      F2R=F2R/STEP
      F2I=F2I/STEP
   60 CONTINUE
      IF(ROT90) GO TO 70
      EI21=-EI21
      EI12=-EI12
      EI22=-EI22
      GO TO 90
   70 TEMP=ER21
      ER21=ER12
      ER12=TEMP
      TEMP=EI21
      EI21=-EI12
      EI12=TEMP
      ER22=ER21*ER12-EI21*EI12
      EI22=ER21*EI12+EI21*ER12
   90 CONTINUE
      FRESIN=SQRT(F2R*F2R+F2I*F2I)*SCALE-DELTA
      IF(IN) RETURN
      IN=.TRUE.
      DELTA=ZEROCR
      SCALE=1.0/FRESIN
      RETURN
 1000 FORMAT('0 TO PREVENT OVERFLOWS IN FRESIN THE F. R. HAS BEEN SCALED
     -             SCALE= ,',G16.7,',    F2R= ',G16.7,',    F2I= ',G16.7)
      DATA COORD,FRES0,ANGLE,FRES1/4*0.0/
      END
```

```
      SUBROUTINE PTPHCC (CC,NF,INORM)
C                                                 JOSEP M. COSTA   1975 1018 1606
C  THIS SUBROUTINE NORMALIZES, PRINTS, AND PUNCHES THE COEFFICIENTS OF
C  A 2D DIGITAL FILTER.
C  IF  INORM=1 THE COEFFICIENTS OF EACH BILINEAR FILTER ARE NORMALIZED
C  WITH RESPECT THE INDEPENDENT TERM IN THE DENOMINATOR (B11).
C
      DIMENSION CC(16,NF)
      LOGICAL LPUN
      LPUN=.FALSE.
      LPUN=.TRUE.
      IF (INORM.NE.1) GO TO 1000
C
C     NORMALIZE WITH RESPECT TO B11(K)
      DO 999 K=1,NF
      U=CC( 9,K)*CC( 9,K)+CC(10,K)*CC(10,K)
      ZPR=CC( 9,K)/U
      ZPI=CC(10,K)/U
      CC( 9,K)=1.0
      CC(10,K)=0.0
      JST=11
      JEND=16
      DO 999 I=1,2
      DO 998 J=JST,JEND,2
      TEMP=CC(J,K)*ZPR+CC(J+1,K)*ZPI
      CC(J+1,K)=CC(J+1,K)*ZPR-CC(J,K)*ZPI
  998 CC(J,K)=TEMP
      IF(I.EQ.2) GO TO 999
      JST=1
      JEND=8
  999 CONTINUE
```

```
C
C   *  PRINT AND PUNCH THE COEFFICIENTS OF THE FILTER
 1000 WRITE(6,6100)
      WRITE(6,7500) CC
      IF(.NOT.LPUN) RETURN
      WRITE(7,7000) CC
      WRITE(7,5600)
      RETURN
C
 6100 FORMAT ('1'/' ','COMPLEX COEFFICIENTS OF THE CASCADE OF ROTATED FI
     -LTERS.')
 5600 FORMAT(2X,78('*'))
 7000 FORMAT(8F10.7)
 7500 FORMAT(1H0,255(   5X,1H(,F10.7,1H,,F10.7,5H) + (,F10.7,1H,,F10.7,
     1                 8H) Z1 + (,F10.7,1H,,F10.7,8H) Z2 + (,F10.7,1H,,
     2                 F10.7,7H) Z1 Z2,/,        '+',5X,113('_'),/,' ',
     3                   5X,1H(,F10.7,1H,,F10.7,5H) + (,F10.7,1H,,F10.7,
     4                 8H) Z1 + (,F10.7,1H,,F10.7,8H) Z2 + (,F10.7,1H,,
     5                 F10.7,7H) Z1 Z2,/,1H0))
      END
```

```
      SUBROUTINE GFRES (A,M,N,X1,X2,Y1,Y2,CC,NF,IFILT,LHBP)
C                                          JOSEP M. COSTA   1975 0728 1602
C  THIS SUBROUTINE EVALUATES THE MAGNITUDE RESPONSE OF A TWO-DIMENSIONAL
C  DIGITAL FILTER.  IT CALLS THE FUNCTION FRESIN.
C
C  A       - MATRIX WHICH ON OUTPUT WILL CONTAIN THE MAGNITUDE RESPONSE.
C  M       - FIRST DIMENSION OF A.
C  N       - SECOND DIMENSION OF A.
C  X1      - LOWER FREQUENCY POINT IN THE X DIRECTION
C  X2      - UPPER FREQUENCY POINT IN THE X DIRECTION
C  Y1      - LOWER FREQUENCY POINT IN THE Y DIRECTION
C  Y2      - UPPER FREQUENCY POINT IN THE Y DIRECTION
C            (NOTE THAT -1.0<X1<X2<1.0 AND -1.0<Y1<Y2<1.0)
C  CC      - 2D ARRAY CONTAINING THE FILTER COEFFICIENTS.
C  NF      - SECOND DIMENSION OF CC.
C  IFILT   - INPUT PARAMETER.  SEE CCP2.
C  LHBP    - INPUT PARAMETER.  SEE FILTER.
C
      DIMENSION A(M,N), CC(16,NF)
      NP=NF
      IF(LHBP.EQ.3) NP=NP/2
      DX=0.
      DY=0.
      IF(M.GT.1) DX=(X2-X1)/FLOAT(M-1)
      IF(N.GT.1) DY=(Y2-Y1)/FLOAT(N-1)
      F=FRESIN(CC,NP,IFILT,0.0)
    5 DO 6 J=1,N
      F=COORD(Y1+DY*FLOAT(J-1))
      DO 6 I=1,M
      A(I,J)=FRESO(X1+DX*FLOAT(I-1))
      IF(LHBP.EQ.2) A(I,J)=1.0-A(I,J)
    6 CONTINUE
      IF(LHBP.LT.3) RETURN
      F=FRESIN(CC(1,NP+1),NP,IFILT,0.0)
      DO 9 J=1,N
      F=COORD(Y1+DY*FLOAT(J-1))
      DO 9 I=1,M
    9 A(I,J)=A(I,J)-FRESO(X1+DX*FLOAT(I-1))
      RETURN
      END
```

```
      SUBROUTINE FILTER (A,B,M,N,LHBP,COEFF,CC,NF,IFILT,W,NW)
C                                               JOSEP M. COSTA  1975 0728 0222
C
C     THIS SUBROUTINE PREPARES THE CALL TO CCP2 FOR HIGH-PASS AND
C     BAND-PASS FILTERS.
C     IT CALLS THE SUBROUTINE ASCALE THAT NORMALIZES THE OUTPUT.
C
C     A        - MATRIX CONTAINING THE DATA TO BE FILTERED.
C                IF LHBP=3 THE CONTENTS OF A WILL BE LOST.
C     B        - SAME AS A.  ON OUTPUT WILL CONTAIN THE FILTERED DATA.
C                IF LHBP=1 (LOW-PASS FILTER) A AND B CAN BE THE SAME ARRAY.
C     M        - FIRST DIMENSION OF A AND B.
C     N        - SECOND DIMENSION OF A AND B.
C     LHBP     - INPUT PARAMETER DETERMINING THE TYPE OF FILTER.
C                =1 LOW-PASS FILTER.
C                =2 HIGH-PASS FILTER.
C                =3 BAND-PASS FILTER.
C     COEFF    - INPUT COEFFICIENT.  SHOULD BE
C                =+1 FOR HIGH-PASS AND BAND-PASS FILTERS.
C                 0<COEFF<1  FOR HIGH-EMPHASIS.
C     CC       - 2D ARRAY OF DIMENSIONS 16 BY NF CONTAINING THE
C                COEFFICIENTS OF A 2D FILTER.
C     NF       - SECOND DIMENSION OF CC.
C     IFILT    - INPUT PARAMETER.  SEE CCP2.
C     W        - WORK ARRAY DIMENSIONED AT LEAST
C                (M+1)*(NF+1)*6  FOR LOW-PASS AND HIGH-PASS FILTERS.
C                (M+1)*(NF/2+1)*6  FOR BAND-PASS FILTERS.
C     NW       - DIMENSION OF W.
C
      DIMENSION A(M,N), B(M,N), CC(16,NF), W(NW)
      MN=M*N
      NP=NF
      IF(LHBP.EQ.3) NP=NP/2
      MP1=M+1
      NPP1=NP+1
      CALL CCP2 (B,M,N,CC,NP,IFILT,W,MP1,NPP1)
      CALL ASCALE (B,MN,+1,BMIN,BMAX)
      IF(LHBP.EQ.1) RETURN
      IF(LHBP.EQ.3) CALL CCP2 (A,M,N,CC( 1,NP+1),NP,IFILT,W,MP1,NPP1)
      CALL ASCALE (A,MN,+1,BMIN,BMAX)
      DO 6 J=1,N
      DO 6 I=1,M
    6 B(I,J)=A(I,J)-COEFF*B(I,J)
      CALL ASCALE (B,MN,+1,BMIN,BMAX)
      RETURN
      END
```

```
      SUBROUTINE CCP2 (D,M,N,CC,NP,IFILT,W,MP1,NPP1)
C
C                                               JOSEP M. COSTA  1975 0727 0400
C     COMPLEX CASCADE PROGRAMMING OF A TWO-DIMENSIONAL
C     RECURSIVE FILTER USING REAL ARITHMETIC.
C     THE FILTRATION IS DONE IN PLACE.
C
C     D          - MATRIX CONTAINING THE DATA TO BE FILTERED
C     M          - FIRST DIMENSION OF D
C     N          - SECOND DIMENSION OF D
C     CC         - 2-D REAL ARRAY OF DIMENSIONS 16 BY NP CONTAINING THE
C                  COEFFICIENTS OF A 2-D ELLIPTICALLY-SHAPED FILTER.
C                  OUTSIDE THIS SUBROUTINE CC CAN BE TREATED AS A 2-D COMPLEX
C                  ARRAY OF DIMENSIONS 8 BY NP.
C     NP         - SECOND DIMENSION OF CC (NUMBER OF BILINEAR FILTERS IN THE
C                  CASCADE NOT INCLUDING COMPLEX CONJUGATES)
C     IFILT      - INPUT PARAMETER
C                  = 0     DO NOTHING (RETURN)
C                  = 1     F
C                  = 2     F    R( 90)    F    R(270)
C                  =-2     F    R(270)    F    R( 90)
C                  = 3     F    R(180)    F    R(180)
C                  = 4     F    R( 90)    F    R( 90)    F    R( 90)    F    R( 90)
C     W          - WORK ARRAY DIMENSIONED AT LEAST (M+1)*(NP+1)*6
C     MP1        = M +1
C     NPP1       = NP+1
C
      LOGICAL COMPLX
      DIMENSION D(M,N), CC(16,NP), COMPLX( 6), W(MP1,NPP1,6)
C
C     INITIALIZATION
      IF(IFILT.EQ.0) RETURN
      JFILT=IABS(MOD(IFILT,5))
      IROT=1
      IROT1=1
      GO TO (11,12,13,14),JFILT
```

```
   11 IROT=0
      GO TO 14
   12 IF (IFILT.LT.0) GO TO 15
      IROT1=3
      GO TO 14
   15 IROT=3
      GO TO 14
   13 JFILT=JFILT-1
      IROT=2
      IROT1=2
   14 IF(NP.LE.0) GO TO 30
      DO 20 J=1,NP
      COMPLX(J)=.TRUE.
      DO 18 I=2,16,2
      IF(CC(I,J).NE.0.0) GO TO 20
   18 CONTINUE
      COMPLX(J)=.FALSE.
   20 CONTINUE
      IEND=NP+1
      KEND=M+1
   30 DO 700 IC=1,JFILT
C
C     SET THE BOUNDARY CONDITIONS
      DO 60 I=1,IEND
      W(1,I,3)=0.0
      W(1,I,4)=0.0
      W(1,I,6)=0.0
      DO 60 K=1,KEND
      W(K,I,1)=0.0
      W(K,I,2)=0.0
   60 W(K,I,5)=0.0
C
C     RECURSE BY ROWS
      DO 666 L=1,N
C
C     RECURSE BY COLUMNS
      DO 606 K1=1,M
      K=K1+1
      W(K,1,6)=D(K1,L)
C
C     CASCADE OF BILINEAR FILTERS
      DO 600 I=2,IEND
      I1=I-1
      IF(COMPLX(I1)) GO TO 200
      W(K,I,6) = CC( 1,I1)*W(K ,I1,6)+CC( 3,I1)*W(K1,I1,6)
     1           +CC( 5,I1)*W(K ,I1,5)+CC( 7,I1)*W(K1,I1,5)
     2           -CC(11,I1)*W(K1,I ,6)-CC(13,I1)*W(K ,I ,5)
     3           -CC(15,I1)*W(K1,I ,5)
      GO TO 600
  200 W(K,I,3) = CC( 1,I1)*W(K ,I1,6)+CC( 3,I1)*W(K1,I1,6)
     1           +CC( 5,I1)*W(K ,I1,5)+CC( 7,I1)*W(K1,I1,5)
     2           -CC(11,I1)*W(K1,I ,3)+CC(12,I1)*W(K1,I ,4)
     3           -CC(13,I1)*W(K ,I ,1)+CC(14,I1)*W(K ,I ,2)
     4           -CC(15,I1)*W(K1,I ,1)+CC(16,I1)*W(K1,I ,2)
      W(K,I,4) = CC( 2,I1)*W(K ,I1,6)+CC( 4,I1)*W(K1,I1,6)
     1           +CC( 6,I1)*W(K ,I1,5)+CC( 8,I1)*W(K1,I1,5)
     2           -CC(12,I1)*W(K1,I ,3)-CC(11,I1)*W(K1,I ,4)
     3           -CC(14,I1)*W(K ,I ,1)-CC(13,I1)*W(K ,I ,2)
     4           -CC(16,I1)*W(K1,I ,1)-CC(15,I1)*W(K1,I ,2)
      W(K,I,6) = CC( 1,I1)*W(K ,I ,3)+CC( 2,I1)*W(K ,I ,4)
     1           +CC( 3,I1)*W(K1,I ,3)+CC( 4,I1)*W(K1,I ,4)
     2           +CC( 5,I1)*W(K ,I ,1)+CC( 6,I1)*W(K ,I ,2)
     3           +CC( 7,I1)*W(K1,I ,1)+CC( 8,I1)*W(K1,I ,2)
     4           -CC(11,I1)*W(K1,I ,6)-CC(13,I1)*W(K ,I ,5)
     5           -CC(15,I1)*W(K1,I ,5)
  600 CONTINUE
C
      D(K1,L)=W(K,IEND,6)
  606 CONTINUE
C
      DO 660 K=2,KEND
      W(K,1,5)=W(K,1,6)
      DO 660 I=2,IEND
      W(K,I,1)=W(K,I,3)
      W(K,I,2)=W(K,I,4)
  660 W(K,I,5)=W(K,I,6)
  666 CONTINUE
C
      CALL TRANSF (D,M,N,IROT)
  700 IROT=IROT1
      RETURN
      END
```

4) Programs Related to Radiologic Systems

```
      SUBROUTINE XRAY (AS,MS,NS,AO,MC,NO,KO,D,AI,MI,NI,ADIM)
C                                            JOSEP M. COSTA   1975 0521 1542
C     THIS SUBROUTINE SIMULATES AN X-RAY SYSTEM.  GIVEN A FOCAL SPOT
C     INTENSITY DISTRIBUTION, AS(MS,NS), AND A 3D OBJECT DEFINED BY THE
C     ATTENUATION FACTORS, AO(MO,NO,KO), THIS ROUTINE DETERMINES
C     THE INTENSITY DISTRIBUTION ON THE FILM PLANE, AI(MI,NI).
C
C     AS   - 2D ARRAY CONTAINING THE INTENSITY DISTRIBUTION OF THE FOCAL
C            SPOT (IF THE FOCAL SPOT IS NOT RECTANGULAR THE ELEMENTS OF AS
C            NOT BELONGING TO THE FOCAL SPOT SHOULD BE SET TO ZERO).
C     MS   - FIRST DIMENSION OF AS.
C     NS   - SECOND DIMENSION OF AS.
C     AO   - 3D ARRAY CONTAINING THE ATTENUATION FACTOR
C            DISTRIBUTION IN THE OBJECT.  THE THIRD ARGUMENT OF THE ARRAY
C            INDICATES THE LAYER NUMBER IN THE OBJECT (THESE LAYERS ARE
C            ASSUMED TO BE PARALLEL TO THE FILM PLANE).
C     MO   - FIRST DIMENSION OF AO.
C     NO   - SECOND DIMENSION OF AO.
C     KO   - THIRD DIMENSION OF AO AND LENGTH OF ARRAY D.
C     D    - 1D ARRAY OF LENGTH KO CONTAINING THE DISTANCES FROM THE FILM
C            PLANE TO THE LAYERS.
C     AI   - 2D ARRAY WHICH ON OUTPUT WILL CONTAIN THE INTENSITY
C            DISTRIBUTION OVER THE FILM PLANE, UNLESS NI=1, SEE NOTE BELOW.
C     MI   - FIRST DIMENSION OF AI.
C     NI   - SECOND DIMENSION OF AI.
C            NOTE: IF(NI.EQ.1) THE FILM PLANE WILL BE DIVIDED IN A GRID
C                  OF SIZE MI*MI AND THE INTENSITY DISTRIBUTION WILL BE
C                  WRITTEN IN AN EXTERNAL DEVICE, UNIT=1, IN UNFORMATTED
C                  BLOCKS OF LENGTH MI.
C     ADIM - 1D ARRAY OF LENGTH 8 CONTAINING THE PHYSICAL DIMENSIONS OF
C            THE X-RAY SYSTEM.  ANY LENGTH UNIT IS VALID BUT IT MUST BE
C            THE SAME FOR ALL DIMENSIONS.
C            ADIM(1) - FOCAL SPOT TO FILM DISTANCE.
C            ADIM(2) - X-LENGTH OF THE FOCAL SPOT.
C            ADIM(3) - Y-LENGTH OF THE FOCAL SPOT.
C            ADIM(4) - X-LENGTH OF THE OBJECT.
C            ADIM(5) - Y-LENGTH OF THE OBJECT.
C            ADIM(6) - X-LENGTH OF THE FILM PLANE.
C            ADIM(7) - Y-LENGTH OF THE FILM PLANE.
C            ADIM(8) - ANGLE IN RADIANS BETWEEN THE PLANE OF THE FOCAL
C                      SPOT AND THE FILM PLANE.
C     N.B.:  ALL ARRAYS ARE ASSUMED TO BE CENTERED WITH RESPECT TO THE
C            CENTRE RAY.
C
      DIMENSION AS(MS,NS), AO(MO,NO,KO), D(KO), AI(MI,NI), ADIM(8)
C
C     INITIALIZATION
      DATA IPRINT/6/, SMALLN/ZFFFFFFF/, GREATP/Z7FFFFFFF/, IUNIT/1/
      AMO=FLOAT(MO)
      ANO=FLOAT(NO)
      ANS=FLOAT(NS)
      MIP=MI
      NIP=NI
      IF(NI.NE.1) GO TO 5
      REWIND IUNIT
      NIP=MI
    5 XIS=ADIM(6)/FLOAT(MIP)
      YIS=ADIM(7)/FLOAT(NIP)
      XOO=(ADIM(6)-ADIM(4))*0.5
      YOO=(ADIM(7)-ADIM(5))*0.5
      XOS=ADIM(4)/AMO
      YOS=ADIM(5)/ANO
       C =COS(ADIM(8))
       S =SIN(ADIM(8))
      XSO=(ADIM(6)-ADIM(2))*0.5
      YSO=(ADIM(7)-ADIM(3)*C)*0.5
      ZSO=ADIM(1)-ADIM(3)*S*0.5
      XSS=ADIM(2)/FLOAT(MS)
      YSS=ADIM(3)*C/ANS
      ZSS=ADIM(3)*S/ANS
      AST=0.0
      DO 6 J=1,NS
      DO 6 I=1,MS
    6 AST=AST+AS(I,J)
      WRITE(IPRINT,*) AST
      AST=1.0/AST
      AIMAX=SMALLN
      AIMIN=GREATP
C
C     TWO LOOPS OVER FILM PLANE
      DO 990 J=1,NIP
      YI2=YIS*FLOAT(J)
```

```
      YI1=YI2-YIS
      JMIN=MINO(J,NI)
C
      DO 900 I=1,MIP
      XI2=XIS*FLOAT(I)
      XI1=XI2-XIS
      AIP=0.0
C
C  TWO LOOPS OVER FOCAL SPOT PLANE
      DO 800 L=1,NS
      AL=FLOAT(L)
      YS2=YS0+YSS*AL
      YS1=YS2-YSS
      ZSC=ZS0+ZSS*AL*0.5
C
      DO 800 K=1,MS
      XS2=XS0+XSS*FLOAT(K)
      XS1=XS2-XSS
      COEFFT=1.0
C
C  ONE LOOP OVER LAYERS IN OBJECT
      DO 700 KV=1,KC
C
C  DETERMINE THE INTERSECTION OF THE X-RAY BEAM WITH THE KV'TH LAYER.
      XO2=(XI2+D(KV)*(XS2-XI2)/ZSC-XO0)/XOS
      IF(XO2.LE.0.0) GO TO 700
      YO2=(YI2+D(KV)*(YS2-YI2)/ZSC-YO0)/YOS
      IF(YO2.LE.0.0) GO TO 700
      XO1=(XI1+D(KV)*(XS1-XI1)/ZSC-XO0)/XOS
      IF(XO1.GE.AMO) GO TO 700
      YO1=(YI1+D(KV)*(YS1-YI1)/ZSC-YO0)/YOS
      IF(YO1.GE.ANO) GO TO 700
C
C  DETERMINE THE AREA OF THE CROSS SECTION.
      AREA=(XO2-XO1)*(YO2-YO1)
C
C  DETERMINE THE AREA WHICH LIES OUTSIDE THE OBJECT.
      COEFF=0.0
      IF(XO1.GE.0.0) GO TO 51
      COEFF=-XO1*(YO2-YO1)
      XO1=0.0
   51 IF(XO2.LE.AMO) GO TO 52
      COEFF=COEFF+(XO2-AMO)*(YO2-YO1)
      XO2=AMO
   52 IF(YO1.GE.0.0) GO TO 53
      COEFF=COEFF-YO1*(XO2-XO1)
      YO1=0.0
   53 IF(YO2.LE.ANO) GO TO 54
      COEFF=COEFF+(YO2-ANO)*(XO2-XO1)
      YO2=ANO
C
C  DETERMINE THE ATTENUATION OF THE BEAM INSIDE THE OBJECT.
   54 IXO1=INT(XO1)+1
      IXO2=INT(XO2)
      JYO1=INT(YO1)+1
      JYO2=INT(YO2)
      XP=XO1
      YP=YO1
      IF(IXO2.LT.IXO1) GO TO 125
      IF(JYO2.LT.JYO1) GO TO 100
      DO 90 II=IXO1,IXO2
      YP=YO1
      XPP=FLOAT(II)
      XPPMXP=XPP-XP
      DO 60 JJ=JYO1,JYO2
      YPP=FLOAT(JJ)
      COEFF=COEFF+XPPMXP*(YPP-YP)*AO(II,JJ,KV)
   60 YP=YPP
   90 XP=XPP
      XP=XO1
  100 YO2MYP=YO2-YP
      DO 120 II=IXO1,IXO2
      XPP=FLOAT(II)
      COEFF=COEFF+(XPP-XP)*YO2MYP*AO(II,JYO2+1,KV)
  120 XP=XPP
  125 IF(JYO2.LT.JYO1) GO TO 200
      YP=YO1
      XO2MXP=XO2-XP
      DO 150 JJ=JYO1,JYO2
      YPP=FLOAT(JJ)
      COEFF=COEFF+XO2MXP*(YPP-YP)*AO(IXO2+1,JJ,KV)
  150 YP=YPP
  200 COEFF=COEFF+(XO2-XP)*(YO2-YP)*AO(IXO2+1,JYO2+1,KV)
C
C  MULTIPLY THE ATTENUATION FACTOR DUE TO EACH LAYER.
      COEFFT=COEFFT*COEFF/AREA
  700 CONTINUE
C
C  ADD ALL THE ATTENUATED INTENSITIES FROM EACH ELEMENT OF THE F.S.
  800 AIP=AIP+AS(K,L)*COEFFT
```

```
C
C   PRENORMALIZE AND FIND THE MAXIMUM AND MINIMUM OF THE IMAGE
      AIP=AIP*AST
      AIMIN=AMIN1(AIP,AIMIN)
      AIMAX=AMAX1(AIP,AIMAX)
  900 AI(I,JMIN)=AIP
C
C   STORE THE RESULTS IN AUXILIARY STORAGE IF NI=1.
      IF(NI.EQ.1) WRITE(IUNIT) AI
  990 CONTINUE
      IF(NI.EQ.1) ENDFILE IUNIT
C
C   PRINT COMPLETION MESSAGES
      WRITE(IPRINT,1000)
      WRITE(IPRINT,1001) ADIM(2),ADIM(4),ADIM(6),ADIM(3),ADIM(5),ADIM(7)
      WRITE(IPRINT,1002) MS,MC,MIP,NS,NC,NIP
      WRITE(IPRINT,1003) XSS,XOS,XIS,YSS,YOS,YIS
      WRITE(IPRINT,1004) ADIM(1),ADIM(8),KO
      WRITE(IPRINT,1005) (I,D(I),I=1,KO)
      WRITE(IPRINT,1006) AIMAX,AIMIN
      IF(NI.EQ.1) WRITE(IPRINT,1007) IUNIT
      WRITE(IPRINT,1008)
      RETURN
C
 1000 FORMAT(1H1,/,77H0XRAY SIMULATION COMPLETED, THE CHARACTERISTICS OF
     - THE SYSTEM ARE AS FOLLOWS:,/,1H-,T43,10HFOCAL SPOT,T62,6HOBJECT,
     - T79,4HFILM,/,1H+,T43,10(1H_),T62,6(1H_),T79 ,4(1H_))
 1001 FORMAT(1H0,T27,3H| X,T42,3(G14.7,3X ),/,11H DIMENSIONS,T27,1H|,/,
     -          1H ,T27,3H| Y,T42,3(G14.7,3X ))
 1002 FORMAT(1H0,T27,3H| X,T42,3(I5,12X),/,18H NUMBER OF SAMPLES,
     -          T27,1H|,/,1H ,T27,3H| Y,T42,3(I5,12X))
 1003 FORMAT(1H0,T27,3H| X,T42,3(G14.7,3X ),/,19H SAMPLING INTERVALS,
     -          T27,1H|,/,1H ,T27,3H| Y,T42,3(G14.7,3X ))
 1004 FORMAT(28H0FOCAL SPOT TO FILM DISTANCE,T42,G14.7,/,
     -          33H0ANGLE OF FOCAL SPOT (IN RADIANS),T42,G14.7,/,
     -          27H0NUMBER OF LAYERS IN OBJECT,T59,I4)
 1005 FORMAT(24H0OBJECT TO FILM DISTANCE,T1,255(T34,I3,T59,G14.7,/,'+',
     -          T27,7H| LAYER,/,1H0))
 1006 FORMAT(1H ,T27,7H| AIMAX,T76 ,G14.7,/,16H INTENSITY RANGE,
     -          T27,1H|,/,1H ,T27,7H| AIMIN,T76 ,G14.7)
 1007 FORMAT(49H-THE SIMULATED RADIOGRAPH HAS BEEN STORED IN UNIT,I4)
 1008 FORMAT(1H1)
      END
```

```
      SUBROUTINE INVFHL (U,V,X,Y,N,HL)
C                                              J.M. COSTA   1975 1229 1203
C   THIS SUBROUTINE CALCULATES THE TRANSFER FUNCTION OF AN INVERSE FILTER
C   WITH HARD-LIMITED MAGNITUDE RESPONSE.
C   THE DFT COEFFICIENTS ARE USED TO DESCRIBE THE TRANSFER FUNCTIONS OF
C   THE SYSTEM AND AND THE INVERSE FILTER.  THE DFT COEFFICIENTS ARE
C   STORED IN THE ARRAYS U, V, X, AND Y.
C   THE SUBROUTINE PARAMETERS ARE AS FOLLOWS.
C   U     - REAL PART OF THE TRANSFER FUNCTION OF THE INVERSE FILTER.
C   V     - IMAGINARY PART OF THE TRANSFER FUNCTION OF THE INVERSE FILTER.
C   X     - REAL PART OF THE TRANSFER FUNCTION OF THE GIVEN FILTER.
C   Y     - IMAGINARY PART OF THE TRANSFER FUNCTION OF THE GIVEN FILTER.
C   N     - NUMBER OF ELEMENTS IN THE ARRAYS X, Y, U, AND V.
C   HL    - LEVEL OF HARD-LIMITING FOR THE MAGNITUDE RESPONSE OF THE
C   N.B. THE TRANSFORMATION MAY BE DONE IN PLACE IF IN THE MAIN PROGRAM
C        THE ARRAYS U AND V ARE EQUIVALENT TO THE ARRAYS X AND Y,
C        RESPECTIVELY.
C
      DIMENSION U(N),V(N),X(N),Y(N)
      CHL=1.0/(HL*HL)
C
      DO 6 I=1,N
      C=X(I)*X(I)+Y(I)*Y(I)
      IF(C.NE.0.0) GO TO 3
C
C THE SQUARE MAGNITUDE IS ZERO
      U(I)=HL
      V(I)=0.0
      GO TO 6
C
C   CALCULATE THE HARD-LIMITING FACTOR IF THE MAGNITUDE RESPONSE OF THE
C   INVERSE FILTER IS GREATER THAN HL.
    3 IF(C.LT.CHL) C=SQRT(C)/HL
C
C   DETERMINE THE REAL AND IMAGINARY PART OF THE INVERSE FILTER.
      U(I)= X(I)/C
      V(I)=-Y(I)/C
    6 CONTINUE
      RETURN
      END
```

5) Utility Programs

```
      SUBROUTINE PICPRT (X,M,N,MX,LI)
C
C                                               JOSEP M. COSTA   1975 0610 1456
C  THIS SUBROUTINE PRODUCES A PICTORIAL OUTPUT ON A LINE PRINTER.
C  THE PICTURE IS DEFINED BY A 2D ARRAY OF REAL NUMBERS BETWEEN 0.0 AND
C  1.0 REPRESENTING THE INTENSITY VALUES.  IF A PIXEL HAS A VALUE LESS
C  THAN ZERO NOTHING IS PRINTED AND IF A PIXEL HAS A VALUE GREATER THAN
C  ONE THE MAXIMUM DENSITY IS PRINTED.
C  X   - 2D ARRAY OF DIMENSIONS M BY N CONTAINING THE INTENSITY VALUES.
C  M   - FIRST DIMENSION OF X
C  N   - SECOND DIMENSION OF X (LENGTH OF PICTURE TO BE PRINTED)
C  MX  - WIDTH OF PICTURE TO BE PRINTED.
C        IF (MX.LT.0) A NEGATIVE OF THE PICTURE IS PRINTED.
C  LI  - NUMBER OF LINES PRINTED PER INCH.
C        THE X-AXIS (FIRST SUBSCRIPT OF ARRAY X) GOES FROM THE LEFT TO
C        THE RIGHT OF THE PAGE.
C        THE Y-AXIS (SECOND SUBSCRIPT OF ARRAY X) GOES FROM THE BOTTOM
C        TO THE TOP OF THE PAGE(S).
C        IF (LI.LT.0) THE Y-AXIS GOES FROM THE TOP TO THE BOTTOM OF THE
C        PAGE(S).
C
      DIMENSION X(M,N)
      LOGICAL FLIP,NEG
      DATA A1/.075/,A2/.185/,A3/.235/,A4/.27/,A5/.31/,A6/.35/,A7/.385/,
     -A8/.41/,A9/.435/,A10/.49/,A11/.545/,A12/.58/,A13/.62/,A14/.655/,
     -A15/.73/,A16/.82/,A17/.87/,A18/.91/,A19/.95/,A20/.985/
      INTEGER   PMAX(8)/9,17,25,33,42,50,58,66/
      LOGICAL*1 P1(133),P2(132),P3(132),P4(132),P5(132),P6(132),
     -P7(132),P8(132),P18(1057),P17(925),P16(793),P15(661),P14(529),
     -P13(397),P12(265),LCARRG,DUMMY(15),
     -C0/' '/,C1/'-'/,C2/'='/,C3/'+'/,C4/')'/,C5/'1'/,C6/'Z'/,C7/'X'/,
     -C8/'A'/,C9/'M'/,C10/'O'/,C11/''''/,C12/'.'/,C13/'H'/,C14/'C'/,
     -C15/'B'/,C16/'V'/
      COMPLEX*16 CP(66),CBLANK/'                '/
      COMMON/P1 TO P8/DUMMY,P1,P2,P3,P4,P5,P6,P7,P8
      EQUIVALENCE(CP(1),P1(2))
      EQUIVALENCE (LCARRG,P1(1),P18(1),P17(1),P16(1),P15(1),P14(1),
     -P13(1),P12(1))
      DATA NCOLPG/132/, NLINPG/60/, NCARIN/10/, NLININ/8/
      L=IABS(MX)
      IF(L.GT.NCOLPG) L=NCOLPG
      NEG=.FALSE.
      IF(MX.LT.0) NEG=.TRUE.
      LCARRG=C5
      IR=IABS(LI)
      IF(IR.EQ.0) IR=NLININ
      FLIP=.FALSE.
      IF(LI.LT.0) FLIP=.TRUE.
      MAXP = 8
      I1=(NCOLPG-L)/2
      I1P1=I1+1
      I2=L+I1
      N1=N*IR/NCARIN
      IF (N1.GE.NLINPG) GO TO 4
      J2=(NLINPG-N1)/2-1
      DO 3 J=1,J2
      WRITE(6,6001) LCARRG
    3 LCARRG=C0
    4 IF(I1.LE.0) GO TO 7
      DO 6 K=1,9
    6 CP(K)=CBLANK
      P1(I1+1)=C3
      P1(I2+2)=C3
      WRITE(6,6001) P1
      LCARRG=C0
    7 AN=FLOAT(N)
      RI=FLOAT(NCARIN)/FLOAT(IR)
      N1P1=N1+1
      DO 900 JJ=1,N1
      J=JJ
      IF(FLIP) J=N1P1-JJ
      IPMAX = PMAX(MAXP)
      DO 9 K=1,IPMAX
    9 CP(K) = CBLANK
      MAXP = 1
      MP=1
      J1=N-(J-1)*NCARIN/IR
      J2=J1-1
      DJ=FLOAT(J1-N)+FLOAT(J-1)*RI
      DO 600 I=I1P1,I2
      IP1=I+1
      Z=X(I-I1,J1)
```

```
      IF (IR.NE.NCARIN) Z=Z+(X(I-I1,J2)-Z)*DJ
      IF(NEG) Z=1.0-Z
      IF (Z.GT.A10) GO TO 90
      IF (Z.GT.A5) GO TO 40
      IF (Z.GT.A3) GO TO 20
      IF (Z.GT.A2) GO TO 10
      IF (Z.GT.A1) P1(IP1)=C1
      GO TO 600
   10 P1(IP1)=C2
      GO TO 600
   20 IF (Z.GT.A4) GO TO 30
      P1(IP1)=C3
      GO TO 600
   30 P1(IP1)=C4
      GO TO 600
   40 IF (Z.GT.A8) GO TO 70
      IF (Z.GT.A7) GO TO 60
      IF (Z.GT.A6) GO TO 50
      P1(IP1)=C5
      GO TO 600
   50 P1(IP1)=C6
      GO TO 600
   60 P1(IP1)=C7
      GO TO 600
   70 IF (Z.GT.A9) GO TO 80
      P1(IP1)=C8
      GO TO 600
   80 P1(IP1)=C9
      GO TO 600
   90 P1(IP1)=C10
      MP=2
      IF (Z.GT.A16) GO TO 130
      IF (Z.GT.A13) GO TO 120
      IF (Z.GT.A11) GO TO 100
      P2(I)=C1
      GO TO 600
  100 IF (Z.GT.A12) GO TO 110
      P2(I)=C2
      GO TO 600
  110 P2(I)=C3
      GO TO 600
  120 P2(I)=C3
      MP=3
      P3(I)=C11
      IF (Z.LE.A14) GO TO 600
      MP=4
      P4(I)=C12
      IF (Z.LE.A15) GO TO 600
      MP=5
      P5(I)=C2
      GO TO 600
  130 MP=5
      P2(I)=C7
      P3(I)=C11
      P4(I)=C12
      IF (Z.GT.A17) GO TO 140
      P5(I)=C1
      GO TO 600
  140 P5(I) =C13
      IF(Z. GT. A19)  GO TO 160
      MP=6
      IF (Z.GT. A18) GO TO 150
      P6 (I) =C14
      GO TO 600
  150 P6 (I) = C15
      GO TO 600
  160 P7(I) =C16
      IF (Z.GT.A20) GO TO 170
      MP=7
      GO TO 600
  170 MP=8
      P8 (I) =C8
  600 MAXP=MAX0(MAXP,MP)
      GO TO ( 610,620,630,640,650,660,670,680),MAXP
  610 WRITE (6,6001) P1
      GO TO 900
  620 WRITE (6,6001) P12
      GO TO 900
  630 WRITE (6,6001) P13
      GO TO 900
  640 WRITE (6,6001) P14
      GO TO 900
  650 WRITE (6,6001) P15
      GO TO 900
  660 WRITE (6,6001) P16
      GO TO 900
  670 WRITE (6,6001) P17
      GO TO 900
  680 WRITE (6,6001) P18
  900 LCARRG=C0
```

```
      IF(I1.LE.0) GO TO 999
      DO 906 K=1,9
  906 CP(K)=CBLANK
      P1(I1+1)=C3
      P1(I2+2)=C3
      WRITE(6,6001) P1
  999 RETURN
 6001 FORMAT(133A1,/,('+',132A1))
      END




      SUBROUTINE ASCALE (A,L,IFN,AMAX,AMIN)
C                                               J.M. COSTA   1976 0102 1555
C   THIS SUBROUTINE FINDS THE MAXIMUM AND MINIMUM OF THE ELEMENTS OF AN
C   ARRAY AND/OR SCALES THESE ELEMENTS BETWEEN 0.0 AND 1.0.
C   THE SUBROUTINE PARAMETERS ARE AS FOLLOWS.
C   A      - ARRAY TO BE SCALED.
C   L      - NUMBER OF ELEMENTS IN A.
C   IFN    - INPUT PARAMETER:
C            IF(IFN.GT.0) THE MAXIMUM AND MINIMUM VALUES ARE DETERMINED
C                         AND THE ELEMENTS OF THE ARRAY ARE SCALED BETWEEN
C                         0.0 AND 1.0.
C            IF(IFN.EQ.0) THE ELEMENTS OF THE ARRAY ARE SCALED ACCORDING
C                         TO THE VALUES OF AMAX AND AMIN SUPPLIED BY THE
C                         CALLING PROGRAM.
C            IF(IFN.LT.0) THE MAXIMUM AND MINIMUM VALUES ARE DETERMINED
C                         BUT THE ARRAY IS NOT SCALED.
C   AMAX   - MAXIMUM VALUE OF ARRAY A.
C   AMIN   - MINIMUM VALUE OF ARRAY A.
C
      DIMENSION A(L)
C
C   DETERMINE AMAX AND AMIN IF THEY ARE NOT SUPPLIED BY
C   THE CALLING PROGRAM
      IF(IFN.EQ.0) GO TO 7
      AMAX=A(1)
      AMIN=AMAX
      DO 6 I=2,L
      AMAX=AMAX1(A(I),AMAX)
      AMIN=AMIN1(A(I),AMIN)
    6 CONTINUE
      WRITE(6,6000) AMAX,AMIN
 6000 FORMAT('0*** IN SUBROUTINE ASCALE: AMAX =',G16.7,' AND AMIN =',
     -        G16.7,' ***')
      IF(IFN.LE.0) RETURN
C
C   SCALE THE ARRAY
    7 D=1.0/(AMAX-AMIN)
      DO 9 I=1,L
    9 A(I)=(A(I)-AMIN)*D
      RETURN
C
      END




      SUBROUTINE DBS (D,X,N,V,F)
C                                               J.M. COSTA   1976 0103 1357
C   THIS SUBROUTINE TRANSFORMS AN ARRAY OF NON NEGATIVE REAL NUMBERS TO
C   DECIBELS.
C   THE SUBROUTINE PARAMETERS ARE AS FOLLOWS.
C   D    - ARRAY OF LENGTH N THAT ON OUTPUT WILL CONTAIN THE DATA IN DB'S.
C   X    - ARRAY OF LENGTH N CONTAINING THE INPUT DATA.
C   N    - NUMBER OF DATA POINTS IN D AND X.
C   V    - HARD-LIMITING PARAMETER FOR VALUES LESS THAN V.
C          IF V IS LESS THAN OR EQUAL TO ZERO THE SUBROUTINE USES INSTEAD
C          THE LEAST POSITIVE NUMBER IN THE ARRAY.
C   F    - INPUT COEFFICIENT. SHOULD BE EQUAL TO 10.0 FOR POWER RATIOS OR
C                             EQUAL TO 20.0 FOR VOLTAGE OR CURRENT RATIOS.
C   N.B. THE TRANSFORMATION MAY BE DONE IN PLACE IF THE ARRAYS D AND X
C        ARE EQUIVALENT IN THE CALLING PROGRAM.
C
      DIMENSION D(N), X(N)
      DATA GREAT/Z7FFFFFFF/, IPRINT/6/
C
C   INITIALIZATION
      VALO=V
      NBV=0
      IF(VALO.GT.0.0) GO TO 4
```

```
C
C   DETERMINE THE LEAST POSITIVE NUMBER IN THE ARRAY
        VALO=GREAT
        DO 3 I=1,N
        IF(X(I).GT.0.0) VALO=AMIN1(VALO,X(I))
      3 CONTINUE
C
C   TRANSFORM TO DB'S
      4 VALODB=F*ALOG10(VALO)
        DO 6 I=1,N
        A=X(I)
        IF(A.GE.VALO) GO TO 5
        NBV=NBV+1
        D(I)=VALODB
        GO TO 6
      5 D(I)=F*ALOG10(A)
      6 CONTINUE
C
C   END OF THE TRANSFORMATION,  A COMPLETION MESSAGE WILL BE PRINTED
        WRITE(IPRINT,9) NBV,VALO
      9 FORMAT ('0*** IN SUBROUTINE DBS:',I6,' DATA VALUES ARE LESS THAN '
       -               ,G16.7,' ***')
        RETURN
C
        END
```

```
        SUBROUTINE CMAG2  (X,MT,NT,ISN)
C                                               J.M. COSTA   1976 0327 1500
C   THIS SUBROUTINE DETERMINES THE SQUARED MAGNITUDE OF THE FOURIER
C   TRANSFORM GIVEN BY FFT2R.
C
        DIMENSION X(MT,NT)
        IF(IABS(ISN).GT.1) GO TO 20
C
        DO 10 J=1,NT
        DO 10 I=1,MT,2
     10 X(I/2+1,J)=X(I,J)*X(I,J)+X(I+1,J)*X(I+1,J)
        RETURN
C
     20 DO 30 J=1,NT,2
        DO 30 I=1,MT
     30 X(I,J/2+1)=X(I,J)*X(I,J)+X(I,J+1)*X(I,J+1)
        RETURN
        END
```

```
        SUBROUTINE COMPLT (X,MT,NT,ISN)
C                                               J.M. COSTA   1976 0327 1500
C   THIS SUBROUTINE COMPLETES THE ARRAY GIVEN BY CMAG2 BY SYMMETRIES.
C
        DIMENSION X(MT,NT)
        IF(IABS(ISN).GT.1) GO TO 50
C
        M2=(MT-2)/2
        DO 10 I=2,M2
     10 X(MT-I,1)=X(I,1)
        X(MT-1,1)=0.0
        X(MT,1)=0.0
        NP2=NT+2
        DO 30 J=2,NT
        X(MT-1,J)=0.0
        X(MT,J)=0.0
        JP=NP2-J
        DO 30 I=2,M2
     30 X(MT-I,JP)=X(I,J)
        RETURN
C
     50 N2=(NT-2)/2
        DO 60 J=2,N2
     60 X(1,NT-J)=X(1,J)
        MP2=MT+2
        DO 90 J=2,N2
        JP=NT-J
        DO 90 I=2,MT
     90 X(MP2-I,JP)=X(I,J)
        RETURN
        END
```

```
      SUBROUTINE CAMOVE (X,M,N,MX)
C                                         JOSEP M. COSTA  1975 1106 1328
C  THIS SUBROUTINE REARRANGES THE ELEMENTS OF A MATRIX TO MEET THE
C  ASSUMPTIONS OF THE TWO-DIMENSIONAL FAST FOURIER TRANSFORM.
C  THE COORDINATE AXES, ASSUMED CENTRED WITHIN THE MATRIX, ARE MOVED TO
C  THE CORNER WITH THE LOWEST INDICES.
C  N. B.  M AND N MUST BE DIVISIBLE BY 2.
C
      DIMENSION X(M,N)
      MBY2=MX/2
      NBY2=N/2
      DO 6 J=1,NBY2
      JP=NBY2+J
      DO 6 I=1,MBY2
      IP=MBY2+I
      T=X(I,J)
      X(I,J)=X(IP,JP)
      X(IP,JP)=T
      T=X(IP,J)
      X(IP,J)=X(I,JP)
    6 X(I,JP)=T
      RETURN
      END
```

```
      SUBROUTINE CTDW2 (X,M,N,MX)
C                                          J.M. COSTA  1976 0327 1500
C  THIS SUBROUTINE MULTIPLIES A GIVEN MATRIX BY A TWO-DIMENSIONAL
C  COSINE TAPER DATA WINDOW (IN PLACE)
C
      DIMENSION X(M,N)
      DATA PI/3.141593/, IR/10/
      IW=MX/IR
      AIW=FLOAT(IW)
      L=N+1
      DO 6 J=1,IW
      CTDW=0.5+0.5*COS(PI*(1+FLOAT(J)/AIW))
      KP=L-J
      DO 6 I=1,MX
      X(I,J)=CTDW*X(I,J)
    6 X(I,KP)=CTDW*X(I,KP)
      IW=N/IR
      AIW=FLOAT(IW)
      L=MX+1
      DO 9 I=1,IW
      CTDW=0.5+0.5*COS(PI*(1+FLOAT(I)/AIW))
      KP=L-I
      DO 9 J=1,N
      X(I,J)=CTDW*X(I,J)
    9 X(KP,J)=CTDW*X(KP,J)
      RETURN
      END
```

```
      SUBROUTINE TRANSF (Z,M,N,IC)
C                                         JOSEP M. COSTA  1975 0611 1246
C  THIS SUBROUTINE IMPLEMENTS ALL LINEAR TRANSFORMATIONS WHICH MAP A
C  SQUARE MATRIX ONTO ITSELF.  THERE ARE 8 SUCH POSSIBLE TRANSFORMATIONS
C  AND THEY HAVE THE ALGEBRAIC STRUCTURE OF A FINITE GROUP.
C  THE TRANSFORMATIONS ARE DONE IN PLACE.
C  Z  - MATRIX TO BE TRANSFORMED.
C  M  - FIRST DIMENSION OF Z.
C  N  - SECOND DIMENSION OF Z, ORDER OF SQUARE MATRIX TO BE TRANSFORMED.
C       N MUST BE LESS THAN OR EQUAL TO M.
C       THE SQUARE MATRIX MAY BE A SUBMATRIX OF A LARGER RECTANGULAR
C       MATRIX IN THE MAIN PROGRAM, IN WHICH CASE THE ADDRESS OF THE
C       UPPER LEFT HAND CORNER OF THE SQUARE MATRIX IS PASSED TO THE
C       SUBROUTINE.
C  IC - INPUT PARAMETER WHICH DETERMINES THE TRANSFORMATION
C       =0 IDENTITY
C       =1 ROTATE BY  90 DEGREES (CLOCKWISE)
C       =2 ROTATE BY 180 DEGREES (CLOCKWISE)
C       =3 ROTATE BY 270 DEGREES (CLOCKWISE)
C       =4 VERTICAL MIRROR IMAGE
C       =5 TRANSPOSE
C       =6 HORIZONTAL MIRROR IMAGE
C       =7 TRANSPOSE WITH RESPECT TO THE SECONDARY DIAGONAL.
C
```

```
      DIMENSION Z(M,N)
C
C   INITIALIZATION
      IROT=MOD(IABS(IC),8)
      NP1=N+1
      MED=N/2
C
C   IDENTITY
      IF(IROT.EQ.0 .OR. N.EQ.1) RETURN
      GO TO (90,180,270,400,500,600,700), IROT
C
C   ROTATE BY 90 DEGREES
   90 DO 95 I=1,MED
      IP=NP1-I
      JND=IP-1
      DO 95 J=I,JND
      JP=NP1-J
      T=Z(I,J)
      Z(I,J)=Z(JP,I)
      Z(JP,I)=Z(IP,JP)
      Z(IP,JP)=Z(J,IP)
   95 Z(J,IP)=T
      RETURN
C
C   ROTATE BY 180 DEGREES
  180 DO 185 I=1,MED
      IP=NP1-I
      JND=IP-1
      DO 185 J=I,JND
      JP=NP1-J
      T=Z(I,J)
      Z(I,J)=Z(IP,JP)
      Z(IP,JP)=T
      T=Z(J,IP)
      Z(J,IP)=Z(JP,I)
  185 Z(JP,I)=T
      RETURN
C
C   ROTATE BY 270 DEGREES
  270 DO 275 I=1,MED
      IP=NP1-I
      JND=IP-1
      DO 275 J=I,JND
      JP=NP1-J
      T=Z(I,J)
      Z(I,J)=Z(J,IP)
      Z(J,IP)=Z(IP,JP)
      Z(IP,JP)=Z(JP,I)
  275 Z(JP,I)=T
      RETURN
C
C   VERTICAL MIPROR IMAGE
  400 DO 405 J=1,MED
      DO 405 I=1,N
      JP=NP1-J
      T=Z(I,J)
      Z(I,J)=Z(I,JP)
  405 Z(I,JP)=T
      RETURN
C
C   TRANSPOSE
  500 DO 505 J=2,N
      JM1=J-1
      DO 505 I=1,JM1
      T=Z(I,J)
      Z(I,J)=Z(J,I)
  505 Z(J,I)=T
      RETURN
C
C   HORIZONTAL MIRROR IMAGE
  600 DO 605 I=1,MED
      DO 605 J=1,N
      IP=NP1-I
      T=Z(I,J)
      Z(I,J)=Z(IP,J)
  605 Z(IP,J)=T
      RETURN
C
C   TRANSPOSE WITH RESPECT TO THE SECONDARY DIAGONAL
  700 JND=N-1
      DO 705 J=1,JND
      JP=NP1-J
      IND=JP-1
      DO 705 I=1,IND
      IP=NP1-I
      T=Z(I,J)
      Z(I,J)=Z(IP,JP)
  705 Z(IP,JP)=T
      RETURN
      END
```

Appendix D

THE COMPUTER SYSTEM

Two digital computer systems were utilized in this work for image digitization, processing and reconstruction, filter design, contour and perspective plots, etc.

Most of the computing was done off-line with an IBM SYSTEM/370 MODEL 165-II (OS/MVT with HASP) with Gould and Calcomp plotters. These are powerful resources but cumbersome to use in image processing because of the lack of interaction.

The digitization and reconstruction of images was done in a modest image processing facility mounted around a DEC PDP-11 minicomputer in the CRF laboratories. A diagram of this facility is shown in Figure D.1.

Magnetic tape (9 track, 800 BPI) was used as the communication medium between the PDP-11 and the IBM 370. The picture elements are represented by integer numbers between 0 and 63 and stored as INTEGER*2 values using A2 format. The records in the tape are of undefined length and the block-size is 512 bytes. The first block contains the number of samples in the image.

We developed some programs for interactive image enhancement. These include determination of the picture histogram, cummulative histogram mapping (for histogram equalization) and piecewise linear intensity mappings (for stretching certain gray levels).

In the remainder of this appendix we give a brief description of the CVI equipment which is used for the digitization and display of images. For more detailed information the reader is referred to the

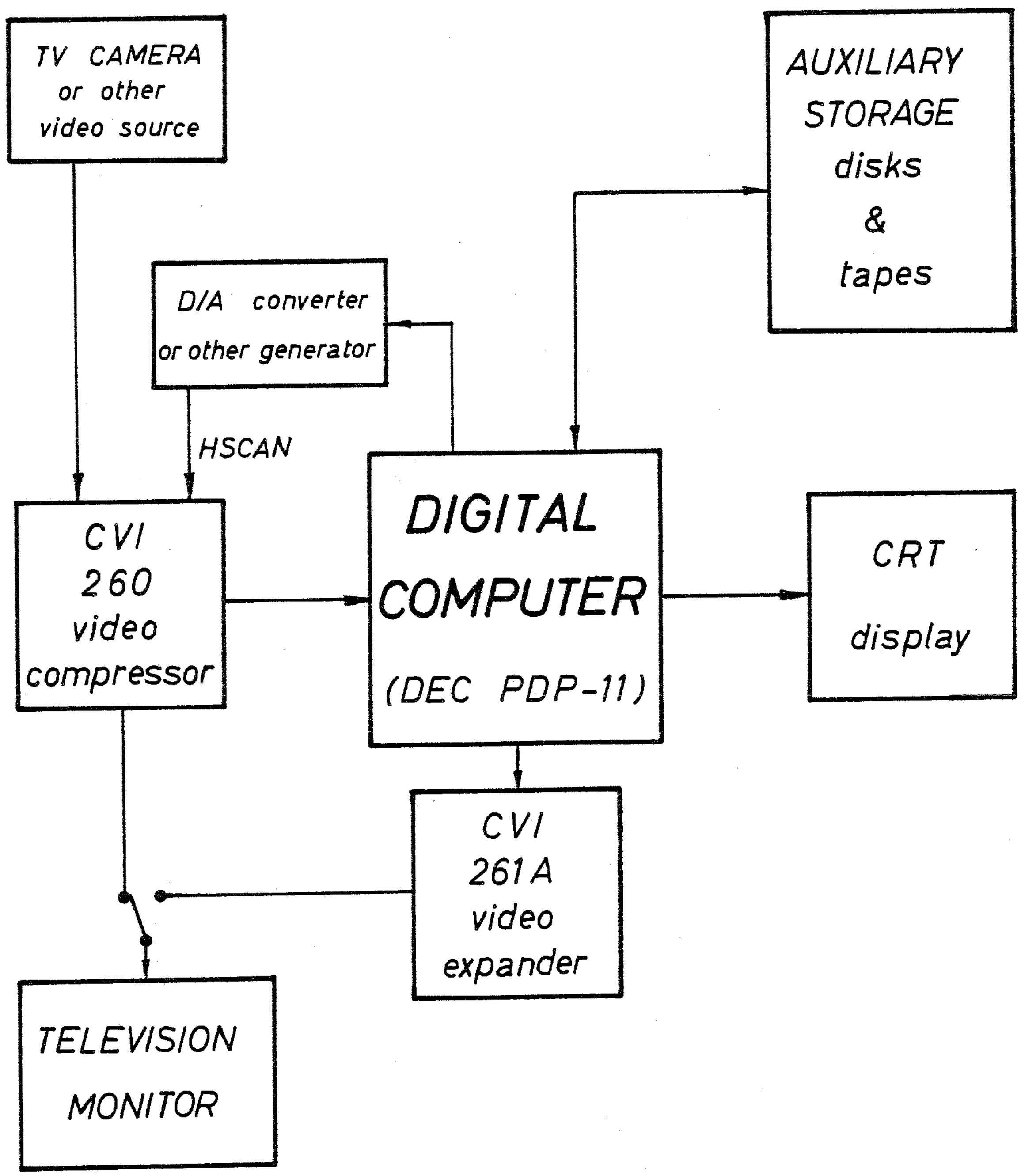

Figure D.1. A computer system for interactive image processing.

equipment manuals.

Video Compressor

The CVI Model 260 Video Compressor is a device that can extract pictorial information from a standard television video signal at a rate compatible with the data rates of computers and other digital processing equipment. This is accomplished by taking one sample from each television scan line; so that the sampling rate is nearly 16,000 samples/second which gives an equivalent analog bandwidth of approximately 8 kHz.

As a result of the sampling technique used in the Model 260, the output data comes from a vertical sampling line that scans from the top to the bottom of the original television raster. This sampling line is normally moved from left to right accross the raster to complete a single frame, but positioning of the sample line can be arbitrary when using the external H-scan capability of the instrument.

The Model 260 incorporates a "real time" video output which allows the user to monitor the sampling process. Location of the sampling line is displayed on a television monitor as a series of superimposed white dots, while the waveform produced by the sampled data is also displayed vertically at the left-hand side of the screen.

Video Expander

The CVI Model 261A Video Expander is a device that accepts digitally encoded pictorial data and stores it on a video disk for display on a standard television monitor. The buildup of the image may be continuously observed, and there is no fadeout or image degradation with time in the resulting display.

The Model 261A accepts parallel six-bit binary data by columns. The input data for one vertical column of picture elements (one picture element per scan line in the final television raster) are read into a buffer storage register into the 261A. This column of data is then recorded on the magnetic disk in the proper field (as selected by the computer) and at the horizontal position in the raster determined by an external position signal. Continuation of this process allows the construction of an entire, interlaced television raster.

Conventional television uses a 2:1 interlaced scanning format. This means that each television frame (a complete picture consisting of 525 scan lines written in 1/30 second) is made up of two fields (each containing 262½ scan lines written in 1/60 second) displaced vertically so that the scan lines interlace. Interlacing is done to minimize flicker in the displayed picture. The number of active lines in each field is 240.

In using the 261A, it is important that the data be interlaced for a proper display. We have chosen to artificially generate the second field by linear interpolating the first. This interpolation is done in real time just before displaying the image, so that redundant digital data do not have to be stored on tape.

The resolution of the system is limited in the vertical direction by the number of active scan lines (240+240=480) and in the horizontal direction by the packing density of the magnetic disk. In the 261A this density limitation requires the use of 200 or fewer points per line; although in practice this horizontal limitation can be exceeded slightly (e.g. to 256 points per line).

REFERENCES

[1] B.G. Ziedses des Plantes, "Body-section radiography: History, image information, various techniques and results", *Australasian Radiology*, Vol. XV, No. 1, pp. 57-64, February 1971.

[2] R.M. Mersereau, "Digital reconstruction of multidimensional signals from their projections", Sc.D. dissertation, Dept. of Electrical Engineering, Massachusetts Institute of Technology, February 1973.

[3] R.M. Mersereau and A.V. Oppenheim, "Digital reconstruction of multidimensional signals from their projections", *Proc. of the IEEE*, Vol. 62, No. 10, pp. 1319-1338, October 1974; reprinted in [15], pp. 210-229.

[4] H.H. Barrett, K. Garewal, and D.T. Wilson, "A spatially-coded X-ray source", *Radiology*, Vol. 104, No. 2, pp. 429-430, August 1972.

[5] W.J. Meredith and J.B. Massey, *Fundamental Physics of Radiology*, Second Edition. Bristol, Great Britain: John Wright & Sons Ltd., 1972.

[6] R.A. Brinker and J. Skucas, *Radiology Special Procedure Room*. Baltimore, Maryland: University Park Press, 1973.

[7] J.W. Goodman, *Introduction to Fourier Optics*. New York: McGraw-Hill, 1968.

[8] T.S. Huang, W.F. Schreiber, and O.J. Tretiak, "Image processing", *Proc. of the IEEE*, Vol. 59, No. 11, pp. 1586-1609, November 1971.

[9] H.C. Andrews, *Computer Techniques in Image Processing*. New York: Academic Press, 1970.

[10] *Proceedings of the IEEE (Special Issue on Digital Picture Processing)*, Vol. 60, No. 7, July 1972.

[11] *Computer (Special Issue on Digital Image Processing)*, Vol. 7, No. 5, May 1974.

[12] A.V. Oppenheim and R.W. Schafer, *Digital Signal Processing*. Englewood Cliffs, New Jersey: Prentice-Hall, 1975.

[13] L.R. Rabiner and B. Gold, *Theory and Application of Digital Signal Processing*. Englewood Cliffs, New Jersey: Prentice-Hall, 1975.

[14] L.R. Rabiner and C.M. Rader, Eds., *Digital Signal Processing*. New York: IEEE Press, 1972.

[15] A.V. Oppenheim *et al.* (Digital Signal Processing Commitee, IEEE Acoustics, Speech, and Signal Processing Society), Eds., *Selected Papers in Digital Signal Processing, II.* New York: IEEE Press, 1976.

[16] K. Rossmann, "Image quality", *Radiologic Clinics of North America (Symposium on the Perception of the Roentgen Image)*, Vol. VII, No. 3, pp. 419-433, December 1969.

[17] E.M. Laasonen, "Information transmission in Roentgen diagnostic chains", *Acta Radiologica*, Supplementum 280, pp. 1-93, 1968.

[18] R.H. Morgan, "The frequency response function, a valuable means of expressing the informational recording capability of diagnostic X-ray systems", *American Journal of Roentgenology, Radiation Therapy and Nuclear Medicine*, Vol. 88, No. 1, pp. 175-186, July 1962.

[19] K. Doi, A. Kaji, T. Takizawa, and K. Sayanagi, "The application of optical transfer function in radiography", in *Proc. of the Conference on Photographic and Spectroscopic Optics*, 1964, *Japanese Journal of Applied Physics*, Vol. 4, Supplement I, pp. 183-190, 1965.

[20] R.D. Moseley, Jr. and J.H. Rust, Eds., *Diagnostic Radiologic Instrumentation, Modulation Transfer Function.* Springfield, Illinois: Charles C. Thomas, Publisher, 1965.

[21] N.C. Beese, "The focusing of electrons in an X-ray tube", *The Review of Scientific Instruments*, Vol. 8, New Series, pp. 258-262, July 1937.

[22] K. Doi, "Optical transfer functions of the focal spot of X-ray tubes", *American Journal of Roentgenology, Radiation Therapy and Nuclear Medicine*, Vol. 94, No. 3, pp. 712-718, July 1965.

[23] G. Lubberts and K. Rossmann, "Modulation transfer function associated with geometrical unsharpness in medical radiography", *Physics in Medicine and Biology*, Vol 12, No. 1, pp. 65-67, January 1967.

[24] E. Takenaka, K. Kinoshita, and R. Nakajima, "Modulation transfer function of the intensity distribution of the Roentgen focal spot", *Acta Radiologica, Therapy, Physics, Biology*, Vol 7, Fasc. 4, pp. 263-272, August 1968.

[25] R.F. Wagner, K.E. Weaver, E.W. Denny, and R.G. Bostrom, "Toward a unified view of radiological imaging systems. Part I: Noiseless images", *Medical Physics*, Vol. 1, No. 1, pp. 11-24, January-February 1974.

[26] E.L. Chaney and W.R. Hendee, "Effects of X-ray tube current and voltage on effective focal-spot size", *Medical Physics*, Vol. 1, No. 3, pp. 141-147, May-June 1974.

[27] G.U.V. Rao and A. Soong, "An intercomparison of the modulation transfer functions of square and circular focal spots", *Medical Physics*, Vol. 1, No. 4, pp. 204-209, July-August 1974.

[28] K. Doi and K. Sayanagi, "Role of optical transfer function for optimum magnification in enlargement radiography", *Japanese Journal of Applied Physics*, Vol. 9, No. 7, pp. 834-839, July 1970.

[29] E.N.C. Milne, "The role and performance of minute focal spots in Roentgenology with special reference to magnification", *CRC Critical Critical Reviews in Radiological Sciences*, Vol. 2, pp. 269-310, May 1971.

[30] J.B. Minkoff, S.K. Hilal, W.F. Konig, M. Arm, and L.B. Lampert, "Optical filtering to compensate for degradation of radiographic images produced by extended sources", *Applied Optics*, Vol. 7, No. 4, pp. 633-641, 1968.

[31] G.A. Krusos, "The amelioration of contrast and resolution of X-ray images using optical signal processing", Eng. Sc. D. dissertation, Columbia University, New York, 1971.

[32] M. Trefler and E.N.C. Milne, "The diagnostic quality of optically processed radiographs", *Radiology*, Vol. 121, No. 1, pp. 211-213, October 1976.

[33] S. Wende, E. Zieler, and N. Nakayama, *Cerebral Magnification Angiography*. New York: Springer-Verlag, 1974, Chapter 8.

[34] B.R. Hunt, D.H. Janney, and R.K. Zeigler, "An introduction to restoration and enhancement of radiographic images", Tech. Rep. LA-4305, Los Alamos Scientific Laboratory, Los Alamos, New Mexico, 1970.

[35] B.R. Hunt, "The inverse problem of radiography", *Mathematical Biosciences*, Vol. 8, pp. 161-179, 1970.

[36] D.G. Falconer, "Image enhancement and film-grain noise", *Optica Acta,* Vol. 17, No. 9, pp. 693-705, September 1970.

[37] B.R. Hunt, "Digital Image Processing", *Proc. of the IEEE*, Vol. 63, No. 4, pp. 693-708, April 1975.

[38] B.R. Hunt and J.R. Breedlove, "Scan and display considerations in processing images by digital computer", *IEEE Trans. on Computers*, Vol. C-24, No. 8, pp. 848-853, August 1975.

[39] L. Biberman, Ed., *Perception of Displayed Information*. New York: Plenum Press, 1973.

[40] A. Rose, "A unified approach to the performance of photographic film, television pickup tubes, and the human eye", *Journal of the Society of Motion Picture Engineers*, Vol. 47, No. 4, pp. 273-294, October 1946.

[41] H.C. Andrews, "Monocrome digital image enhancement", *Applied Optics*, Vol. 15, No. 2, pp. 495-503, February 1976.

[42] B.S. Lipkin and A. Rosenfeld, Eds., *Picture Processing and Psychopictorics*. New York: Academic Press, 1970.

[43] R.H. Selzer, "Improving biomedical image quality with computers", Tech. Rep. 32-1336, Jet Propulsion Laboratory, Pasadena, California, October 1, 1968.

[44] E.L. Hall, "Digital filtering of images", Ph.D. dissertation, University of Missouri, Columbia, January 1971.

[45] B.R. Hunt, D.H. Hanney, and R.K. Ziegler, "A survey of radiographic image enhancement experience", Tech. Rep. LA-DC-72-69, Los Alamos Scientific Laboratory, University of California, Los Alamos, New Mexico, 1972.

[46] P.W. Hesse, "Fourier transform enhancement of radiographs", in *Proc. of the Eighth Symposium on Nondestructive Evaluation in Aerospace Weapons Systems, and Nuclear Applications*, April 21-23, 1971, pp. 155-167.

[47] E.L. Hall, R.P. Kruger, S.J. Dwyer, III, D.L. Hall, R.W. McLaren, and G.S. Lodwick, "A survey of preprocessing and feature extraction techniques for radiographic images", *IEEE Trans. on Computers*, Vol. C-20, No. 9, pp. 1032-1044, September 1971.

[48] S.C. Orphanoudakis and J.W. Strohbehn, "Mathematical model of conventional tomography", *Medical Physics*, Vol. 3, No. 4, pp. 224-232, Jul./Aug. 1976.

[49] E.R. Cole, "The removal of unknown image blurs by homomorphic filtering", Ph.D. dissertation, Computer Science Department, University of Utah, Salt Lake City, Utah, June 1973.

[50] B.R. Hunt and H.C. Andrews, "Comparison of different filter structures for image restoration", in *Proc. 6th Annual Hawaii International Conference on Systems Sciences*, January 1973.

[51] H.C. Andrews, "Digital image restoration: A survey", *op. cit.* [11], pp. 36-45.

[52] M.M. Sondhi, "Image restoration: The removal of spatially invariant degradations", *op. cit.* [10], pp. 842-853.

[53] T.G. Stockham, Jr., "Image processing in the context of a visual model", *op. cit.* [10], pp. 828-842.

[54] M. Trefler and J.E. Gray, "Characterization of the imaging properties of X-ray focal spots", *Applied Optics*, Vol. 15, No. 12, pp. 3099-3104, December 1976.

[55] T.M. Cannon, "Digital image deblurring by nonlinear homomorphic filtering", Ph.D. dissertation, Computer Science Department, University of Utah, Salt Lake City, Utah, August 1974.

[56] R. Rom, "On the cepstrum of two-dimensional functions", *IEEE Trans. on Information Theory*, Vol. IT-21, No. 2, pp. 214-217, March 1975.

[57] H.D. Helms, "Nonrecursive digital filters: Design methods for achieving specifications on frequency response", *IEEE Trans. on Audio and Electroacustics*, Vol. AU-16, No. 3, pp. 336-342, September 1968.

[58] T.S. Huang, "Two-dimensional windows", *IEEE Trans. on Audio and Electroacustics*, Vol. AU-20, No. 1, pp. 88-89, March 1972; reprinted in *op. cit.* [15], pp. 249-250.

[59] J.F. Kaiser, "Nonrecursive digital filter design using the I_0-sinh window function", in *Proc. 1974 IEEE Symposium on Circuits and Systems*, April 22-25, 1974, pp. 20-23; reprinted in *op. cit.* [15], pp. 123-126.

[60] J.L. Shanks, S. Treitel, and J.H. Justice, "Stability and synthesis of two-dimensional recursive filters", *IEEE Trans. on Audio and Electroacustics*, Vol. AU-20, No. 2, pp. 115-128, June 1972; reprinted in *op. cit.* [15], pp. 276-289.

[61] T.S. Huang, "Stability of two-dimensional recursive filters", *IEEE Trans. on Audio and Electroacustics*, Vol. AU-20, No. 2, pp. 158-163, June 1972; reprinted in *op. cit.* [15], pp. 290-295.

[62] R.M. Mersereau and D.E. Dudgeon, "Two-dimensional digital filtering", *Proc. of the IEEE*, Vol. 63, No. 4, pp. 610-623, April 1975; reprinted in *op. cit.* [15], pp. 230-243.

[63] J.M. Costa and A.N. Venetsanopoulos, "Design of circularly symmetric two-dimensional recursive filters", *IEEE Trans. on Acoustics, Speech, and Signal Processing*, Vol. ASSP-22, No. 6, pp. 432-443, December 1974; reprinted in *op. cit.* [15], pp. 321-332.

[64] N.A. Pendergrass, S.K. Mitra, and E.I. Jury, "Spectral transformations for two-dimensional digital filters", *IEEE Trans. on Circuits and Systems*, Vol. CAS-23, No. 1, pp. 26-35, January 1976.

[65] J.M. Costa and A.N. Venetsanopoulos, "A group of linear spectral transformations for two-dimensional digital filters", *IEEE Trans. on Acoustics, Speech, and Signal Processing*, Vol. ASSP-24, No. 5, pp. 424-425, October 1976.

[66] W.W. Peterson and E.J. Weldon, Jr., *Error-Correcting Codes*, Second Edition. Cambridge, Massachusetts: MIT Press, 1972, pp. 21-22.

[67] J.H. Justice and J.L. Shanks, "Stability criterion for n-dimensional recursive filters", *IEEE Trans. on Automatic Control* Vol. AC-18, No. 3, pp. 284-286, June 1973.

[68] J.M. Costa, "Design and realization of stable two-dimensional recursive filters", M.A.Sc. thesis, University of Toronto, Toronto, Ontario, September 1973.

[69] B.R. Hunt, "Data structures and computational organization in digital image enhancement", *op. cit.* [10], pp. 884-887.

[70] B.R. Hunt, "Minimizing the computation time for using the technique of sectioning for digital filtering of pictures", *IEEE Trans. on Computers*, Vol. C-21, No. 11, pp. 1219-1222, November 1972.

[71] M. Onoe, "A method for computing large-scale two-dimensional transforms without transposing data matrix", *Proc. of the IEEE*, Vol. 63, No. 1, pp. 196-197, January 1975.

[72] G. Southworth, "The TV camera as a computer input", *EE/Systems Engineering Today*, Vol. 32, No. 7, July 1973.

[73] H.C. Andrews, "Spatial resolution requirements for real-time digital displays", Image Processing Application Note 3, Comtal Corporation, Pasadena, California.

[74] H.C. Andrews, "Digital Fourier transforms as means for scanner evaluation", *Applied Optics*, Vol. 13, No. 1, pp. 146-149, January 1974.

[75] H.C. Andrews and C.L. Patterson, III, "Digital interpolation of discrete images", *IEEE Trans. on Computers*, Vol. C-25, No. 2, pp. 196-202, February 1976.

[76] H.C. Andrews, "Positive digital image restoration techniques — a survey", Tech. Rep. No. ATR-73(8139)-2, Aerospace Corporation, 26 February 1973.

[77] T.S. Huang, Ed., *Picture Processing and Digital Filtering*. New York: Springer-Verlag, 1975.

[78] B.K. Gilbert, M.T. Storma, C.E. James, L.W. Hobrock, E.S. Yang, K.C. Ballard, and E.H. Wood, "A real-time hardware system for digital processing of wide-band video images", *IEEE Trans. on Computers*, Vol. C-25, No. 11, pp. 1089-1100, November 1976.

[79] W.F. Schreiber, "Precise transmission and duplication of radiographs", *Quaterly Progress Report*, Massachusetts Institute of Technology, No. 112, pp. 95-99, January 1974.

[80] P. Edholm, "The tomogram, its formation and content", *Acta Radiologica (Stockholm), Supplementum 193*, 1960.

[81] A. Berrett, S. Brünner, and G.E. Valvassory, Eds., *Modern Thin-Section Tomography*. Springfield, Illinois: Charles C. Thomas, 1973.

[82] D. Westra, "Zonography. The narrow-angle tomography", thesis, Excerpta Medica Foundation, Amsterdam, 1966.

[83] K. Lindblom, "On microtomography", *Acta Radiologica (Stockholm)*, Vol. 42, p.465, 1954.

[84] W. Maue-Dickson and M. Trefler, "Image quality in computerized and conventional tomography in the assessment of craniofacial anomalies", University of Miami School of Medicine, Miami, Florida, August 26, 1977.

[85] B.G. Ziedses des Plantes, "Relative patient dose in conventional radiology, tomography, multisection radiography, and radiographic subtraction", in R.D. Moseley and J.H. Rust, Eds., *The Reduction of Patient Dose by Diagnostic Radiologic Instrumentation*. Springfield, Illinois: Charles C. Thomas, 1964, p. 71.

[86] D. Meyer-Ebrecht, "Hospital picture communication systems", in *Proc. EUROCON'77*, Venezia, Italy, 3-7 May 1977, pp. 4.2.3 1-7.

[87] A. Rosenfeld and A.C. Kak, *Digital Picture Processing*. New York: Academic Press, 1966.

[88] H.C. Andrews and B.R. Hunt, *Digital Image Restoration*. Englewood Cliffs, New Jersey: Prentice Hall, 1977.

[89] B.R. Hunt, "Digital Image Processing", in A.V. Oppenheim, Ed., *Applications of Digital Signal Processing*. Englewood Cliffs, New Jersey: Prentice Hall, 1978, pp. 169-237.

[90] W.K. Pratt, *Digital Image Processing*. New York: Wiley, 1978.

[91] J. L. Harris, Sr., "Image evaluation and restoration", *Journal of the Optical Society of America*, Vol. 56, No. 5, pp. 569-574, May 1966.

[92] J. L. Harris, Sr., "Potential and limitation of techniques for processing linear motion-degraded imagery", in *Evaluation of Motion Degraded Images (Prof. NASA/ERC Seminar)*, Cambridge, Mass., NASA Publ., SP-193, pp. 149-159, December 1968.

[93] D. Slepian, "On the restoration of photographs blurred by image motion", Miscellaneous Paper No. 3, *Woods Hole 1966 Summer Study Report on Restoration of Atmospherically Degraded Images*, National Academy of Sciences, July 1966.

[94] D. Slepian, "Restoration of photographs blurred by image motion", *The Bell System Technical Journal*, Vol. 46, pp. 2353-2362, December 1967.

[95] L. J. Cutrona and W.D. Hall, "Some considerations in post-facto blur removal", in *Evaluation of Motion Degraded Images (Proc. NASA/ERC Seminar)*, Cambridge, Mass., NASA Publ. SP-193, pp. 149-159, December 1968.

[96] D. W. Brown, D.L.Kirch, T.W. Ryerson, A.J. Throckmorton, A.L. Kilbourn, and N.M. Brenner, " Computer processing of scans using Fourier and other transformations", *Journal of Nuclear Medicine*, Vol. 12, No. 6, pp. 287-291, 1971.

[97] D. R. Dance, B.C. Wilson, and R.P. Parker, "Digital reconstruction of point sources imaged by a zone plate camera", *Physics in Medicine and Biology*, Vol. 20, No.5, pp. 747-756, 1975.

[98] K. R. Hetzel, "Cost-effectiveness of radiopharmaceuticals in medical imaging", in J.L. Quinn, III, editor, *The Year Book of Nuclear Medicine 1978*. Chicago, Ill.: Year Book Medical Publishers, Inc., 1978.

[99] C. J. Harrison, "The design and application of two-dimensional digital filters", M.Sc. thesis, Dept. of Geophysics, The Univeristy of Western Ontario, London, Ontario, May 1978.

[100] D. J. Goodman, "A design technique for circularly symmetric low-pass filters", *IEEE Trans. on Acoustics, Speech, and Signal Processing*, Vol. ASSP-26, No.4, pp. 290-304, August 1978.

[101] B. T. O'Connor and T.S. Huang, "Stability of general two-dimensional recursive digital filters", *IEEE Trans. on Acoustics, Speech, and Signal Processing*, Vol. ASSP-26, No.6, pp. 550-560, December 1978.